Université Fédérale
Toulouse Midi-Pyrénées

THÈSE

En vue de l'obtention du

DOCTORAT DE L'UNIVERSITÉ DE TOULOUSE

Délivré par : *l'Institut Supérieur de l'Aéronautique et de l'Espace (ISAE)*

Présentée et soutenue le *30 Octobre 2020* **par :**

Andrea BRUGNOLI

A port-Hamiltonian formulation of flexible structures
Modelling and symplectic finite element discretization

JURY

Daniel ALAZARD	ISAE-Supaeŕo, Toulouse	Directeur
Valérie P. BUDINGER	ISAE-Supaeŕo, Toulouse	Co-directeur
Denis Matignon	ISAE-Supaéro, Toulouse	Examinateur
Thomas Hélie	Directeur des Recherches CNRS	Examinateur
Yann LE GORREC	Institut FEMTO-ST	Rapporteur
Alessandro MACCHELLI	Universitá di Bologna	Rapporteur
?????	??????	Président

École doctorale et spécialité :
EDSYS : Automatique
Unité de Recherche :
CSDV - Commande des Systèmes et Dynamique du Vol - ONERA - ISAE
Directeur de Thèse :
Daniel ALAZARD et *Valérie POMMIER-BUDINGER*
Rapporteurs :
Yann LE GORREC et *Alessandro MACCHELLI*

Abstract

This thesis aims at extending the port-Hamiltonian (pH) approach to continuum mechanics in higher geometrical dimensions (particularly in 2D). The pH formalism has a strong multiphysics character and represents a unified framework to model, analyze and control both finite- and infinite-dimensional systems. Despite the large literature on this topic, elasticity problems in higher geometrical dimensions have almost never been considered. This work establishes the connection between port-Hamiltonian distributed systems and elasticity problems. The originality resides in three major contributions. First, the novel pH formulation of plate models and coupled thermoelastic phenomena is presented. The use of tensor calculus is mandatory for continuum mechanical models and the inclusion of tensor variables is necessary to obtain an intrinsic, i.e. coordinate free, and equivalent pH description. Second, a finite element based discretization technique, capable of preserving the structure of the infinite-dimensional problem at a discrete level, is developed and validated. The discretization of elasticity problems in port-Hamiltonian form requires the use of non-standard finite elements. Nevertheless, the numerical implementation is performed thanks to well-established open-source libraries, providing external users with an easy to use tool for simulating flexible systems in pH form. Third, flexible multibody systems are recast in pH form by making use of a floating frame description valid under small deformations assumptions. This reformulation include all kinds of linear elastic models and exploits the intrinsic modularity of pH systems.

Résumé

Cette thèse vise à étendre l'approche port-Hamiltonienne (pH) à la mécanique des milieux continus dans des dimensions géométriques plus élevées (en particulier on se focalise sur la dimension 2). Le formalisme pH, avec son fort caractère multiphysique, représente un cadre unifié pour modéliser, analyser et contrôler les systèmes de dimension finie et infinie. Malgré l'abondante littérature sur ce sujet, les problèmes d'élasticité en deux ou trois dimensions géométriques n'ont presque jamais été considérés. Dans ce travail de thèse la connexion entre problèmes d'élasticité et systèmes distribués port-Hamiltoniens est établie. L'originalité apportée réside dans trois contributions majeures. Tout d'abord, une nouvelle formulation pH des modèles de plaques et des phénomènes thermoélastiques couplés est présentée. L'utilisation du calcul tensoriel est obligatoire pour modéliser les milieux continus et l'introduction de variables tensorielles est nécessaire pour obtenir une description pH équivalente qui soit intrinsèque, c'est-à-dire indépendante des coordonnées choisies. Deuxièmement, une technique de discrétisation basée sur les éléments finis et capable de préserver la structure du problème de la dimension infinie au niveau discret est développée et validée. La discrétisation des problèmes d'élasticité écrits en forme port-Hamiltonienne nécessite l'utilisation d'éléments finis non standards. Néanmoins, l'implémentation numérique est réalisée grâce à des bibliothèques open source bien établies, fournissant aux utilisateurs externes un outil facile à utiliser pour simuler des systèmes flexibles sous forme pH. Troisièmement, une nouvelle formulation pH de la dynamique multicorps flexible est dérivée. Cette reformulation, valable sous de petites hypothèses de déformations, inclut toutes sortes de modèles élastiques linéaires et exploite la modularité intrinsèque des systèmes pH.

43

Acknowledgments

44

Remerciements

Ringraziamenti

Alla mia famiglia

Contents

Abstract i

Résumé iii

Acknowledgments v

Remerciements vii

Ringraziamenti ix

List of Acronyms xxi

I Introduction and state of the art 1

1 Introduction 3

1.1 Motivation and context 3

1.2 Overview of chapters 3

1.3 Contributions 3

2 Literature review 5

2.1 Port-Hamiltonian distributed systems 5

2.2 Structure-preserving discretization 5

2.3 Mixed finite element for elasticity 5

2.4 Multibody dynamics 6

3 Reminder on port-Hamiltonian systems 7

3.1 Finite dimensional setting 8

3.1.1 Dirac structure 8

3.1.2 Finite dimensional port-Hamiltonian systems 9
3.2 Infinite dimensional setting 9
3.2.1 Linear differential operators 10
3.2.2 Constant Stokes-Dirac structures 12
3.2.3 Distributed port-Hamiltonian systems 14
3.3 Some examples of known distributed port-Hamiltonian systems 15
3.3.1 Wave equation 16
3.3.2 Euler Bernoulli beam 17
3.3.3 2D shallow water equations 19
3.4 Conclusion 21

II Port-Hamiltonian elasticity and thermoelasticity **23**

4 Elasticity in port-Hamiltonian form **25**
4.1 Continuum mechanics 25
4.1.1 Non linear formulation of elasticity 25
4.1.2 The linear elastodynamics problem 27
4.2 Port-Hamiltonian formulation of linear elasticity 29
4.2.1 Energy and co-energy variables 29
4.2.2 Final system and associated Stokes-Dirac structure 31
4.3 Conclusion 35

5 Port-Hamiltonian plate theory **37**
5.1 First order plate theory 38
5.1.1 Mindlin-Reissner model 39
5.1.2 Kirchhoff-Love model 40
5.2 Port-Hamiltonian formulation of isotropic plates 42
5.2.1 Port-Hamiltonian Mindlin plate 43

5.2.2 Port-Hamiltonian Kirchhoff plate . . . 47
5.3 Laminated anisotropic plates . . . 52
5.3.1 Port-Hamiltonian laminated Mindlin plate . . . 54
5.3.2 Port-Hamiltonian laminated Kirchhoff plate . . . 55
5.4 Conclusion . . . 56

6 Thermoelasticity in port-Hamiltonian form **59**
6.1 Port-Hamiltonian linear coupled thermoelasticity . . . 59
6.1.1 The heat equation as a pH descriptor system . . . 60
6.1.2 Classical thermoelasticity . . . 61
6.1.3 Thermoelasticity as two coupled pHs . . . 63
6.2 Thermoelastic port-Hamiltonian bending . . . 65
6.2.1 Thermoelastic Euler-Bernoulli beam . . . 65
6.2.2 Thermoelastic Kirchhoff plate . . . 67
6.3 Conclusion . . . 69

III Finite element structure preserving discretization **71**

7 Partitioned finite element method **73**
7.1 Discretization under uniform boundary condition . . . 73
7.1.1 General procedure . . . 75
7.1.2 Linear case . . . 84
7.1.3 Linear flexible structures . . . 86
7.2 Mixed boundary conditions . . . 95
7.2.1 Solution using Lagrange multipliers . . . 97
7.2.2 Virtual domain decomposition . . . 99
7.3 Conclusion . . . 103

8 Numerical convergence study **105**

8.1 Discretization of the Euler-Bernoulli beam 107
8.1.1 Mixed discretization for the free-free beam 107
8.1.2 Mixed discretization for the clamped-clamped beam 108
8.1.3 Mixed discretization with lower regularity requirement 108
8.2 Plate problems using known mixed finite elements 109
8.2.1 Mindlin plate mixed discretization 109
8.2.2 The Hellan-Herrmann-Johnson scheme for the Kirchhoff plate 112
8.3 Dual mixed discretization of plate problems 113
8.3.1 Dual mixed discretization of the Mindlin plate 113
8.3.2 Dual mixed discretization of the Kirchhoff plate 114
8.4 Numerical experiments 115
8.4.1 Numerical test for the Euler-Bernoulli beam 116
8.4.2 Numerical test for the Mindlin plate 118
8.4.3 Numerical test for the Kirchhoff plate 120
8.5 Conclusion 125

9 Numerical applications **127**
9.1 Boundary stabilization 128
9.1.1 Cantilever Kirchhoff plate 128
9.1.2 Irrotational shallow water equations 130
9.2 Mixed boundary conditions enforcement 135
9.2.1 Motion planning of a thin beam 135
9.2.2 Vibroacoustics under mixed boundary conditions 139
9.3 Thermoelastic wave propagation 145
9.4 Modal analysis of plates 145

IV Port-Hamiltonian flexible multibody dynamics 147

10 Modular multibody systems in port-Hamiltonian form 149

10.1 Reminder of the rigid case 149

10.2 Flexible floating body 149

10.3 Modular construction of multibody systems 149

11 Validation 151

11.1 Beam systems 151

11.1.1 Modal analysis of a flexible mechanism 151

11.1.2 Non-linear crank slider 151

11.1.3 Hinged beam 151

11.2 Plate systems 151

11.2.1 Boundary interconnection with a rigid element 151

11.2.2 Actuated plate 151

Conclusions and future directions 155

A Mathematical tools 157

A.1 Differential operators 157

A.2 Integration by parts 158

A.3 Bilinear forms 159

B Supplementary material: tabulated results of Chapter 8 161

C Implementation using FEniCS and Firedrake 167

Bibliography 169

List of Figures

4.1 A 2D continuum with Neumann and Dirichlet boundary conditions 33

5.1 Kinematic assumption for the Kirchhoff plate 41
5.2 Cauchy law for momenta and forces at the boundary. 44
5.3 Reference frames and notations. 44
5.4 Boundary conditions for the Mindlin plate. 45
5.5 Boundary conditions for the Kirchhoff plate. 50
5.6 Laminated plate with 4 layers. 52

6.1 Boundary conditions for the thermoelastic problem. 62

7.1 Partition of boundary into two connected sets. 96
7.2 Splitting of the domain. 99
7.3 Interconnection at the interface Γ_{12}. 99

8.1 Error for the Euler Bernoulli beam (HerDG1 elements). 116
8.2 Error for the Euler Bernoulli beam (DG1Her elements). 117
8.3 Error for the Euler Bernoulli beam (CGCG elements). 117
8.4 Error for the clamped Mindlin plate (BJT elements). 119
8.5 Error for the clamped Mindlin plate (AFW elements). 121
8.6 Error for the clamped Mindlin plate (CGDG elements). 122
8.7 Error for the simply supported Kirchhoff plate (HHJ elements). 123
8.8 Error for the SSSS Kirchhoff plate (BellDG3 elements). 124
8.9 Error for the CSFS Kirchhoff plate (HHJ elements) 125
8.10 Error for the CSFS Kirchhoff plate (BellDG3 elements). 126

9.1 Cantilever plate subjected to a control forces on the lateral sides. 128

9.2 Hamiltonian trend for the cantilever Kirchhoff plate. 130

9.3 Snapshots at different times of the simulation of the boundary controlled cantilever Kirchhoff plate ($t_{\text{end}} = 5\,[s]$). 131

9.4 Total energy and Lyapunov function for the Shallow water equations. 133

9.5 Snapshots at different times of the simulation for the boundary controlled irrotational shallow water equations ($t_{\text{end}} = 3\,[s]$). 134

9.6 Boundary conditions for the motion planning problem. 135

9.7 Virtual decomposition of the Euler Bernoulli beam. 137

9.8 Interconnection for the Euler-Bernoulli beam. 137

9.9 Computed vertical displacement. 138

9.10 Analytical reference displacement and numerical predictions. 138

9.11 Analytical reference velocity and numerical predictions. 138

9.12 Boundary conditions for the 3D vibroacoustic problem. 139

9.13 Boundary partition for the 2D vibroacoustic problem. 140

9.14 Virtual decomposition of the vibroacoustic domain. 142

9.15 Interconnection for the vibroacoustic domain.. 142

List of Tables

8.1 Physical parameters for the Euler Bernoulli beam. 116

8.2 Physical parameters for the Mindlin plate. 119

8.3 Physical parameters for the Kirchhoff plate. 123

9.1 Settings and parameters for the boundary control of the Kirchhoff plate. . . . 130

9.2 Settings and parameters for the irrotational shallow water equations. 133

9.3 Settings and parameters for the vibroacoustic problem. 143

9.4 Elapsed simulation time for the vibroacoustic experiment. 145

B.1 Euler Bernoulli convergence result for the HerDG1 scheme. 161

B.2 Euler Bernoulli convergence result for the DG1Her scheme. 161

B.3 Euler Bernoulli convergence result for the CGCG scheme $k = 1$. 161

B.4 Euler Bernoulli convergence result for the CGCG scheme $k = 2$. 162

B.5 Euler Bernoulli convergence result for the CGCG scheme $k = 3$. 162

B.6 Mindlin plate convergence result for the BJT scheme $k = 1$. 162

B.7 Mindlin plate convergence result for the BJT scheme $k = 2$. 162

B.8 Mindlin plate convergence result for the BJT scheme $k = 3$. 163

B.9 Mindlin plate convergence result for the AFW scheme $k = 1$. 163

B.10 Mindlin plate convergence result for the AFW scheme $k = 2$. 163

B.11 Mindlin plate convergence result for the AFW scheme $k = 3$. 163

B.12 Mindlin plate convergence result for the Lagrange multiplier $\boldsymbol{E}_r$. 163

B.13 Mindlin plate convergence result for the CGDG scheme $k = 1$. 164

B.14 Mindlin plate convergence result for the CGDG scheme $k = 2$. 164

B.15 Mindlin plate convergence result for the CGDG scheme $k = 3$. 164

B.16 Kirchoff plate convergence result for the HHJ scheme $k = 1$ (SSSS test). . . . 164

B.17 Kirchoff plate convergence result for the HHJ scheme $k = 2$ (SSSS test). . . . 165

B.18 Kirchoff plate convergence result for the HHJ scheme $k = 3$ (SSSS test). . . . 165

B.19 Kirchoff plate convergence result for the BellDG3 scheme (SSSS test). 165

B.20 Kirchoff plate convergence result for the HHJ scheme $k = 1$ (CSFS test). . . . 165

B.21 Kirchoff plate convergence result for the HHJ scheme $k = 2$ (CSFS test). . . . 166

B.22 Kirchoff plate convergence result for the HHJ scheme $k = 3$ (CSFS test). . . . 166

B.23 Kirchoff plate convergence result for the BellDG3 scheme (CSFS test). 166

List of Acronyms

AFW	*Arnold-Falk-Winther*
BDM	*Brezzi-Douglas-Marini*
BJT	*Bécache-Joly-Tsogka*
CG	*Continuous Galerkin*
DAE	*Differential-Algebraic Equation*
DG	*Discontinuous Galerkin*
dpHs	*distributed port-Hamiltonian systems*
FEM	*Finite Element Method*
FMS	*Flexible Multibody System*
IDA-PBC	*Interconnection and Damping Assignment Passivity Based Control*
HHJ	*Hellan-Herrmann-Johnson*
PDE	*Partial Differential Equation*
PFEM	*Partitioned Finite Element Method*
pH	*port-Hamiltonian*
pHs	*port-Hamiltonian systems*
pHDAE	*port-Hamiltonian Descriptor System*
RT	*Raviart-Thomas*

Part I

Introduction and state of the art

Chapter 1

Introduction

I was born not knowing and have had only a little time to change that here and there.

Richard Feynman
Letter to Armando Garcia J.

Contents

1.1 Motivation and context 3
1.2 Overview of chapters 3
1.3 Contributions 3

1.1 Motivation and context

1.2 Overview of chapters

1.3 Contributions

Chapter 2

Literature review

Books serve to show a man that those original thoughts of his aren't very new after all.

Abraham Lincoln

2.1 Port-Hamiltonian distributed systems

Differential geometry An interesting reference that can provide some ideas in this direction is [Yao11, NY04].

For 1D linear PH systems with a generalized skew-adjoint system operator, [LGZM05] gives conditions on the assignment of boundary inputs and outputs for the system operator to generate a contraction semigroup. The latter is instrumental to show well-posedness of a linear PH system, see [JZ12]. Essentially, at most half the number of boundary port variables can be imposed as control inputs for a well-posed PH system in one-dimensional domains. The complete characterization of pH in arbitrary dimension is still an open research field. Two notable exceptions [KZ15, Skr19] provide partial answers to this problem. The first demonstrate the well-posedness of the linear wave equation in arbitrary geometrical dimensions. The second generalizes this result to treat the case of generic first order linear pHs in arbitrary geometrical dimensions.

2.2 Structure-preserving discretization

2.3 Mixed finite element for elasticity

Thanks to [CRML18], it has become evident that there is a strict link between discretization of port-Hamiltonian (pH) systems and mixed finite elements. Velocity-stress formulation for the wave dynamics and elastodynamics problems are indeed Hamiltonian and their mixed discretization preserves such a structure. For instance in [KK15] the authors employed mixed finite elements to obtain a symplectic semi-discretization for the wave equation. This allows using known finite element scheme to preserve the pH structure at the discrete level.

Mixed finite elements for the wave equation have been studied in [Gev88, BJT00]. For elastodynamics the construction of stable elements gets more complicated because of the presence of the symmetric stress tensor. Existing elements enforce symmetry either strongly [BJT01] or weakly [AL14].

2.4 Multibody dynamics

Chapter 3

Reminder on port-Hamiltonian systems

Contents

3.1 Finite dimensional setting 8

3.1.1 Dirac structure 8

3.1.2 Finite dimensional port-Hamiltonian systems 9

3.2 Infinite dimensional setting 9

3.2.1 Linear differential operators 10

3.2.2 Constant Stokes-Dirac structures 12

3.2.3 Distributed port-Hamiltonian systems 14

3.3 Some examples of known distributed port-Hamiltonian systems . . . 15

3.3.1 Wave equation 16

3.3.2 Euler Bernoulli beam 17

3.3.3 2D shallow water equations 19

3.4 Conclusion 21

The main mathematical aspects behind the pH formalism are recalled in this chapter. First, the finite dimensional case is considered. The geometric concept of Dirac structure [Cou90] is first presented. Finite dimensional port-Hamiltonian system are then introduced by making clear their intimate connection with the concept of Dirac structure. Second, the infinite dimensional case is recalled. The equivalent of Dirac structures for the infinite-dimensional case is the concept of Stokes-Dirac structure. Analogously to what happens in the finite-dimensional case, infinite-dimensional (or distributed) port-Hamiltonian systems are intimately related to the concept of Stokes-Dirac structure.

This notion of Stokes-Dirac structure was first introduced in the literature by making use of a differential geometry approach [vdSM02]. Despite being really insightful in terms of geometrical structure, this approach does not encompass the case of higher-order differential operators. An extension in this sense is still an open question. Since bending problems in elasticity introduce higher-order differential operators, the language of PDE will be privileged over the one of differential forms.

In the last section some examples are presented to demonstrate the general character of the port-Hamiltonian formalism.

3.1 Finite dimensional setting

Finite dimensional port-Hamiltonian are characterized by geometrical structures called Dirac structures. It is important to define this geometric concept and see how pHs relate to it.

3.1.1 Dirac structure

Consider a finite dimensional space F over the field $\mathbb{R}$ and $E \equiv F'$ its dual, i.e. the space of linear operator $\mathbf{e} : F \to \mathbb{R}$. The elements of F are called flows, while the elements of E are called efforts. Those are port variables and their combination gives the power flowing inside the system. The space $B := F \times E$ is called the bond space of power variables. Therefore the power is defined as $\langle \mathbf{e}, \mathbf{f} \rangle = \boldsymbol{e}(\mathbf{f})$, where $\langle \mathbf{e}, \mathbf{f} \rangle$ is the dual product between $\mathbf{f}$ and $\mathbf{e}$.

Definition 1 (Dirac Structure [Cou90], Def. 1.1.1)
Given the finite-dimensional space F and its dual E with respect to the inner product $\langle \cdot, \cdot \rangle_{E \times F} : F \times E \to \mathbb{R}$, consider the symmetric bilinear form:

$$\langle\langle\, (\mathbf{f}_1, \mathbf{e}_1), (\mathbf{f}_2, \mathbf{e}_2)\, \rangle\rangle := \langle \mathbf{e}_1,\, \mathbf{f}_2 \rangle_{E \times F} + \langle \mathbf{e}_2,\, \mathbf{f}_1 \rangle_{E \times F}\,, \qquad \textit{where} \qquad \mathbf{f}_i, \mathbf{e}_i \in B,\ i = 1, 2 \tag{3.1}$$

A Dirac structure on $B := F \times E$ is a subspace $D \subset B$, which is maximally isotropic under $\langle\langle \cdot, \cdot \rangle\rangle$. Equivalently, a Dirac structure on $B := F \times E$ is a subspace $D \subset B$ which equals its orthogonal complement with respect to $\langle\langle \cdot, \cdot \rangle\rangle : D = D^{\perp}$.

This definition can be extended to consider distributed forces and dissipation [Vil07].

Proposition 1 (Characterization of Dirac structures)
Consider the space of power variables $F \times E$ and let X denote an n-dimensional space, the space of energy variables. Suppose that $F := F_s \times F_e$ and that $E := E_s \times E_e$, with $\dim F_s = \dim E_s = n$ and $\dim F_e = \dim E_e = m$. Moreover, let $\mathbf{J}(\mathbf{x})$ denote a skew-symmetric matrix of dimension n and $\mathbf{B}(\mathbf{x})$ a matrix of dimension $n \times m$. Then, the set

$$D := \left\{ (\mathbf{f}_s, \mathbf{f}_e, \mathbf{e}_s, \mathbf{e}_e) \in F \times E | \quad \mathbf{f}_s = \mathbf{J}(\mathbf{x})\mathbf{e}_s + \mathbf{B}(\mathbf{x})\mathbf{f}_e,\ \mathbf{e}_e = -\mathbf{B}(\mathbf{x})^{\top}\mathbf{e}_s \right\} \tag{3.2}$$

is a Dirac structure.

It is now possible to make the connection between Dirac structures and pH system explicit.

3.1.2 Finite dimensional port-Hamiltonian systems

Consider the time-invariant dynamical system:

$$\begin{cases} \dot{\mathbf{x}} &= \mathbf{J}(\mathbf{x})\nabla H(\mathbf{x}) + \mathbf{B}(\mathbf{x})\mathbf{u}, \\ \mathbf{y} &= \mathbf{B}(\mathbf{x})^\top \nabla H(\mathbf{x}), \end{cases} \tag{3.3}$$

where $H(\mathbf{x}) : X \subset \mathbb{R}^n \to \mathbb{R}$, the Hamiltonian, is a real-valued function bounded from below. Such a system is called port-Hamiltonian, as it arises from the Hamiltonian modelling of a physical system and it interacts with the environment through the input $\mathbf{u}$ and the output $\mathbf{y}$, included in the formulation. The connection with the concept of Dirac structure is achieved by considering the following port behavior:

$$\begin{aligned} \mathbf{f}_s &= \dot{\mathbf{x}}, \qquad & \mathbf{e}_s &= \nabla H(\mathbf{x}), \\ \mathbf{f}_e &= \mathbf{u}, \qquad & \mathbf{e}_e &= -\mathbf{y}. \end{aligned} \tag{3.4}$$

With this choice of the port variables, system (3.3) defines, by Proposition 1, a Dirac structure. Dissipation and distributed forces can be included and the corresponding system defines an extended Dirac structure, once the proper port variables have been introduced.

System 3.3 is a pH system in canonical form. Recently, finite dimensional differential algebraic port-Hamiltonian systems (pHDAE) have been introduced both for linear [BMXZ18] and non linear systems [MM19]. This enriched description share all the crucial features of ordinary pHs, but easily account for algebraic constraints, time-dependent transformations and explicit dependence on time in the Hamiltonian. The application of the proposed discretization method lead naturally to pHDAE systems.

3.2 Infinite dimensional setting

Infinite dimensional spaces appears whenever differential operators have to be considered. In this section we first explain what defines a differential operator. Then Stokes-Dirac structures, characterized by a skew-symmetric differential operator, are introduced. Finally distributed port-Hamiltonian systems and their connection to the concept of Stokes-Dirac structure are illustrated.

Before starting we recall how inner products of square integrable function are computed. Let Ω denote a compact subset of $\mathbb{R}^d$ and let $L^2(\Omega, \mathbb{A})$ be the space of square integrable functions over the set $\mathbb{A}$ in Ω, with inner product denoted by $\langle \cdot, \cdot \rangle_{L^2(\Omega,\mathbb{A})}$. The set $\mathbb{A}$ can either denote scalars $\mathbb{R}$, vectors $\mathbb{R}^d$, tensors $\mathbb{R}^{d\times d}$ or a Cartesian product of those. For scalars

$(a,b) \in L^2(\Omega)$, vectors $(\boldsymbol{a}, \boldsymbol{b}) \in L^2(\Omega, \mathbb{R}^d)$ and tensors $(\boldsymbol{A}, \boldsymbol{B}) \in L^2(\Omega, \mathbb{R}^{d\times d})$ the L^2 inner product is given by

$$\langle a,\, b\rangle_{L^2(\Omega)} = \int_\Omega ab \,\mathrm{d}\Omega, \qquad \langle \boldsymbol{a},\, \boldsymbol{b}\rangle_{L^2(\Omega,\mathbb{R}^d)} = \int_\Omega \boldsymbol{a}\cdot\boldsymbol{b} \,\mathrm{d}\Omega, \qquad \langle \boldsymbol{A},\, \boldsymbol{B}\rangle_{L^2(\Omega,\mathbb{R}^{d\times d})} = \int_\Omega \boldsymbol{A}:\boldsymbol{B} \,\mathrm{d}\Omega. \tag{3.5}$$

The notation $\boldsymbol{A}:\boldsymbol{B} = \sum_{i,j} A_{ij}B_{ij}$ denotes the tensor contraction. Furthermore, the space of square integrable vector-valued functions over the boundary of Ω is indicated by $L^2(\partial\Omega, \mathbb{R}^m)$. This space is endowed with the inner product

$$\langle \boldsymbol{a}_\partial,\, \boldsymbol{b}_\partial\rangle_{L^2(\partial\Omega,\mathbb{R}^m)} = \int_{\partial\Omega} \boldsymbol{a}_\partial\cdot\boldsymbol{b}_\partial \,\mathrm{d}S, \qquad \boldsymbol{a}_\partial, \boldsymbol{b}_\partial \in \mathbb{R}^m. \tag{3.6}$$

3.2.1 Linear differential operators

Let Ω denote a compact subset of $\mathbb{R}^d$ representing the spatial domain of the distributed parameter system. Consider two function spaces F_1, F_2 over the sets $\mathbb{A}$, $\mathbb{B}$ defined on $\Omega \subset \mathbb{R}^d$ and a map $\mathcal{L}$ relating the two

$$\begin{aligned} \mathcal{L} : F_1(\Omega, \mathbb{A}) &\longrightarrow F_2(\Omega, \mathbb{B}), \\ \boldsymbol{u} &\longrightarrow \boldsymbol{v}. \end{aligned} \tag{3.7}$$

Sets $\mathbb{A}, \mathbb{B}$ can either denote scalars $\mathbb{R}$, vectors $\mathbb{R}^d$, tensors $\mathbb{R}^{d\times d}$ or a Cartesian product of those. Given $\boldsymbol{u} \in F_1$, $\boldsymbol{v} \in F_2$ The map $\mathcal{L}$ is a linear differential operator if it can be represented by a linear combination of derivatives of $\boldsymbol{u}$

$$\boldsymbol{v} = \mathcal{L}\boldsymbol{u} \iff \boldsymbol{v} := \sum_{|\alpha|=0}^{n} \mathcal{P}_\alpha \partial^\alpha \boldsymbol{u}, \tag{3.8}$$

where $\alpha := (\alpha_1, \dots, \alpha_d)$ is a multi-index of order $|\alpha| := \sum_{i=1}^d \alpha_i$ and $\partial^\alpha := \partial_{x_1}^{\alpha_1} \dots \partial_{x_d}^{\alpha_d}$ is a differential operator of order $|\alpha|$ resulting from a combination of spatial derivatives. $\mathcal{P}_\alpha : \mathbb{A} \to \mathbb{B}$ is a constant algebraic operator from set $\mathbb{A}$ to $\mathbb{B}$.

Example 1 (Divergence operator in $\mathbb{R}^d$)
Given $\boldsymbol{u} \in C^\infty(\Omega, \mathbb{R}^d)$, $v \in C^\infty(\Omega)$, where $C^\infty(\Omega, \mathbb{R}^d)$, $C^\infty(\Omega)$ denotes the set of smooth vector- and scalar-valued function defined on Ω, the divergence operator in Cartesian coordinate is expressed as

$$v = \operatorname{div} \boldsymbol{u} = \sum_{i=1}^{d} \boldsymbol{e}_i \cdot \partial_{x_i} \boldsymbol{u}, \tag{3.9}$$

where $\boldsymbol{e}_i$ is the $i-$th element of the canonical basis in $\mathbb{R}^d$.

The differential operators employed in this thesis are reported in Appendix A.
A very important notion related to a differential operator is the one of formal adjoint.

Definition 2 (Formal Adjoint)
Let $\mathcal{L} = L^2(\Omega, \mathbb{A}) \to L^2(\Omega, \mathbb{B})$ be a differential operator and $\boldsymbol{u} \in C_0^\infty(\Omega, \mathbb{A})$, $\boldsymbol{v}(\Omega, \mathbb{B})$ be smooth variables with compact support on Ω. The formal adjoint of the differential operator $\mathcal{L}$, denoted by $\mathcal{L}^* = L^2(\Omega, \mathbb{B}) \to L^2(\Omega, \mathbb{A})$, is defined by the relation

$$\langle \mathcal{L}\boldsymbol{u},\, \boldsymbol{v} \rangle_{L^2(\Omega,\mathbb{B})} = \langle \boldsymbol{u},\, \mathcal{L}^*\boldsymbol{v} \rangle_{L^2(\Omega,\mathbb{A})} \,. \tag{3.10}$$

This definition represent an extension to generic sets $\mathbb{A}$, $\mathbb{B}$ of Def. 5.80 in [RR04] (reported in Appendix A).

Remark 1 (Differences between adjoint and formal adjoint)
The definition of formal adjoint is such that the integration by parts formula is respected. Contrarily to the adjoint of an operator, the formal adjoint definition does not regard the actual domain of the operator nor the boundary conditions. For example, the differential operators div, grad *are unbounded in the L^2 topology. Whenever unbounded operators are considered, it is important to define their domain. To avoid the need of specifying domains, the notion of formal adjoint is used. The formal adjoint respects the integration by parts formula and is defined only for sufficiently smooth functions with compact support. In this sense the formal adjoint of* div *is* $-$grad*, since for smooth functions with compact support, it holds*

$$\langle \mathrm{div}\, \boldsymbol{y},\, x \rangle_{L^2(\Omega,\mathbb{R})} \underbrace{=}_{I.B.P.} - \langle \boldsymbol{y},\, \mathrm{grad}\, x \rangle_{L^2(\Omega,\mathbb{R}^d)} \,,$$

for $\boldsymbol{y} \in C_0^\infty(\Omega, \mathbb{R}^d)$, $x \in C_0^\infty(\Omega)$ (I.B.P. stands for integration by parts). The definition of the domain of the operators, that requires the knowledge of the boundary conditions, has not been specified.

For pHs formally skew-adjoint operators (or simply skew-symmetric) plays a fundamental role.

Definition 3 (Formally skew-adjoint operator)
Let $\mathcal{J} : L^2(\Omega, \mathbb{F}) \to L^2(\Omega, \mathbb{F})$ be a linear differential operator. Notice that the set $\mathbb{F}$ in the domain and co-domain is the same. Then, $\mathcal{J}$ is formally skew-adjoint (or skew-symmetric) if and only if $\mathcal{J} = -\mathcal{J}^*$.

If functions with compact support are considered, i.e. $\boldsymbol{u}_1, \boldsymbol{u}_2 \in C_0^\infty(\Omega, \mathbb{F})$ a formally skew-adjoint operator is characterized by the relation

$$\langle \mathcal{J}\boldsymbol{u}_1,\, \boldsymbol{u}_2 \rangle_{L^2(\Omega,\mathbb{B})} + \langle \boldsymbol{u}_1,\, \mathcal{J}\boldsymbol{u}_2 \rangle_{L^2(\Omega,\mathbb{A})} = 0. \tag{3.11}$$

3.2.2 Constant Stokes-Dirac structures

Constant Stokes-Dirac structures are the infinite-dimensional generalization of constant Dirac structures (i.e. Dirac structures for which the matrices $\mathbf{J}$, $\mathbf{B}$ in (3.3) are constant). Stokes-Dirac structure are characterized by the fact that they equal their orthogonal complement with respect to a bilinear product. So we recall the definition of orthogonal companion for the case of smooth functions.

Definition 4 (Orthogonal complement)
Let $\Omega \subset \mathbb{R}^d,\ d \in \{1,2,3\}$ be an open connected set and $C^\infty(\partial\Omega, \mathbb{R}^m)$ the space of smooth functions over its boundary. Consider the space

$$B = C^\infty(\Omega, \mathbb{F}) \times C^\infty(\partial\Omega, \mathbb{R}^m) \times C^\infty(\Omega, \mathbb{F}) \times C^\infty(\partial\Omega, \mathbb{R}^m) \tag{3.12}$$

and the bilinear pairing defined by

$$\begin{aligned} \langle\langle \cdot, \cdot \rangle\rangle : B \times B &\longrightarrow \mathbb{R}, \\ (\boldsymbol{a},\ \boldsymbol{a}_\partial,\ \boldsymbol{b},\ \boldsymbol{b}_\partial) \times (\boldsymbol{c},\ \boldsymbol{c}_\partial,\ \boldsymbol{d},\ \boldsymbol{d}_\partial) &\longrightarrow \begin{array}{l} \langle \boldsymbol{a},\ \boldsymbol{d} \rangle_{L^2(\Omega,\mathbb{F})} + \langle \boldsymbol{b},\ \boldsymbol{c} \rangle_{L^2(\Omega,\mathbb{F})} + \\ \langle \boldsymbol{a}_\partial,\ \boldsymbol{d}_\partial \rangle_{L^2(\partial\Omega,\mathbb{R}^m)} + \langle \boldsymbol{b}_\partial,\ \boldsymbol{c}_\partial \rangle_{L^2(\partial\Omega,\mathbb{R}^m)}\,. \end{array} \end{aligned} \tag{3.13}$$

Given a linear subspace $W \subset B$, its orthogonal complement is the set

$$W^\perp = \{\boldsymbol{v} \in B |\ \langle\langle \boldsymbol{v}, \boldsymbol{w} \rangle\rangle = 0,\ \forall \boldsymbol{w} \in W\} \tag{3.14}$$

We can now define what a Stokes-Dirac structure is.

Definition 5 (Stokes-Dirac structure)
A subset $D \subset B$, with B defined in (3.12), is a Stokes-Dirac structure iff

$$D = D^\perp, \tag{3.15}$$

where the orthogonal complement has been defined in Eq. (3.14)

For a subset to be a Stokes-Dirac structures a link between flow and effort variables must hold. Consider $\boldsymbol{f} \in C^\infty(\Omega, \mathbb{F})$ and $\boldsymbol{e} \in C^\infty(\Omega, \mathbb{F})$ and te following relation between the two

$$\boldsymbol{f} = \mathcal{J}\boldsymbol{e}, \qquad \mathcal{J} = -\mathcal{J}^*, \tag{3.16}$$

where $\mathcal{J}$ is a formally skew-adjoint operator. A Stokes-Dirac structure requires the specification of boundary variables in order to express a general power conservation property for *open* physical systems. We make therefore the following assumption, over the existence of appropriate boundary operators.

Assumption 1 (Existence of boundary operators)

Assume that exist two linear boundary operators $\mathcal{B}_\partial$, $\mathcal{C}_\partial$ such that for $\boldsymbol{u}_1,\ \boldsymbol{u}_2 \in C^\infty(\Omega, \mathbb{F})$ the following integration by parts formula holds

$$\langle \mathcal{J}\boldsymbol{u}_1,\, \boldsymbol{u}_2 \rangle_{L^2(\Omega,\mathbb{B})} + \langle \boldsymbol{u}_1,\, \mathcal{J}\boldsymbol{u}_2 \rangle_{L^2(\Omega,\mathbb{A})} = \langle \mathcal{B}_\partial \boldsymbol{u}_1,\, \mathcal{C}_\partial \boldsymbol{u}_2 \rangle_{L^2(\partial\Omega,\mathbb{R}^m)} + \langle \mathcal{B}_\partial \boldsymbol{u}_2,\, \mathcal{C}_\partial \boldsymbol{u}_1 \rangle_{L^2(\partial\Omega,\mathbb{R}^m)} . \tag{3.17}$$

This assumption is necessary to appropriately define a Stokes-Dirac structure. Only few particular cases, like the transport equation, do not verify it. We can now characterize generic Stokes-Dirac structure for smooth functions spaces.

Proposition 2 (Characterization of Stokes-Dirac structures)
Let B be defined as in Eq. (3.12) and $\mathcal{J}$ be a formally skew adjoint operator verifying Assumption 1. The set

$$D_\mathcal{J} = \{(\boldsymbol{f},\ \boldsymbol{f}_\partial,\ \boldsymbol{e},\ \boldsymbol{e}_\partial) \in B | \boldsymbol{f} = \mathcal{J}\boldsymbol{e},\ \boldsymbol{f}_\partial = \mathcal{B}_\partial \boldsymbol{e},\ \boldsymbol{e}_\partial = -\mathcal{C}_\partial \boldsymbol{e}\} \tag{3.18}$$

is a Stokes-Dirac structure with respect to the bilinear pairing (3.13).

Proof. A Stokes-Dirac is characterized by the fact that $D_\mathcal{J} = D_\mathcal{J}^\perp$. Then one has to show that $D_\mathcal{J} \subset D_\mathcal{J}^\perp$ and $D_\mathcal{J}^\perp \subset D_\mathcal{J}$. Following [LGZM05], the proof is obtained following three steps.

Step 1. To show that $D_\mathcal{J} \subset D_\mathcal{J}^\perp$, take $(\boldsymbol{f},\ \boldsymbol{f}_\partial,\ \boldsymbol{e},\ \boldsymbol{e}_\partial) \in D_\mathcal{J}$. Then

$$\begin{aligned}
\langle\langle\, (\boldsymbol{f}, \boldsymbol{f}_\partial, \boldsymbol{e}, \boldsymbol{e}_\partial), (\boldsymbol{f}, \boldsymbol{f}_\partial, \boldsymbol{e}, \boldsymbol{e}_\partial)\, \rangle\rangle =& 2 \langle \boldsymbol{e},\, \boldsymbol{f} \rangle_{L^2(\Omega,\mathbb{F})} + 2 \langle \boldsymbol{e}_\partial,\, \boldsymbol{f}_\partial \rangle_{L^2(\partial\Omega,\mathbb{R}^m)} , \\
=& 2 \langle \boldsymbol{e},\, \mathcal{J}\boldsymbol{e} \rangle_{L^2(\Omega,\mathbb{F})} + 2 \langle \boldsymbol{e}_\partial,\, \boldsymbol{f}_\partial \rangle_{L^2(\partial\Omega,\mathbb{R}^m)} , \\
\overset{\text{Eq. (3.17)}}{=}& 2 \langle \mathcal{B}_\partial \boldsymbol{e},\, \mathcal{C}_\partial \boldsymbol{e} \rangle_{L^2(\partial\Omega,\mathbb{R}^m)} + 2 \langle \boldsymbol{e}_\partial,\, \boldsymbol{f}_\partial \rangle_{L^2(\partial\Omega,\mathbb{R}^m)} , \\
\overset{\text{Eq. (3.18)}}{=}& 2 \langle \mathcal{B}_\partial \boldsymbol{e},\, \mathcal{C}_\partial \boldsymbol{e} \rangle_{L^2(\partial\Omega,\mathbb{R}^m)} - 2 \langle \mathcal{B}_\partial \boldsymbol{e},\, \mathcal{C}_\partial \boldsymbol{e} \rangle_{L^2(\partial\Omega,\mathbb{R}^m)} , \\
=& 0.
\end{aligned}$$

This implies $D_\mathcal{J} \subset D_\mathcal{J}^\perp$.

Step 2. Take $(\boldsymbol{\phi},\ \boldsymbol{\phi}_\partial,\ \boldsymbol{\epsilon},\ \boldsymbol{\epsilon}_\partial) \in D_\mathcal{J}^\perp$ and $\boldsymbol{e}_0 \in C_0^\infty(\Omega, \mathbb{F})$. This implies $\mathcal{B}_\partial \boldsymbol{e}_0 = (\boldsymbol{0},\ \boldsymbol{0})$ and $\mathcal{C}_\partial \boldsymbol{e}_0 = (\boldsymbol{0},\ \boldsymbol{0})$. Taking $(\mathcal{J}\boldsymbol{e}_0, \boldsymbol{0}, \boldsymbol{e}_0, \boldsymbol{0}) \in D_\mathcal{J}$ then

$$\langle\langle\, (\boldsymbol{\phi}, \boldsymbol{\phi}_\partial, \boldsymbol{\epsilon}, \boldsymbol{\epsilon}_\partial), (\mathcal{J}\boldsymbol{e}_0, \boldsymbol{0}, \boldsymbol{e}_0, \boldsymbol{0})\, \rangle\rangle = \langle \boldsymbol{\epsilon},\, \mathcal{J}\boldsymbol{e}_0 \rangle_{L^2(\Omega,\mathbb{F})} + \langle \boldsymbol{e}_0,\, \boldsymbol{\phi} \rangle_{L^2(\Omega,\mathbb{F})} = 0, \quad \forall \boldsymbol{e}_0 \in C_0^\infty(\Omega, \mathbb{F}).$$

It follows that $\boldsymbol{\epsilon} \in C_0^\infty(\Omega, \mathbb{F})$ and $\boldsymbol{\phi} = \mathcal{J}\boldsymbol{\epsilon}$.

Step 3. Take $(\boldsymbol{\phi},\ \boldsymbol{\phi}_\partial,\ \boldsymbol{\epsilon},\ \boldsymbol{\epsilon}_\partial) \in D_\mathcal{J}^\perp$ and $(\boldsymbol{f},\ \boldsymbol{f}_\partial,\ \boldsymbol{e},\ \boldsymbol{e}_\partial) \in D_\mathcal{J}$. From step 2 and (3.17)

$$
\begin{aligned}
0 &= \langle \mathcal{J}\boldsymbol{e},\, \boldsymbol{\epsilon}\rangle_{L^2(\Omega,\mathbb{F})} + \langle \boldsymbol{e},\, \mathcal{J}\boldsymbol{\epsilon}\rangle_{L^2(\Omega,\mathbb{F})} + \langle \boldsymbol{e}_\partial,\, \boldsymbol{\phi}_\partial\rangle_{L^2(\partial\Omega,\mathbb{R}^m)} + \langle \boldsymbol{\epsilon}_\partial,\, \boldsymbol{f}_\partial\rangle_{L^2(\partial\Omega,\mathbb{R}^m)}\,, \\
&\overset{\text{Eq. (3.17)}}{=} \langle \mathcal{B}_\partial\boldsymbol{e},\, \mathcal{C}_\partial\boldsymbol{\epsilon}\rangle_{L^2(\partial\Omega,\mathbb{R}^m)} + \langle \mathcal{B}_\partial\boldsymbol{\epsilon},\, \mathcal{C}_\partial\boldsymbol{e}\rangle_{L^2(\partial\Omega,\mathbb{R}^m)} + \langle \boldsymbol{e}_\partial,\, \boldsymbol{\phi}_\partial\rangle_{L^2(\partial\Omega,\mathbb{R}^m)} + \langle \boldsymbol{\epsilon}_\partial,\, \boldsymbol{f}_\partial\rangle_{L^2(\partial\Omega,\mathbb{R}^m)}\,, \\
&= \langle \mathcal{B}_\partial\boldsymbol{e},\, \mathcal{C}_\partial\boldsymbol{\epsilon}\rangle_{L^2(\partial\Omega,\mathbb{R}^m)} + \langle \mathcal{B}_\partial\boldsymbol{\epsilon},\, \mathcal{C}_\partial\boldsymbol{e}\rangle_{L^2(\partial\Omega,\mathbb{R}^m)} + \langle -\mathcal{C}_\partial\boldsymbol{e},\, \boldsymbol{\phi}_\partial\rangle_{L^2(\partial\Omega,\mathbb{R}^m)} + \langle \boldsymbol{\epsilon}_\partial,\, \mathcal{B}_\partial\boldsymbol{e}\rangle_{L^2(\partial\Omega,\mathbb{R}^m)}\,, \\
&= \langle \mathcal{B}_\partial\boldsymbol{e},\, \mathcal{C}_\partial\boldsymbol{\epsilon} + \boldsymbol{\epsilon}_\partial\rangle_{L^2(\partial\Omega,\mathbb{R}^m)} + \langle \mathcal{B}_\partial\boldsymbol{\epsilon} - \boldsymbol{\phi}_\partial,\, \mathcal{C}_\partial\boldsymbol{e}\rangle_{L^2(\partial\Omega,\mathbb{R}^m)}\,, \qquad \text{By linearity,} \\
&= \langle \boldsymbol{e}_\partial,\, \mathcal{C}_\partial\boldsymbol{\epsilon} + \boldsymbol{\epsilon}_\partial\rangle_{L^2(\partial\Omega,\mathbb{R}^m)} - \langle \mathcal{B}_\partial\boldsymbol{\epsilon} - \boldsymbol{\phi}_\partial,\, \boldsymbol{f}_\partial\rangle_{L^2(\partial\Omega,\mathbb{R}^m)}\,.
\end{aligned}
$$

Given the fact that $\boldsymbol{e}_\partial,\ \boldsymbol{f}_\partial$ are arbitrary then

$$\boldsymbol{\phi}_\partial = \mathcal{B}_\partial\boldsymbol{\epsilon}, \qquad \boldsymbol{\epsilon}_\partial = -\mathcal{C}_\partial\boldsymbol{\epsilon},$$

meaning that $D_{\mathcal{J}}^{\perp} \subset D_{\mathcal{J}}$. This concludes the proof. □

3.2.3 Distributed port-Hamiltonian systems

A distributed lossless port-Hamiltonian system is defined by a set of variables that describes the unknowns, by a formally skew-adjoint differential operator, an energy functional and a set of boundary inputs and corresponding conjugated outputs. Such a system is described by the following set of equations, defined on an open connected set $\Omega \subset \mathbb{R}^d$

$$
\begin{aligned}
\partial_t\boldsymbol{\alpha} &= \mathcal{J}\,\delta_{\boldsymbol{\alpha}}H, & \boldsymbol{\alpha} &\in C^\infty(\Omega,\mathbb{F}), \\
\boldsymbol{u}_\partial &= \mathcal{B}_\partial\,\delta_{\boldsymbol{\alpha}}H, & \boldsymbol{u}_\partial &\in \mathbb{R}^m, \\
\boldsymbol{y}_\partial &= \mathcal{C}_\partial\,\delta_{\boldsymbol{\alpha}}H, & \boldsymbol{y}_\partial &\in \mathbb{R}^m.
\end{aligned} \tag{3.19}
$$

The unknowns $\boldsymbol{\alpha}$ are called energy variables in the port-Hamiltonian framework, the formally skew-adjoint operator $\mathcal{J}$ is named interconnection operator (see Def. 3 for a precise definition of formal skew adjointness). $\mathcal{B}_\partial, \mathcal{C}_\partial$ are boundary operators, that provide the boundary input $\boldsymbol{u}_\partial$ and output $\boldsymbol{y}_\partial$ [TW09, Chapter 4]. The functional $H(\boldsymbol{\alpha}) : C^\infty(\Omega,\mathbb{F}) \to \mathbb{R}$ corresponds to the Hamiltonian functional and in all the examples considered in this thesis coincide with the total energy of the system. Notation $\delta_{\boldsymbol{\alpha}}H$ indicates the variational derivative of H.

Definition 6 (Variational derivative, Def. 4.1 in [Olv93])
Consider a functional $H(\boldsymbol{\alpha}) : C^\infty(\Omega,\mathbb{F}) \to \mathbb{R}$

$$H(\boldsymbol{\alpha}) = \int_\Omega \mathcal{H}(\boldsymbol{\alpha})\, \mathrm{d}\Omega.$$

Given a variation $\boldsymbol{\alpha} = \bar{\boldsymbol{\alpha}} + \eta\boldsymbol{\delta\alpha}$ *the variational derivative* $\frac{\delta H}{\delta\boldsymbol{\alpha}}$ *is defined as*

$$H(\bar{\boldsymbol{\alpha}} + \eta\boldsymbol{\delta\alpha}) = H(\bar{\boldsymbol{\alpha}}) + \eta\,\langle \delta_{\boldsymbol{\alpha}}H,\, \boldsymbol{\delta\alpha}\rangle_{L^2(\Omega,\mathbb{F})} + O(\eta^2).$$

Remark 2

If the integrand does not contain derivative of the argument $\boldsymbol{\alpha}$ then the variational derivative is equal to the partial derivative of the Hamiltonian density $\mathcal{H}$

$$\frac{\delta H}{\delta \boldsymbol{\alpha}} = \frac{\partial \mathcal{H}}{\partial \boldsymbol{\alpha}}.$$

Remark 3 (Co-energy variables)
The variational derivative of the Hamiltonian defines the co-energy variables $\boldsymbol{e} := \delta_{\boldsymbol{\alpha}} H$. These are equivalent to the effort variables of the Stokes-Dirac structure as we will immediately show.

Suppose that operators $\mathcal{J}$, $\mathcal{B}_\partial$, $\mathcal{C}_\partial$ in Eq. 3.19 verify Ass. 1. Then, System (3.19) is lossless since the energy rate is given by

$$\begin{aligned}
\dot{H} &= \langle \delta_{\boldsymbol{\alpha}} H, \, \partial_t \boldsymbol{\alpha} \rangle_{L^2(\Omega, \mathbb{F})}, \\
&\overset{Eq.(3.17)}{=} \langle \mathcal{B}_\partial \delta_{\boldsymbol{\alpha}} H, \, \mathcal{C}_\partial \delta_{\boldsymbol{\alpha}} H \rangle_{L^2(\partial\Omega, \mathbb{R}^m)}, \\
&= \langle \boldsymbol{u}_\partial, \, \boldsymbol{y}_\partial \rangle_{L^2(\partial\Omega, \mathbb{R}^m)}.
\end{aligned} \tag{3.20}$$

The connection between the concept of Stokes-Dirac structure and dpHs becomes clear if the following port behavior is considered

$$\begin{aligned}
\boldsymbol{f} &= \partial_t \boldsymbol{\alpha}, \qquad & \boldsymbol{e} &= \delta_{\boldsymbol{\alpha}} H, \\
\boldsymbol{f}_\partial &= \boldsymbol{u}_\partial, \qquad & \boldsymbol{e}_\partial &= -\boldsymbol{y}_\partial.
\end{aligned} \tag{3.21}$$

By proposition (2) System (3.19) under the port behavior (3.21) defines a Stokes-Dirac structure. No rigorous characterization has been given so far for operators $\mathcal{J}$, $\mathcal{B}_\partial$, $\mathcal{C}_\partial$ in system (3.19). A formal characterization of these operators has been given in [LGZM05] for pH of generic order only in one geometrical dimensional. In Chapter 7 the operator $\mathcal{J}$ will be better characterize using an appropriate partition. By applying a general integration by parts formula, the operators $\mathcal{B}_\partial$, $\mathcal{C}_\partial$ associated to $\mathcal{J}$ can be defined as well. The following examples clarifies this assertion for some known pHs.

3.3 Some examples of known distributed port-Hamiltonian systems

In this section the generality of the pH framework is illustrated through three different examples: the wave equation in a 2D geometry, the Euler-Bernoulli beam and the non linear Saint-Venant equations.

3.3.1 Wave equation

Given an open bounded connected set $\Omega \subset \mathbb{R}^d,\ d = \{2, 3\}$ with Lipschitz continuous boundary $\partial\Omega$, the propagation of sound in air can be described by the following model [TRLGK18]

$$\begin{aligned} \chi_s \partial_t p(\boldsymbol{x}, t) &= -\operatorname{div} \boldsymbol{v}, \\ \mu_0 \partial_t \boldsymbol{v}(\boldsymbol{x}, t) &= -\operatorname{grad} p, \end{aligned} \tag{3.22}$$

where the scalars χ_s, μ_0 are the constant adiabatic compressibility factor and the steady state mass density respectively. The scalar field $p \in \mathbb{R}$ and vector field $\boldsymbol{v} \in \mathbb{R}^d$ represents the variation of pressure and velocity from the steady state. The Hamiltonian (total energy) reads

$$H = \frac{1}{2} \int_\Omega \left\{ \chi_s p^2 + \mu_0 \left\| \boldsymbol{v} \right\|^2 \right\} \, \mathrm{d}\Omega.$$

To recast (3.22) in pH form the energy variables has to be introduced $\boldsymbol{\alpha} = [\alpha_p, \, \boldsymbol{\alpha}_v]^\top$

$$\alpha_p := \chi_s p, \qquad \boldsymbol{\alpha}_v := \mu_0 \boldsymbol{v}.$$

The Hamiltonian is rewritten as

$$H = \frac{1}{2} \int_\Omega \left\{ \frac{1}{\chi_s} \alpha_p^2 + \frac{1}{\mu_0} \left\| \boldsymbol{\alpha}_v \right\|^2 \right\} \, \mathrm{d}\Omega.$$

By definition, the co-energy are

$$e_p = \frac{\delta H}{\delta \alpha_p} = \frac{1}{\chi_s} \alpha_p = p, \qquad \boldsymbol{e}_v = \frac{\delta H}{\delta \boldsymbol{\alpha}_v} = \frac{1}{\mu_0} \boldsymbol{\alpha}_v = \boldsymbol{v}.$$

Equation (3.22) can be recast in port-Hamiltonian form

$$\frac{\partial}{\partial t} \begin{pmatrix} \alpha_p \\ \boldsymbol{\alpha}_v \end{pmatrix} = - \begin{bmatrix} 0 & \operatorname{div} \\ \operatorname{grad} & \boldsymbol{0} \end{bmatrix} \begin{pmatrix} e_p \\ \boldsymbol{e}_v \end{pmatrix}. \tag{3.23}$$

From the energy rate it is possible to identify the boundary variables.

$$\begin{aligned} \dot{H} &= + \int_\Omega \left\{ e_p \, \partial_t \alpha_p + \boldsymbol{e}_v \cdot \partial_t \boldsymbol{\alpha}_v \right\} \, \mathrm{d}\Omega, \\ &= - \int_\Omega \left\{ e_p \, \operatorname{div} \boldsymbol{e}_v + \boldsymbol{e}_v \cdot \operatorname{grad} e_p \right\} \, \mathrm{d}\Omega, && \text{Chain rule,} \\ &= - \int_\Omega \operatorname{div}(e_p \, \boldsymbol{e}_v) \, \mathrm{d}\Omega, && \text{Stokes theorem,} \\ &= - \int_{\partial\Omega} e_p \, \boldsymbol{e}_v \cdot \boldsymbol{n} \, \mathrm{d}S = - \left\langle e_p, \, \boldsymbol{e}_v \cdot \boldsymbol{n} \right\rangle_{L^2(\partial\Omega, \mathbb{R}^2)}. \end{aligned}$$

The boundary term $\left\langle e_p, \, \boldsymbol{e}_v \cdot \boldsymbol{n} \right\rangle_{L^2(\partial\Omega, \mathbb{R}^2)}$ pairs two power variables. One is taken as control input, the other plays the role of power-conjugated output. The assignment of these roles to the boundary power variables is referred to as causality of the boundary port [KML18],[Kot19, Chapter 2]. Under uniform causality assumption, either e_p or $\boldsymbol{e}_v$ can assume the role of (distributed) boundary input, but not both. This leads to two possible selections:

- First case $u_\partial = e_p, \quad y_\partial = \boldsymbol{e}_v \cdot \boldsymbol{n}$.
  This imposes the variable $e_p := p$ as boundary input and corresponds to a classical Dirichlet condition. The boundary operator for this case are given by
  $$\mathcal{B}_\partial \begin{pmatrix} e_p \\ \boldsymbol{e}_v \end{pmatrix} = e_p|_{\partial\Omega}, \qquad \mathcal{C}_\partial \begin{pmatrix} e_p \\ \boldsymbol{e}_v \end{pmatrix} = \boldsymbol{e}_v \cdot \boldsymbol{n}|_{\partial\Omega},$$
  corresponding to the standard trace and normal trace operators.

- Second case $u_\partial = \boldsymbol{e}_v \cdot \boldsymbol{n}, \quad y_\partial = e_p$.
  This imposes the variable $\boldsymbol{e}_v \cdot \boldsymbol{n} := \boldsymbol{v} \cdot \boldsymbol{n}$ as boundary input and corresponds to a Neumann condition. The boundary operators are therefore switched with respect to the previous case
  $$\mathcal{B}_\partial \begin{pmatrix} e_p \\ \boldsymbol{e}_v \end{pmatrix} = \boldsymbol{e}_v \cdot \boldsymbol{n}|_{\partial\Omega}, \qquad \mathcal{C}_\partial \begin{pmatrix} e_p \\ \boldsymbol{e}_v \end{pmatrix} = e_p|_{\partial\Omega}.$$

3.3.2 Euler Bernoulli beam

The Euler-Bernoulli beam model consists of one PDE, describing the vertical displacement along the beam length:

$$\rho A(x) \frac{\partial^2 w}{\partial t^2}(x,t) + \frac{\partial^2}{\partial x^2}\left(EI(x)\frac{\partial^2 w}{\partial x^2}\right) = 0, \quad x \in \Omega = \{0, L\}, \tag{3.24}$$

where $w(x,t)$ is the transverse displacement of the beam. The coefficients $\rho(x), A(x)E(x)$ and $I(x)$ are the mass density, cross section, Young's modulus of elasticity and the moment of inertia of a cross section. The energy variables are then chosen as follows:

$$\alpha_w = \rho A(x)\frac{\partial w}{\partial t}(x,t), \quad \text{Linear Momentum}, \quad \alpha_\kappa = \frac{\partial^2 w}{\partial x^2}(x,t), \quad \text{Curvature}. \tag{3.25}$$

Those variables are collected in the vector $\boldsymbol{\alpha} = (\alpha_w, \alpha_\kappa)^T$, so that the Hamiltonian can be written as a quadratic functional in the energy variables:

$$H = \frac{1}{2}\int_\Omega \left\{\frac{1}{\rho A}\alpha_w^2 + EI\alpha_\kappa^2\right\} \mathrm{d}\Omega \tag{3.26}$$

The co-energy variables are found by computing the variational derivative of the Hamiltonian:

$$\begin{aligned} e_w &:= \frac{\delta H}{\delta \alpha_w} = \frac{\partial w}{\partial t}(x,t), && \text{Vertical velocity}, \\ e_\kappa &:= \frac{\delta H}{\delta \alpha_\kappa} = EI(x)\frac{\partial^2 w}{\partial x^2}(x,t), && \text{Flexural momentum}. \end{aligned} \tag{3.27}$$

The underlying interconnection structure is then found to be:

$$\frac{\partial}{\partial t}\begin{pmatrix}\alpha_w\\ \alpha_\kappa\end{pmatrix} = \begin{bmatrix}0 & -\partial_{xx}\\ \partial_{xx} & 0\end{bmatrix}\begin{pmatrix}e_w\\ e_\kappa\end{pmatrix}. \tag{3.28}$$

The power flow gives access to the boundary variables:

$$\begin{aligned}\dot{H} &= \int_\Omega \{e_w\partial_t\alpha_w + e_\kappa\partial_t\alpha_\kappa\}\ \mathrm{d}\Omega,\\ &= \int_\Omega \{-e_w\partial_{xx}e_\kappa + e_\kappa\partial_{xx}e_w\}\ \mathrm{d}\Omega, \qquad \text{Integration by parts,}\\ &= \int_{\partial\Omega}\{-e_w\partial_x e_\kappa + e_\kappa\partial_x e_w\}\ \mathrm{d}s = \langle -e_w|_{\partial\Omega},\, \partial_x e_\kappa|_{\partial\Omega}\rangle_{\mathbb{R}^4} + \langle e_\kappa|_{\partial\Omega},\, \partial_x e_w|_{\partial\Omega}\rangle_{\mathbb{R}^4}\end{aligned} \tag{3.29}$$

Since the system is of differential order two, two pairing appears, giving rise to four combination of uniform boundary causality

- First case $u_{\partial,1} = e_w, \quad u_{\partial,2} = \partial_x e_w, \quad y_{\partial,1} = -\partial_x e_\kappa, \quad y_{\partial,2} = e_\kappa$.
  This imposes the vertical $e_w := \partial_t w$ and angular velocity $\partial_x e_w := \partial_{xt} w$ as boundary inputs

  $$\mathcal{B}_\partial\begin{pmatrix}e_w\\ e_\kappa\end{pmatrix} = \begin{pmatrix}e_w(L)\\ -e_w(0)\\ \partial_x e_w(L)\\ -\partial_x e_w(0)\end{pmatrix} \in \mathbb{R}^4 \qquad \mathcal{C}_\partial\begin{pmatrix}e_w\\ e_\kappa\end{pmatrix} = \begin{pmatrix}-\partial_x e_\kappa(L)\\ \partial_x e_\kappa(0)\\ e_\kappa(L)\\ -e_\kappa(0)\end{pmatrix} \in \mathbb{R}^4 \tag{3.30}$$

  If the inputs are null a clamped boundary condition is obtained.

- Second case $u_{\partial,1} = e_w, \quad u_{\partial,2} = e_\kappa, \quad y_{\partial,1} = -\partial_x e_\kappa, \quad y_{\partial,2} = \partial_x e_w$.
  This imposes the vertical velocity and flexural momentum $e_\kappa := EI\partial_{xx} w$ as boundary inputs

  $$\mathcal{B}_\partial\begin{pmatrix}e_w\\ e_\kappa\end{pmatrix} = \begin{pmatrix}e_w(L)\\ -e_w(0)\\ e_\kappa(L)\\ -e_\kappa(0)\end{pmatrix} \in \mathbb{R}^4 \qquad \mathcal{C}_\partial\begin{pmatrix}e_w\\ e_\kappa\end{pmatrix} = \begin{pmatrix}-\partial_x e_\kappa(L)\\ \partial_x e_\kappa(0)\\ \partial_x e_w(L)\\ -\partial_x e_w(0)\end{pmatrix} \in \mathbb{R}^4 \tag{3.31}$$

  Zero inputs lead to a simply supported condition.

- Third case $u_{\partial,1} = -\partial_x e_\kappa, \quad u_{\partial,2} = e_\kappa, \quad y_{\partial,1} = e_w, \quad y_{\partial,2} = \partial_x e_w$.
  This imposes the shear force $\partial_x e_\kappa := \partial_x(EI\partial_{xx} w)$ and flexural momentum as boundary inputs

  $$\mathcal{B}_\partial\begin{pmatrix}e_w\\ e_\kappa\end{pmatrix} = \begin{pmatrix}-\partial_x e_\kappa(L)\\ \partial_x e_\kappa(0)\\ e_\kappa(L)\\ -e_\kappa(0)\end{pmatrix} \in \mathbb{R}^4 \qquad \mathcal{C}_\partial\begin{pmatrix}e_w\\ e_\kappa\end{pmatrix} = \begin{pmatrix}e_w(L)\\ -e_w(0)\\ \partial_x e_w(L)\\ -\partial_x e_w(0)\end{pmatrix} \in \mathbb{R}^4 \tag{3.32}$$

  Null inputs correspond to a free condition.

- Fourth case $u_{\partial,1} = -\partial_x e_\kappa, \quad u_{\partial,2} = \partial_x e_w, \quad y_{\partial,1} = e_w, \quad y_{\partial,2} = e_\kappa$.
  This imposes the shear force and angular velocity as boundary inputs

$$\mathcal{B}_\partial \begin{pmatrix} e_w \\ e_\kappa \end{pmatrix} = \begin{pmatrix} -\partial_x e_\kappa(L) \\ \partial_x e_\kappa(0) \\ \partial_x e_w(L) \\ -\partial_x e_w(0) \end{pmatrix} \in \mathbb{R}^4 \qquad \mathcal{C}_\partial \begin{pmatrix} e_w \\ e_\kappa \end{pmatrix} = \begin{pmatrix} e_w(L) \\ -e_w(0) \\ e_\kappa(L) \\ -e_\kappa(0) \end{pmatrix} \in \mathbb{R}^4 \tag{3.33}$$

3.3.3 2D shallow water equations

This formulation may be found in [CR16, Section 6.2]. This model describes a thin fluid layer of constant density in hydrostatic balance, like the propagation of a tsunami wave far from shore. Consider an open bounded connected set $\Omega \subset \mathbb{R}^2$ and a constant bed profile. The mass conservation implies

$$\frac{\partial h}{\partial t} + \mathrm{div}(h\boldsymbol{v}) = 0,$$

where $h(x, y, t) \in \mathbb{R}$ is a scalar field representing the fluid height, $\boldsymbol{v}(x, y, t) \in \mathbb{R}^2$ is the fluid velocity field. The conservation of linear momentum reads

$$\frac{\partial \rho \boldsymbol{v}}{\partial t} + \rho(\boldsymbol{v} \cdot \nabla)\boldsymbol{v} + \nabla(\rho g h) = 0,$$

where ρ is the mass density and g the gravitational acceleration constant. Using the identity

$$(\boldsymbol{v} \cdot \nabla)\boldsymbol{v} = \frac{1}{2}\nabla(\|\boldsymbol{v}\|^2) + (\nabla \times \boldsymbol{v}) \times \boldsymbol{v},$$

where $\nabla\times$ is the rotational of $\boldsymbol{v}$ (also denoted $\mathrm{curl}\, \boldsymbol{v}$), the momentum is rearranged as follows

$$\frac{\partial \rho \boldsymbol{v}}{\partial t} = -\nabla \left(\frac{1}{2}\rho \|\boldsymbol{v}\|^2 + \rho g h \right) - \rho(\nabla \times \boldsymbol{v}) \times \boldsymbol{v}.$$

The last term on the right-hand side can be rewritten

$$\rho(\nabla \times \boldsymbol{v}) \times \boldsymbol{v} = \begin{bmatrix} 0 & -\rho\omega \\ \rho\omega & 0 \end{bmatrix} \boldsymbol{v},$$

with $\omega = \partial_x v_y - \partial_y v_x$ the local vorticity term. To derive a suitable pH formulation, the total energy, made up of kinetic and potential contribution, has to be invoked

$$H = \frac{1}{2}\int_\Omega \left\{ \rho h \|\boldsymbol{v}\|^2 + \rho g h^2 \right\} \, \mathrm{d}\Omega.$$

As energy variable the fluid height and the linear momentum are chosen

$$\alpha_h = h, \qquad \boldsymbol{\alpha}_v = \rho \boldsymbol{v}. \tag{3.34}$$

The Hamiltonian is a non separable functional of the energy variables

$$H(\alpha_h, \boldsymbol{\alpha}_v) = \frac{1}{2}\int_\Omega \left\{ \frac{1}{\rho}\alpha_h \left\|\boldsymbol{\alpha}_v\right\|^2 + \rho g \alpha_h^2 \right\} \, \mathrm{d}\Omega. \tag{3.35}$$

The co-energy variables are given by

$$e_h := \frac{\delta H}{\delta \alpha_h} = \frac{1}{2\rho}\left\|\boldsymbol{\alpha}_v\right\|^2 + \rho g \alpha_h, \qquad \boldsymbol{e}_v := \frac{\delta H}{\delta \boldsymbol{\alpha}_v} = \frac{1}{\rho}\alpha_h \boldsymbol{\alpha}_v. \tag{3.36}$$

The mass and momentum conservation are then rewritten as follows

$$\frac{\partial}{\partial t}\begin{pmatrix} \alpha_h \\ \boldsymbol{\alpha}_v \end{pmatrix} = \begin{bmatrix} 0 & -\operatorname{div} \\ -\operatorname{grad} & \boldsymbol{\mathcal{G}} \end{bmatrix} \begin{pmatrix} e_h \\ \boldsymbol{e}_v \end{pmatrix}, \tag{3.37}$$

The gyroscopic skew-symmetric term $\boldsymbol{\mathcal{G}}$ introduces a non-linearity as it depends on the energy variables

$$\boldsymbol{\mathcal{G}}(\alpha_h, \boldsymbol{\alpha}_v) = \frac{\omega}{\alpha_h}\begin{bmatrix} 0 & -1 \\ 1 & 0 \end{bmatrix}, \qquad \omega = \partial_x \alpha_{v,y} - \partial_y \alpha_{v,x}.$$

Despite the non-standard formulation, the energy rate provides anyway the boundary variables

$$\begin{aligned}
\dot{H} &= + \int_\Omega \left\{ e_h \, \partial_t \alpha_h + \boldsymbol{e}_v \cdot \partial_t \boldsymbol{\alpha}_v \right\} \, \mathrm{d}\Omega, \\
&= - \int_\Omega \left\{ e_h \, \operatorname{div} \boldsymbol{e}_v + \boldsymbol{e}_v \cdot (\operatorname{grad} e_h - \mathcal{G}\boldsymbol{e}_v) \right\} \, \mathrm{d}\Omega, && \text{skew-symmetry of } \mathcal{G}, \\
&= - \int_\Omega \left\{ e_h \, \operatorname{div} \boldsymbol{e}_v + \boldsymbol{e}_v \cdot \operatorname{grad} e_h \right\} \, \mathrm{d}\Omega, && \text{Chain rule,} \\
&= - \int_\Omega \operatorname{div}(e_h \, \boldsymbol{e}_v) \, \mathrm{d}\Omega, && \text{Stokes theorem,} \\
&= - \int_{\partial\Omega} e_h \, \boldsymbol{e}_v \cdot \boldsymbol{n} \, \mathrm{d}S = - \left\langle e_h, \, \boldsymbol{e}_v \cdot \boldsymbol{n} \right\rangle_{\partial\Omega}.
\end{aligned} \tag{3.38}$$

Again two possible cases of uniform boundary causality arise:

- First case $u_\partial = e_h, \quad y_\partial = \boldsymbol{e}_v \cdot \boldsymbol{n}$.
  This imposes the variable $e_h := h$ as boundary input and corresponds to a given water level for a fluid boundary.

- Second case $u_\partial = \boldsymbol{e}_v \cdot \boldsymbol{n}, \quad y_\partial = e_p$.
  This imposes the variable $\boldsymbol{e}_v \cdot \boldsymbol{n} := h\boldsymbol{v} \cdot \boldsymbol{n}$ as boundary input and corresponds to a given volumetric flow rate.

3.4 Conclusion

In this chapter, the main mathematical tools needed to understand infinite-dimensional pHs were recalled. A general characterization of the underlying operators behind a boundary control pH system is still an open topic. In Chapter 7, these operators are characterized, in connection to the discretization method developed.

Part II

Port-Hamiltonian elasticity and thermoelasticity

Chapter 4

Elasticity in port-Hamiltonian form

I try not to break the rules but merely to test their elasticity.

Bill Veeck

Contents

4.1 Continuum mechanics 25
4.1.1 Non linear formulation of elasticity 25
4.1.2 The linear elastodynamics problem 27
4.2 Port-Hamiltonian formulation of linear elasticity 29
4.2.1 Energy and co-energy variables 29
4.2.2 Final system and associated Stokes-Dirac structure 31
4.3 Conclusion 35

Continuum mechanics is the mathematical description of how materials behave kinematically under external excitations. In this framework, the microscopic structure of a material body is neglected and a macroscopic viewpoint, that describes the body as a continuum, is adopted. This leads to a PDE based model. In this chapter, the general linear elastodynamics problem is recalled. A suitable port-Hamiltonian formulation is then derived.

4.1 Continuum mechanics

In this section, the main concepts behind a deformable continuum are briefly recalled following [Lee12]. For a detailed discussion on this topic, the reader may consult [Abe12, LPKL12].

4.1.1 Non linear formulation of elasticity

The bounded region of $\mathbb{R}^d,\ d \in \{2, 3\}$ occupied by a solid is called configuration. The reference configuration Ω is the domain that a body occupies at the initial state. To describe how the

body deforms in time the deformation map $\mathbf{\Phi} : \Omega \times [0, T_f] \to \Omega' \subset \mathbb{R}^d$ is introduced. This map is differentiable and orientation preserving, and the image of Ω under $\mathbf{\Phi}(\cdot, t)$ $\forall t \in [0, T_f]$ is called the deformed configuration Ω_t. Given a specific point in the reference frame its image is denoted by $\boldsymbol{y} = \mathbf{\Phi}(\boldsymbol{x}, t)$. The gradient of the deformation map is called the deformation gradient $\boldsymbol{F} := \nabla_x \mathbf{\Phi} = \frac{\partial \boldsymbol{y}}{\partial \boldsymbol{x}}$. A rigid deformation maps a point $\boldsymbol{x} \in \Omega \to \boldsymbol{A}(t)\boldsymbol{x} + \boldsymbol{b}(t)$, where $\boldsymbol{A}(t)$ is an orthogonal matrix and $\boldsymbol{b}(t) \in \mathbb{R}^d$ a vector. A differentiable deformation map $\mathbf{\Phi}$ is a rigid deformation iff $\boldsymbol{F}^\top \boldsymbol{F} - \boldsymbol{I} = 0$, where $\boldsymbol{I}$ is the identity in $\mathbb{R}^{d \times d}$ (for the proof see [Cia88], page 44). For this reason, a suitable measure of the deformation is the Green-St.Venant strain tensor $\frac{1}{2}(\boldsymbol{F}^\top \boldsymbol{F} - \boldsymbol{I})$.
A quantity of interest is the displacement $\boldsymbol{u} : \Omega \times [0, T_f] \to \mathbb{R}^d$ with respect to the reference configuration. It is defined as $\boldsymbol{u}(\boldsymbol{x}, t) = \mathbf{\Phi}(\boldsymbol{x}, t) - \boldsymbol{x}$. The gradient of the displacement verifies $\nabla_x \boldsymbol{u} = \boldsymbol{F} - \boldsymbol{I}$. The strain tensor can now be written in terms of the displacement

$$\begin{aligned}
\frac{1}{2}(\boldsymbol{F}^\top \boldsymbol{F} - \boldsymbol{I}) &= \frac{1}{2}\left[(\nabla_x \boldsymbol{u} + \boldsymbol{I})^\top (\nabla_x \boldsymbol{u} + \boldsymbol{I}) - \boldsymbol{I}\right] \\
&= \frac{1}{2}\left[\nabla_x \boldsymbol{u} + (\nabla_x \boldsymbol{u})^\top + (\nabla_x \boldsymbol{u})^\top (\nabla_x \boldsymbol{u})\right],
\end{aligned}$$

or in components

$$\frac{1}{2}(F_{ik}^\top F_{kj} - I_{ij}) = \frac{1}{2}\left(\frac{\partial u_i}{\partial x_j} + \frac{\partial u_j}{\partial x_i} + \frac{\partial u_i}{\partial x_j}\frac{\partial u_j}{\partial x_i}\right).$$

To state the balance laws the actual deformed configuration is considered. The linear and angular momenta in a subdomain $\omega_t \subset \Omega_t$ are computed as

$$\int_{\omega_t} \rho\, \boldsymbol{v} \,\mathrm{d}\omega_t, \quad \text{and} \quad \int_{\omega_t} \rho\, \boldsymbol{y} \times \boldsymbol{v} \,\mathrm{d}\omega_t,$$

where ρ is the mass density and the velocity $\boldsymbol{v} = \frac{D\boldsymbol{u}}{Dt}(\boldsymbol{y}, t) = \frac{\partial \boldsymbol{u}}{\partial t}(\boldsymbol{x}, t)$ is the material time derivative of the displacement (see [Abe12, Chapter 1]). Let $\omega_{t,1}$, $\omega_{t,2}$ be two subregions in a deformed continuum Ω_t with contacting surface S_{12}. There is a force acting on this surface for a continuum that is called stress vector. If $\boldsymbol{n}$ is the outward normal at $\boldsymbol{y}$ on S_{12} with respect to $\omega_{t,1}$, then the surface force that $\omega_{t,1}$ exerts on $\omega_{t,2}$ is denoted by $\boldsymbol{t}(\boldsymbol{y}, \boldsymbol{n}) \in \mathbb{R}^d$. By the Newton third law, the surface force that $\omega_{t,2}$ applies on $\omega_{t,1}$ is given by $\boldsymbol{t}(\boldsymbol{y}, -\boldsymbol{n}) = -\boldsymbol{t}(\boldsymbol{y}, \boldsymbol{n})$. It is assumed that the linear and angular momentum balances hold for any subregion $\omega_t \in \Omega_t$

$$\begin{aligned}
\frac{d}{dt}\int_{\omega_t} \rho \boldsymbol{v} \,\mathrm{d}\omega_t &= \int_{\partial\omega_t} \boldsymbol{t}(\boldsymbol{y}, \boldsymbol{n}) \,\mathrm{d}S + \int_{\omega_t} \boldsymbol{f} \,\mathrm{d}\omega_t, \\
\frac{d}{dt}\int_{\omega_t} \rho \boldsymbol{y} \times \boldsymbol{v} \,\mathrm{d}\omega_t &= \int_{\partial\omega_t} \boldsymbol{y} \times \boldsymbol{t}(\boldsymbol{y}, \boldsymbol{n}) \,\mathrm{d}S + \int_{\omega_t} \boldsymbol{y} \times \boldsymbol{f} \,\mathrm{d}\omega_t,
\end{aligned}$$

where $\partial\omega_t$ stands for the boundary surface of the subdomain ω_t, $\boldsymbol{n}$ is the outward normal to the surface $\partial\omega_t$ and $\boldsymbol{f}$ represents an exterior body force. The following theorem characterizes the stress vector (see [Cia88, Chapter 2]):

Theorem 1 (Cauchy's theorem)

If the linear and angular momenta balances hold, then there exists a matrix-valued function $\boldsymbol{\Sigma}$ *from* Ω_t *to* $\mathbb{S}$ *such that* $\boldsymbol{t}(\boldsymbol{y},\boldsymbol{n}) = \boldsymbol{\Sigma}(\boldsymbol{y})\boldsymbol{n}$, $\forall \boldsymbol{y} \in \Omega_t$ *where the right-hand side is the matrix-vector multiplication.*

The set $\mathbb{S} = \mathbb{R}^{d\times d}_{\mathrm{sym}}$ denotes the field of symmetric matrices in $\mathbb{R}^{d\times d}$. The symmetry of the stress tensor $\boldsymbol{\Sigma}$ is due to the balance of angular momentum. The divergence theorem can then be applied

$$\int_{\partial\omega_t} \boldsymbol{\Sigma}\,\boldsymbol{n}\,\mathrm{d}S = \int_{\omega_t} \nabla_y \cdot \boldsymbol{\Sigma}\,\mathrm{d}\omega_t,$$

where $\nabla_y \cdot$ is the tensor divergence with respect to the deformed configuration, $\nabla_y \cdot \boldsymbol{\Sigma} = \sum_{i=1}^{d} \frac{\partial \Sigma_{ij}}{\partial y_i}$. Because the considered subregion ω_t is arbitrary, using the linear balance momentum and the conservation of mass, the following PDE is found

$$\rho \frac{D\boldsymbol{v}}{Dt} - \nabla_y \cdot \boldsymbol{\Sigma} = \boldsymbol{f}, \qquad \boldsymbol{y} \in \Omega_t.$$

This equation is written with respect to the deformed configuration Ω_t. For a detailed derivation of this equation the reader may consult [Abe12, Chapter 4]. To obtain a closed formulation, the constitutive law, namely the link between the stress tensor $\boldsymbol{\Sigma}$ and the strain tensor $\frac{1}{2}(\boldsymbol{F}^\top \boldsymbol{F} - \boldsymbol{I})$, has to be introduced. In the next section such relation will be discussed for the case of linear elasticity.

4.1.2 The linear elastodynamics problem

Whenever deformations are small, $\|\nabla_x \boldsymbol{u}\| \ll 1$, then the reference and deformed configurations are almost indistinguishable $\boldsymbol{y} = \boldsymbol{x} + \boldsymbol{u} = \boldsymbol{x} + O(\nabla_x \boldsymbol{u}) \approx \boldsymbol{x}$. This allows writing the linear momentum balance in the reference configuration

$$\rho \frac{\partial \boldsymbol{v}}{\partial t}(\boldsymbol{x},\boldsymbol{t}) - \operatorname{Div} \boldsymbol{\Sigma}(\boldsymbol{x},t) = \boldsymbol{f}, \qquad \boldsymbol{x} \in \Omega.$$

The material derivative simplifies to a partial one. The operator Div is the divergence of a tensor field with respect to the reference configuration (see Appendix A for a description of the differential operators)

$$\operatorname{Div} \boldsymbol{\Sigma}(\boldsymbol{x},t) = \nabla_x \cdot \boldsymbol{\Sigma}(\boldsymbol{x},t) = \left(\sum_{i=1}^{d} \frac{\partial \Sigma_{ij}}{\partial x_i} \right)_{1\le j\le d}.$$

Furthermore, the non-linear terms in the Green-St. Venant strain tensor can be dropped

$$\frac{1}{2}(\boldsymbol{F}^\top \boldsymbol{F} - \boldsymbol{I}) = \frac{1}{2}\left[\nabla_x \boldsymbol{u} + (\nabla_x \boldsymbol{u})^\top + (\nabla_x \boldsymbol{u})^\top (\nabla_x \boldsymbol{u})\right] \approx \frac{1}{2}\left[\nabla_x \boldsymbol{u} + (\nabla_x \boldsymbol{u})^\top\right].$$

The linearized strain tensor (also called infinitesimal strain tensor) is the symmetric gradient of the displacement

$$\boldsymbol{\varepsilon} := \operatorname{Grad} \boldsymbol{u}, \qquad \text{where} \qquad \operatorname{Grad} \boldsymbol{u} = \frac{1}{2}\left[\nabla_x \boldsymbol{u} + (\nabla_x \boldsymbol{u})^\top\right]. \tag{4.1}$$

To obtain a closed system of equations, it is now necessary to characterize the relation between stress and strain. This relation is normally called *constitutive law*. In the following, the particular case of elastic materials is considered. These materials are able to return back to their original size and shapes after forces are removed. For this class of materials, the stress tensor is solely determined from the deformed configuration at a given time (Hooke's law)

$$\boldsymbol{\Sigma}(\boldsymbol{x}) = \boldsymbol{\mathcal{D}}(\boldsymbol{x})\, \boldsymbol{\varepsilon}(\boldsymbol{u}(\boldsymbol{x})).$$

The *stiffness tensor* or *elasticity tensor* $\boldsymbol{\mathcal{D}} : \mathbb{S} \to \mathbb{S}$ is a rank 4 tensor that is symmetric positive definite and uniformly bounded above and below. Because of symmetry, its components satisfy

$$\mathcal{D}_{ijkl} = \mathcal{D}_{jikl} = \mathcal{D}_{klij}.$$

From the uniform boundedness of $\boldsymbol{\mathcal{D}}$, the map $\boldsymbol{\mathcal{D}} : L^2(\Omega, \mathbb{S}) \to L^2(\Omega, \mathbb{S})$ is a symmetric positive definite bounded linear operator ($L^2(\Omega, \mathbb{S})$ is the space of square integrable symmetric tensor-valued functions). The compliance tensor $\boldsymbol{\mathcal{C}}$ is defined by $\boldsymbol{\mathcal{C}} = \boldsymbol{\mathcal{D}}^{-1}$. Thus $\boldsymbol{\mathcal{C}} : \mathbb{S} \to \mathbb{S}$ is as well symmetric positive definite and uniformly bounded above and below. An isotropic elastic medium has the same kinematic properties in any direction and at each point. If an elastic medium is isotropic, then the stiffness and compliance tensors assume the form

$$\boldsymbol{\mathcal{D}}(\cdot) = 2\mu(\cdot) + \lambda \operatorname{Tr}(\cdot)\boldsymbol{I}, \qquad \boldsymbol{\mathcal{C}}(\cdot) = \frac{1}{2\mu}\left[(\cdot) - \frac{\lambda}{2\mu + d\lambda}\operatorname{Tr}(\cdot)\boldsymbol{I}\right], \qquad d = \{2, 3\}, \tag{4.2}$$

where Tr is the trace operator and the positive scalar functions μ, λ, defined on Ω, are called the Lamé coefficients. In engineering applications it is easier to compute experimentally two other parameters: the Young modulus E and Poisson's ratio ν. Those are expressed in terms of the Lamé coefficients as

$$\nu = \frac{\lambda}{2(\lambda + \mu)}, \qquad E = \frac{\mu(3\lambda + 2\mu)}{\lambda + \mu}, \tag{4.3}$$

and conversely

$$\lambda = \frac{E\nu}{(1+\nu)(1-2\nu)}, \qquad \mu = \frac{E}{2(1+\nu)}. \tag{4.4}$$

The stiffness and compliant tensor are expressed as

$$\boldsymbol{\mathcal{D}}(\cdot) = \frac{E}{1+\nu}\left[(\cdot) + \frac{\nu}{1-2\nu}\operatorname{Tr}(\cdot)\boldsymbol{I}\right], \tag{4.5}$$

$$\boldsymbol{\mathcal{C}}(\cdot) = \frac{1+\nu}{E}\left[(\cdot) - \frac{\nu}{1+\nu(d-2)}\operatorname{Tr}(\cdot)\boldsymbol{I}\right]. \tag{4.6}$$

The linear elastodynamics problem is formulated through a vector-valued PDE

$$\rho \frac{\partial^2 \boldsymbol{u}}{\partial t^2} - \mathrm{Div}(\boldsymbol{\mathcal{D}}\, \mathrm{Grad}\, \boldsymbol{u}) = \boldsymbol{f}. \tag{4.7}$$

The classical elastodynamics problem is expressed considering the displacement $\boldsymbol{u}$ as the unknown. This PDE goes together with appropriate boundary conditions that will be specified in 4.2.

4.2 Port-Hamiltonian formulation of linear elasticity

In this section a port-Hamiltonian formulation for elasticity is deduced from the classical elastodynamics problem. It must be highlighted that already in the seventies a purely hyperbolic formulation for elasticity was detailed [HM78]. The missing point is the clear connection with the theory of Hamiltonian PDEs. An Hamiltonian formulation can be found in [Gri15, Chapter 16], but without any connection to the concept of Stokes-Dirac structure induced by the underlying geometry.

4.2.1 Energy and co-energy variables

Consider an open connected set $\Omega \subset \mathbb{R}^d$, $d \in \{2, 3\}$. The displacement within a deformable continuum is given by Eq. (4.7).

$$\rho \frac{\partial^2 \boldsymbol{u}}{\partial t^2} - \mathrm{Div}(\boldsymbol{\mathcal{D}}\, \mathrm{Grad}\, \boldsymbol{u}) = 0, \qquad \boldsymbol{x} \in \Omega. \tag{4.8}$$

The contribution of the body force $\boldsymbol{f}$ has been removed for ease of presentation. To derive a pH formulation, the total energy, that includes the kinetic and deformation energy, is needed

$$H = \frac{1}{2} \int_\Omega \left\{ \rho \left\| \partial_t \boldsymbol{u} \right\|^2 + \boldsymbol{\Sigma} : \boldsymbol{\varepsilon} \right\} \, \mathrm{d}\Omega. \tag{4.9}$$

The notation $\boldsymbol{A} : \boldsymbol{B} = \mathrm{Tr}(\boldsymbol{A}^\top \boldsymbol{B}) = \sum_{i,j} A_{ij} B_{ij}$ denotes the tensor contraction. Recall that $\boldsymbol{\varepsilon} = \mathrm{Grad}\, \boldsymbol{u}$ and $\boldsymbol{\Sigma} = \boldsymbol{\mathcal{D}} \boldsymbol{\varepsilon}$. The energy variables are then the linear momentum and the deformation field

$$\boldsymbol{\alpha}_v = \rho \boldsymbol{v}, \qquad \boldsymbol{A}_\varepsilon = \boldsymbol{\varepsilon},$$

where $\boldsymbol{v} := \partial_t \boldsymbol{u}$. The Hamiltonian can be rewritten as a quadratic functional in the energy variables

$$H = \frac{1}{2} \int_\Omega \left\{ \frac{1}{\rho} \boldsymbol{\alpha}_v^2 + (\boldsymbol{\mathcal{D}} \boldsymbol{A}_\varepsilon) : \boldsymbol{A}_\varepsilon \right\} \, \mathrm{d}\Omega. \tag{4.10}$$

The co-energy variables are given by

$$\boldsymbol{e}_v := \frac{\delta H}{\delta \boldsymbol{\alpha}_v} = \boldsymbol{v}, \qquad \boldsymbol{E}_\varepsilon := \frac{\delta H}{\delta \boldsymbol{A}_\varepsilon} = \boldsymbol{\Sigma}. \tag{4.11}$$

The tensor-valued co-energy $\boldsymbol{E}_\varepsilon$ is obtained by taking the variational derivative with respect to a tensor.

Proposition 3
The variational derivative of the Hamiltonian with respect to the strain tensor is the stress tensor $\delta_{\boldsymbol{A}_\varepsilon} H = \boldsymbol{\Sigma}$.

Proof. Let $\mathbb{S} : \mathbb{R}^{d\times d}_{\text{sym}}$ be the space of symmetric tensor and $L^2(\Omega, \mathbb{S})$ the space of the square integrable symmetric tensors endowed with the tensor contraction as inner product

$$\langle \boldsymbol{A},\, \boldsymbol{B}\rangle_{L^2(\Omega,\mathbb{S})} = \int_\Omega \boldsymbol{A} : \boldsymbol{B} \,\mathrm{d}\Omega. \tag{4.12}$$

The contribution due to the deformation part in Hamiltonian is given by:

$$H_{\text{def}}(\boldsymbol{A}_\varepsilon) = \frac{1}{2}\int_\Omega (\boldsymbol{\mathcal{D}} \boldsymbol{A}_\varepsilon) : \boldsymbol{A}_\varepsilon \;\, \mathrm{d}\Omega.$$

A variation $\boldsymbol{\Delta A}_\varepsilon$ of the strain tensor with respect to a given value $\bar{\boldsymbol{A}}_\varepsilon$ leads to:

$$\begin{aligned} H_{\text{def}}(\bar{\boldsymbol{A}}_\varepsilon + \eta \boldsymbol{\Delta A}_\varepsilon) = &+ \frac{1}{2}\int_\Omega (\boldsymbol{\mathcal{D}} \bar{\boldsymbol{A}}_\varepsilon) : \bar{\boldsymbol{A}}_\varepsilon \;\, \mathrm{d}\Omega \\ &+ \eta \frac{1}{2}\int_\Omega \left\{ (\boldsymbol{\mathcal{D}} \bar{\boldsymbol{A}}_\varepsilon) : \boldsymbol{\Delta A}_\varepsilon + (\boldsymbol{\mathcal{D}} \boldsymbol{\Delta A}_\varepsilon) : \bar{\boldsymbol{A}}_\varepsilon \right\} \;\, \mathrm{d}\Omega + O(\eta^2). \end{aligned}$$

The term $(\boldsymbol{\mathcal{D}} \boldsymbol{\Delta A}_\varepsilon) : \bar{\boldsymbol{A}}_\varepsilon$ can be further rearranged using the symmetry of $\boldsymbol{\mathcal{D}}$ and the commutativity of the tensor contraction

$$(\boldsymbol{\mathcal{D}} \boldsymbol{\Delta A}_\varepsilon) : \bar{\boldsymbol{A}}_\varepsilon = (\boldsymbol{\mathcal{D}} \bar{\boldsymbol{A}}_\varepsilon) : \boldsymbol{\Delta A}_\varepsilon,$$

so that

$$H_{\text{def}}(\bar{\boldsymbol{A}}_\varepsilon + \eta \boldsymbol{\Delta A}_\varepsilon) = \frac{1}{2}\int_\Omega (\boldsymbol{\mathcal{D}} \bar{\boldsymbol{A}}_\varepsilon) : \bar{\boldsymbol{A}}_\varepsilon \;\, \mathrm{d}\Omega + \eta \int_\Omega (\boldsymbol{\mathcal{D}} \bar{\boldsymbol{A}}_\varepsilon) : \boldsymbol{\Delta A}_\varepsilon \;\, \mathrm{d}\Omega + O(\eta^2).$$

By definition of variational derivative it can be written:

$$H_{\text{def}}(\bar{\boldsymbol{A}}_\varepsilon + \eta \boldsymbol{\Delta A}_\varepsilon) = H_{\text{def}}(\bar{\boldsymbol{A}}_\varepsilon) + \eta \left\langle \frac{\delta H}{\delta \boldsymbol{A}_\varepsilon},\, \boldsymbol{\Delta A}_\varepsilon \right\rangle_{L^2(\Omega,\mathbb{S})} + O(\eta^2),$$

Then, by identification

$$\frac{\delta H_{\text{def}}}{\delta \boldsymbol{A}_\varepsilon} = \boldsymbol{\mathcal{D}} \bar{\boldsymbol{A}}_\varepsilon = \boldsymbol{\Sigma}.$$

Since the Hamiltonian is separable then $\delta_{\boldsymbol{A}_\varepsilon} H_{\text{def}} = \delta_{\boldsymbol{A}_\varepsilon} H$, leading to the final result. □

4.2.2 Final system and associated Stokes-Dirac structure

It is now possible to state the final pH form

$$\frac{\partial}{\partial t}\begin{pmatrix}\boldsymbol{\alpha}_v \\ \boldsymbol{A}_\varepsilon\end{pmatrix} = \begin{bmatrix}\mathbf{0} & \mathrm{Div} \\ \mathrm{Grad} & \mathbf{0}\end{bmatrix}\begin{pmatrix}\boldsymbol{e}_v \\ \boldsymbol{E}_\varepsilon\end{pmatrix}. \tag{4.13}$$

The first equation of the system is the conservation of linear momentum. The second represents a compatibility condition

$$\begin{aligned}\partial_t \boldsymbol{A}_\varepsilon &= \mathrm{Grad}(\boldsymbol{e}_v), \\ \partial_t \boldsymbol{\varepsilon} &= \mathrm{Grad}(\boldsymbol{v}), \\ \partial_t \,\mathrm{Grad}\,\boldsymbol{u} &= \mathrm{Grad}(\partial_t \boldsymbol{u}).\end{aligned} \tag{4.14}$$

Assuming that $\boldsymbol{u} \in C^2$, higher order derivatives commute (Clairaut's theorem). Hence, the equation is verified. The following theorem ensures the differential operator is formally skew-adjoint (one can also find this result in the recent article [PZ20, Lemma 3.3], available as arXiv preprint).

Theorem 2
The formal adjoint of the tensor divergence Div *is* $-$Grad*, the opposite of the symmetric gradient.*

Proof. We denote by $\mathbb{V} = \mathbb{R}^d$ the space of vector field in $\mathbb{R}^d$ and by $\mathbb{S} = \mathbb{R}^{d\times d}$ the space of symmetric tensor field in $\mathbb{R}^{d\times d}$. Let us consider the Hilbert space of the square integrable symmetric tensors $L^2(\Omega, \mathbb{S})$ with scalar product defined in (4.12). Moreover consider the Hilbert space of the square integrable vector function $L^2(\Omega, \mathbb{V})$, endowed with the usual scalar product

$$\langle \boldsymbol{a}, \boldsymbol{b}\rangle_{L^2(\Omega,\mathbb{V})} = \int_\Omega \boldsymbol{a}\cdot\boldsymbol{b} \;\, \mathrm{d}\Omega.$$

Let us consider the tensor divergence operator defined as:

$$\begin{aligned}\mathrm{Div}:\ L^2(\Omega,\mathbb{S}) &\to L^2(\Omega,\mathbb{V}), \\ \boldsymbol{\Psi} &\to \mathrm{Div}\,\boldsymbol{\Psi} = \boldsymbol{\psi},\end{aligned} \qquad \text{with } \psi_j = \mathrm{div}(\Psi_{ij}) = \sum_{i=1}^{d}\frac{\partial \Psi_{ij}}{\partial x_i}.$$

We try to identify Div^*

$$\begin{aligned}\mathrm{Div}^*:\ L^2(\Omega,\mathbb{V}) &\to L^2(\Omega,\mathbb{S}), \\ \boldsymbol{\phi} &\to \mathrm{Div}^*\boldsymbol{\phi} = \boldsymbol{\Phi},\end{aligned}$$

such that

$$\langle \mathrm{Div}\,\boldsymbol{\Psi},\, \boldsymbol{\phi}\rangle_{L^2(\Omega,\mathbb{V})} = \langle \boldsymbol{\Psi},\, \mathrm{Div}^*\boldsymbol{\phi}\rangle_{L^2(\Omega,\mathbb{S})}, \qquad \begin{aligned}&\forall \boldsymbol{\Psi} \in \mathrm{Dom}(\mathrm{Div}) \subset L^2(\Omega,\mathbb{S}), \\ &\forall \boldsymbol{\phi} \in \mathrm{Dom}(\mathrm{Div}^*) \subset L^2(\Omega,\mathbb{V}).\end{aligned}$$

Now let us take $\boldsymbol{\Psi} \in C_0^1(\Omega,\mathbb{S}) \subset \mathrm{Domain}(\mathrm{Div})$ the space of differentiable symmetric tensors with compact support in Ω. Additionally $\boldsymbol{\phi}$ will belong to $C_0^1(\Omega, \mathbb{V}) \subset \mathrm{Dom}(\mathrm{Div}^*)$, the space of differentiable vector functions with compact support in Ω. Then

$$\begin{aligned}
\langle \mathrm{Div}\, \boldsymbol{\Psi}, \boldsymbol{\phi} \rangle_{L^2(\Omega,\mathbb{V})} &= \int_\Omega \boldsymbol{\psi} \cdot \boldsymbol{\phi} \ \mathrm{d}\Omega, \\
&= \int_\Omega \sum_{i=1}^{d} \sum_{j=1}^{d} \frac{\partial \Psi_{ij}}{\partial x_i} \phi_j \ \mathrm{d}\Omega, \\
&= -\int_\Omega \sum_{i=1}^{d} \sum_{j=1}^{d} \Psi_{ij} \frac{\partial \phi_j}{\partial x_i} \ \mathrm{d}\Omega\,, && \text{since the functions vanish at the boundary,} \\
&= -\int_\Omega \sum_{i=1}^{d} \sum_{j=1}^{d} \Psi_{ij} F_{ij} \ \mathrm{d}\Omega, && \text{where} \qquad F_{ij} = \frac{\partial \phi_j}{\partial x_i}, \\
&= -\langle \boldsymbol{\Psi}, \boldsymbol{F} \rangle_{L^2(\Omega,\mathbb{S})}\,, && \boldsymbol{F} = \mathrm{grad}\, \boldsymbol{\phi}.
\end{aligned}$$

But in this latter case, it could not be stated that $\boldsymbol{F} \in L^2(\Omega, \mathbb{S})$. Now, since $\boldsymbol{\Psi} \in L^2(\Omega, \mathbb{S})$, $\Psi_{ji} = \Psi_{ij}$, thus the last equality can be further decomposed as

$$\sum_{i,j} \Psi_{ij} \frac{\partial \phi_j}{\partial x_i} = \sum_{i,j} \Psi_{ij} \frac{1}{2} \left(\frac{\partial \phi_i}{\partial x_j} + \frac{\partial \phi_j}{\partial x_i} \right) = \sum_{i,j} \Psi_{ij} \Phi_{ij}, \qquad \text{with } \Phi_{ij} := \frac{1}{2} \left(\frac{\partial \phi_i}{\partial x_j} + \frac{\partial \phi_j}{\partial x_i} \right).$$

Thus $\boldsymbol{\Phi} = \mathrm{Grad}\, \boldsymbol{\phi} \in L^2(\Omega, \mathbb{S})$ and it can be stated that:

$$\begin{aligned}
\langle \mathrm{Div}\, \boldsymbol{\Psi},\, \boldsymbol{\phi} \rangle_{L^2(\Omega,\mathbb{V})} &= -\int_\Omega \sum_{i,j} \Psi_{ij} \frac{1}{2} \left(\frac{\partial \phi_i}{\partial x_j} + \frac{\partial \phi_j}{\partial x_i} \right) \ \mathrm{d}\Omega \\
&= -\int_\Omega \sum_{i,j} \Psi_{ij} \Phi_{ij} \ \mathrm{d}\Omega = \langle \boldsymbol{\Psi},\, -\mathrm{Grad}\, \boldsymbol{\phi} \rangle_{L^2(\Omega,\mathbb{S})}\,.
\end{aligned}$$

It can be concluded that the formal adjoint of Div is $\mathrm{Div}^* = -\mathrm{Grad}$. □

The boundary values are then found by evaluating the energy rate

$$\begin{aligned}
\dot{H} &= \int_\Omega \{ \boldsymbol{e}_v \cdot \partial_t \boldsymbol{\alpha}_v + \boldsymbol{E}_\varepsilon : \partial_t \boldsymbol{A}_\varepsilon \} \ \mathrm{d}\Omega, \\
&= \int_\Omega \{ \boldsymbol{e}_v \cdot \mathrm{Div}\, \boldsymbol{E}_\varepsilon + \boldsymbol{E}_\varepsilon : \mathrm{Grad}\, \boldsymbol{e}_v \} \ \mathrm{d}\Omega, \\
&= \int_\Omega \mathrm{div}(\boldsymbol{E}_\varepsilon\, \boldsymbol{e}_v)\ \mathrm{d}\Omega, && \text{Stokes theorem (see Appendix A Eq. (A.6)),} \\
&= \int_{\partial\Omega} \boldsymbol{e}_v \cdot (\boldsymbol{E}_\varepsilon \boldsymbol{n})\ \mathrm{d}S = \langle \boldsymbol{e}_v,\, \boldsymbol{E}_\varepsilon\, \boldsymbol{n} \rangle_{L^2(\partial\Omega,\mathbb{R}^d)}\,.
\end{aligned} \tag{4.15}$$

The imposition of the velocity field along the boundary $\boldsymbol{e}_v = \partial_t \boldsymbol{u}$ corresponds to a Dirichlet condition. Setting $\boldsymbol{E}_\varepsilon\, \boldsymbol{n} = \boldsymbol{\Sigma}\, \boldsymbol{n} = \boldsymbol{t}$ (the traction) corresponds to a Neumann condition.

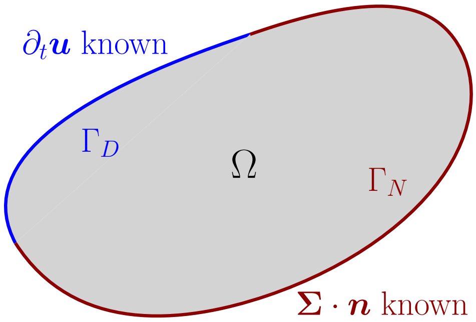

Figure 4.1: A 2D continuum with Neumann and Dirichlet boundary conditions

Consider a partition of the boundary $\partial\Omega = \overline{\Gamma}_N \cup \overline{\Gamma}_D$ and $\Gamma_N \cap \Gamma_D = \{\emptyset\}$, where a Dirichlet and a Neumann condition applies on the open subset Γ_D and Γ_N respectively (see Fig. 4.1). Then the final pH formulation reads

$$
\begin{aligned}
\frac{\partial}{\partial t}\begin{pmatrix}\boldsymbol{\alpha}_v \\ \boldsymbol{A}_\varepsilon\end{pmatrix} &= \underbrace{\begin{bmatrix}\mathbf{0} & \mathrm{Div} \\ \mathrm{Grad} & \mathbf{0}\end{bmatrix}}_{\mathcal{J}}\begin{pmatrix}\boldsymbol{e}_v \\ \boldsymbol{E}_\varepsilon\end{pmatrix}, \\
\boldsymbol{u}_\partial &= \underbrace{\begin{bmatrix}\gamma_0^{\Gamma_D} & \mathbf{0} \\ \mathbf{0} & \gamma_n^{\Gamma_N}\end{bmatrix}}_{\mathcal{B}_\partial}\begin{pmatrix}\boldsymbol{e}_v \\ \boldsymbol{E}_\varepsilon\end{pmatrix}, \\
\boldsymbol{y}_\partial &= \underbrace{\begin{bmatrix}\mathbf{0} & \gamma_n^{\Gamma_D} \\ \gamma_0^{\Gamma_N} & \mathbf{0}\end{bmatrix}}_{\mathcal{C}_\partial}\begin{pmatrix}\boldsymbol{e}_v \\ \boldsymbol{E}_\varepsilon\end{pmatrix},
\end{aligned}
\tag{4.16}
$$

where $\boldsymbol{\gamma}_0^{\Gamma_*}$ denotes the trace over the set Γ_*, namely $\boldsymbol{\gamma}_0^{\Gamma_*}\boldsymbol{e}_v = \boldsymbol{e}_v|_{\Gamma_*}$. Furthermore, $\boldsymbol{\gamma}_n^{\Gamma_*}$ denotes the normal trace over the set Γ_*, namely $\boldsymbol{\gamma}_n^{\Gamma_*}\boldsymbol{E}_\varepsilon = \boldsymbol{E}_\varepsilon\boldsymbol{n}|_{\Gamma_*}$.

Conjecture 1 (Stokes-Dirac structure for elastodynamics)
Let $H^{\mathrm{Grad}}(\Omega, \mathbb{V})$ denote the space of vectors with symmetric gradient in $L^2(\Omega, \mathbb{S})$ and $H^{\mathrm{Div}}(\Omega, \mathbb{S})$ be the space of symmetric tensors with divergence in $L^2(\Omega, \mathbb{V})$. Consider the following definitions

$$
\begin{aligned}
H &:= H^{\mathrm{Grad}}(\Omega, \mathbb{V}) \times H^{\mathrm{Div}}(\Omega, \mathbb{S}), \\
F &:= L^2(\Omega, \mathbb{V}) \times L^2(\Omega, \mathbb{S}), \\
F_\partial &:= L^2(\Gamma_D, \mathbb{V}) \times L^2(\Gamma_N, \mathbb{V}).
\end{aligned}
$$

The set

$$
D_{\mathcal{J}} = \left\{ \begin{pmatrix}\boldsymbol{f} \\ \boldsymbol{f}_\partial \\ \boldsymbol{e} \\ \boldsymbol{e}_\partial\end{pmatrix} \mid \boldsymbol{e} \in H, \; \boldsymbol{f} = \mathcal{J}\boldsymbol{e}, \; \boldsymbol{f}_\partial = \mathcal{B}_\partial\boldsymbol{e}, \; \boldsymbol{e}_\partial = -\mathcal{C}_\partial\boldsymbol{e} \right\}, \tag{4.17}
$$

where $\boldsymbol{e} = (\boldsymbol{e}_v, \boldsymbol{E}_\varepsilon)$ *and* $\mathcal{J}, \mathcal{B}_\partial, \mathcal{C}_\partial$ *are defined in* (4.16), *is a Stokes–Dirac structure with respect to the pairing*

$$\left\langle\left\langle (\boldsymbol{f}^1, \boldsymbol{f}_\partial^1, \boldsymbol{e}^1, \boldsymbol{e}_\partial^1), (\boldsymbol{f}^2, \boldsymbol{f}_\partial^2, \boldsymbol{e}^2, \boldsymbol{e}_\partial^2) \right\rangle\right\rangle := \left\langle \boldsymbol{e}^1, \boldsymbol{f}^2 \right\rangle_F + \left\langle \boldsymbol{e}^2, \boldsymbol{f}^1 \right\rangle_F + \left\langle \boldsymbol{e}_\partial^1, \boldsymbol{f}_\partial^2 \right\rangle_{F_\partial} + \left\langle \boldsymbol{e}_\partial^2, \boldsymbol{f}_\partial^1 \right\rangle_{F_\partial}, \tag{4.18}$$

where

$$\langle (\boldsymbol{a}, \boldsymbol{b}), (\boldsymbol{c}, \boldsymbol{d}) \rangle_{F_\partial} = \int_{\Gamma_D} \boldsymbol{a} \cdot \boldsymbol{c} \, \mathrm{d}S + \int_{\Gamma_N} \boldsymbol{b} \cdot \boldsymbol{d} \, \mathrm{d}S, \quad \boldsymbol{a}, \boldsymbol{b}, \boldsymbol{c}, \boldsymbol{d} \in \mathbb{V}.$$

Crucial points to obtain a rigorous proof *The crucial point that needs to be elucidated is where the boundary variables live. These variables belong to the fractional Sobolev spaces* $H^{\frac{1}{2}}(\partial\Omega, \mathbb{V})$, $H^{-\frac{1}{2}}(\partial\Omega, \mathbb{V})$ *linked by duality with respect to the pivot space* $L^2(\partial\Omega, \mathbb{V})$. *This is why a* L^2 *inner product has been assumed as boundary inner product.*
Furthermore, the partition of the boundary due to the non uniform boundary control complicates the proof, since one has to properly connect the two partitions at their interconnection.

Elements to support the conjecture *A Stokes-Dirac is characterized by the fact that* $D_\mathcal{J} = D_\mathcal{J}^\perp$. *Then one has to show that* $D_\mathcal{J} \subset D_\mathcal{J}^\perp$ *and* $D_\mathcal{J}^\perp \subset D_\mathcal{J}$. *The main steps of Theorem 3.6 in [LGZM05] are followed here to support the substantiation of the conjecture. The integration by parts formula is applied as in* (4.15).

Step 1. To show that $D_\mathcal{J} \subset D_\mathcal{J}^\perp$, *take* $(\boldsymbol{f}, \boldsymbol{f}_\partial, \boldsymbol{e}, \boldsymbol{e}_\partial) \in D_\mathcal{J}$. *Then*

$$\begin{aligned}
\langle\langle (\boldsymbol{f}, \boldsymbol{f}_\partial, \boldsymbol{e}, \boldsymbol{e}_\partial), (\boldsymbol{f}, \boldsymbol{f}_\partial, \boldsymbol{e}, \boldsymbol{e}_\partial) \rangle\rangle =& 2 \langle \boldsymbol{e}, \boldsymbol{f} \rangle_F + 2 \langle \boldsymbol{e}_\partial, \boldsymbol{f}_\partial \rangle_{F_\partial}, \\
=& 2 \langle \boldsymbol{e}, \mathcal{J} \boldsymbol{e} \rangle_F + 2 \langle \boldsymbol{e}_\partial, \boldsymbol{f}_\partial \rangle_{F_\partial}, \\
=& + 2 \int_\Omega \{ \boldsymbol{e}_v \cdot \mathrm{Div}\, \boldsymbol{E}_\varepsilon + \boldsymbol{E}_\varepsilon : \mathrm{Grad}\, \boldsymbol{e}_v \} \, \mathrm{d}\Omega \\
& - 2 \int_{\Gamma_D} \boldsymbol{e}_v \cdot (\boldsymbol{E}_\varepsilon \boldsymbol{n}) \, \mathrm{d}S - 2 \int_{\Gamma_N} \boldsymbol{e}_v \cdot (\boldsymbol{E}_\varepsilon \boldsymbol{n}) \, \mathrm{d}S, \\
=& + 2 \int_\Omega \{ \boldsymbol{e}_v \cdot \mathrm{Div}\, \boldsymbol{E}_\varepsilon + \boldsymbol{E}_\varepsilon : \mathrm{Grad}\, \boldsymbol{e}_v \} \, \mathrm{d}\Omega \\
& - 2 \int_{\partial\Omega} \boldsymbol{e}_v \cdot (\boldsymbol{E}_\varepsilon \boldsymbol{n}) \, \mathrm{d}S, = 0, \quad \textit{from } (4.15).
\end{aligned}$$

This implies $D_\mathcal{J} \subset D_\mathcal{J}^\perp$.

Step 2. Take $(\boldsymbol{\phi}, \boldsymbol{\phi}_\partial, \boldsymbol{\epsilon}, \boldsymbol{\epsilon}_\partial) \in D_\mathcal{J}^\perp$ *and* $\boldsymbol{e}_0 \in H$ *with compact support on* Ω. *This implies* $\mathcal{B}_\partial \boldsymbol{e}_0 = (\mathbf{0}, \mathbf{0})$ *and* $\mathcal{C}_\partial \boldsymbol{e}_0 = (\mathbf{0}, \mathbf{0})$. *Taking* $(\mathcal{J}\boldsymbol{e}_0, \mathbf{0}, \boldsymbol{e}_0, \mathbf{0}) \in D_\mathcal{J}$ *then*

$$\langle\langle (\boldsymbol{\phi}, \boldsymbol{\phi}_\partial, \boldsymbol{\epsilon}, \boldsymbol{\epsilon}_\partial), (\mathcal{J}\boldsymbol{e}_0, \mathbf{0}, \boldsymbol{e}_0, \mathbf{0}) \rangle\rangle = \langle \boldsymbol{\epsilon}, \mathcal{J}\boldsymbol{e}_0 \rangle_F + \langle \boldsymbol{e}_0, \boldsymbol{\phi} \rangle_F = 0, \quad \forall \boldsymbol{e}_0 \in H.$$

It follows that $\boldsymbol{\epsilon} \in H$ *and* $\boldsymbol{\phi} = \mathcal{J}\boldsymbol{\epsilon}$.

Step 3. Take $(\boldsymbol{\phi},\, \boldsymbol{\phi}_\partial,\, \boldsymbol{\epsilon},\, \boldsymbol{\epsilon}_\partial) \in D_{\mathcal{J}}^{\perp}$ *and* $(\boldsymbol{f},\, \boldsymbol{f}_\partial,\, \boldsymbol{e},\, \boldsymbol{e}_\partial) \in D_{\mathcal{J}}$*. Variables* $\boldsymbol{e}, \boldsymbol{\epsilon}$ *are indeed tuples containing a vector and a tensor, namely* $\boldsymbol{e} = (\boldsymbol{e}_v,\, \boldsymbol{E}_\varepsilon)$*,* $\boldsymbol{\epsilon} = (\boldsymbol{\epsilon}_v,\, \boldsymbol{\mathcal{E}}_\varepsilon)$*. From step 2 and* (4.18)

$$
\begin{aligned}
0 &= \langle \boldsymbol{e},\, \mathcal{J}\boldsymbol{\epsilon} \rangle_F + \langle \mathcal{J}\boldsymbol{e},\, \boldsymbol{\epsilon} \rangle_F + \langle \boldsymbol{e}_\partial,\, \boldsymbol{\phi}_\partial \rangle_{F_\partial} + \langle \boldsymbol{\epsilon}_\partial,\, \boldsymbol{f}_\partial \rangle_{F_\partial}\,, \\
&= \int_{\partial\Omega} \{\boldsymbol{e}_v \cdot (\boldsymbol{\mathcal{E}}_\varepsilon\, \boldsymbol{n}) + \boldsymbol{\epsilon}_v \cdot (\boldsymbol{E}_\varepsilon\, \boldsymbol{n})\} \; \mathrm{d}S + \langle -\mathcal{C}_\partial \boldsymbol{e},\, \boldsymbol{\phi}_\partial \rangle_{F_\partial} + \langle \boldsymbol{\epsilon}_\partial,\, \mathcal{B}_\partial \boldsymbol{e} \rangle_{F_\partial}
\end{aligned}
$$

Consider the splitting of the boundary $\partial\Omega = \overline{\Gamma}_N \cup \overline{\Gamma}_D$

$$
\begin{aligned}
\int_{\partial\Omega} \{\boldsymbol{e}_v \cdot (\boldsymbol{\mathcal{E}}_\varepsilon \cdot \boldsymbol{n}) + \boldsymbol{\epsilon}_v \cdot (\boldsymbol{E}_\varepsilon \cdot \boldsymbol{n})\} \; \mathrm{d}S = &+ \int_{\Gamma_N} \{\boldsymbol{e}_{\partial,2} \cdot (\boldsymbol{\mathcal{E}}_\varepsilon \cdot \boldsymbol{n}) + \boldsymbol{\epsilon}_v \cdot \boldsymbol{f}_{\partial,2}\} \; \mathrm{d}S, \\
&+ \int_{\Gamma_D} \{\boldsymbol{f}_{\partial,1} \cdot (\boldsymbol{\mathcal{E}}_\varepsilon \cdot \boldsymbol{n}) + \boldsymbol{\epsilon}_v \cdot \boldsymbol{e}_{\partial,1}\} \; \mathrm{d}S,
\end{aligned}
$$

where the elements of the vectors $\boldsymbol{f}_\partial = (\boldsymbol{f}_{\partial,1}, \boldsymbol{f}_{\partial,2})$*,* $\boldsymbol{e}_\partial = (\boldsymbol{e}_{\partial,1}, \boldsymbol{e}_{\partial,2})$ *have been considered. By expanding of the terms* $\langle \boldsymbol{e}_\partial,\, \boldsymbol{\phi}_\partial \rangle_{F_\partial} + \langle \boldsymbol{\epsilon}_\partial,\, \boldsymbol{f}_\partial \rangle_{F_\partial}$ *and given the fact that* $\boldsymbol{e}$ *is arbitrary then*

$$
\boldsymbol{\phi}_\partial = \begin{bmatrix} \gamma_0^{\Gamma_D} & \boldsymbol{0} \\ \boldsymbol{0} & \gamma_n^{\Gamma_N} \end{bmatrix} \begin{pmatrix} \boldsymbol{\epsilon}_v \\ \boldsymbol{\mathcal{E}}_\varepsilon \end{pmatrix}, \qquad \boldsymbol{\epsilon}_\partial = -\begin{bmatrix} \boldsymbol{0} & \gamma_n^{\Gamma_D} \\ \gamma_0^{\Gamma_N} & \boldsymbol{0} \end{bmatrix} \begin{pmatrix} \boldsymbol{\epsilon}_v \\ \boldsymbol{\mathcal{E}}_\varepsilon \end{pmatrix},
$$

meaning that $D_{\mathcal{J}}^{\perp} \subset D_{\mathcal{J}}$*.*

Linear elasticity falls within the assumption of [Skr19]. Therefore, it is a well posed boundary control pH system. A question that naturally arises is how to reformulate this system using the language of differential geometry. This is possible through the usage of vector-valued differential forms. The interested reader may consult [Bre08].

4.3 Conclusion

In this chapter, the pH formulation of elasticity has been obtained. This model represents a generalization of the wave equation to higher dimensional variables. This leads to the introduction of symmetric tensorial quantities describing the state of stress and deformation within the body.

For a plane continuum with moderate thickness, it is possible to reduce the general three-dimensional mode to two uncoupled systems: one representing the in-plane behavior ruled by 2D elasticity and one representing the out-of-plane deflection. This will be the object of the next chapter dedicated to the study of a pH formulation of plate bending. It is important to remember that plate models are just particular cases of three-dimensional elasticity.

CHAPTER 5

Port-Hamiltonian plate theory

You get tragedy where the tree, instead of bending, breaks.

Culture and Value
Ludwig Wittgenstein

Contents

5.1 First order plate theory **38**
5.1.1 Mindlin-Reissner model 39
5.1.2 Kirchhoff-Love model 40
5.2 Port-Hamiltonian formulation of isotropic plates **42**
5.2.1 Port-Hamiltonian Mindlin plate 43
5.2.2 Port-Hamiltonian Kirchhoff plate 47
5.3 Laminated anisotropic plates **52**
5.3.1 Port-Hamiltonian laminated Mindlin plate 54
5.3.2 Port-Hamiltonian laminated Kirchhoff plate 55
5.4 Conclusion **56**

Plates are plane structural elements with a small thickness compared to the planar dimensions. Thanks to this feature, it is not necessary to model plate structures using three-dimensional elasticity. Dimensional reduction strategies are employed to describe plate structures as two-dimensional problems. These strategies rely on an educated guess of the displacement field. For beams and plates this field is expressed in terms of unknown functions $\phi_i^j(x, y, t)$ that solely depends on the midplane coordinates (x, y)

$$u_i(x, y, z, t) = \sum_{j=0}^{m} (z)^j \phi_i^j(x, y, t).$$

where u_i, $i = \{x, y, z\}$ are the components of the displacement field. A first-order approximation is commonly used, meaning that a linear dependence on z is considered. Two main models arise from such a framework:

- the Mindlin-Reissner model for thick plates;

- the Kirchhoff-Love model for thin plates.

In this chapter it is shown how to formulate first-order plate models as pHs.

5.1 First order plate theory

As previously stated, first order theories assume a linear dependence on the vertical coordinate (cf. [Red06])

$$u_i(x, y, z, t) = \phi_i^0(x, y, t) + z\phi_i^1(x, y, t).$$

This hypothesis implies that the fibers, i.e. segments perpendicular to the mid-plane before deformation, remain straight after deformation. Additionally, for plate with moderate thickness the fibers are considered inextensible, meaning that $\phi_z^1 = 0$. These assumptions lead to the following displacement field

$$\begin{aligned} u_x(x, y, z, t) &= u_x^0(x, y, t) - z\theta_x(x, y, t), \\ u_y(x, y, z, t) &= u_y^0(x, y, t) - z\theta_y(x, y, t), \\ u_z(x, y, z, t) &= u_z^0(x, y, t), \end{aligned} \tag{5.1}$$

where $u_i^0(x, y, t) = \phi_i^0(x, y, t)$, $\theta_i(x, y, t) = -\phi_i^1(x, y, t)$. Assuming a linear elastic behavior, the 3D strain tensors for such a displacement field takes the form

$$\varepsilon_{\alpha\beta} = \frac{1}{2}\left(\partial_\beta u_\alpha + \partial_\alpha u_\beta\right) - z\frac{1}{2}\left(\partial_\beta \theta_\alpha + \partial_\alpha \theta_\beta\right) = \varepsilon_{\alpha\beta}^0 - z\kappa_{\alpha\beta}, \tag{5.2}$$

$$\varepsilon_{\alpha z} = \frac{1}{2}\left(\partial_a u_z - \theta_\alpha\right) = \frac{1}{2}\gamma_\alpha, \tag{5.3}$$

where $\alpha = \{x, y\}$, $\beta = \{x, y\}$. The tensors $\boldsymbol{\varepsilon}^0$, $\boldsymbol{\kappa}$, $\boldsymbol{\gamma}$ are called membrane, bending (or curvature) and shear strain tensor

$$\boldsymbol{\varepsilon}^0 = \operatorname{Grad} \boldsymbol{u}^0, \tag{5.4}$$

$$\boldsymbol{\kappa} = \operatorname{Grad} \boldsymbol{\theta}, \tag{5.5}$$

$$\boldsymbol{\gamma} = \operatorname{grad} u_z - \boldsymbol{\theta}. \tag{5.6}$$

where $\boldsymbol{u}^0 = (u_x, u_y)^\top$, $\boldsymbol{\theta} = (\theta_x, \theta_y)^\top$. For now, it is assumed that the material is isotropic, linear elastic (in Section §5.3 this hypothesis is removed). Recall the Hooke's law for 3D continua (see Eq. (4.5))

$$\boldsymbol{\Sigma} = \frac{E}{1+\nu}\left[\boldsymbol{\varepsilon} + \frac{\nu}{1-2\nu}\operatorname{Tr}(\boldsymbol{\varepsilon})\boldsymbol{I}_{3\times 3}\right].$$

where E, ν are the Young modulus and Poisson ratio. The hypothesis of inextensible fibers implies $\varepsilon_{zz} = 0$. However, imposing a plane strain condition provides a model that is too stiff. Rather than a plain strain assumption, a plain stress hypothesis is used to derive the constitutive law for plates. The displacement field (5.1) is left unchanged, but, instead of ε_{zz},

Σ_{zz} is set to zero. If $\Sigma_{zz} = 0$, one gets

$$\varepsilon_{zz} = -\frac{\nu}{1-\nu}(\varepsilon_{xx} + \varepsilon_{yy}).$$

Consequently, it is computed

$$\mathrm{Tr}(\boldsymbol{\varepsilon}) = \frac{1-2\nu}{1-\nu}(\varepsilon_{xx} + \varepsilon_{yy}).$$

The constitutive law for the in-plane stress takes the form

$$\boldsymbol{\Sigma}_{2D} = \boldsymbol{\mathcal{D}}_{2D}\,\boldsymbol{\varepsilon}_{2D},$$

where $\boldsymbol{\Sigma}_{2D} = \Sigma_{\alpha\beta}$, $\boldsymbol{\varepsilon}_{2D} = \varepsilon_{\alpha\beta}$ and

$$\boldsymbol{\mathcal{D}}_{2D} = \frac{E}{1-\nu^2}\left[(1-\nu)(\cdot) + \nu\,\mathrm{Tr}(\cdot)\boldsymbol{I}_{2\times 2}\right]. \tag{5.7}$$

Concerning the shear deformation, the constitutive law reduces to

$$\boldsymbol{\sigma}_s = G\boldsymbol{\gamma}, \tag{5.8}$$

where $\boldsymbol{\sigma}_s := \boldsymbol{\Sigma}_{\alpha,3}$ and $G = \frac{E}{2(1+\nu)}$ is the shear modulus. In the following sections, the most common plate models will be presented.

5.1.1 Mindlin-Reissner model

The Mindlin-Reissner model [Rei47, Min51] represents a first-order shear deformation theory for describing the bending of plate. The in-plane midplane displacement are zero $\boldsymbol{u}^0(x,y) = \mathbf{0}$ for an isotropic plate that experiences only bending. Hence, the displacement field reduces to

$$\begin{aligned} u_x(x,y,z) &= -z\partial_x\theta_x, \\ u_y(x,y,z) &= -z\partial_y\theta_y, \\ u_z(x,y,z) &= u_z^0(x,y). \end{aligned} \tag{5.9}$$

In pure bending, the strain tensor is given by

$$\boldsymbol{\varepsilon}_b := \boldsymbol{\varepsilon}_{2D}(\boldsymbol{u}^0 = \mathbf{0}) = -z\boldsymbol{\kappa},$$

with $\boldsymbol{\kappa}$ given by (5.5). Consequently, the stress tensor reads

$$\boldsymbol{\Sigma}_b := \boldsymbol{\Sigma}_{2D}(\boldsymbol{u}^0 = \mathbf{0}) = -z\boldsymbol{\mathcal{D}}_{2D}\boldsymbol{\kappa},$$

where $\boldsymbol{\mathcal{D}}_{2D}$ is defined in Eq. (5.7).

The undeformed middle plane of the plate is denoted by Ω. The total domain of the plate is the product $\Omega \times (-h/2, h/2)$, where h is the constant thickness. To effectively reduce the problem from three- to two-dimensional, the stresses have to be integrated along the fibers. Since the stress varies linearly across the thickness, the stress has to be multiplied by z before the integration to get a non null contribution. The resulting quantity is called bending momenta tensor and is given by

$$\boldsymbol{M} := -\int_{-h/2}^{h/2} z\boldsymbol{\Sigma}_b \, \mathrm{d}z = \boldsymbol{\mathcal{D}}_b \, \boldsymbol{\kappa}, \tag{5.10}$$

where

$$\boldsymbol{\mathcal{D}}_b = D_b \left[(1-\nu)(\cdot) + \nu \operatorname{Tr}(\cdot)\boldsymbol{I}_{2\times 2}\right], \qquad \text{where} \qquad D_b = \frac{Eh^3}{12(1-\nu^2)}. \tag{5.11}$$

The shear stress has to be integrated along the fibers as well. Given the excessive rigidity of the shear contribution, a correction factor $K_{\mathrm{sh}} = 5/6$ [Red06, Chapter 10] is introduced

$$\boldsymbol{q} = \int_{-h/2}^{h/2} K_{\mathrm{sh}} \boldsymbol{\sigma}_{\boldsymbol{s}} = K_{\mathrm{sh}} G h \boldsymbol{\gamma}, \tag{5.12}$$

where $\boldsymbol{\gamma}$ is defined in Eq. (5.6). The equations of motion can be obtained using Hamilton's principle. It consists in minimizing the total Lagrangian, given by $L = E_{\mathrm{def}} - E_{\mathrm{kin}}$, where E_{def} and E_{kin} are the deformation and kinetic energies

$$E_{\mathrm{def}} = \frac{1}{2}\int_\Omega \int_{-h/2}^{h/2} \boldsymbol{\Sigma} : \boldsymbol{\varepsilon} \, \mathrm{d}\Omega \, \mathrm{d}z = \frac{1}{2}\int_\Omega \left\{ \boldsymbol{M} : \boldsymbol{\kappa} + \boldsymbol{q} \cdot \boldsymbol{\gamma} \right\} \, \mathrm{d}\Omega, \tag{5.13}$$

$$E_{\mathrm{kin}} = \frac{1}{2}\int_\Omega \int_{-h/2}^{h/2} \rho \, \|\partial_t \boldsymbol{u}\|^2 \, \mathrm{d}\Omega \, \mathrm{d}z = \frac{1}{2}\int_\Omega \left\{ \frac{\rho h^3}{12} \|\partial_t \boldsymbol{\theta}\|^2 + \rho h (\partial_t u_z)^2 \right\} \, \mathrm{d}\Omega, \tag{5.14}$$

where ρ is the mass density. The Hamilton principle states that

$$\int_0^T \delta L \, \mathrm{d}t = \int_0^T \left\{ \delta E_{\mathrm{def}} - \delta E_{\mathrm{kin}} \right\} \, \mathrm{d}t = 0.$$

The final result is the following system of PDEs (for the detailed computations see [Red06, Chapter 10])

$$\begin{aligned} \rho h \frac{\partial^2 u_z}{\partial t^2} &= \operatorname{div} \boldsymbol{q}, \qquad (x, y) \in \Omega, \\ \frac{\rho h^3}{12} \frac{\partial^2 \boldsymbol{\theta}}{\partial t^2} &= \operatorname{Div} \boldsymbol{M} + \boldsymbol{q}, \end{aligned} \tag{5.15}$$

with $\boldsymbol{M} = \boldsymbol{\mathcal{D}}_b \operatorname{Grad} \boldsymbol{\theta}$ and $\boldsymbol{q} = K_{\mathrm{sh}} G h \, (\operatorname{grad} u_z - \boldsymbol{\theta})$. This PDE goes together with specified boundary conditions. Those will be detailed in 5.2.1.

5.1.2 Kirchhoff-Love model

The Kirchhoff model was formulated around 1850 and it is referred to as classical plate theory. The hypotheses on the displacement field consist of the following three points (see Fig. 5.1):

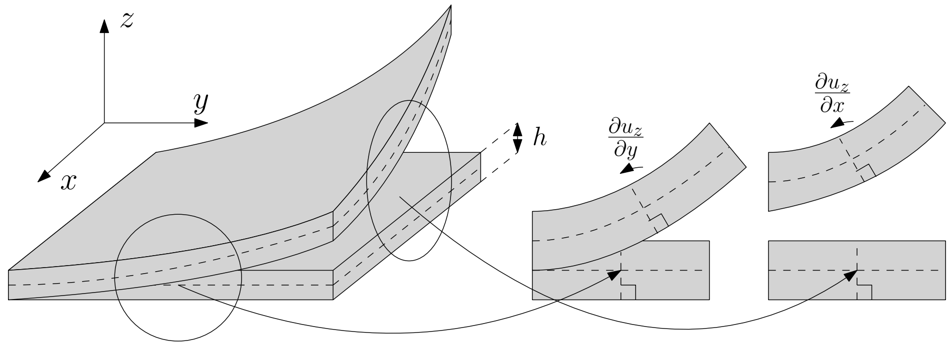

Figure 5.1: Kinematic assumption for the Kirchhoff plate

1. The fibers, segments perpendicular to the mid-plane before deformation, remain straight after deformation.

2. The fibers are inextensible.

3. While rotating, fibers remain perpendicular to the middle surface after deformation.

While the first two points are valid also for the Mindlin plate, the third assumption is specific to the Kirchhoff-Love model. Such an approximation is valid for plates having span-to-thickness ratio of the order of $L/h \approx 100-1000$ and implies zero transverse shear deformation

$$\boldsymbol{\gamma} = 0 \implies \varepsilon_{xz} = -\theta_x + \frac{\partial u_z}{\partial x} = 0, \qquad \varepsilon_{yz} = -\theta_y + \frac{\partial u_z}{\partial y} = 0.$$

The rotation vector is then related to the vertical displacement $\boldsymbol{\theta} = \mathrm{grad}\, u_z$. Plugging this into (5.5), it is found

$$\boldsymbol{\kappa} = \mathrm{Grad}\,\mathrm{grad}\, u_z = \mathrm{Hess}\, u_z. \tag{5.16}$$

Since the focus is on bending behavior, the in-plane displacement of the mid-plane are assumed to be zero $\boldsymbol{u}^0(x, y) = \boldsymbol{0}$. Hence, the displacement field assumes the form

$$\begin{aligned} u_x(x, y, z) &= -z\partial_x u_z, \\ u_y(x, y, z) &= -z\partial_y u_z, \\ u_z(x, y, z) &= u_z^0(x, y). \end{aligned} \tag{5.17}$$

For the Kirchhoff plate, the same link between the momenta and bending tensor holds

$$\boldsymbol{M} = \boldsymbol{\mathcal{D}}_b \boldsymbol{\kappa},$$

where $\boldsymbol{\mathcal{D}}_b$ and $\boldsymbol{\kappa}$ are given in (5.11), (5.16) respectively. The equations of motion can be obtained using Hamilton's principle [Red06, Chapter 2]. The deformation energy, kinetic energy and external work read

$$E_{\text{def}} = \frac{1}{2}\int_{\Omega}\int_{-h/2}^{h/2} \boldsymbol{\Sigma} : \boldsymbol{\varepsilon} \, \mathrm{d}\Omega \, \mathrm{d}z = \frac{1}{2}\int_{\Omega} \{\boldsymbol{M} : \boldsymbol{\kappa}\} \, \mathrm{d}\Omega, \tag{5.18}$$

$$E_{\text{kin}} = \frac{1}{2}\int_{\Omega}\int_{-h/2}^{h/2} \rho \, \|\partial_t \boldsymbol{u}\|^2 \, \mathrm{d}\Omega \, \mathrm{d}z \approx \frac{1}{2}\int_{\Omega} \rho h (\partial_t u_z)^2 \, \mathrm{d}\Omega. \tag{5.19}$$

Remark 4 (Rotational energy)
For the kinetic energy the rotational contribution

$$E_{rot} = \frac{1}{2}\int_{\Omega}\int_{-h/2}^{h/2} \left\{\rho \, (\partial_t u_x)^2 + (\partial_t u_y)^2\right\} \, \mathrm{d}\Omega \, \mathrm{d}z = \frac{h^3}{24}\int_{\Omega} \rho \left\{ (\partial_{tx} u_z)^2 + (\partial_{ty} u_z)^2 \right\} \, \mathrm{d}\Omega = O(h^3),$$

is neglected given the small thickness assumption.

The final result from the Hamilton's principle is the following PDE (for the detailed computations the reader may consult [Red06, Chapter 3])

$$\rho h \frac{\partial^2 u_z}{\partial t^2} = -\operatorname{div} \operatorname{Div}(\boldsymbol{\mathcal{D}}_b \operatorname{Grad} \operatorname{grad} u_z), \qquad (x, y) \in \Omega. \tag{5.20}$$

Developing the calculations, one obtains

$$\rho h \frac{\partial^2 u_z}{\partial t^2} = -D_b \Delta^2 u_z, \qquad (x, y) \in \Omega,$$

where $\Delta^2 = \frac{\partial^4}{\partial x^4} + 2\frac{\partial^2}{\partial x^2}\frac{\partial^2}{\partial y^2} + \frac{\partial^4}{\partial y^4}$ is the bi-Laplacian. Appropriate boundary conditions for this problem will be detailed in 5.2.2.

5.2 Port-Hamiltonian formulation of isotropic plates

In this section the pH formulation of the isotropic Mindlin and Kirchhoff plate models is detailed. In [MMB05], the Mindlin plate model was put in pH form by appropriate selection of the energy variables. However, the final system does not consider the nature of the different variables that come into play, leading to a non intrinsic final formulation. Additionally, this model was presented using the jet bundle formalism in [SS17]. The Kirchhoff model was never explored in the pH framework and represents an original contribution of this thesis. The interested reader can find in [RZ18] a rigorous mathematical treatment of the biharmonic problem and its decomposition in 2D geometries, but only for the static case (the 3D case, that does not relate to plate bending, is treated in [PZ18]).

5.2.1 Port-Hamiltonian Mindlin plate

Let $w := u_z$ denote the vertical displacement of the plate. Consider a bounded, connected domain $\Omega \subset \mathbb{R}^2$ and the Hamiltonian (total energy)

$$H = \frac{1}{2} \int_\Omega \left\{ \rho h \left(\frac{\partial w}{\partial t} \right)^2 + \frac{\rho h^3}{12} \left\| \frac{\partial \boldsymbol{\theta}}{\partial t} \right\|^2 + \boldsymbol{M} : \boldsymbol{\kappa} + \boldsymbol{q} \cdot \boldsymbol{\gamma} \right\} \mathrm{d}\Omega, \tag{5.21}$$

where $\boldsymbol{M}$, $\boldsymbol{\kappa}$, $\boldsymbol{q}$, $\boldsymbol{\gamma}$ are defined in Eqs. (5.10), (5.5), (5.12), (5.6) respectively. The choice of the energy variables is the same as in [MMB05] but here scalar-, vector- and tensor-valued variables are gathered together:

$$\begin{aligned}
\alpha_w &= \rho h \frac{\partial w}{\partial t}, && \text{Linear momentum}, & \boldsymbol{\alpha}_\theta &= \frac{\rho h^3}{12} \frac{\partial \boldsymbol{\theta}}{\partial t}, && \text{Angular momentum}, \\
\boldsymbol{A}_\kappa &= \boldsymbol{\kappa}, && \text{Curvature tensor}, & \boldsymbol{\alpha}_\gamma &= \boldsymbol{\gamma}. && \text{Shear deformation}.
\end{aligned} \tag{5.22}$$

The energy is now a quadratic function of the energy variables

$$H = \frac{1}{2} \int_\Omega \left\{ \frac{1}{\rho h} \alpha_w^2 + \frac{12}{\rho h^3} \left\| \boldsymbol{\alpha}_\theta \right\|^2 + (\boldsymbol{\mathcal{D}}_b \boldsymbol{A}_\kappa) : \boldsymbol{A}_\kappa + (\boldsymbol{\mathcal{D}}_s \boldsymbol{\alpha}_\gamma) \cdot \boldsymbol{\alpha}_\gamma \right\} \mathrm{d}\Omega, \tag{5.23}$$

where $\boldsymbol{\mathcal{D}}_s := G h K_{\mathrm{sh}} \boldsymbol{I}_{2\times 2}$, G is the shear modulus and K_{sh} the correction factor. The co-energy variables are found by computing the variational derivative of the Hamiltonian:

$$\begin{aligned}
e_w &:= \frac{\delta H}{\delta \alpha_w} = \frac{\partial w}{\partial t}, && \text{Linear velocity}, & \boldsymbol{e}_\theta &:= \frac{\delta H}{\delta \boldsymbol{\alpha}_\theta} = \frac{\partial \boldsymbol{\theta}}{\partial t}, && \text{Angular velocity}, \\
\boldsymbol{E}_\kappa &:= \frac{\delta H}{\delta \boldsymbol{A}_\kappa} = \boldsymbol{M}, && \text{Momenta tensor}, & \boldsymbol{e}_\gamma &:= \frac{\delta H}{\delta \boldsymbol{\alpha}_\gamma} = \boldsymbol{q} && \text{Shear stress}.
\end{aligned} \tag{5.24}$$

Proposition 4
The variational derivative of the Hamiltonian with respect to the curvature tensor is the momenta tensor $\frac{\delta H}{\delta \boldsymbol{A}_\kappa} = \boldsymbol{M}$.

Proof. The proof is analogous to the one already detailed in Prop. 3 □

Once the variables are concatenated together, the pH system is expressed as follows

$$\frac{\partial}{\partial t} \begin{pmatrix} \alpha_w \\ \boldsymbol{\alpha}_\theta \\ \boldsymbol{A}_\kappa \\ \boldsymbol{\alpha}_\gamma \end{pmatrix} = \begin{bmatrix} 0 & 0 & 0 & \mathrm{div} \\ \boldsymbol{0} & \boldsymbol{0} & \mathrm{Div} & \boldsymbol{I}_{2\times 2} \\ \boldsymbol{0} & \mathrm{Grad} & \boldsymbol{0} & \boldsymbol{0} \\ \mathrm{grad} & -\boldsymbol{I}_{2\times 2} & \boldsymbol{0} & \boldsymbol{0} \end{bmatrix} \begin{pmatrix} e_w \\ \boldsymbol{e}_\theta \\ \boldsymbol{E}_\kappa \\ \boldsymbol{e}_\gamma \end{pmatrix}. \tag{5.25}$$

The first two equations are equivalent to (5.15). The last two equations, like (4.14) for 3D elasticity, represent the fact that the higher order derivatives commute. We shall now establish the total energy balance in terms of boundary variables as they will be part of the

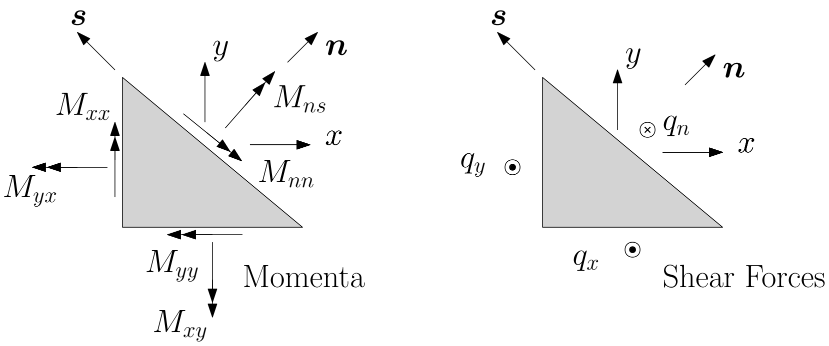

Figure 5.2: Cauchy law for momenta and forces at the boundary.

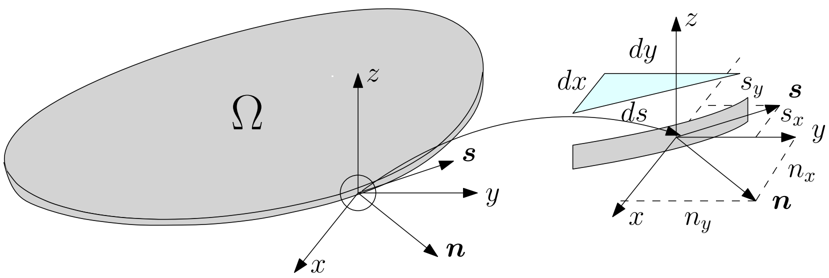

Figure 5.3: Reference frames and notations.

underlying Stokes-Dirac structure of this model. The energy rate reads

$$
\begin{aligned}
\dot{H} &= \int_\Omega \left\{ \frac{\partial \alpha_w}{\partial t} e_w + \frac{\partial \boldsymbol{\alpha}_\theta}{\partial t} \cdot \boldsymbol{e}_\theta + \frac{\partial \boldsymbol{A}_\kappa}{\partial t} : \boldsymbol{E}_\kappa + \frac{\partial \boldsymbol{\alpha}_\gamma}{\partial t} \cdot \boldsymbol{e}_\gamma \right\} \, \mathrm{d}\Omega \\
&= \int_\Omega \left\{ \mathrm{div}(\boldsymbol{e}_\gamma) e_w + \mathrm{Div}(\boldsymbol{E}_\kappa) \cdot \boldsymbol{e}_\theta + \ \mathrm{Grad}(\boldsymbol{e}_\theta) : \boldsymbol{E}_\kappa + \mathrm{grad}(e_w) \cdot \boldsymbol{e}_\gamma \right\} \, \mathrm{d}\Omega \qquad \text{Stokes theorem,} \\
&= \int_{\partial\Omega} \left\{ w_t \, q_n + \omega_n \, M_{nn} + \omega_s \, M_{ns} \right\} \, \mathrm{d}s,
\end{aligned}
\tag{5.26}
$$

where s is the curvilinear abscissa. The last integral is obtained by applying the Stokes theorem. The boundary variables appearing in the last line of (5.26) and illustrated in Fig. 5.2 are defined as follows:

$$
\begin{aligned}
\text{Shear force} \quad & q_n := \boldsymbol{q} \cdot \boldsymbol{n} = \boldsymbol{e}_\gamma \cdot \boldsymbol{n}, \\
\text{Flexural momentum} \quad & M_{nn} := \boldsymbol{M} : (\boldsymbol{n} \otimes \boldsymbol{n}) = \boldsymbol{E}_\kappa : (\boldsymbol{n} \otimes \boldsymbol{n}), \\
\text{Torsional momentum} \quad & M_{ns} := \boldsymbol{M} : (\boldsymbol{s} \otimes \boldsymbol{n}) = \boldsymbol{E}_\kappa : (\boldsymbol{s} \otimes \boldsymbol{n}),
\end{aligned}
\tag{5.27}
$$

Given two vectors $\boldsymbol{a} \in \mathbb{R}^n$, $\boldsymbol{b} \in \mathbb{R}^m$, the notation $\boldsymbol{a} \otimes \boldsymbol{b} = \boldsymbol{a}\boldsymbol{b}^\top \in \mathbb{R}^{n \times m}$ denotes the outer (or dyadic) product of two vectors. Vectors $\boldsymbol{n}$ and $\boldsymbol{s}$ designate the normal and tangential unit vectors to the boundary, as shown in Fig. 5.3. The corresponding power conjugated

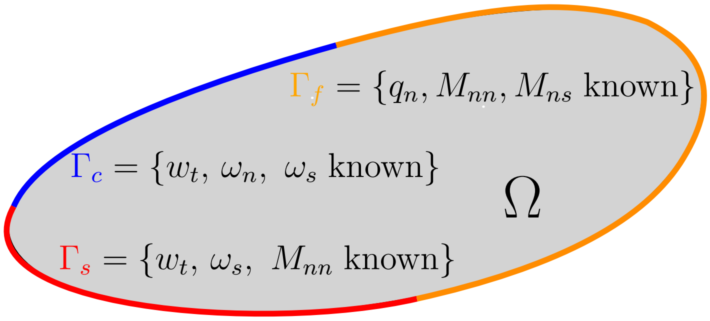

Figure 5.4: Boundary conditions for the Mindlin plate.

variables are

$$
\begin{aligned}
\text{Vertical velocity} \quad & w_t := \frac{\partial w}{\partial t} = e_w, \\
\text{Flexural rotation} \quad & \omega_n := \frac{\partial \boldsymbol{\theta}}{\partial t} \cdot \boldsymbol{n} = \boldsymbol{e}_\theta \cdot \boldsymbol{n}, \\
\text{Torsional rotation} \quad & \omega_s := \frac{\partial \boldsymbol{\theta}}{\partial t} \cdot \boldsymbol{s} = \boldsymbol{e}_\theta \cdot \boldsymbol{s}.
\end{aligned}
\tag{5.28}
$$

Consider a partition of the boundary $\partial\Omega = \overline{\Gamma}_C \cup \overline{\Gamma}_S \cup \overline{\Gamma}_F$, $\Gamma_C \cap \Gamma_S \cap \Gamma_F = \{\emptyset\}$. The open subset Γ_C, Γ_S, Γ_F could be empty. Given definitions (5.27), (5.28), the boundary conditions for the Mindlin plate [DHNLS99] (see Fig. 5.4) that are considered are:

- Clamped (C) on $\Gamma_C \subseteq \partial\Omega :\ w_t,\ \omega_n,\ \omega_s$ known;

- Simply supported hard (S) on $\Gamma_S \subseteq \partial\Omega$: $w_t,\ \omega_s,\ M_{nn}$ known;

- Free (F) on $\Gamma_F \subseteq \partial\Omega$: $M_{nn},\ M_{ns},\ q_n$ known.

Then the final pH formulation reads

$$
\begin{aligned}
\frac{\partial}{\partial t}\begin{pmatrix}\alpha_w\\ \boldsymbol{\alpha}_\theta\\ \boldsymbol{A}_\kappa\\ \boldsymbol{\alpha}_\gamma\end{pmatrix} &= \underbrace{\begin{bmatrix} 0 & 0 & 0 & \mathrm{div}\\ \mathbf{0} & \mathbf{0} & \mathrm{Div} & \boldsymbol{I}_{2\times 2}\\ \mathbf{0} & \mathrm{Grad} & \mathbf{0} & \mathbf{0}\\ \mathrm{grad} & -\boldsymbol{I}_{2\times 2} & \mathbf{0} & \mathbf{0}\end{bmatrix}}_{\mathcal{J}}\begin{pmatrix}e_w\\ \boldsymbol{e}_\theta\\ \boldsymbol{E}_\kappa\\ \boldsymbol{e}_\gamma\end{pmatrix},\\
\boldsymbol{u}_\partial &= \underbrace{\begin{bmatrix} \gamma_0^{\Gamma_C} & 0 & 0 & 0\\ 0 & \gamma_n^{\Gamma_C} & 0 & 0\\ 0 & \gamma_s^{\Gamma_C} & 0 & 0\\ \gamma_0^{\Gamma_S} & 0 & 0 & 0\\ 0 & \gamma_s^{\Gamma_S} & 0 & 0\\ 0 & 0 & \gamma_{nn}^{\Gamma_S} & 0\\ 0 & 0 & \gamma_{nn}^{\Gamma_F} & 0\\ 0 & 0 & \gamma_{ns}^{\Gamma_F} & 0\\ 0 & 0 & 0 & \gamma_n^{\Gamma_F}\end{bmatrix}}_{\mathcal{B}_\partial}\begin{pmatrix}e_w\\ \boldsymbol{e}_\theta\\ \boldsymbol{E}_\kappa\\ \boldsymbol{e}_\gamma\end{pmatrix},\\
\boldsymbol{y}_\partial &= \underbrace{\begin{bmatrix} 0 & 0 & 0 & \gamma_n^{\Gamma_C}\\ 0 & 0 & \gamma_{nn}^{\Gamma_C} & 0\\ 0 & 0 & \gamma_{ns}^{\Gamma_C} & 0\\ 0 & 0 & 0 & \gamma_n^{\Gamma_S}\\ 0 & 0 & \gamma_{ns}^{\Gamma_S} & 0\\ 0 & \gamma_n^{\Gamma_S} & 0 & 0\\ 0 & \gamma_n^{\Gamma_F} & 0 & 0\\ 0 & \gamma_s^{\Gamma_F} & 0 & 0\\ \gamma_0^{\Gamma_F} & 0 & 0 & 0\end{bmatrix}}_{\mathcal{C}_\partial}\begin{pmatrix}e_w\\ \boldsymbol{e}_\theta\\ \boldsymbol{E}_\kappa\\ \boldsymbol{e}_\gamma\end{pmatrix},
\end{aligned}
\tag{5.29}
$$

where $\gamma_0^{\Gamma_*}a = a|_{\Gamma_*}$ denotes the trace over the set Γ_*. Furthermore, notations $\gamma_n^{\Gamma_*}\boldsymbol{a} = \boldsymbol{a}\cdot\boldsymbol{n}|_{\Gamma_*}$, $\gamma_s^{\Gamma_*}\boldsymbol{a} = \boldsymbol{a}\cdot\boldsymbol{s}|_{\Gamma_*}$ indicate respectively the normal and tangential traces over the set Γ_*. Symbols $\gamma_{nn}^{\Gamma_*}, \gamma_{ns}^{\Gamma_*}$ denote the normal-normal trace and the normal-tangential trace of tensor-valued functions and $\gamma_{nn}^{\Gamma_*}\boldsymbol{A} = \boldsymbol{A} : (\boldsymbol{n}\otimes\boldsymbol{n})|_{\Gamma_*}$, $\gamma_{ns}^{\Gamma_*}\boldsymbol{A} = \boldsymbol{A} : (\boldsymbol{n}\otimes\boldsymbol{s})|_{\Gamma_*}$.

Remark 5
It can be observed that the interconnection structure given by $\mathcal{J}$ in (5.29) mimics that of the Timoshenko beam [JZ12, Chapter 7].

Conjecture 2 (Stokes-Dirac structure for the Mindlin plate)
Consider $\mathbb{V} = \mathbb{R}^2$, $\mathbb{S} = \mathbb{R}^{2\times 2}_{sym}$ and let $H^1(\Omega)$ be the space of functions with gradient in $L^2(\Omega, \mathbb{V})$ and $H^{\mathrm{div}}(\Omega, \mathbb{V})$ the space of vector-valued functions with divergence in $L^2(\Omega)$. Furthermore, $H^1(\Omega, \mathbb{V})$ is the space of vectors with symmetric gradient in $L^2(\Omega, \mathbb{S})$ and $H^{\mathrm{Div}}(\Omega, \mathbb{S})$ denotes

the space of symmetric tensors with divergence in $L^2(\Omega, \mathbb{V})$. Consider the definitions

$$
\begin{aligned}
H &:= H^1(\Omega) \times H^{\mathrm{Grad}}(\Omega, \mathbb{V}) \times H^{\mathrm{Div}}(\Omega, \mathbb{S}) \times H^{\mathrm{div}}(\Omega, \mathbb{V}), \\
F &:= L^2(\Omega) \times L^2(\Omega, \mathbb{V}) \times L^2(\Omega, \mathbb{S}) \times L^2(\Omega, \mathbb{V}), \\
F_\partial &:= L^2(\Gamma_C, \mathbb{R}^3) \times L^2(\Gamma_S, \mathbb{R}^3) \times L^2(\Gamma_F, \mathbb{R}^3).
\end{aligned}
$$

The set

$$
D_{\mathcal{J}} = \left\{ \begin{pmatrix} \boldsymbol{f} \\ \boldsymbol{f}_\partial \\ \boldsymbol{e} \\ \boldsymbol{e}_\partial \end{pmatrix} \mid \boldsymbol{e} \in H, \ \boldsymbol{f} = \mathcal{J}\boldsymbol{e}, \ \boldsymbol{f}_\partial = \mathcal{B}_\partial \boldsymbol{e}, \ \boldsymbol{e}_\partial = -\mathcal{C}_\partial \boldsymbol{e} \right\}, \tag{5.30}
$$

where $\boldsymbol{e} = (e_w, \boldsymbol{e}_\theta, \boldsymbol{E}_\kappa, \boldsymbol{e}_\gamma)$ and $\mathcal{J}, \mathcal{B}_\partial, \mathcal{C}_\partial$ are defined in (5.29), is a Stokes–Dirac structure with respect to the pairing

$$
\left\langle\left\langle (\boldsymbol{f}^1, \boldsymbol{f}_\partial^1, \boldsymbol{e}^1, \boldsymbol{e}_\partial^1), (\boldsymbol{f}^2, \boldsymbol{f}_\partial^2, \boldsymbol{e}^2, \boldsymbol{e}_\partial^2) \right\rangle\right\rangle := \left\langle \boldsymbol{e}^1, \, \boldsymbol{f}^2 \right\rangle_F + \left\langle \boldsymbol{e}^2, \, \boldsymbol{f}^1 \right\rangle_F + \left\langle \boldsymbol{e}_\partial^1, \, \boldsymbol{f}_\partial^2 \right\rangle_{F_\partial} + \left\langle \boldsymbol{e}_\partial^2, \, \boldsymbol{f}_\partial^1 \right\rangle_{F_\partial}, \tag{5.31}
$$

where $\boldsymbol{e}_\partial^i = (\boldsymbol{e}_{\partial,1}^i, \ \boldsymbol{e}_{\partial,2}^i, \ \boldsymbol{e}_{\partial,3}^i)$, $\boldsymbol{f}_\partial^i = (\boldsymbol{f}_{\partial,1}^i, \ \boldsymbol{f}_{\partial,2}^i, \ \boldsymbol{f}_{\partial,3}^i)$ and

$$
\langle (\boldsymbol{a}, \, \boldsymbol{b}, \, \boldsymbol{c}), \, (\boldsymbol{d}, \, \boldsymbol{e}, \, \boldsymbol{f}) \rangle_{F_\partial} = \int_{\Gamma_C} \boldsymbol{a} \cdot \boldsymbol{d} \, \mathrm{d}S + \int_{\Gamma_S} \boldsymbol{b} \cdot \boldsymbol{e} \, \mathrm{d}S + \int_{\Gamma_F} \boldsymbol{c} \cdot \boldsymbol{f} \, \mathrm{d}S, \quad \boldsymbol{a}, \ \boldsymbol{b}, \ \boldsymbol{c}, \ \boldsymbol{d}, \ \boldsymbol{e}, \ \boldsymbol{f} \in \mathbb{R}^3.
$$

Crucial points and elements in favor of the conjecture *Analogously to what was stated in Conjecture 1, the boundary spaces have to properly defined. If the integration by parts is carried out as in Eq. (5.26), one can follow the same lines of Conjecture 1 to support the present Conjecture.*

The Mindlin plate falls within the assumption of [Skr19], hence it is a well posed boundary control pH systems.

5.2.2 Port-Hamiltonian Kirchhoff plate

Again the starting point is the Hamiltonian (total energy)

$$
H = \frac{1}{2} \int_\Omega \left\{ \rho h \left(\frac{\partial w}{\partial t} \right)^2 + \boldsymbol{M} : \boldsymbol{\kappa} \right\} \, \mathrm{d}\Omega, \tag{5.32}
$$

where $\boldsymbol{M}, \ \boldsymbol{\kappa}$ are defined in Eqs. (5.10), (5.16). For what concerns the choice of the energy variables, a scalar and a tensor variable are considered:

$$
\alpha_w = \rho h \frac{\partial w}{\partial t}, \quad \text{Linear momentum}, \qquad \boldsymbol{A}_\kappa = \boldsymbol{\kappa}, \quad \text{Curvature tensor}. \tag{5.33}
$$

The co-energy variables are found by computing the variational derivative of the Hamiltonian:

$$e_w := \frac{\delta H}{\delta \alpha_w} = \frac{\partial w}{\partial t}, \quad \text{Linear velocity}, \qquad \boldsymbol{E}_\kappa := \frac{\delta H}{\delta \boldsymbol{A}_\kappa} = \boldsymbol{M}, \quad \text{Curvature tensor}. \tag{5.34}$$

The port-Hamiltonian system is then written as

$$\frac{\partial}{\partial t}\begin{pmatrix} \alpha_w \\ \boldsymbol{A}_\kappa \end{pmatrix} = \begin{bmatrix} 0 & -\operatorname{div}\circ\operatorname{Div} \\ \operatorname{Grad}\circ\operatorname{grad} & \boldsymbol{0} \end{bmatrix}\begin{pmatrix} e_w \\ \boldsymbol{E}_\kappa \end{pmatrix}. \tag{5.35}$$

The first equation is equivalent to (5.20). The last equation represents the fact that higher order derivatives commute

$$\begin{aligned} \partial_t \boldsymbol{A}_\kappa &= \operatorname{Grad}\operatorname{grad} e_w, \\ \partial_t \boldsymbol{\kappa} &= \operatorname{Grad}\operatorname{grad} \partial_t w, \\ \partial_t \operatorname{Grad}\operatorname{grad} w &= \operatorname{Grad}\operatorname{grad} \partial_t w. \end{aligned}$$

The last equation holds for $w \in C^3(\Omega)$.

Theorem 3
The operator $\operatorname{Grad}\circ\operatorname{grad}$, *corresponding to the Hessian operator, is the adjoint of the double divergence* $\operatorname{div}\circ\operatorname{Div}$.

Proof. Let $\mathbb{S} = \mathbb{R}^{d\times d}_{\text{sym}}$ and consider the Hilbert space of the square integrable symmetric square tensors $L^2(\Omega, \mathbb{S})$ over an open connected set Ω (its inner product is defined in (4.12)). Consider the Hilbert space $L^2(\Omega)$ of scalar square integrable functions, endowed with the standard inner product. Consider the double divergence operator defined as:

$$\begin{aligned} \operatorname{div}\operatorname{Div}:\ L^2(\Omega,\mathbb{S}) &\to L^2(\Omega), \\ \boldsymbol{\Psi} &\to \operatorname{div}\operatorname{Div}\boldsymbol{\Psi} = \psi, \end{aligned} \qquad \text{with } \psi = \operatorname{div}\operatorname{Div}\boldsymbol{\Psi} = \sum_{i=1}^{d}\sum_{j=1}^{d}\frac{\partial^2 \boldsymbol{\Psi}_{ij}}{\partial x_i \partial x_j}.$$

We shall identify $\operatorname{div}\operatorname{Div}^*$

$$\begin{aligned} \operatorname{div}\operatorname{Div}^*:\ L^2(\Omega) &\to L^2(\Omega,\mathbb{S}), \\ f &\to \operatorname{div}\operatorname{Div}^* f = \boldsymbol{F}, \end{aligned}$$

such that

$$\langle \operatorname{div}\operatorname{Div}\boldsymbol{\Psi}, f\rangle_{L^2(\Omega)} = \langle \boldsymbol{\Psi}, \operatorname{div}\operatorname{Div}^* f\rangle_{L^2(\Omega,\mathbb{S})}, \qquad \begin{aligned} &\forall\, \boldsymbol{\Psi} \in \operatorname{Dom}(\operatorname{div}\operatorname{Div}) \subset L^2(\Omega,\mathbb{S}) \\ &\forall\, f \in \operatorname{Dom}(\operatorname{div}\operatorname{Div}^*) \subset L^2(\Omega) \end{aligned}$$

The function has to belong to the operator domain, so for instance $f \in C_0^2(\Omega) \in \operatorname{Dom}(\operatorname{div}\operatorname{Div}^*)$ the space of twice differentiable scalar functions with compact support and $\boldsymbol{\Psi}$ can be chosen in the set $C_0^2(\Omega, \mathbb{S}) \in \operatorname{Dom}(\operatorname{div}\operatorname{Div})$, the space of twice differentiable symmetric tensors with compact support on Ω. A classical result is the fact that the adjoint of the vector divergence is $\mathrm{div}^* = -\mathrm{grad}$ as stated in [KZ15]. By theorem 2, it holds $\mathrm{Div}^* = -\mathrm{Grad}$. Considering that $\mathrm{div}\,\mathrm{Div} = \mathrm{div} \circ \mathrm{Div}$ is the composition of two different operators and that the adjoint of a composed operator is the adjoint of each operator in reverse order, i.e. $(B \circ C)^* = C^* \circ B^*$, then it can be stated

$$(\mathrm{div} \circ \mathrm{Div})^* = \mathrm{Div}^* \circ \mathrm{div}^* = \mathrm{Grad} \circ \mathrm{grad}\,.$$

Since only formal adjoints are being looked for, this concludes the proof. $\square$

The energy rate provides the boundary port variables

$$\begin{aligned}
\dot{H} &= \int_\Omega \left\{\partial_t \alpha_w \, e_w + \partial_t \boldsymbol{A}_\kappa : \boldsymbol{E}_\kappa \right\} \,\mathrm{d}\Omega \\
&= \int_\Omega \left\{- \mathrm{div}\,\mathrm{Div}\, \boldsymbol{E}_\kappa \, e_w + \mathrm{Grad}\,\mathrm{grad}\, e_w : \boldsymbol{E}_\kappa \right\} \,\mathrm{d}\Omega, && \text{Stokes theorem} \\
&= \int_{\partial\Omega} \left\{-\boldsymbol{n} \cdot \mathrm{Div}\, \boldsymbol{E}_\kappa \, e_w + (\boldsymbol{n} \otimes \mathrm{grad}\, e_w) : \boldsymbol{E}_\kappa \right\} \,\mathrm{d}s, \\
&= \int_{\partial\Omega} \left\{-\boldsymbol{n} \cdot \mathrm{Div}\, \boldsymbol{E}_\kappa \, e_w + \partial_{\boldsymbol{n}} e_w \, (\boldsymbol{n} \otimes \boldsymbol{n}) : \boldsymbol{E}_\kappa + \partial_{\boldsymbol{s}} e_w \, (\boldsymbol{n} \otimes \boldsymbol{s}) : \boldsymbol{E}_\kappa \right\} \,\mathrm{d}s, && \text{Dyadic properties} \\
&= \int_{\partial\Omega} \left\{\widehat{q}_n \, w_t + \partial_{\boldsymbol{n}} w_t \, M_{nn} + \partial_{\boldsymbol{s}} w_t \, M_{ns} \right\} \,\mathrm{d}s.
\end{aligned} \tag{5.36}$$

where s is the curvilinear abscissa, $w_t := \partial_t w$ and $\partial_{\boldsymbol{s}} w_t$ denotes the directional derivative along the tangential versor at the boundary. Additionally, the following definitions have been introduced

$$\widehat{q}_n := -\boldsymbol{n} \cdot \mathrm{Div}(\boldsymbol{E}_\kappa), \quad M_{nn} := (\boldsymbol{n} \otimes \boldsymbol{n}) : \boldsymbol{E}_\kappa, \quad M_{ns} := (\boldsymbol{n} \otimes \boldsymbol{s}) : \boldsymbol{E}_\kappa. \tag{5.37}$$

Variables w_t and $\partial_{\boldsymbol{s}} w_t$ are not independent as they are differentially related with respect to derivation along $\boldsymbol{s}$ (see for instance [TWK59, Chapter 4]). The tangential derivative has to be moved on the torsional momentum M_{ns}. For sake of simplicity, $\partial\Omega$ is supposed to be regular. Then the integration by parts provides

$$\int_{\partial\Omega} \partial_{\boldsymbol{s}} w_t \, M_{ns} \,\mathrm{d}s = -\int_{\partial\Omega} \partial_{\boldsymbol{s}} M_{ns} \, w_t \,\mathrm{d}s. \tag{5.38}$$

The final energy balance reads

$$\dot{H} = \int_{\partial\Omega} \left\{ w_t \, \widetilde{q}_n + \partial_{\boldsymbol{n}} w_t \, M_{nn} \right\} \,\mathrm{d}s, \tag{5.39}$$

where the boundary variables are

$$\begin{aligned}
&\text{Effective shear force} && \widetilde{q}_n := \widehat{q}_n - \partial_{\boldsymbol{s}} M_{ns}, \\
&\text{Flexural momentum} && M_{nn} := \boldsymbol{M} : (\boldsymbol{n} \otimes \boldsymbol{n}) = \boldsymbol{E}_\kappa : (\boldsymbol{n} \otimes \boldsymbol{n}),
\end{aligned} \tag{5.40}$$

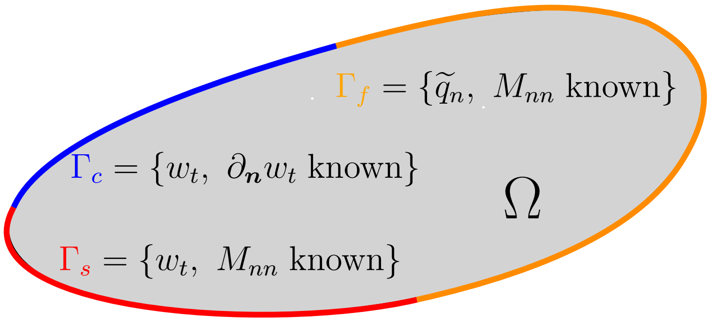

Figure 5.5: Boundary conditions for the Kirchhoff plate.

and $\widehat{q}_n$ is defined in (5.37). The corresponding power conjugated variables are:

$$\begin{aligned} &\text{Vertical velocity} \qquad w_t := \frac{\partial w}{\partial t} = e_w, \\ &\text{Flexural rotation} \quad \partial_{\boldsymbol{n}} w_t := \nabla e_w \cdot \boldsymbol{n}. \end{aligned}, \tag{5.41}$$

Consider a partition of the boundary $\partial\Omega = \overline{\Gamma}_C \cup \overline{\Gamma}_S \cup \overline{\Gamma}_F$, $\Gamma_C \cap \Gamma_S \cap \Gamma_F = \{\emptyset\}$, where $\Gamma_C, \Gamma_S, \Gamma_F$ are open subset of $\partial\Omega$. Given definitions (5.40), (5.41), the boundary conditions for the Kirchhoff plate [GSV18] are the following (see Fig. 5.5):

- Clamped (C) on $\Gamma_C \subseteq \partial\Omega :\ w_t,\ \partial_{\boldsymbol{n}} w_t$ known;

- Simply supported (S) on $\Gamma_S \subseteq \partial\Omega$: $w_t,\ M_{nn}$ known;

- Free (F) on $\Gamma_F \subseteq \partial\Omega$: $\widetilde{q}_n,\ M_{nn}$ known.

Then the final pH formulation reads

$$
\begin{aligned}
\frac{\partial}{\partial t}\begin{pmatrix}\alpha_w \\ \boldsymbol{A}_\kappa\end{pmatrix} &= \underbrace{\begin{bmatrix} 0 & -\operatorname{div}\circ\operatorname{Div} \\ \operatorname{Grad}\circ\operatorname{grad} & \boldsymbol{0}\end{bmatrix}}_{\mathcal{J}} \begin{pmatrix} e_w \\ \boldsymbol{E}_\kappa\end{pmatrix}, \\
\boldsymbol{u}_\partial &= \underbrace{\begin{bmatrix} \gamma_0^{\Gamma_C} & 0 \\ \gamma_1^{\Gamma_C} & 0 \\ \gamma_0^{\Gamma_S} & 0 \\ 0 & \gamma_{nn}^{\Gamma_S} \\ 0 & \gamma_{nn,1}^{\Gamma_F} \\ 0 & \gamma_{nn}^{\Gamma_F} \end{bmatrix}}_{\mathcal{B}_\partial} \begin{pmatrix} e_w \\ \boldsymbol{E}_\kappa\end{pmatrix}, \\
\boldsymbol{y}_\partial &= \underbrace{\begin{bmatrix} 0 & \gamma_{nn,1}^{\Gamma_C} \\ 0 & \gamma_{nn}^{\Gamma_C} \\ 0 & \gamma_{nn,1}^{\Gamma_S} \\ \gamma_1^{\Gamma_S} & 0 \\ \gamma_0^{\Gamma_F} & 0 \\ \gamma_1^{\Gamma_F} & 0 \end{bmatrix}}_{\mathcal{C}_\partial} \begin{pmatrix} e_w \\ \boldsymbol{E}_\kappa\end{pmatrix},
\end{aligned}
\tag{5.42}
$$

where $\gamma_0^{\Gamma_*} a = a|_{\Gamma_*}$ and $\gamma_1^{\Gamma_*} a = \partial_{\boldsymbol{n}} a|_{\Gamma_*}$ denote the standard and the normal derivative trace over the set Γ_* respectively. The symbol $\gamma_{nn,1}^{\Gamma_*}$ denotes the map $\gamma_{nn,1}^{\Gamma_*}\boldsymbol{A} = -\boldsymbol{n}\cdot\operatorname{Div}\boldsymbol{A} - \partial_{\boldsymbol{s}}(\boldsymbol{A} : (\boldsymbol{n}\otimes\boldsymbol{s}))|_{\Gamma_*}$,, while $\gamma_{nn}^{\Gamma_*}\boldsymbol{A} = \boldsymbol{A} : (\boldsymbol{n}\otimes\boldsymbol{n})|_{\Gamma_*}$ indicates the normal-normal trace of a tensor-valued function.

Remark 6
The interconnection structure $\mathcal{J}$ in (5.42) mimics that of the Bernoulli beam [CRMPB17]. The double divergence and the Hessian coincide, in dimension one, with the second derivative.

Conjecture 3 (Stokes-Dirac structure for the Kirchhoff plate)
Consider $\mathbb{S} = \mathbb{R}^{2\times 2}_{sym}$ and let $H^2(\Omega)$ be the space of functions with Hessian in $L^2(\Omega,\mathbb{S})$ and $H^{\operatorname{div}\operatorname{Div}}(\Omega,\mathbb{S})$ the space of vector-valued functions with double divergence in $L^2(\Omega)$. Consider the definitions

$$
\begin{aligned}
H &:= H^2(\Omega)\times H^{\operatorname{div}\operatorname{Div}}(\Omega,\mathbb{S}), \\
F &:= L^2(\Omega)\times L^2(\Omega,\mathbb{S}), \\
F_\partial &:= L^2(\Gamma_C,\mathbb{R}^2)\times L^2(\Gamma_S,\mathbb{R}^2)\times L^2(\Gamma_F,\mathbb{R}^2).
\end{aligned}
$$

The set

$$
D_{\mathcal{J}} = \left\{ \begin{pmatrix} \boldsymbol{f} \\ \boldsymbol{f}_\partial \\ \boldsymbol{e} \\ \boldsymbol{e}_\partial \end{pmatrix} \mid \boldsymbol{e}\in H,\ \boldsymbol{f} = \mathcal{J}\boldsymbol{e},\ \boldsymbol{f}_\partial = \mathcal{B}_\partial\boldsymbol{e},\ \boldsymbol{e}_\partial = -\mathcal{C}_\partial\boldsymbol{e} \right\}, \tag{5.43}
$$

where $\boldsymbol{e} = (e_w, \boldsymbol{E}_\kappa)$ and $\mathcal{J},\mathcal{B}_\partial,\mathcal{C}_\partial$ are defined in (5.42), is a Stokes–Dirac structure with

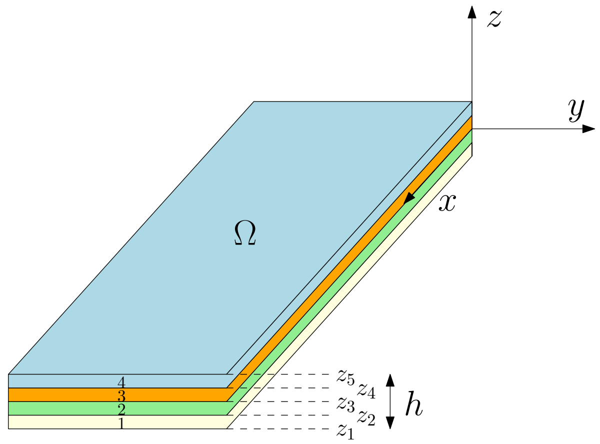

Figure 5.6: Laminated plate with 4 layers.

respect to the pairing

$$\left\langle\left\langle (\boldsymbol{f}^1, \boldsymbol{f}^1_\partial, \boldsymbol{e}^1, \boldsymbol{e}^1_\partial), (\boldsymbol{f}^2, \boldsymbol{f}^2_\partial, \boldsymbol{e}^2, \boldsymbol{e}^2_\partial) \right\rangle\right\rangle := \left\langle \boldsymbol{e}^1,\, \boldsymbol{f}^2 \right\rangle_F + \left\langle \boldsymbol{e}^2,\, \boldsymbol{f}^1 \right\rangle_F + \left\langle \boldsymbol{e}^1_\partial,\, \boldsymbol{f}^2_\partial \right\rangle_{F_\partial} + \left\langle \boldsymbol{e}^2_\partial,\, \boldsymbol{f}^1_\partial \right\rangle_{F_\partial}, \tag{5.44}$$

where $\boldsymbol{e}^i_\partial = (\boldsymbol{e}^i_{\partial,1},\ \boldsymbol{e}^i_{\partial,2})$, $\boldsymbol{f}^i_\partial = (\boldsymbol{f}^i_{\partial,1},\ \boldsymbol{f}^i_{\partial,2})$ *and*

$$\langle (\boldsymbol{a},\, \boldsymbol{b},\, \boldsymbol{c}),\, (\boldsymbol{d},\, \boldsymbol{e},\, \boldsymbol{f}) \rangle_{F_\partial} = \int_{\Gamma_C} \boldsymbol{a}\cdot\boldsymbol{d}\,\mathrm{d}S + \int_{\Gamma_S} \boldsymbol{b}\cdot\boldsymbol{e}\,\mathrm{d}S + \int_{\Gamma_F} \boldsymbol{c}\cdot\boldsymbol{f}\,\mathrm{d}S, \quad \boldsymbol{a},\ \boldsymbol{b},\ \boldsymbol{c},\ \boldsymbol{d},\ \boldsymbol{e},\ \boldsymbol{f} \in \mathbb{R}^2.$$

Validity of the conjecture *The integration by parts has to be carried as in Eq.* (5.36) *to retrieve a similar discussion to the one in Conjecture 1.*

5.3 Laminated anisotropic plates

Until now homogeneous isotropic materials have been considered. For this class of materials, the membrane and bending problems are decoupled. In aeronautical applications, structure are made up of laminae of different materials to enhance the mechanical properties of the resulting structure. In some cases, a certain coupling is desired, to increase the aerodynamical performance of the wing as it deforms.

Consider again the deformation field given by (5.1)

$$\begin{aligned} \boldsymbol{u}(x, y, z, t) &= \boldsymbol{u}^0(x, y, t) - z\boldsymbol{\theta}(x, y, t), \\ u_z(x, y, z, t) &= u_z^0(x, y, t), \end{aligned}$$

where $\boldsymbol{u} = (u_x,\, u_y)$. The link between in-plane deformation (5.2) and the membrane and bending contribution (5.4), (5.5).

$$\boldsymbol{\varepsilon}_{2D} = \boldsymbol{\varepsilon}^0 - z\boldsymbol{\kappa} \qquad \text{where} \qquad \boldsymbol{\varepsilon}^0 = \operatorname{Grad} \boldsymbol{u}^0, \quad \boldsymbol{\kappa} = \operatorname{Grad} \boldsymbol{\theta}. \tag{5.45}$$

Assume that each layer is an anisotropic material under plane stress condition. Then, it holds (see [Red03, Chapter 1] for details)

$$\boldsymbol{\Sigma}_{2D}^i = \boldsymbol{\mathcal{D}}_{2D}^i \boldsymbol{\varepsilon}_{2D}^i,$$

where i indicates the layer under consideration. The matrix $\boldsymbol{\mathcal{D}}_{2D}^i$ depends on the properties of each material. To reduce the problem to bi-dimensional, the stresses have to be integrated along the thickness. Consider the membrane and bending resultant of the stress

$$\boldsymbol{N} := \sum_{i=1}^{n_{\text{layer}}} \int_{z_i}^{z_{i+1}} \boldsymbol{\Sigma}_{2D}^i \, \mathrm{d}z, \qquad \boldsymbol{M} := \sum_{i=1}^{n_{\text{layer}}} \int_{z_i}^{z_{i+1}} -z\boldsymbol{\Sigma}_{2D}^i \, \mathrm{d}z. \tag{5.46}$$

where n_{layer} is the number of layers and z_i represents the height of the i^{th} layer (see Fig. 5.6) Since the stress are discontinuous due to the change of constitutive law along the thickness, the integration has to be performed lamina-wise. Once the computations are carried out, it is found

$$\begin{pmatrix} \boldsymbol{N} \\ \boldsymbol{M} \end{pmatrix} = \begin{bmatrix} \boldsymbol{\mathcal{D}}_m & \boldsymbol{\mathcal{D}}_c \\ \boldsymbol{\mathcal{D}}_c & \boldsymbol{\mathcal{D}}_b \end{bmatrix} \begin{pmatrix} \boldsymbol{\varepsilon}^0 \\ \boldsymbol{\kappa} \end{pmatrix}, \tag{5.47}$$

where

$$\boldsymbol{\mathcal{D}}_m = \sum_{i=1}^{n_{\text{layer}}} \boldsymbol{\mathcal{D}}_{2D}^i (z_{i+1} - z_i), \quad \boldsymbol{\mathcal{D}}_c = -\frac{1}{2} \sum_{i=1}^{n_{\text{layer}}} \boldsymbol{\mathcal{D}}_{2D}^i (z_{i+1}^2 - z_i^2), \quad \boldsymbol{\mathcal{D}}_b = \frac{1}{3} \sum_{i=1}^{n_{\text{layer}}} \boldsymbol{\mathcal{D}}_{2D}^i (z_{i+1}^3 - z_i^3), \tag{5.48}$$

Differently from isotropic plate, for laminated anisotropic plates the membrane and bending behavior are coupled. The coupling term $\boldsymbol{\mathcal{D}}_c$ disappears if a symmetric configuration is considered. For the shear contribution it is obtained

$$\boldsymbol{q} := \int_{-h/2}^{h/2} \boldsymbol{\sigma}_s \, \mathrm{d}z = \boldsymbol{\mathcal{D}}_s \boldsymbol{\gamma}, \qquad \text{where} \qquad \boldsymbol{\gamma} = \operatorname{grad} u_z - \boldsymbol{\theta}. \tag{5.49}$$

The tensor $\boldsymbol{\mathcal{D}}_s$ is not diagonal as in the isotropic case, cf. §5.2.1.

In the following section it is shown how anisotropic laminated plates can be formulated as pHs.

5.3.1 Port-Hamiltonian laminated Mindlin plate

For a shear deformable laminated plate the kinetic and deformation energy read

$$
\begin{aligned}
E_{\text{kin}} &= \frac{1}{2}\int_\Omega \left\{ \rho h \left\| \frac{\partial \boldsymbol{u}^0}{\partial t} \right\|^2 + \rho h \left(\frac{\partial u_z}{\partial t} \right)^2 + \frac{\rho h^3}{12} \left\| \frac{\partial \boldsymbol{\theta}}{\partial t} \right\|^2 \right\} \, \mathrm{d}\Omega, \\
E_{\text{def}} &= \frac{1}{2}\int_\Omega \left\{ \boldsymbol{N} : \boldsymbol{\varepsilon}^0 + \boldsymbol{M} : \boldsymbol{\kappa} + \boldsymbol{q} \cdot \boldsymbol{\gamma} \right\} \, \mathrm{d}\Omega.
\end{aligned}
$$

By using Hamilton's principle the equations of motion are retrieved (see [Red03, Chapter 3] for an exhaustive explanation)

$$
\begin{aligned}
\rho h \frac{\partial^2 \boldsymbol{u}^0}{\partial t^2} &= \mathrm{Div}\, \boldsymbol{N}, \\
\rho h \frac{\partial^2 u_z}{\partial t^2} &= \mathrm{div}\, \boldsymbol{q}, \\
\frac{\rho h^3}{12} \frac{\partial^2 \boldsymbol{\theta}}{\partial t^2} &= \mathrm{Div}\, \boldsymbol{M} + \boldsymbol{q},
\end{aligned} \tag{5.50}
$$

where $\boldsymbol{N}$, $\boldsymbol{M}$, $\boldsymbol{q}$ are defined in Eqs. (5.47), (5.49). To get a port-Hamiltonian formulation, the following energy variables are chosen

$$
\begin{aligned}
\boldsymbol{\alpha}_u &= \rho h \frac{\partial \boldsymbol{u}^0}{\partial t}, \qquad & \alpha_w &= \rho h \frac{\partial u_z}{\partial t}, \qquad & \boldsymbol{\alpha}_\theta &= \frac{\rho h^3}{12} \frac{\partial \boldsymbol{\theta}}{\partial t}, \\
\boldsymbol{A}_{\varepsilon^0} &= \boldsymbol{\varepsilon}^0, & \boldsymbol{A}_\kappa &= \boldsymbol{\kappa}, & \boldsymbol{\alpha}_\gamma &= \boldsymbol{\gamma}.
\end{aligned} \tag{5.51}
$$

This choice highlights the nature of the problem in which the membrane part (equivalent to a 2D elasticity problem) and the bending part interact. The total energy $H = E_{\text{kin}} + E_{\text{def}}$ is now a quadratic function of the energy variables

$$
\begin{aligned}
E_{\text{kin}} &= \frac{1}{2}\int_\Omega \left\{ \frac{1}{\rho h} \left\| \frac{\partial \boldsymbol{\alpha}_u}{\partial t} \right\|^2 + \frac{1}{\rho h} \left(\frac{\partial \alpha_w}{\partial t} \right)^2 + \frac{12}{\rho h^3} \left\| \frac{\partial \boldsymbol{\alpha}_\theta}{\partial t} \right\|^2 \right\} \, \mathrm{d}\Omega, \\
E_{\text{def}} &= \frac{1}{2}\int_\Omega \{ (\boldsymbol{\mathcal{D}}_m \boldsymbol{A}_{\varepsilon^0} + \boldsymbol{\mathcal{D}}_c \boldsymbol{A}_\kappa) : \boldsymbol{A}_{\varepsilon^0} + (\boldsymbol{\mathcal{D}}_c \boldsymbol{A}_{\varepsilon^0} + \boldsymbol{\mathcal{D}}_b \boldsymbol{A}_\kappa) : \boldsymbol{A}_\kappa + (\boldsymbol{\mathcal{D}}_s \boldsymbol{\alpha}_\gamma) \cdot \boldsymbol{\alpha}_\gamma \} \, \mathrm{d}\Omega,
\end{aligned}
$$

The co-energies are equal to

$$
\begin{aligned}
e_w &:= \frac{\delta H}{\delta \boldsymbol{\alpha}_u} = \frac{\partial \boldsymbol{u}^0}{\partial t}, \qquad & e_w &:= \frac{\delta H}{\delta \alpha_w} = \frac{\partial u_z}{\partial t}, \qquad & \boldsymbol{e}_\theta &:= \frac{\delta H}{\delta \boldsymbol{\alpha}_\theta} = \frac{\partial \boldsymbol{\theta}}{\partial t}, \\
\boldsymbol{E}_\kappa &:= \frac{\delta H}{\delta \boldsymbol{A}_{\varepsilon^0}} = \boldsymbol{N}, & \boldsymbol{E}_\kappa &:= \frac{\delta H}{\delta \boldsymbol{A}_\kappa} = \boldsymbol{M}, & \boldsymbol{e}_\gamma &:= \frac{\delta H}{\delta \boldsymbol{\alpha}_\gamma} = \boldsymbol{q}
\end{aligned} \tag{5.52}
$$

The final pH formulation is found as usual considering the dynamics (5.50) and Clairaut's theorem

$$\frac{\partial}{\partial t}\begin{pmatrix}\boldsymbol{\alpha}_u\\ \alpha_w\\ \boldsymbol{\alpha}_\theta\\ \boldsymbol{A}_{\varepsilon^0}\\ \boldsymbol{A}_\kappa\\ \boldsymbol{\alpha}_\gamma\end{pmatrix}=\begin{bmatrix}\mathbf{0} & \mathbf{0} & \mathbf{0} & \mathrm{Div} & \mathbf{0} & \mathbf{0}\\ 0 & 0 & 0 & 0 & 0 & \mathrm{div}\\ \mathbf{0} & \mathbf{0} & \mathbf{0} & \mathbf{0} & \mathrm{Div} & \boldsymbol{I}_{2\times 2}\\ \mathrm{Grad} & \mathbf{0} & \mathbf{0} & \mathbf{0} & \mathbf{0} & \mathbf{0}\\ \mathbf{0} & \mathbf{0} & \mathrm{Grad} & \mathbf{0} & \mathbf{0} & \mathbf{0}\\ \mathbf{0} & \mathrm{grad} & -\boldsymbol{I}_{2\times 2} & \mathbf{0} & \mathbf{0} & \mathbf{0}\end{bmatrix}\begin{pmatrix}\boldsymbol{e}_u\\ e_w\\ \boldsymbol{e}_\theta\\ \boldsymbol{E}_{\varepsilon^0}\\ \boldsymbol{E}_\kappa\\ \boldsymbol{e}_\gamma\end{pmatrix}. \tag{5.53}$$

The coupling between the membrane and bending part is clear when considering the link between energy and co-energy variables

$$\begin{pmatrix}\boldsymbol{e}_u\\ e_w\\ \boldsymbol{e}_\theta\\ \boldsymbol{E}_{\varepsilon^0}\\ \boldsymbol{E}_\kappa\\ \boldsymbol{e}_\gamma\end{pmatrix}=\begin{bmatrix}\frac{1}{\rho h}\boldsymbol{I}_{2\times 2} & \mathbf{0} & \mathbf{0} & \mathbf{0} & \mathbf{0} & \mathbf{0}\\ 0 & \frac{1}{\rho h} & 0 & 0 & 0 & 0\\ \mathbf{0} & \mathbf{0} & \frac{12}{\rho h^3}\boldsymbol{I}_{2\times 2} & \mathbf{0} & \mathbf{0} & \mathbf{0}\\ \mathbf{0} & \mathbf{0} & \mathbf{0} & \boldsymbol{\mathcal{D}}_m & \boldsymbol{\mathcal{D}}_c & \mathbf{0}\\ \mathbf{0} & \mathbf{0} & \mathbf{0} & \boldsymbol{\mathcal{D}}_c & \boldsymbol{\mathcal{D}}_b & \mathbf{0}\\ \mathbf{0} & \mathbf{0} & \mathbf{0} & \mathbf{0} & \mathbf{0} & \boldsymbol{\mathcal{D}}_s\end{bmatrix}\begin{pmatrix}\boldsymbol{\alpha}_u\\ \alpha_w\\ \boldsymbol{\alpha}_\theta\\ \boldsymbol{A}_{\varepsilon^0}\\ \boldsymbol{A}_\kappa\\ \boldsymbol{\alpha}_\gamma\end{pmatrix}. \tag{5.54}$$

Again appropriate boundary variables and a suitable Stokes-Dirac structure can be found for this model. The final formulation is just a superposition of systems (4.16) and (5.29).

5.3.2 Port-Hamiltonian laminated Kirchhoff plate

According to the Kirchhoff hypotheses the kinetic and deformation energies reduce to

$$\begin{aligned}E_{\mathrm{kin}}&=\frac{1}{2}\int_\Omega\left\{\rho h\left\|\frac{\partial \boldsymbol{u}^0}{\partial t}\right\|^2+\rho h\left(\frac{\partial u_z}{\partial t}\right)^2\right\}\,\mathrm{d}\Omega,\\ E_{\mathrm{def}}&=\frac{1}{2}\int_\Omega\left\{\boldsymbol{N}:\boldsymbol{\varepsilon}^0+\boldsymbol{M}:\boldsymbol{\kappa}\right\}\,\mathrm{d}\Omega,\end{aligned}$$

where $\boldsymbol{\kappa}$ is defined in Eq. (5.5). Furthermore, as stated in Remark 4, the rotational contribution in the kinetic energy has been neglected. The equations of motion are (see [Red03, Chapter 3] for an exhaustive explanation)

$$\begin{aligned}\rho h\frac{\partial^2 \boldsymbol{u}^0}{\partial t^2}&=\mathrm{Div}\,\boldsymbol{N},\\ \rho h\frac{\partial^2 u_z}{\partial t^2}&=-\,\mathrm{div}\,\mathrm{Div}\,\boldsymbol{M},\end{aligned} \tag{5.55}$$

where $\boldsymbol{N}$, $\boldsymbol{M}$ are defined in Eqs. (5.47). To get a port-Hamiltonian formulation, the following energy variables are chosen

$$
\begin{aligned}
\boldsymbol{\alpha}_u &= \rho h \frac{\partial \boldsymbol{u}^0}{\partial t}, & \alpha_w &= \rho h \frac{\partial u_z}{\partial t}, \\
\boldsymbol{A}_{\varepsilon^0} &= \boldsymbol{\varepsilon}^0, & \boldsymbol{A}_\kappa &= \boldsymbol{\kappa}.
\end{aligned}
\tag{5.56}
$$

The total energy $H = E_{\text{kin}} + E_{\text{def}}$ is now a quadratic function of the energy variables

$$
\begin{aligned}
E_{\text{kin}} &= \frac{1}{2} \int_\Omega \left\{ \frac{1}{\rho h} \left\| \frac{\partial \boldsymbol{\alpha}_u}{\partial t} \right\|^2 + \frac{1}{\rho h} \left(\frac{\partial \alpha_w}{\partial t} \right)^2 \right\} \mathrm{d}\Omega, \\
E_{\text{def}} &= \frac{1}{2} \int_\Omega \left\{ (\boldsymbol{\mathcal{D}}_m \boldsymbol{A}_{\varepsilon^0} + \boldsymbol{\mathcal{D}}_c \boldsymbol{A}_\kappa) : \boldsymbol{A}_{\varepsilon^0} + (\boldsymbol{\mathcal{D}}_c \boldsymbol{A}_{\varepsilon^0} + \boldsymbol{\mathcal{D}}_b \boldsymbol{A}_\kappa) : \boldsymbol{A}_\kappa \right\} \mathrm{d}\Omega,
\end{aligned}
$$

The co-energies are equal to

$$
\begin{aligned}
e_w &:= \frac{\delta H}{\delta \boldsymbol{\alpha}_u} = \frac{\partial \boldsymbol{u}^0}{\partial t}, & e_w &:= \frac{\delta H}{\delta \alpha_w} = \frac{\partial u_z}{\partial t}, \\
\boldsymbol{E}_\kappa &:= \frac{\delta H}{\delta \boldsymbol{A}_{\varepsilon^0}} = \boldsymbol{N}, & \boldsymbol{E}_\kappa &:= \frac{\delta H}{\delta \boldsymbol{A}_\kappa} = \boldsymbol{M},
\end{aligned}
\tag{5.57}
$$

The final pH formulation is found to be

$$
\frac{\partial}{\partial t} \begin{pmatrix} \boldsymbol{\alpha}_u \\ \alpha_w \\ \boldsymbol{A}_{\varepsilon^0} \\ \boldsymbol{A}_\kappa \end{pmatrix} = \begin{bmatrix} \boldsymbol{0} & \boldsymbol{0} & \mathrm{Div} & \boldsymbol{0} \\ 0 & 0 & 0 & -\mathrm{div} \circ \mathrm{Div} \\ \mathrm{Grad} & \boldsymbol{0} & \boldsymbol{0} & \boldsymbol{0} \\ \boldsymbol{0} & \mathrm{Grad} \circ \mathrm{grad} & \boldsymbol{0} & \boldsymbol{0} \end{bmatrix} \begin{pmatrix} \boldsymbol{e}_u \\ e_w \\ \boldsymbol{E}_{\varepsilon^0} \\ \boldsymbol{E}_\kappa \end{pmatrix}.
\tag{5.58}
$$

Again, the coupling appears when considering the link between energy and co-energy variables

$$
\begin{pmatrix} \boldsymbol{e}_u \\ e_w \\ \boldsymbol{E}_{\varepsilon^0} \\ \boldsymbol{E}_\kappa \end{pmatrix} = \begin{bmatrix} \frac{1}{\rho h} \boldsymbol{I}_{2\times 2} & \boldsymbol{0} & \boldsymbol{0} & \boldsymbol{0} \\ 0 & \frac{1}{\rho h} & 0 & 0 \\ \boldsymbol{0} & \boldsymbol{0} & \boldsymbol{\mathcal{D}}_m & \boldsymbol{\mathcal{D}}_c \\ \boldsymbol{0} & \boldsymbol{0} & \boldsymbol{\mathcal{D}}_c & \boldsymbol{\mathcal{D}}_b \end{bmatrix} \begin{pmatrix} \boldsymbol{\alpha}_u \\ \alpha_w \\ \boldsymbol{A}_{\varepsilon^0} \\ \boldsymbol{A}_\kappa \end{pmatrix}.
\tag{5.59}
$$

The energy rate provides the appropriate boundary conditions from which one can construct the Stokes-Dirac structure. The necessary computations are not performed here as the final result is just a juxtaposition of systems (4.16), (5.42).

5.4 Conclusion

In this chapter, a pH formulation for the most commonly used plate models has been detailed. Many open questions remain. In particular, how to generalize the results to shell problems, for which the domain is a surface embedded in the three dimensional space (a manifold). Computations get more involved in this case since the usage of differential geometry concepts is unavoidable. These models are important since they are widely used in the aerospace industry and ubiquitous in nature.

The reformulation of plate models using the language of differential geometry is another open research topic. Indeed, while for the Mindlin plate it should be possible to use vector-valued forms to obtain an equivalent system, for the Kirchhoff plate higher order Stokes-Dirac structure are needed [NY04].

Chapter 6

Thermoelasticity in port-Hamiltonian form

Eh bien, mon ami, la terre sera un jour ce cadavre refroidi. Elle deviendra inhabitable et sera inhabitée comme la lune, qui depuis longtemps a perdu sa chaleur vitale.

Vingt mille lieues sous les mers
Jules Verne

Contents

6.1 Port-Hamiltonian linear coupled thermoelasticity **59**
6.1.1 The heat equation as a pH descriptor system 60
6.1.2 Classical thermoelasticity 61
6.1.3 Thermoelasticity as two coupled pHs 63
6.2 Thermoelastic port-Hamiltonian bending **65**
6.2.1 Thermoelastic Euler-Bernoulli beam 65
6.2.2 Thermoelastic Kirchhoff plate 67
6.3 Conclusion **69**

Thermoelasticity is the study of deformable bodies undergoing thermal excitations. It is a clear example of a multiphysics phenomenon since the heat transfer and elastic vibrations within the body mutually interact. In this chapter, a linear model of thermoelasticity is obtained under the pH formalism. Each physics is described separately and the final system is obtained considering a power-preserving interconnection of two pHs.

6.1 Port-Hamiltonian linear coupled thermoelasticity

In this section, a pH formulation of heat transfer is first introduced. The classical model of thermoelasticity is then recalled. The same model is found by interconnecting the heat equation and the linear elastodynamics problem seen as pHs. It is shown that the interconnection preserves a quadratic functional that plays the role of a fictitious energy. The resulting system is dissipative with respect to this functional. The construction makes use of the intrinsic modularity of pHs [KZvdSB10].

6.1.1 The heat equation as a pH descriptor system

Consider the heat equation in a bounded connected set $\Omega \subset \mathbb{R}^d$, $d \in \{1,2,3\}$, describing the evolution of the temperature field $T(\boldsymbol{x}, t)$

$$\rho c_\epsilon \frac{\partial T}{\partial t} = k \Delta T + r_Q, \qquad \boldsymbol{x} \in \Omega, \tag{6.1}$$

where ρ, c_ϵ, k, r_Q are the mass density, the specific heat density at constant strain, the thermal diffusivity and an heat source. Symbol Δ denotes the Laplacian in $\mathbb{R}^d$. The Dirichlet and Neumann condition of this problem are

$$\begin{aligned} T \text{ known on } \Gamma_D^T, &\qquad \text{Dirichlet condition}, \\ -k \operatorname{grad} T \cdot \boldsymbol{n} \text{ known on } \Gamma_N^T, &\qquad \text{Neumann condition}, \end{aligned}$$

where a partition of the boundary $\partial\Omega = \Gamma_D^T \cup \Gamma_N^T$ has been considered. This model can be put in pH form by means of a canonical interconnection structure. An algebraic relationship that describes the Fourier law has to be incorporated in the model (cf. [Kot19, Chapter 2]). Here, a differential-algebraic formulation is exploited to obtain the same system.

Let T_0 be a constant reference temperature (the introduction of this variables is instrumental for coupled thermoelasticity). The functional

$$H_T = \frac{1}{2} \int_\Omega \rho c_\epsilon T_0 \left(\frac{T - T_0}{T_0} \right)^2 \, \mathrm{d}\Omega$$

has the physical dimension of an energy and represents a Lyapunov functional of this system. Even though it does not represent the internal energy, it has some important properties. Select as energy variable

$$\alpha_T := \rho c_\epsilon (T - T_0),$$

whose corresponding co-energy is

$$e_T := \frac{\delta H_T}{\delta \alpha_T} = \frac{\alpha_T}{\rho c_\epsilon T_0} = \frac{T - T_0}{T_0} =: \theta.$$

Introducing the heat flux $\boldsymbol{j}_Q := -k \operatorname{grad} T$ as additional variable, the heat equation (6.1) is equivalently reformulated as

$$\begin{aligned}
\begin{bmatrix} 1 & 0 \\ \mathbf{0} & \mathbf{0} \end{bmatrix} \frac{\partial}{\partial t} \begin{pmatrix} \alpha_T \\ \boldsymbol{j}_Q \end{pmatrix} &= \begin{bmatrix} 0 & -\operatorname{div} \\ -\operatorname{grad} & -(T_0 k)^{-1} \end{bmatrix} \begin{pmatrix} e_T \\ \boldsymbol{j}_Q \end{pmatrix} + \begin{bmatrix} 1 \\ \mathbf{0} \end{bmatrix} u_T, \\
y_T &= \begin{bmatrix} 1 & \mathbf{0} \end{bmatrix} \begin{pmatrix} e_T \\ \boldsymbol{j}_Q \end{pmatrix}.
\end{aligned} \tag{6.2}$$

with $u_T := r_Q$ and y_T represents the corresponding power-conjugated variable. In matrix notation, it is obtained

$$\begin{aligned}
\mathcal{E}_T \partial_t \boldsymbol{\alpha}_T &= (\mathcal{J}_T - \mathcal{R}_T)\, \boldsymbol{e}_T + \mathcal{B}_T\, u_T, \\
y_d &= \mathcal{B}_T^* \, \boldsymbol{e}_T
\end{aligned} \tag{6.3}$$

where $\boldsymbol{\alpha}_T = (\alpha_T,\ \boldsymbol{j}_Q)$, $\boldsymbol{e}_T = (e_T,\ \boldsymbol{j}_Q)$ and

$$\mathcal{E}_T = \begin{bmatrix} 1 & 0 \\ \mathbf{0} & \mathbf{0} \end{bmatrix}, \quad \mathcal{J}_T = \begin{bmatrix} 0 & -\operatorname{div} \\ -\operatorname{grad} & \mathbf{0} \end{bmatrix}, \quad \mathcal{R}_T = \begin{bmatrix} 0 & 0 \\ \mathbf{0} & (T_0 k)^{-1} \end{bmatrix}, \quad \mathcal{B}_T = \begin{bmatrix} 1 \\ \mathbf{0} \end{bmatrix}.$$

The system is an example of pH descriptor system (cf. [BMXZ18] for the finite dimensional case). The Hamiltonian reads

$$H_T = \frac{1}{2} \int_\Omega \boldsymbol{e}_T \cdot \mathcal{E}_T \boldsymbol{\alpha}_T \, \mathrm{d}\Omega. \tag{6.4}$$

The power rate is then deduced

$$\begin{aligned}
\dot{H}_T &= \int_\Omega \boldsymbol{e}_T \cdot \mathcal{E}_T \, \partial_t \boldsymbol{\alpha}_T \, \mathrm{d}\Omega, \\
&= \int_\Omega \boldsymbol{e}_T \cdot \{(\mathcal{J}_T - \mathcal{R}_T)\boldsymbol{e} + \mathcal{B}_T u_T\} \, \mathrm{d}\Omega, \\
&= \int_\Omega u_T \, y_T \, \mathrm{d}\Omega - \int_\Omega \left(e_T \operatorname{div} \boldsymbol{j}_Q + \boldsymbol{j}_Q \operatorname{grad} e_T + \frac{\|\boldsymbol{j}_Q\|^2}{k T_0} \right) \mathrm{d}\Omega, \\
&\leq \int_\Omega u_T \, y_T \, \mathrm{d}\Omega - \int_{\partial\Omega} e_T \, \boldsymbol{j}_Q \cdot \boldsymbol{n} \, \mathrm{d}S.
\end{aligned} \tag{6.5}$$

This choice of Hamiltonian allows retrieving the classical boundary conditions and leads to a dissipative system. Other formulations, based on an entropy or internal energy functionals, are possible for the heat equation [DMSB09, SHM19a]. These provide an accrescent or a lossless system. Unfortunately these formulations are non linear and their discretization is a difficult task [SHM19b].

6.1.2 Classical thermoelasticity

The derivation of the classical theory of thermoelasticity is not carried out here. The reader may consult in [HE09, Chapter 1] or [Abe12, Chapter 8] for a detailed discussion on this topic.

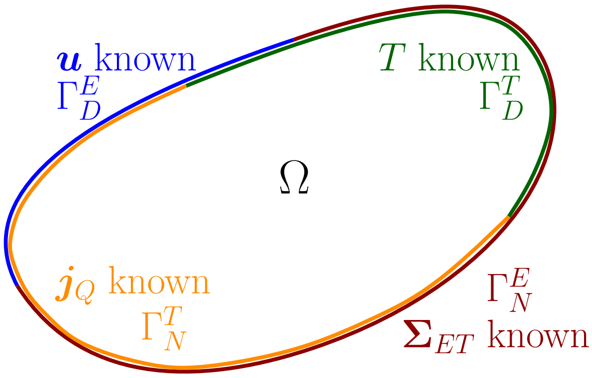

Figure 6.1: Boundary conditions for the thermoelastic problem.

Consider a bounded connected set $\Omega \subset \mathbb{R}^d$, $d \in \{1, 2, 3\}$. The classical equations for linear fully-coupled thermoelasticity for an isotropic thermoelastic material are [Bio56, Car73]

$$
\begin{aligned}
\rho \frac{\partial^2 \boldsymbol{u}}{\partial t^2} &= \mathrm{Div}(\boldsymbol{\Sigma}_{ET}), \\
\rho c_\epsilon \frac{\partial T}{\partial t} &= -\operatorname{div}(\boldsymbol{j}_Q) - \mathcal{C}_\beta : \frac{\partial \boldsymbol{\varepsilon}}{\partial t}, \\
\boldsymbol{\Sigma}_{ET} &= \boldsymbol{\Sigma}_E + \boldsymbol{\Sigma}_T, \\
\boldsymbol{\Sigma}_E &= 2\mu\boldsymbol{\varepsilon} + \lambda \operatorname{Tr}(\boldsymbol{\varepsilon}) \boldsymbol{I}_{d\times d}, \\
\boldsymbol{\Sigma}_T &= -\mathcal{C}_\beta \theta, \\
\boldsymbol{\varepsilon} &= \mathrm{Grad}(\boldsymbol{u}), \\
\boldsymbol{j}_Q &= -k \operatorname{grad} T.
\end{aligned}
\tag{6.6}
$$

For simplicity the coupling term

$$
\mathcal{C}_\beta := T_0 \beta (2\mu + d\lambda) \boldsymbol{I}_{d\times d}
$$

has been introduced. Field $\boldsymbol{u}$ is the displacement, $\boldsymbol{\varepsilon}$ is the infinitesimal strain tensor, $\boldsymbol{\Sigma}_E, \boldsymbol{\Sigma}_T$ are the stress tensor contribution due to mechanical deformation and a thermal field. Coefficients λ, μ are the Lamé parameters, and β the thermal expansion coefficient. Given a partition of the boundary $\partial\Omega = \Gamma_D^E \cup \Gamma_N^E = \Gamma_D^T \cup \Gamma_N^T$ for the elastic and thermal domain. The general boundary conditions read (see Fig. 6.1)

$$
\begin{aligned}
\boldsymbol{u} \text{ known on } \Gamma_D^E \times (0, +\infty), &\qquad T \text{ known on } \Gamma_D^T \times (0, +\infty), \\
\boldsymbol{\Sigma}_{ET} \cdot \boldsymbol{n} \text{ known on } \Gamma_N^E \times (0, +\infty), &\qquad \boldsymbol{j}_Q \cdot \boldsymbol{n} \text{ known on } \Gamma_N^T \times (0, +\infty).
\end{aligned}
\tag{6.7}
$$

In the following section an equivalent system is constructed by interconnecting the heat equation and the elastodynamics system in a structured manner.

6.1.3 Thermoelasticity as two coupled pHs

Consider again the equation of elasticity on $\Omega \subset \mathbb{R}^d$, $d \in \{1, 2, 3\}$ (cf. Eq. (4.16)), together with a distributed input $\boldsymbol{u}_E$ that plays the role of a distributed force

$$
\begin{aligned}
\frac{\partial}{\partial t}\begin{pmatrix} \boldsymbol{\alpha}_v \\ \boldsymbol{A}_\varepsilon \end{pmatrix} &= \begin{bmatrix} \boldsymbol{0} & \mathrm{Div} \\ \mathrm{Grad} & \boldsymbol{0} \end{bmatrix} \begin{pmatrix} \boldsymbol{e}_v \\ \boldsymbol{E}_\varepsilon \end{pmatrix} + \begin{bmatrix} \boldsymbol{I}_{d\times d} \\ \boldsymbol{0} \end{bmatrix} \boldsymbol{u}_E, \\
\boldsymbol{y}_E &= \begin{bmatrix} \boldsymbol{I}_{d\times d} & \boldsymbol{0} \end{bmatrix} \begin{pmatrix} \boldsymbol{e}_v \\ \boldsymbol{E}_\varepsilon \end{pmatrix},
\end{aligned} \tag{6.8}
$$

with Hamiltonian

$$
H_E = \frac{1}{2}\int_\Omega \{\boldsymbol{\alpha}_v \cdot \boldsymbol{e}_v + \boldsymbol{A}_\varepsilon : \boldsymbol{E}_\varepsilon\} \, \mathrm{d}\Omega.
$$

Recall the pH formulation of the heat equation (6.2)

$$
\begin{aligned}
\begin{bmatrix} 1 & 0 \\ \boldsymbol{0} & \boldsymbol{0} \end{bmatrix} \frac{\partial}{\partial t}\begin{pmatrix} \alpha_T \\ \boldsymbol{j}_Q \end{pmatrix} &= \begin{bmatrix} 0 & -\mathrm{div} \\ -\mathrm{grad} & -(T_0 k)^{-1} \end{bmatrix} \begin{pmatrix} e_T \\ \boldsymbol{j}_Q \end{pmatrix} + \begin{bmatrix} 1 \\ \boldsymbol{0} \end{bmatrix} u_T, \\
y_T &= \begin{bmatrix} 1 & \boldsymbol{0} \end{bmatrix} \begin{pmatrix} e_T \\ \boldsymbol{j}_Q \end{pmatrix},
\end{aligned} \tag{6.9}
$$

with Hamiltonian H_T defined in (6.4). The linear thermoelastic problem can be expressed as a coupled port-Hamiltonian system. Consider the following interconnection

$$
\boldsymbol{u}_E = -\mathrm{Div}(\mathcal{C}_\beta \, y_T), \qquad u_T = -\mathcal{C}_\beta : \mathrm{Grad}(\boldsymbol{y}_E). \tag{6.10}
$$

The interconnection is power preserving as it can be compactly written as

$$
\boldsymbol{u}_E = \mathcal{A}_\beta(y_T), \qquad u_T = -\mathcal{A}_\beta^*(\boldsymbol{y}_E).
$$

where $\mathcal{A}_\beta^*$ denotes the formal adjoint. The assertion is justified by the following proposition.

Proposition 5
Let $C_0^\infty(\Omega)$, $C_0^\infty(\Omega, \mathbb{R}^d)$ be the space of smooth functions and vector-valued functions respectively. Given $y_T \in C_0^\infty(\Omega)$, $\boldsymbol{y}_E \in C_0^\infty(\Omega, \mathbb{R}^d)$, the coupling operator

$$
\begin{aligned}
\mathcal{A}_\beta : C_0^\infty(\Omega) &\to C_0^\infty(\Omega, \mathbb{R}^d), \\
y_T &\to -\mathrm{Div}(\mathcal{C}_\beta y_T)
\end{aligned} \tag{6.11}
$$

has formal adjoint

$$
\begin{aligned}
\mathcal{A}_\beta^* : C_0^\infty(\Omega, \mathbb{R}^d) &\to C_0^\infty(\Omega) \\
\boldsymbol{y}_E &\to +\mathcal{C}_\beta : \mathrm{Grad}(\boldsymbol{y}_E)
\end{aligned} \tag{6.12}
$$

Proof. It is necessary to show

$$
\langle \boldsymbol{y}_E, \, \mathcal{A}_\beta y_T \rangle_{L^2(\Omega, \mathbb{R}^d)} = \left\langle \mathcal{A}_\beta^* \boldsymbol{y}_E, \, y_T \right\rangle_{L^2(\Omega)}, \tag{6.13}
$$

where for $\boldsymbol{u}_E, \boldsymbol{y}_E \in C_0^\infty(\Omega),\ u_T, y_T \in C_0^\infty(\Omega)$

$$\langle \boldsymbol{u}_E,\, \boldsymbol{y}_E \rangle_{L^2(\Omega, \mathbb{R}^d)} = \int_{\Omega_E} \boldsymbol{u}_E \cdot \boldsymbol{y}_E \,\mathrm{d}\Omega, \qquad \langle u_T,\, y_T \rangle_{L^2(\Omega)} = \int_{\Omega_T} u_T y_T \,\mathrm{d}\Omega. \tag{6.14}$$

The proof is a simple application of Theorem 5

$$\begin{aligned}
\langle \boldsymbol{y}_E,\, \mathcal{A}_\beta y_T \rangle_{L^2(\Omega, \mathbb{R}^d)} &= -\int_\Omega \boldsymbol{y}_E \cdot \mathrm{Div}(\mathcal{C}_\beta y_T) \,\mathrm{d}\Omega, \\
&= \int_\Omega \mathrm{Grad}(\boldsymbol{y}_E) : \mathcal{C}_\beta y_T \,\mathrm{d}\Omega, \\
&= \int_\Omega \mathcal{A}_\beta^*(\boldsymbol{y}_E) y_T \,\mathrm{d}\Omega, \\
&= \left\langle \mathcal{A}_\beta^* \boldsymbol{y}_E,\, y_T \right\rangle_{L^2(\Omega)}.
\end{aligned} \tag{6.15}$$

This concludes the proof. □

If the compact support assumption is removed, it is obtained

$$\begin{aligned}
\langle u_T, y_T \rangle_{L^2(\Omega)} + \langle \boldsymbol{u}_E, \boldsymbol{y}_E \rangle_{L^2(\Omega, \mathbb{R}^3)} &= -\int_\Omega \left\{ (\mathcal{C}_\beta : \mathrm{Grad}\, \boldsymbol{e}_v) e_T + \mathrm{Div}(\mathcal{C}_\beta e_T) \cdot \boldsymbol{e}_v \right\} \,\mathrm{d}\Omega, \\
&= -\int_\Omega \mathrm{div}(e_T \mathcal{C}_\beta \cdot \boldsymbol{e}_v) \,\mathrm{d}\Omega, \\
&= -\int_{\partial\Omega} (e_T \mathcal{C}_\beta \cdot \boldsymbol{n}) \cdot \boldsymbol{e}_v \,\mathrm{d}S.
\end{aligned} \tag{6.16}$$

Using the expression of $y_T, \boldsymbol{y}_E$, considering that T_0 is constant and applying Schwarz theorem for smooth function, the inputs are equal to

$$\boldsymbol{u}_E = \mathrm{Div}(\boldsymbol{\Sigma}_T), \qquad u_T = -\mathcal{C}_\beta : \mathrm{Grad}(\boldsymbol{v}) = -\mathcal{C}_\beta : \frac{\partial \boldsymbol{\varepsilon}}{\partial t}.$$

The coupled thermoelastic problem can now be written as

$$\begin{bmatrix} \mathbf{1} & \mathbf{0} & \mathbf{0} & \mathbf{0} \\ \mathbf{0} & \mathbf{1} & \mathbf{0} & \mathbf{0} \\ 0 & 0 & 1 & 0 \\ \mathbf{0} & \mathbf{0} & \mathbf{0} & \mathbf{0} \end{bmatrix} \frac{\partial}{\partial t} \begin{pmatrix} \boldsymbol{\alpha}_v \\ \boldsymbol{A}_\varepsilon \\ \alpha_T \\ \boldsymbol{j}_Q \end{pmatrix} = \begin{bmatrix} \mathbf{0} & \mathrm{Div} & \mathcal{A}_\beta & \mathbf{0} \\ \mathrm{Grad} & \mathbf{0} & \mathbf{0} & \mathbf{0} \\ -\mathcal{A}_\beta^* & 0 & 0 & -\mathrm{div} \\ \mathbf{0} & \mathbf{0} & -\mathrm{grad} & -(T_0 k)^{-1} \end{bmatrix} \begin{pmatrix} \boldsymbol{e}_v \\ \boldsymbol{E}_\varepsilon \\ e_T \\ \boldsymbol{j}_Q \end{pmatrix}, \tag{6.17}$$

with total energy given by $H = H_E + H_T$. The power balance for each subsystem is given by

$$\dot{H}_E = \int_\Omega \boldsymbol{u}_E \cdot \boldsymbol{y}_E \,\mathrm{d}\Omega + \int_{\partial\Omega} \boldsymbol{e}_v \cdot (\boldsymbol{E}_\varepsilon \cdot \boldsymbol{n}) \,\mathrm{d}S, \tag{6.18}$$

$$\dot{H}_T \leq \int_\Omega u_T\ y_T \,\mathrm{d}\Omega - \int_{\partial\Omega} \theta\ \boldsymbol{j}_Q \cdot \boldsymbol{n} \,\mathrm{d}S, \tag{6.19}$$

The overall power balance is easily computed considering Eqs. (6.18) (6.19) and (6.16)

$$\dot{H} = \dot{H}_E + \dot{H}_T \leq \int_{\partial\Omega} \{[\boldsymbol{E}_\varepsilon - e_T \mathcal{C}_\beta] \cdot \boldsymbol{n}\} \cdot \boldsymbol{e}_v \, \mathrm{d}S - \int_{\partial\Omega} \theta \, \boldsymbol{j}_Q \cdot \boldsymbol{n} \, \mathrm{d}S. \tag{6.20}$$

This result is the same stated in [Car73], page 332. From the power balance the classical boundary conditions are retrieved. This allows defining appropriate boundary operators for the thermoelastic problem

$$\boldsymbol{u}_\partial = \underbrace{\begin{bmatrix} \boldsymbol{\gamma}_0^{\Gamma_D^E} & \boldsymbol{0} & \boldsymbol{0} & \boldsymbol{0} \\ \boldsymbol{0} & \boldsymbol{\gamma}_n^{\Gamma_N^E} & -\boldsymbol{\gamma}_n^{\Gamma_N^E}(\mathcal{C}_\beta \, \cdot) & \boldsymbol{0} \\ 0 & 0 & \gamma_0^{\Gamma_D^T} & 0 \\ \boldsymbol{0} & \boldsymbol{0} & \boldsymbol{0} & \boldsymbol{\gamma}_n^{\Gamma_N^T} \end{bmatrix}}_{\mathcal{B}_\partial} \begin{pmatrix} \boldsymbol{e}_v \\ \boldsymbol{E}_\varepsilon \\ e_T \\ \boldsymbol{j}_Q \end{pmatrix}, \quad \boldsymbol{y}_\partial = \underbrace{\begin{bmatrix} \boldsymbol{0} & \boldsymbol{\gamma}_n^{\Gamma_D^E} & -\boldsymbol{\gamma}_n^{\Gamma_D^E}(\mathcal{C}_\beta \, \cdot) & \boldsymbol{0} \\ \boldsymbol{\gamma}_0^{\Gamma_N^E} & \boldsymbol{0} & \boldsymbol{0} & \boldsymbol{0} \\ \boldsymbol{0} & \boldsymbol{0} & \boldsymbol{0} & \boldsymbol{\gamma}_n^{\Gamma_D^T} \\ 0 & 0 & \gamma_0^{\Gamma_N^T} & 0 \end{bmatrix}}_{\mathcal{C}_\partial} \begin{pmatrix} \boldsymbol{e}_v \\ \boldsymbol{E}_\varepsilon \\ e_T \\ \boldsymbol{j}_Q \end{pmatrix}. \tag{6.21}$$

System (6.17) together with (6.21) is a pH system with boundary control and observation. Indeed, the classical thermoelastic problem can be modeled as two coupled systems, demonstrating the modularity of the pH paradigm.

6.2 Thermoelastic port-Hamiltonian bending

In this section, the thermoelastic bending of thin beam and plate structures is described as coupled interconnection pf pHs. Starting from classical thermoelastic models a suitable pH formulation can be obtained. This couples a mechanical system defined on a reduced domain (uni-dimensional for beams, bi-dimensional for plates), to a thermal domain defined in the three-dimensional space.

6.2.1 Thermoelastic Euler-Bernoulli beam

The model for the linear thermoelastic vibrations of an isotropic thin rod is detailed in [Cha62, LR00]. The domain of the beam is uni-dimensional $\Omega_E = \{0, L\}$, while the thermal domain is three-dimensional $\Omega_T = \{0, L\} \times S$, where S is the set representing the beam cross section. The set S is assumed to constant along the axis for simplicity. The ruling equations are

$$\begin{aligned} \rho A \frac{\partial^2 w}{\partial t^2} &= -EI \frac{\partial^4 w}{\partial x^4} - \beta E T_0 \frac{\partial^2}{\partial x^2} \int_S z\theta \, \mathrm{d}x \, \mathrm{d}y, \qquad && x \in \{0, L\} = \Omega_E, \\ \rho c_{\epsilon,B} T_0 \frac{\partial \theta}{\partial t} &= k T_0 \Delta\theta + \beta T_0 E z \frac{\partial^3 w}{\partial x^2 \, \partial t}, && (x, y, z) \in \Omega_E \times S = \Omega_T, \end{aligned} \tag{6.22}$$

where $w(x, t)$ is the vertical displacement of the beam $I = \int_S z^2 \, \mathrm{d}x \, \mathrm{d}y$ the second moment of area, E the Young modulus and A the cross section. The constant $c_{\epsilon,B}$ is due to the thermoelastic coupling (cf. [Cha62, LR00] for a detailed explanation). The other terms have meaning than in Section §6.1. Since the normalized temperature $\theta(x, y, z, t)$ depends on all spatial coordinates, the symbol $\Delta = \partial_{xx} + \partial_{yy} + \partial_{zz}$ is the Laplacian in three dimensions. The physical constants are assumed to be constant for simplicity.

The coupling operator is defined as

$$\mathcal{A}_{\beta,B}(y_T) := -\beta E T_0 \partial_{xx} \left(\int_S z y_T \, \mathrm{d}x \, \mathrm{d}y \right). \tag{6.23}$$

To unveil an interconnection that is power with respect to a certain function, the formal adjoint of the coupling operator is needed.

Proposition 6
Let $C_0^\infty(\Omega_T)$, $C_0^\infty(\Omega_E)$ be the space of smooth functions with compact support defined on Ω_T and Ω_E respectively. Given $y_T \in C_0^\infty(\Omega_T)$, $y_E \in C_0^\infty(\Omega_E)$ the formal adjoint of the coupling operator is

$$\mathcal{A}^*_{\beta,B}(y_E) = -\beta E T_0 z \, \partial_{xx} y_E. \tag{6.24}$$

Proof. The formal adjoint is defined by the relation

$$\langle y_E, \, \mathcal{A}_{\beta,B} y_T \rangle_{L^2(\Omega_E)} = \left\langle \mathcal{A}^*_{\beta,B} y_E, \, y_T \right\rangle_{L^2(\Omega_T)}, \tag{6.25}$$

where for $u_E, y_E \in C_0^\infty(\Omega_E)$, $u_T, y_T \in C_0^\infty(\Omega_T)$

$$\langle u_E, \, y_E \rangle_{L^2(\Omega_E)} = \int_{\Omega_E} u_E y_E \, \mathrm{d}x, \qquad \langle u_T, \, y_T \rangle_{L^2(\Omega_T)} = \int_{\Omega_T} y_T y_T \, \mathrm{d}x \, \mathrm{d}y \, \mathrm{d}z. \tag{6.26}$$

Using Def. (6.23) and the integration by parts, one finds

$$\begin{aligned} \langle y_E, \, \mathcal{A}_{\beta,B} y_T \rangle_{L^2(\Omega_E)} &= \int_{\Omega_E} y_E \mathcal{A}_{\beta,B} y_T \, \mathrm{d}x, \\ &= -\int_{\Omega_E} y_E \beta E T_0 \partial_{xx} \left(\int_S z y_T \, \mathrm{d}x \, \mathrm{d}y \right) \, \mathrm{d}x, \\ &= -\int_{\Omega_E} (\partial_{xx} y_E) \beta E T_0 \left(\int_S z y_T \, \mathrm{d}x \, \mathrm{d}y \right) \, \mathrm{d}x, \end{aligned} \tag{6.27}$$

Since $\Omega_T = \Omega_E \times S$ and from the properties of multiple integrals, it is found

$$\begin{aligned} -\int_{\Omega_E} \partial_{xx}(y_E) \beta E T_0 \left(\int_S z \, y_T \, \mathrm{d}x \, \mathrm{d}y \right) \, \mathrm{d}x &= -\int_{\Omega_E} \int_S (\partial_{xx} y_E) \beta E T_0 z \, y_T \, \mathrm{d}x \, \mathrm{d}x \, \mathrm{d}y, \\ &= -\int_{\Omega_T} (\partial_{xx} y_E) \beta E T_0 z \, y_T \, \mathrm{d}x \, \mathrm{d}x \, \mathrm{d}y, \\ &= \left\langle \mathcal{A}^*_{\beta,B} y_E, \, y_T \right\rangle_{L^2(\Omega_T)}. \end{aligned} \tag{6.28}$$

This concludes the proof. □

Using Eqs. (6.23) and (6.24), System (6.22), is rewritten as

$$
\begin{aligned}
\rho A \frac{\partial^2 w}{\partial t^2} &= -EI \frac{\partial^4 w}{\partial x^4} + \mathcal{A}_{\beta,B}\theta, \\
\rho c_{\epsilon,B} T_0 \frac{\partial \theta}{\partial t} &= k T_0 \Delta\theta - \mathcal{A}^*_{\beta,B} \frac{\partial w}{\partial t}.
\end{aligned}
\tag{6.29}
$$

Consider the Hamiltonian functional

$$
H = H_E + H_T = \frac{1}{2} \int_{\Omega_E} \left\{ \rho A \left(\frac{\partial w}{\partial t}\right)^2 + EI \left(\frac{\partial^2 w}{\partial x^2}\right)^2 \right\} \mathrm{d}x + \frac{1}{2} \int_{\Omega_T} \rho c_{\epsilon,B} T_0 \theta^2 \,\mathrm{d}x \,\mathrm{d}y \,\mathrm{d}z. \tag{6.30}
$$

The energy variables are chosen to make the Hamiltonian functional quadratic

$$
\alpha_w = \rho A \partial_t w, \qquad \alpha_\kappa = \partial_{xx} w, \qquad \alpha_T = \rho c_{\epsilon,B} T_0 \theta. \tag{6.31}
$$

The corresponding co-energy variables evaluate to

$$
e_w := \frac{\delta H}{\delta \alpha_w} = \partial_t w, \qquad e_\kappa := \frac{\delta H}{\delta \alpha_\kappa} = EI \partial_{xx} w, \qquad e_T := \frac{\delta H}{\delta \alpha_T} = \theta. \tag{6.32}
$$

System (6.29) can now be rewritten as

$$
\begin{bmatrix} 1 & 0 & 0 & 0 \\ 0 & 1 & 0 & 0 \\ 0 & 0 & 1 & 0 \\ \mathbf{0} & \mathbf{0} & \mathbf{0} & \mathbf{0} \end{bmatrix} \frac{\partial}{\partial t} \begin{pmatrix} \alpha_w \\ \alpha_\kappa \\ \alpha_T \\ \boldsymbol{j}_Q \end{pmatrix} = \begin{bmatrix} 0 & -\partial_{xx} & \mathcal{A}_{\beta,B} & 0 \\ \partial_{xx} & 0 & 0 & 0 \\ -\mathcal{A}^*_{\beta,B} & 0 & 0 & -\operatorname{div} \\ \mathbf{0} & \mathbf{0} & -\operatorname{grad} & -(kT_0)^{-1} \end{bmatrix} \begin{pmatrix} e_w \\ e_\kappa \\ e_T \\ \boldsymbol{j}_Q \end{pmatrix}, \tag{6.33}
$$

This system is the equivalent of (6.17) for bending of beams. Hence, following the same reasoning, it can be obtained starting from each subsystem in pH form by means of an appropriate interconnection.

6.2.2 Thermoelastic Kirchhoff plate

For the bending of thin plate, several different models have been proposed [Cha62, Lag89, Sim99, Nor06]. Here, the Chadwick model [Cha62] is considered. The thin plate occupies the open connected set $\Omega_E \times \left\{-\frac{h}{2}, \frac{h}{2}\right\}$, where h is the plate thickness. The system of equations describe the midplane vertical displacement and the evolution of the temperature in the 3D domain

$$
\begin{aligned}
\rho h \frac{\partial^2 w}{\partial t^2} &= -D_b \Delta^2_{2D} w - \frac{\beta T_0 E}{1-\nu} \Delta_{2D} \left(\int_{-h/2}^{h/2} z\theta \,\mathrm{d}z \right), & (x,y) &\in \Omega_E, \\
\rho c_{\epsilon,P} T_0 \frac{\partial \theta}{\partial t} &= -k T_0 \Delta_{3D} + \frac{\beta T_0 E z}{1-\nu} \Delta_{2D} \left(\frac{\partial w}{\partial t} \right), & (x,y,z) &\in \Omega_E \times \left\{ -\frac{h}{2}, \frac{h}{2} \right\} = \Omega_T,
\end{aligned}
\tag{6.34}
$$

where $w(x,y,t)$ is the vertical deflection, $D_b = \frac{Eh^3}{12(1-\nu^2)}$ the bending rigidity (cf. Eq. (5.11)), ν the Poisson modulus and $c_{\epsilon,P}$ a constant (depending on the heat capacity at constant strain and other coupling parameters, cf. [Cha62]). Symbols $\Delta_{2D} = \partial_{xx} + \partial_{yy}$, $\Delta_{3D} = \partial_{xx} + \partial_{yy} + \partial_{zz}$ are the two- and three-dimensional Laplacian.

The coupling operator is here defined as

$$\mathcal{A}_{\beta,P}(y_T) := -\frac{\beta T_0 E}{1-\nu}\Delta_{2D}\left(\int_{-h/2}^{h/2} z y_T \,\mathrm{d}z\right). \tag{6.35}$$

Analouglsy with respect to the Euler-Bernoulli beam its formal adjoint is sought for.

Proposition 7
Let $C_0^\infty(\Omega_T)$, $C_0^\infty(\Omega_E)$ be the space of smooth functions with compact support defined on Ω_T and Ω_E respectively. Given $y_T \in C_0^\infty(\Omega_T)$, $y_E \in C_0^\infty(\Omega_E)$ the formal adjoint of the coupling operator is

$$\mathcal{A}^*_{\beta,B}(y_E) = -\frac{\beta T_0 E z}{1-\nu}\Delta_{2D} y_E. \tag{6.36}$$

Proof. The proof is completely identical to Prop. 6. □

System 6.34 is rewritten as

$$\begin{aligned} \rho h \frac{\partial^2 w}{\partial t^2} &= -D_b \Delta_{2D}^2 w + \mathcal{A}_{\beta,P}\theta, \\ \rho c_{\epsilon,P} T_0 \frac{\partial \theta}{\partial t} &= -k T_0 \Delta_{3D}\theta - \mathcal{A}^*_{\beta,P}\left(\frac{\partial w}{\partial t}\right), \end{aligned} \tag{6.37}$$

The Hamiltonian functional equals

$$\begin{aligned} H = H_E + H_T =& \frac{1}{2}\int_{\Omega_E} \left\{\rho h \left(\frac{\partial w}{\partial t}\right)^2 + (\boldsymbol{\mathcal{D}}_b \mathrm{Hess}_{2D} w) : \mathrm{Hess}_{2D} w\right\} \mathrm{d}x\,\mathrm{d}y \\ &+ \frac{1}{2}\int_{\Omega_T} \rho c_{\epsilon,P} T_0 \theta^2 \,\mathrm{d}x\,\mathrm{d}y\,\mathrm{d}z, \end{aligned} \tag{6.38}$$

where Hess_{2D} is the Hessian in two dimensions and $\boldsymbol{\mathcal{D}}_b$ was defined in (5.11) (cf. Sec. §5.1.1). The energy and co-energy variables are

$$\begin{aligned} \alpha_w &= \rho h \partial_t w, & \boldsymbol{A}_\kappa &= \mathrm{Hess}_{2D} w, & \alpha_T &= \rho c_{\epsilon,P} T_0 \theta, \\ e_w &= \partial_t w, & \boldsymbol{E}_\kappa &= \boldsymbol{\mathcal{D}}_b \mathrm{Hess}_{2D} w, & e_T &= \theta. \end{aligned} \tag{6.39}$$

System (6.37) is rewritten as

$$\begin{bmatrix} 1 & 0 & 0 & 0 \\ \mathbf{0} & \mathbf{1} & \mathbf{0} & \mathbf{0} \\ 0 & 0 & 1 & 0 \\ \mathbf{0} & \mathbf{0} & \mathbf{0} & \mathbf{0} \end{bmatrix} \frac{\partial}{\partial t}\begin{pmatrix} \alpha_w \\ \boldsymbol{A}_\kappa \\ \alpha_T \\ \boldsymbol{j}_Q \end{pmatrix} = \begin{bmatrix} 0 & -\operatorname{div}\mathrm{Div}_{2D} & \mathcal{A}_{\beta,P} & 0 \\ \mathrm{Hess}_{2D} & \mathbf{0} & \mathbf{0} & 0 \\ -\mathcal{A}^*_{\beta,P} & 0 & 0 & -\operatorname{div}_{3D} \\ \mathbf{0} & \mathbf{0} & -\operatorname{grad}_{3D} & -(kT_0)^{-1} \end{bmatrix}\begin{pmatrix} e_w \\ \boldsymbol{E}_\kappa \\ e_T \\ \boldsymbol{j}_Q \end{pmatrix}, \tag{6.40}$$

The subscript $2D$, $3D$ refers to two- and three-dimensional operators respectively. The final system reproduces the same structured coupling already observed for (6.17), (6.33).

Remark 7
The thermoelastic bending can be reduced to two problems defined on the same domain (cf. [HZ97] for beams and [AL00] for plates) by introducing the following approximation of the temperature field

$$\theta(x, y, z) = \theta_0 + z\theta_1, \tag{6.41}$$

where $\theta_0 = \theta_0(x)$, $\theta_1 = \theta_1(x)$ for beams and $\theta_0 = \theta_0(x, y)$, $\theta_1 = \theta_1(x, y)$ for plates. However, this introducing a strong simplication as the thermal phenomena typically occur in the whole three-dimensional space.

6.3 Conclusion

In this chapter, it was shown classical linear thermoelastic problem are equivalent to two coupled port-Hamiltonian systems. This is especially interesting for the simulation of thermoelastic phenomena: each subsystem can be discretized separately and then coupled to the other using the discretized coupling operator. This allows to track easily how the energy flows within the two physics.

Part III

Finite element structure preserving discretization

Chapter 7

Partitioned finite element method

Every truth is simple... is that not doubly a lie?

Twilight of the Idols
Friedrich Nietzsche

Contents

7.1 Discretization under uniform boundary condition 73
7.1.1 General procedure 75
7.1.2 Linear case 84
7.1.3 Linear flexible structures 86
7.2 Mixed boundary conditions 95
7.2.1 Solution using Lagrange multipliers 97
7.2.2 Virtual domain decomposition 99
7.3 Conclusion 103

Discretization is the process of transferring continuous models into discrete counterparts. The discrete model should be faithful to the continuous one. To this aim, it is usually essential that the main properties of the continuous system are preserved at the discrete level. An algorithm that is capable of conserving properties at the discrete level is called structure-preserving [CMKO11]. In this chapter, a method to spatially discretize infinite-dimensional pHs into finite-dimensional ones in a structure preserving manner is illustrated.

7.1 Discretization under uniform boundary condition

A discrete version of a infinite-dimensional pH system is meant to preserve the underlying properties related to power continuity. To achieve this purpose, the discretization procedure consists of two steps [KML18]:

- Finite-dimensional approximation of the Stokes-Dirac structure, i.e. the formally skew symmetric differential operator that defines the structure. The duality of the power variables has to be mapped onto the finite approximation. The subspace of the discrete variables will be represented by a Dirac structure.

- The Hamiltonian requires as well a suitable discretization, which gives rise to a discrete Hamiltonian.

A structure-preserving discretization is able to construct an equivalent pH system that possesses the structural properties of the original model:

Infinite dimensional pH system

PDE with distributed inputs:

$$
\begin{aligned}
\frac{\partial \boldsymbol{\alpha}}{\partial t}(\boldsymbol{x}, t) &= \mathcal{J}\frac{\delta H}{\delta \boldsymbol{\alpha}} + \mathcal{B}\boldsymbol{u}_\Omega(\boldsymbol{x}, t), \\
\boldsymbol{y}_\Omega(\boldsymbol{x}, t) &= \mathcal{B}^*\frac{\delta H}{\delta \boldsymbol{\alpha}}.
\end{aligned}
$$

Boundary conditions:

$$
\boldsymbol{u}_\partial = \mathcal{B}_\partial \frac{\delta H}{\delta \boldsymbol{\alpha}}, \qquad \boldsymbol{y}_\partial = \mathcal{C}_\partial \frac{\delta H}{\delta \boldsymbol{\alpha}}.
$$

Power balance (Stokes Theorem):

$$
\dot{H} = \int_{\partial\Omega} \boldsymbol{u}_\partial \cdot \boldsymbol{y}_\partial \, \mathrm{d}S + \int_{\Omega} \boldsymbol{u}_\Omega \cdot \boldsymbol{y}_\Omega \, \mathrm{d}\Omega.
$$

Structure-preserving discretization

Resulting ODE:

$$
\begin{aligned}
\dot{\boldsymbol{\alpha}}_d &= \mathbf{J}\,\nabla H_d + \mathbf{B}_\Omega \mathbf{u}_\Omega + \mathbf{B}_\partial \mathbf{u}_\partial, \\
\mathbf{y}_\Omega &= \mathbf{B}_\Omega^\top \nabla H_d, \\
\mathbf{y}_\partial &= \mathbf{B}_\partial^\top \nabla H_d.
\end{aligned}
$$

Discretized Hamiltonian:

$$
H_d := H(\boldsymbol{\alpha} \equiv \boldsymbol{\alpha}_d).
$$

Power balance:

$$
\dot{H} = \mathbf{u}_\partial^\top \mathbf{y}_\partial + \mathbf{u}_\Omega^\top \mathbf{y}_\Omega.
$$

In this thesis the Partitioned Finite Element Method (PFEM), originally presented in [CRML18, CRML19], is chosen to obtain discretized models of dpHs. This procedure boils down to three simple steps

1. The system is written in weak form;

2. An integration by parts is applied to highlight the appropriate boundary control;

3. A Galerkin method is employed to obtain a finite-dimensional system. For the approximation basis the finite element method is here employed but spectral methods can be used as well.

Once the system has been put into weak form, a subset of the equations is integrated by parts, so that boundary variables are naturally included into the formulation and appear as control inputs, the collocated outputs being defined accordingly. The discretization of energy and co-energy variables (and the associated test functions) leads directly to a full rank representation for the finite-dimensional pH system. This approach makes possible the usage of FEM software, like FEniCS [LMW+12], or Firedrake [RHM+17]. The procedure is universal, as it relies on a general integration by parts formula that characterizes multi-dimensional pHs. This is why the methodology is illustrated in all its generality and then detailed for some particular examples.

This methodology is easily applicable under a uniform causality assumption. The case of mixed boundary conditions requires additional care and will be treated in the subsequent Section §7.2.

7.1.1 General procedure

Given an open connected set $\Omega \in \mathbb{R}^d$, $d \in \{1, 2, 3\}$, consider a generic pH system defined on Ω

$$
\begin{aligned}
\partial_t \boldsymbol{\alpha} &= \mathcal{J}\boldsymbol{e}, & \boldsymbol{\alpha} &\in L^2(\Omega, \mathbb{F}), \quad \mathcal{J} : L^2(\Omega, \mathbb{F}) \rightarrow L^2(\Omega, \mathbb{F}) |\ \mathcal{J} = -\mathcal{J}^*, && \text{(7.1a)} \\
\boldsymbol{e} &:= \delta_{\boldsymbol{\alpha}} H, & \boldsymbol{e} &\in H^{\mathcal{J}} := \left\{ \boldsymbol{e} \in L^2(\Omega, \mathbb{F}) |\ \mathcal{J}\boldsymbol{e} \in L^2(\Omega, \mathbb{F}) \right\}, && \text{(7.1b)} \\
\boldsymbol{u}_\partial &= \mathcal{B}_\partial \boldsymbol{e}, & \boldsymbol{u}_\partial &\in \mathbb{R}^m, && \text{(7.1c)} \\
\boldsymbol{y}_\partial &= \mathcal{C}_\partial \boldsymbol{e}, & \boldsymbol{y}_\partial &\in \mathbb{R}^m. && \text{(7.1d)}
\end{aligned}
$$

The operator $\mathcal{J} : L^2(\Omega, \mathbb{F}) \rightarrow L^2(\Omega, \mathbb{F})$ is a differential, formally skew adjoint operator $\mathcal{J} = -\mathcal{J}^*$ over the space $L^2(\Omega, \mathbb{F})$. The set $\mathbb{F}$ is an appropriate Cartesian product of either scalar, vectorial or tensorial quantities. Its precise definition depends on the example upon consideration. For scalars $(a, b) \in L^2(\Omega)$, vectors $(\boldsymbol{a}, \boldsymbol{b}) \in L^2(\Omega, \mathbb{R}^d)$ and tensors $(\boldsymbol{A}, \boldsymbol{B}) \in L^2(\Omega, \mathbb{R}^{d \times d})$ the L^2 inner product is given by

$$
\langle a,\, b \rangle_{L^2(\Omega)} = \int_\Omega ab \; \mathrm{d}\Omega, \qquad \langle \boldsymbol{a},\, \boldsymbol{b} \rangle_{L^2(\Omega, \mathbb{R}^d)} = \int_\Omega \boldsymbol{a} \cdot \boldsymbol{b} \; \mathrm{d}\Omega, \qquad \langle \boldsymbol{A},\, \boldsymbol{B} \rangle_{L^2(\Omega, \mathbb{R}^{d \times d})} = \int_\Omega \boldsymbol{A} : \boldsymbol{B} \; \mathrm{d}\Omega. \tag{7.2}
$$

For scalars $a_\partial, b_\partial \in L^2(\partial\Omega)$ and vectors $\boldsymbol{a}_\partial, \boldsymbol{b}_\partial \in L^2(\partial\Omega, \mathbb{R}^m)$ defined on the boundary the inner product is defined as

$$
\langle a_\partial,\, b_\partial \rangle_{L^2(\partial\Omega)} = \int_{\partial\Omega} a_\partial b_\partial \; \mathrm{d}S, \qquad \langle \boldsymbol{a}_\partial,\, \boldsymbol{b}_\partial \rangle_{L^2(\partial\Omega, \mathbb{R}^m)} = \int_{\partial\Omega} \boldsymbol{a}_\partial \cdot \boldsymbol{b}_\partial \; \mathrm{d}S. \tag{7.3}
$$

The Hamiltonian functional of Eq. (7.1b) is allowed to be non linear in the energy variables

$$
H = \int_\Omega \mathcal{H}(\boldsymbol{\alpha}) \; \mathrm{d}\Omega,
$$

where $\mathcal{H}(\boldsymbol{\alpha}) : L^2(\Omega, \mathbb{F}) \rightarrow \mathbb{R}$ is a non linear function.

To applied this methodology the non linearities are restricted to the Hamiltonian and a uniform causality condition is supposed to characterize the system. It is required as well that the system admits a partition of the variables. This requirement is always encountered in the following examples. These hypotheses are resumed in the following assumptions.

Assumption 2 (Partitioning of the system)

Consider system (7.1a)*. It is assumed that the Hilbert space* $L^2(\Omega, \mathbb{F}) := L^2(\Omega, \mathbb{F})$ *admits the splitting* $L^2(\Omega, \mathbb{F}) = L^2(\Omega, \mathbb{A}) \times L^2(\Omega, \mathbb{B})$ *This means that* $\mathbb{F} = \mathbb{A} \times \mathbb{B}$*.*

The operator $\mathcal{J}$ *is assumed to be skew-symmetric (or formally skew-adjoint) on* $L^2(\Omega, \mathbb{F})$ *and linear:*

$$\mathcal{J} = \mathcal{J}_a + \mathcal{J}_d, \tag{7.4}$$

where $\mathcal{J}_a$ *is the algebraic contribution (a skew-symmetric matrix) and* $\mathcal{J}_d$ *the differential contribution. The algebraic part is assumed to take the form*

$$\mathcal{J}_a = \begin{bmatrix} 0 & -\boldsymbol{L}^\top \\ \boldsymbol{L} & 0 \end{bmatrix}, \qquad \begin{aligned} \boldsymbol{L}^\top &: L^2(\Omega, \mathbb{B}) \to L^2(\Omega, \mathbb{A}), \\ \boldsymbol{L} &: L^2(\Omega, \mathbb{A}) \to L^2(\Omega, \mathbb{B}), \end{aligned} \tag{7.5}$$

where $\boldsymbol{L}$ *is a bounded operator. Analogously, the linear differential operator* $\mathcal{J}_d$ *is assumed to be of the form*

$$\mathcal{J}_d = \begin{bmatrix} 0 & -\mathcal{L}^* \\ \mathcal{L} & 0 \end{bmatrix}, \qquad \begin{aligned} \mathcal{L}^* &: L^2(\Omega, \mathbb{B}) \to L^2(\Omega, \mathbb{A}), \\ \mathcal{L} &: L^2(\Omega, \mathbb{A}) \to L^2(\Omega, \mathbb{B}), \end{aligned} \tag{7.6}$$

where $\mathcal{L}^*$ *denotes the formal adjoint of the linear differential operator* $\mathcal{L}$*. The operator* $\mathcal{L}$ *is unbounded and can be either a first or a second order differential operator (in the latter case it can be expressed as* $\mathcal{L} = \mathcal{L}_1 \circ \mathcal{L}_2$*). Given the splitting* $L^2(\Omega, \mathbb{A}) \times L^2(\Omega, \mathbb{B}) = L^2(\Omega, \mathbb{F})$ *the Hilbert space* $H^{\mathcal{J}}$ *can be split as well as*

$$H^{\mathcal{J}} = H^{\mathcal{L}} \times H^{-\mathcal{L}^*}, \qquad \begin{aligned} H^{\mathcal{L}} &:= \left\{ \boldsymbol{u}_1 \in L^2(\Omega, \mathbb{A}) |\; \mathcal{L}\boldsymbol{u}_1 \in L^2(\Omega, \mathbb{B}) \right\}, \\ H^{-\mathcal{L}^*} &:= \left\{ \boldsymbol{u}_2 \in L^2(\Omega, \mathbb{B}) |\; -\mathcal{L}^*\boldsymbol{u}_2 \in L^2(\Omega, \mathbb{A}) \right\} \end{aligned} \tag{7.7}$$

Remark 8
Notice that this assumption is also made in [Skr19] (using a vectorial notation for tensors) to demonstrate the well-posedness of linear pHs in arbitrary geometrical domains.

The boundary operators are then supposed to fulfill the following assumption, that guarantees a uniform causality condition.

Assumption 3 (Abstract integration by parts formula)
Assume that there exist two boundary operators $\mathcal{N}_{\partial,1}$, $\mathcal{N}_{\partial,2}$ *such that for* $(\boldsymbol{u}_1, \boldsymbol{u}_2) \in H^{\mathcal{L}} \times H^{-\mathcal{L}^*}$ *a general integration by parts formula holds*

$$\langle \boldsymbol{u}_2,\, \mathcal{L}\, \boldsymbol{u}_1 \rangle_{L^2(\Omega,\mathbb{B})} - \langle \mathcal{L}^*\, \boldsymbol{u}_2,\, \boldsymbol{u}_1 \rangle_{L^2(\Omega,\mathbb{A})} = \langle \mathcal{N}_{\partial,1} \boldsymbol{u}_1,\, \mathcal{N}_{\partial,2} \boldsymbol{u}_2 \rangle_{L^2(\partial\Omega,\mathbb{R}^m)}. \tag{7.8}$$

The boundary operators $\mathcal{B}_\partial, \mathcal{C}_\partial$ *of Eqs.* (7.1c)*,* (7.1d)*, are then assumed to verify, in an exclusive manner, either*

$$\mathcal{B}_\partial = \begin{bmatrix} 0 & \mathcal{N}_{\partial,2} \end{bmatrix}, \quad \mathcal{C}_\partial = \begin{bmatrix} \mathcal{N}_{\partial,1} & 0 \end{bmatrix}, \tag{7.9}$$

or

$$\mathcal{B}_\partial = \begin{bmatrix} \mathcal{N}_{\partial,1} & 0 \end{bmatrix}, \quad \mathcal{C}_\partial = \begin{bmatrix} 0 & \mathcal{N}_{\partial,2} \end{bmatrix}. \tag{7.10}$$

Remark 9 (Duality pairing for rigged Hilbert spaces)
The integration by part formula establishes a duality pairing between Sobolev spaces. This duality pairing is then compatible with an L^2 inner product in presence of a rigged Hilbert space (or Gelfand triple [GV64]). Without entering into technical details, we shall always use this equivalence of representation. Therefore, the boundary integrals are expressed as L^2 inner product over the boundary.

Thanks to Assumption 2, System (7.1) is rewritten as

$$\partial_t \begin{pmatrix} \boldsymbol{\alpha}_1 \\ \boldsymbol{\alpha}_2 \end{pmatrix} = \begin{bmatrix} 0 & -\boldsymbol{L}^\top - \mathcal{L}^* \\ \boldsymbol{L} + \mathcal{L} & 0 \end{bmatrix} \begin{pmatrix} \boldsymbol{e}_1 \\ \boldsymbol{e}_2 \end{pmatrix}, \qquad \begin{aligned} \boldsymbol{\alpha}_1 &\in L^2(\Omega, \mathbb{A}), \\ \boldsymbol{\alpha}_2 &\in L^2(\Omega, \mathbb{B}), \end{aligned} \tag{7.11a}$$

$$\begin{pmatrix} \boldsymbol{e}_1 \\ \boldsymbol{e}_2 \end{pmatrix} := \begin{pmatrix} \delta_{\boldsymbol{\alpha}_1} H \\ \delta_{\boldsymbol{\alpha}_2} H \end{pmatrix}, \qquad \begin{aligned} \boldsymbol{e}_1 &\in H^{\mathcal{L}}, \\ \boldsymbol{e}_2 &\in H^{-\mathcal{L}^*}. \end{aligned} \tag{7.11b}$$

In light of Assumption 3, if Eq. (7.9) holds the boundary variables are given by

$$\boldsymbol{u}_\partial = \mathcal{N}_2 \boldsymbol{e}_2, \qquad \boldsymbol{y}_\partial = \mathcal{N}_1 \boldsymbol{e}_1, \qquad \boldsymbol{u}_\partial, \, \boldsymbol{y}_\partial \in \mathbb{R}^m. \tag{7.12}$$

Otherwise, if Eq. (7.10) applies, then

$$\boldsymbol{u}_\partial = \mathcal{N}_1 \boldsymbol{e}_1, \qquad \boldsymbol{y}_\partial = \mathcal{N}_2 \boldsymbol{e}_2, \qquad \boldsymbol{u}_\partial, \, \boldsymbol{y}_\partial \in \mathbb{R}^m. \tag{7.13}$$

In both cases, the power balance reads

$$\begin{aligned} \dot{H} &= \langle \boldsymbol{e}_1, \, \partial_t \boldsymbol{\alpha}_1 \rangle_{L^2(\Omega,\mathbb{A})} + \langle \boldsymbol{e}_2, \, \partial_t \boldsymbol{\alpha}_2 \rangle_{L^2(\Omega,\mathbb{B})}, \\ &= \langle \boldsymbol{e}_1, \, -\mathcal{L}^* \boldsymbol{e}_2 \rangle_{L^2(\Omega,\mathbb{A})} + \langle \boldsymbol{e}_2, \, \mathcal{L} \boldsymbol{e}_1 \rangle_{L^2(\Omega,\mathbb{B})}, \\ &= \langle \mathcal{N}_{\partial,1} \boldsymbol{e}_1, \, \mathcal{N}_{\partial,2} \boldsymbol{e}_2 \rangle_{L^2(\partial\Omega,\mathbb{R}^m)}, \\ &= \langle \boldsymbol{y}_\partial, \, \boldsymbol{u}_\partial \rangle_{L^2(\partial\Omega,\mathbb{R}^m)}. \end{aligned} \tag{7.14}$$

We are now in a position to illustrate the methodology.

Step 1 First consider the weak form of system (7.11a), obtained by taking the L^2 inner product introducing an appropriate test function $\boldsymbol{v} = (\boldsymbol{v}_1, \boldsymbol{v}_2) \in \mathbb{A} \times \mathbb{B} = \mathbb{F}$ and integrating over the domain Ω

$$\begin{aligned} \langle \boldsymbol{v}_1, \, \partial_t \boldsymbol{\alpha}_1 \rangle_{L^2(\Omega,\mathbb{A})} &= -\langle \boldsymbol{v}_1, \, \boldsymbol{L}^\top \boldsymbol{e}_2 \rangle_{L^2(\Omega,\mathbb{A})} - \langle \boldsymbol{v}_1, \, \mathcal{L}^* \boldsymbol{e}_2 \rangle_{L^2(\Omega,\mathbb{A})}, \\ \langle \boldsymbol{v}_2, \, \partial_t \boldsymbol{\alpha}_2 \rangle_{L^2(\Omega,\mathbb{B})} &= \langle \boldsymbol{v}_2, \, \boldsymbol{L} \boldsymbol{e}_1 \rangle_{L^2(\Omega,\mathbb{B})} + \langle \boldsymbol{v}_2, \, \mathcal{L} \boldsymbol{e}_1 \rangle_{L^2(\Omega,\mathbb{B})}. \end{aligned} \tag{7.15}$$

To obtain a closed system, the constitutive law (7.11b) and the output variables (7.1d) are put in weak form

$$
\begin{aligned}
\langle \boldsymbol{v}_1,\, \boldsymbol{e}_1 \rangle_{L^2(\Omega,\mathbb{A})} &= \langle \boldsymbol{v}_1,\, \delta_{\boldsymbol{\alpha}_1} H \rangle_{L^2(\Omega,\mathbb{A})}\,, \\
\langle \boldsymbol{v}_2,\, \boldsymbol{e}_2 \rangle_{L^2(\Omega,\mathbb{B})} &= \langle \boldsymbol{v}_2,\, \delta_{\boldsymbol{\alpha}_2} H \rangle_{L^2(\Omega,\mathbb{B})}\,, \\
\langle \boldsymbol{v}_\partial,\, \boldsymbol{y}_\partial \rangle_{L^2(\partial\Omega,\mathbb{R}^m)} &= \langle \boldsymbol{v}_\partial,\, \mathcal{C}_\partial \boldsymbol{e} \rangle_{L^2(\partial\Omega,\mathbb{R}^m)}\,,
\end{aligned}
\tag{7.16}
$$

where the test function $\boldsymbol{v}_\partial \in L^2(\partial\Omega, \mathbb{R}^m)$ is defined on the boundary $\partial\Omega$ and $\mathcal{C}_\partial$ is defined either by Eq. (7.9) or (7.10).

Step 2 Next the integration by part has to be carried out. The choice is dictated by the boundary control to be imposed on the system. Consider again Eq. (7.15). The integration by parts can be carried out either on term $-\langle \boldsymbol{v}_1,\, \mathcal{L}^* \boldsymbol{e}_2 \rangle_{L^2(\Omega,\mathbb{A})}$, or on term $\langle \boldsymbol{v}_2,\, \mathcal{L} \boldsymbol{e}_1 \rangle_{L^2(\Omega,\mathbb{B})}$. Depending on which line undergoes the integration by parts (this is why the name Partitioned Finite Element method), two structure preserving weak forms are obtained. These differ by the boundary causality imposed to the system.

Integration by parts of the term $-\langle \boldsymbol{v}_1,\, \mathcal{L}^* \boldsymbol{e}_2 \rangle_{L^2(\Omega,\mathbb{A})}$ In this case case, using Eq. (7.8), it is obtained

$$
-\langle \boldsymbol{v}_1,\, \mathcal{L}^* \boldsymbol{e}_2 \rangle_{L^2(\Omega,\mathbb{A})} = -\langle \mathcal{L} \boldsymbol{v}_1,\, \boldsymbol{e}_2 \rangle_{L^2(\Omega,\mathbb{B})} + \langle \mathcal{N}_{\partial,1} \boldsymbol{v}_1,\, \mathcal{N}_{\partial,2} \boldsymbol{e}_2 \rangle_{L^2(\partial\Omega,\mathbb{R}^m)}\,. \tag{7.17}
$$

Then the weak form of the system dynamics reads

$$
\begin{aligned}
\langle \boldsymbol{v}_1,\, \partial_t \boldsymbol{\alpha}_1 \rangle_{L^2(\Omega,\mathbb{A})} &= -\langle \boldsymbol{v}_1,\, \boldsymbol{L}^\top \boldsymbol{e}_2 \rangle_{L^2(\Omega,\mathbb{A})} - \langle \mathcal{L} \boldsymbol{v}_1,\, \boldsymbol{e}_2 \rangle_{L^2(\Omega,\mathbb{B})} + \langle \mathcal{N}_{\partial,1} \boldsymbol{v}_1,\, \boldsymbol{u}_\partial \rangle_{L^2(\partial\Omega,\mathbb{R}^m)}\,, \\
\langle \boldsymbol{v}_2,\, \partial_t \boldsymbol{\alpha}_2 \rangle_{L^2(\Omega,\mathbb{B})} &= \langle \boldsymbol{v}_2,\, \boldsymbol{L} \boldsymbol{e}_1 \rangle_{L^2(\Omega,\mathbb{B})} + \langle \boldsymbol{v}_2,\, \mathcal{L} \boldsymbol{e}_1 \rangle_{L^2(\Omega,\mathbb{B})}\,,
\end{aligned}
\tag{7.18}
$$

The following proposition is crucial as the lossless character of the infinite-dimensional system (due to the formally skew-adjoint operator) translates into an equivalent property for the corresponding bilinear form in the weak form.

Proposition 8
Given the Hilbert space $H_2^{\mathcal{L}} := H^{\mathcal{L}} \times L^2(\Omega, \mathbb{B})$ and variables $\boldsymbol{v} = (\boldsymbol{v}_1, \boldsymbol{v}_2) \in H_2^{\mathcal{L}}$, $\boldsymbol{e} = (\boldsymbol{e}_1, \boldsymbol{e}_2) \in H_2^{\mathcal{L}}$, the bilinear form

$$
\begin{aligned}
j_{\mathcal{L}} : H_2^{\mathcal{L}} \times H_2^{\mathcal{L}} &\longrightarrow \mathbb{R}, \\
(\boldsymbol{v}, \boldsymbol{e}) &\longrightarrow -\langle \mathcal{L} \boldsymbol{v}_1,\, \boldsymbol{e}_2 \rangle_{L^2(\Omega,\mathbb{B})} + \langle \boldsymbol{v}_2,\, \mathcal{L} \boldsymbol{e}_1 \rangle_{L^2(\Omega,\mathbb{B})}
\end{aligned}
$$

is skew-symmetric.

Proof. The proof is obtained by the following computation

$$
\begin{aligned}
j_{\mathcal{L}}(\boldsymbol{v}, \boldsymbol{e}) &= -\langle \mathcal{L} \boldsymbol{v}_1,\, \boldsymbol{e}_2 \rangle_{L^2(\Omega,\mathbb{B})} + \langle \boldsymbol{v}_2,\, \mathcal{L} \boldsymbol{e}_1 \rangle_{L^2(\Omega,\mathbb{B})}\,, \\
&= -\Big(-\langle \boldsymbol{v}_2,\, \mathcal{L} \boldsymbol{e}_1 \rangle_{L^2(\Omega,\mathbb{B})} + \langle \mathcal{L} \boldsymbol{v}_1,\, \boldsymbol{e}_2 \rangle_{L^2(\Omega,\mathbb{B})} \Big)\,, \\
&= -\Big(-\langle \mathcal{L} \boldsymbol{e}_1,\, \boldsymbol{v}_2 \rangle_{L^2(\Omega,\mathbb{B})} + \langle \boldsymbol{e}_2,\, \mathcal{L} \boldsymbol{v}_1 \rangle_{L^2(\Omega,\mathbb{B})} \Big) = -j_{\mathcal{L}}(\boldsymbol{e}, \boldsymbol{v}).
\end{aligned}
$$

□

Now assume that the system satisfies the boundary causality condition 7.12. Then, this choice of the integration by parts leads to the following weak formulation

$$
\begin{aligned}
\langle \boldsymbol{v}_1,\, \partial_t \boldsymbol{\alpha}_1\rangle_{L^2(\Omega,\mathbb{A})} &= -\langle \boldsymbol{v}_1,\, \boldsymbol{L}^\top \boldsymbol{e}_2\rangle_{L^2(\Omega,\mathbb{A})} - \langle \mathcal{L}\boldsymbol{v}_1,\, \boldsymbol{e}_2\rangle_{L^2(\Omega,\mathbb{B})} + \langle \mathcal{N}_{\partial,1}\boldsymbol{v}_1,\, \boldsymbol{u}_\partial\rangle_{L^2(\partial\Omega,\mathbb{R}^m)}\,, \\
\langle \boldsymbol{v}_2,\, \partial_t \boldsymbol{\alpha}_2\rangle_{L^2(\Omega,\mathbb{B})} &= \langle \boldsymbol{v}_2,\, \boldsymbol{L}\boldsymbol{e}_1\rangle_{L^2(\Omega,\mathbb{B})} + \langle \boldsymbol{v}_2,\, \mathcal{L}\boldsymbol{e}_1\rangle_{L^2(\Omega,\mathbb{B})}\,, \\
\langle \boldsymbol{v}_1,\, \boldsymbol{e}_1\rangle_{L^2(\Omega,\mathbb{A})} &= \langle \boldsymbol{v}_1,\, \delta_{\boldsymbol{\alpha}_1} H\rangle_{L^2(\Omega,\mathbb{A})}\,, \\
\langle \boldsymbol{v}_2,\, \boldsymbol{e}_2\rangle_{L^2(\Omega,\mathbb{B})} &= \langle \boldsymbol{v}_2,\, \delta_{\boldsymbol{\alpha}_2} H\rangle_{L^2(\Omega,\mathbb{B})}\,, \\
\langle \boldsymbol{v}_\partial,\, \boldsymbol{y}_\partial\rangle_{L^2(\partial\Omega,\mathbb{R}^m)} &= \langle \boldsymbol{v}_\partial,\, \mathcal{N}_{\partial,1}\boldsymbol{e}_1\rangle_{L^2(\partial\Omega,\mathbb{R}^m)}\,.
\end{aligned}
\tag{7.19}
$$

Integration by parts of the term $\langle \boldsymbol{v}_2,\, \mathcal{L}\boldsymbol{e}_1\rangle_{L^2(\Omega,\mathbb{B})}$ Using Eq. (7.8), it is obtained

$$
\langle \boldsymbol{v}_2,\, \mathcal{L}\boldsymbol{e}_1\rangle_{L^2(\Omega,\mathbb{B})} = \langle \mathcal{L}^*\boldsymbol{v}_2,\, \boldsymbol{e}_1\rangle_{L^2(\Omega,\mathbb{A})} + \langle \mathcal{N}_{\partial,2}\boldsymbol{v}_2,\, \mathcal{N}_{\partial,1}\boldsymbol{e}_1\rangle_{L^2(\partial\Omega,\mathbb{R}^m)}\,. \tag{7.20}
$$

Then the weak form of the system dynamics reads

$$
\begin{aligned}
\langle \boldsymbol{v}_1,\, \partial_t \boldsymbol{\alpha}_1\rangle_{L^2(\Omega,\mathbb{A})} &= -\langle \boldsymbol{v}_1,\, \boldsymbol{L}^\top \boldsymbol{e}_2\rangle_{L^2(\Omega,\mathbb{A})} - \langle \boldsymbol{v}_1,\, \mathcal{L}^*\boldsymbol{e}_2\rangle_{L^2(\Omega,\mathbb{A})}\,, \\
\langle \boldsymbol{v}_2,\, \partial_t \boldsymbol{\alpha}_2\rangle_{L^2(\Omega,\mathbb{B})} &= \langle \boldsymbol{v}_2,\, \boldsymbol{L}\boldsymbol{e}_1\rangle_{L^2(\Omega,\mathbb{B})} + \langle \mathcal{L}^*\boldsymbol{v}_2,\, \boldsymbol{e}_1\rangle_{L^2(\Omega,\mathbb{A})} + \langle \mathcal{N}_{\partial,2}\boldsymbol{v}_2,\, \boldsymbol{u}_\partial\rangle_{L^2(\partial\Omega,\mathbb{R}^m)}\,,
\end{aligned}
\tag{7.21}
$$

Again the bilinear form arising from the formally skew-adjoint operator is skew-symmetric.

Proposition 9
Given the Hilbert space $H_1^{-\mathcal{L}^*} = L^2(\Omega,\mathbb{A}) \times H^{-\mathcal{L}^*}$ and variables $\boldsymbol{v} = (\boldsymbol{v}_1, \boldsymbol{v}_2) \in H_1^{-\mathcal{L}^*}$, $\boldsymbol{e} = (\boldsymbol{e}_1, \boldsymbol{e}_2) \in H_1^{-\mathcal{L}^*}$, the bilinear form

$$
\begin{aligned}
j_{-\mathcal{L}^*} : H_1^{-\mathcal{L}^*} \times H_1^{-\mathcal{L}^*} &\longrightarrow \mathbb{R}, \\
(\boldsymbol{v}, \boldsymbol{e}) &\longrightarrow -\langle \boldsymbol{v}_1,\, \mathcal{L}^*\boldsymbol{e}_2\rangle_{L^2(\Omega,\mathbb{A})} + \langle \mathcal{L}^*\boldsymbol{v}_2,\, \boldsymbol{e}_1\rangle_{L^2(\Omega,\mathbb{A})}
\end{aligned}
$$

is skew-symmetric.

Proof. The proof follows from the computation

$$
\begin{aligned}
j_{-\mathcal{L}^*}(\boldsymbol{v}, \boldsymbol{e}) &= -\langle \boldsymbol{v}_1,\, \mathcal{L}^*\boldsymbol{e}_2\rangle_{L^2(\Omega,\mathbb{A})} + \langle \mathcal{L}^*\boldsymbol{v}_2,\, \boldsymbol{e}_1\rangle_{L^2(\Omega,\mathbb{A})}\,, \\
&= -\left(-\langle \mathcal{L}^*\boldsymbol{v}_2,\, \boldsymbol{e}_1\rangle_{L^2(\Omega,\mathbb{A})} + \langle \boldsymbol{v}_1,\, \mathcal{L}^*\boldsymbol{e}_2\rangle_{L^2(\Omega,\mathbb{A})}\right), \\
&= -\left(-\langle \boldsymbol{e}_1,\, \mathcal{L}^*\boldsymbol{v}_2\rangle_{L^2(\Omega,\mathbb{A})} + \langle \mathcal{L}^*\boldsymbol{e}_2,\, \boldsymbol{v}_1\rangle_{L^2(\Omega,\mathbb{A})}\right) = -j_{-\mathcal{L}^*}(\boldsymbol{e}, \boldsymbol{v}).
\end{aligned}
$$

□

Now assume that the system satisfies the boundary causality condition (7.13). Then, the final weak formulation reads

$$
\begin{aligned}
\langle \boldsymbol{v}_1,\, \partial_t \boldsymbol{\alpha}_1 \rangle_{L^2(\Omega,\mathbb{A})} &= -\langle \boldsymbol{v}_1,\, \boldsymbol{L}^\top \boldsymbol{e}_2 \rangle_{L^2(\Omega,\mathbb{A})} - \langle \boldsymbol{v}_1,\, \mathcal{L}^* \boldsymbol{e}_2 \rangle_{L^2(\Omega,\mathbb{A})}\,, \\
\langle \boldsymbol{v}_2,\, \partial_t \boldsymbol{\alpha}_2 \rangle_{L^2(\Omega,\mathbb{B})} &= \langle \boldsymbol{v}_2,\, \boldsymbol{L} \boldsymbol{e}_1 \rangle_{L^2(\Omega,\mathbb{B})} + \langle \mathcal{L}^* \boldsymbol{v}_2,\, \boldsymbol{e}_1 \rangle_{L^2(\Omega,\mathbb{A})} + \langle \mathcal{N}_{\partial,2} \boldsymbol{v}_2,\, \boldsymbol{u}_\partial \rangle_{L^2(\partial\Omega,\mathbb{R}^m)}\,, \\
\langle \boldsymbol{v}_1,\, \boldsymbol{e}_1 \rangle_{L^2(\Omega,\mathbb{A})} &= \langle \boldsymbol{v}_1,\, \delta_{\boldsymbol{\alpha}_1} H \rangle_{L^2(\Omega,\mathbb{A})}\,, \\
\langle \boldsymbol{v}_2,\, \boldsymbol{e}_2 \rangle_{L^2(\Omega,\mathbb{B})} &= \langle \boldsymbol{v}_2,\, \delta_{\boldsymbol{\alpha}_2} H \rangle_{L^2(\Omega,\mathbb{B})}\,, \\
\langle \boldsymbol{v}_\partial,\, \boldsymbol{y}_\partial \rangle_{L^2(\partial\Omega,\mathbb{R}^m)} &= \langle \boldsymbol{v}_\partial,\, \mathcal{N}_{\partial,2} \boldsymbol{e}_2 \rangle_{L^2(\partial\Omega,\mathbb{R}^m)}\,.
\end{aligned}
\tag{7.22}
$$

Galerkin discretization To conclude the illustration of this methodology, a Galerkin discretization is introduced. This means that test, energy and co-energy functions are discretized using the same basis. Furthermore the boundary variables are discretized as well using bases defined over the boundary

$$
\begin{aligned}
\boldsymbol{v}_1 &\approx \sum_{i=1}^{n_1} \boldsymbol{\phi}_1^i(\boldsymbol{x}) v_1^i, &\quad \boldsymbol{\alpha}_1 &\approx \sum_{i=1}^{n_1} \boldsymbol{\phi}_1^i(\boldsymbol{x}) \alpha_1^i(t), &\quad \boldsymbol{e}_1 &\approx \sum_{i=1}^{n_1} \boldsymbol{\phi}_1^i(\boldsymbol{x}) e_1^i(t), &\quad \boldsymbol{x} &\in \Omega, \\
\boldsymbol{v}_2 &\approx \sum_{i=1}^{n_2} \boldsymbol{\phi}_2^i(\boldsymbol{x}) v_2^i, &\quad \boldsymbol{\alpha}_2 &\approx \sum_{i=1}^{n_2} \boldsymbol{\phi}_2^i(\boldsymbol{x}) \alpha_2^i(t), &\quad \boldsymbol{e}_2 &\approx \sum_{i=1}^{n_2} \boldsymbol{\phi}_2^i(\boldsymbol{x}) e_2^i(t), &\quad \boldsymbol{x} &\in \Omega, \\
\boldsymbol{v}_\partial &\approx \sum_{i=1}^{n_\partial} \boldsymbol{\phi}_\partial^i(\boldsymbol{s}) v_\partial^i, &\quad \boldsymbol{u}_\partial &\approx \sum_{i=1}^{n_\partial} \boldsymbol{\phi}_\partial^i(\boldsymbol{s}) u_\partial^i(t), &\quad \boldsymbol{y}_\partial &\approx \sum_{i=1}^{n_\partial} \boldsymbol{\phi}_\partial^i(\boldsymbol{s}) y_\partial^i(t), &\quad \boldsymbol{s} &\in \partial\Omega,
\end{aligned}
\tag{7.23}
$$

where $\boldsymbol{\phi}_1^i \in \mathbb{A},\ \boldsymbol{\phi}_2^i \in \mathbb{B},\ \boldsymbol{\phi}_\partial^i \in \mathbb{R}^m$.

Discretization of the weak form (7.19) Plugging the approximation into the weak form (7.19) and considering that the resulting equation holds $\forall\, v_1^i,\, v_2^j,\, v_\partial^k$ $(i \in \{1, n_1\}\,,\ j \in \{1, n_2\}\,,\ k \in \{1, n_\partial\})$, the finite dimensional system is obtained

$$
\begin{aligned}
\begin{bmatrix} \mathbf{M}_1 & \mathbf{0} \\ \mathbf{0} & \mathbf{M}_2 \end{bmatrix} \begin{pmatrix} \dot{\boldsymbol{\alpha}}_{d,1} \\ \dot{\boldsymbol{\alpha}}_{d,2} \end{pmatrix} &= \begin{bmatrix} \mathbf{0} & -\mathbf{D}_0^\top - \mathbf{D}_\mathcal{L}^\top \\ \mathbf{D}_0 + \mathbf{D}_\mathcal{L} & \mathbf{0} \end{bmatrix} \begin{pmatrix} \mathbf{e}_1 \\ \mathbf{e}_2 \end{pmatrix} + \begin{bmatrix} \mathbf{B}_1 \\ \mathbf{0} \end{bmatrix} \mathbf{u}_\partial, \\
\begin{bmatrix} \mathbf{M}_1 & \mathbf{0} \\ \mathbf{0} & \mathbf{M}_2 \end{bmatrix} \begin{pmatrix} \mathbf{e}_1 \\ \mathbf{e}_2 \end{pmatrix} &= \begin{bmatrix} \partial_{\boldsymbol{\alpha}_{d,1}} H_d(\boldsymbol{\alpha}_d) \\ \partial_{\boldsymbol{\alpha}_{d,2}} H_d(\boldsymbol{\alpha}_d) \end{bmatrix}, \\
\mathbf{M}_\partial \mathbf{y}_\partial &= \begin{bmatrix} \mathbf{B}_1^\top & \mathbf{0} \end{bmatrix} \begin{pmatrix} \mathbf{e}_1 \\ \mathbf{e}_2 \end{pmatrix}.
\end{aligned}
\tag{7.24}
$$

Vectors $\boldsymbol{\alpha}_{d,1}$, $\boldsymbol{\alpha}_{d,2}$, $\mathbf{e}_1$, $\mathbf{e}_2$, $\mathbf{u}_\partial$, $\mathbf{y}_\partial$ are given by the column-wise concatenation of their respective degrees of freedom. The matrices are defined as follows

$$
\begin{aligned}
M_1^{ij} &= \left\langle \boldsymbol{\phi}_1^i,\, \boldsymbol{\phi}_1^j \right\rangle_{L^2(\Omega,\mathbb{A})}, &\quad D_0^{mi} &= \left\langle \boldsymbol{\phi}_2^m,\, \boldsymbol{L} \boldsymbol{\phi}_1^i \right\rangle_{L^2(\Omega,\mathbb{B})}, &\quad B_1^{ik} &= \left\langle \mathcal{N}_{\partial,1} \boldsymbol{\phi}_1^i,\, \boldsymbol{\phi}_\partial^k \right\rangle_{L^2(\partial\Omega,\mathbb{R}^m)}, \\
M_2^{mn} &= \langle \boldsymbol{\phi}_2^m,\, \boldsymbol{\phi}_2^n \rangle_{L^2(\Omega,\mathbb{B})}, &\quad D_\mathcal{L}^{mi} &= \left\langle \boldsymbol{\phi}_2^m,\, \mathcal{L} \boldsymbol{\phi}_1^i \right\rangle_{L^2(\Omega,\mathbb{B})}, &\quad M_\partial^{lk} &= \left\langle \boldsymbol{\phi}_\partial^l,\, \boldsymbol{\phi}_\delta^k \right\rangle_{L^2(\partial\Omega,\mathbb{R}^m)},
\end{aligned}
\tag{7.25}
$$

where $i, j \in \{1, n_1\}$, $m, n \in \{1, n_2\}$, $l, k \in \{1, n_\partial\}$. Introducing the definitions

$$
\begin{aligned}
\delta_{\boldsymbol{\alpha}_{d,1}} H_d &:= \delta_{\boldsymbol{\alpha}_1} H \left(\boldsymbol{\alpha}_1 = \sum_{i=1}^{n_1} \boldsymbol{\phi}_1^i \alpha_1^i, \; \boldsymbol{\alpha}_2 = \sum_{i=1}^{n_1} \boldsymbol{\phi}_2^i \alpha_2^i \right), \\
\delta_{\boldsymbol{\alpha}_{d,2}} H_d &:= \delta_{\boldsymbol{\alpha}_2} H \left(\boldsymbol{\alpha}_1 = \sum_{i=1}^{n_1} \boldsymbol{\phi}_1^i \alpha_1^i, \; \boldsymbol{\alpha}_2 = \sum_{i=1}^{n_1} \boldsymbol{\phi}_2^i \alpha_2^i \right),
\end{aligned}
$$

the discretized gradient of the Hamiltonian reads

$$
\begin{aligned}
\partial_{\alpha_{d,1}^i} H_d(\boldsymbol{\alpha}_d) &= \left\langle \boldsymbol{\phi}_1^i, \, \delta_{\boldsymbol{\alpha}_{d,1}} H_d \right\rangle_{L^2(\Omega, \mathbb{A})}, \qquad & i \in \{1, n_1\}, \\
\partial_{\alpha_{d,2}^j} H_d(\boldsymbol{\alpha}_d) &= \left\langle \boldsymbol{\phi}_2^j, \, \delta_{\boldsymbol{\alpha}_{d,2}} H_d \right\rangle_{L^2(\Omega, \mathbb{B})}, \qquad & j \in \{1, n_2\}.
\end{aligned} \tag{7.26}
$$

A pH system in canonical form is found observing that Sys. (7.24) is compactly rewritten as

$$
\mathbf{M} \dot{\boldsymbol{\alpha}}_d = \mathbf{J}_{\mathcal{L}} \mathbf{e} + \mathbf{B} \mathbf{u}_\partial, \tag{7.27}
$$

$$
\mathbf{M} \mathbf{e} = \nabla H_d(\boldsymbol{\alpha}_d), \tag{7.28}
$$

$$
\mathbf{M}_\partial \mathbf{y}_\partial = \mathbf{B}^\top \mathbf{e}, \tag{7.29}
$$

where $\boldsymbol{\alpha}_d = (\boldsymbol{\alpha}_{d,1}^\top \;\; \boldsymbol{\alpha}_{d,2}^\top)^\top$, $\mathbf{e} = (\mathbf{e}_1^\top \;\; \mathbf{e}_2^\top)^\top$, $\nabla H_d(\boldsymbol{\alpha}_d) = (\partial_{\boldsymbol{\alpha}_{d,1}}^\top H_d(\boldsymbol{\alpha}_d) \;\; \partial_{\boldsymbol{\alpha}_{d,2}}^\top H_d(\boldsymbol{\alpha}_d))^\top$ and

$$
\mathbf{M} = \begin{bmatrix} \mathbf{M}_1 & \mathbf{0} \\ \mathbf{0} & \mathbf{M}_2 \end{bmatrix}, \qquad \mathbf{J}_{\mathcal{L}} = \begin{bmatrix} \mathbf{0} & -\mathbf{D}_0^\top - \mathbf{D}_{\mathcal{L}}^\top \\ \mathbf{D}_0 + \mathbf{D}_{\mathcal{L}} & \mathbf{0} \end{bmatrix}, \qquad \mathbf{B} = \begin{bmatrix} \mathbf{B}_1 \\ \mathbf{0} \end{bmatrix}. \tag{7.30}
$$

Plugging (7.28) into (7.27), a pH system in canonical form is obtained

$$
\begin{aligned}
\dot{\boldsymbol{\alpha}}_d &= \mathbf{J} \, \nabla H_d(\boldsymbol{\alpha}_d) + \mathbf{B} \, \mathbf{u}_\partial, \qquad & \text{where} \qquad \mathbf{J} &= \mathbf{M}^{-1} \mathbf{J}_{\mathcal{L}} \mathbf{M}^{-1}, \\
\widehat{\mathbf{y}}_\partial &= \mathbf{B}^\top \nabla H_d(\boldsymbol{\alpha}_d), \qquad & \text{where} \qquad \widehat{\mathbf{y}}_\partial &= \mathbf{M}_\partial \mathbf{y}_\partial.
\end{aligned} \tag{7.31}
$$

The structure preserving character of the method is evident from the preservation at the discrete level of the power balance. The finite dimensional counterpart of the energy rate is given by

$$
\begin{aligned}
\dot{H}_d &= \nabla^\top H_d(\boldsymbol{\alpha}_d) \dot{\boldsymbol{\alpha}}_d, \\
&= \nabla^\top H_d(\boldsymbol{\alpha}_d) \mathbf{J} \, \nabla H_d(\boldsymbol{\alpha}_d) + \nabla^\top H_d(\boldsymbol{\alpha}_d) \mathbf{B} \, \mathbf{u}_\partial, \qquad \text{Skew-symmetry of } \mathbf{J} \\
&= \mathbf{y}_\partial^\top \mathbf{M}_\partial \mathbf{u}_\partial = \widehat{\mathbf{y}}_\partial^\top \mathbf{u}_\partial.
\end{aligned} \tag{7.32}
$$

This result mimics its infinite dimensional equivalent (7.14).

Discretization of the weak form (7.22) Plugging the approximation into the weak form (7.22) a finite dimensional system with a different causality is obtained

$$
\begin{aligned}
\begin{bmatrix} \mathbf{M}_1 & \mathbf{0} \\ \mathbf{0} & \mathbf{M}_2 \end{bmatrix} \begin{pmatrix} \dot{\boldsymbol{\alpha}}_{d,1} \\ \dot{\boldsymbol{\alpha}}_{d,2} \end{pmatrix} &= \begin{bmatrix} \mathbf{0} & -\mathbf{D}_0^\top + \mathbf{D}_{-\mathcal{L}^*} \\ \mathbf{D}_0 - \mathbf{D}_{-\mathcal{L}^*}^\top & \mathbf{0} \end{bmatrix} \begin{pmatrix} \mathbf{e}_1 \\ \mathbf{e}_2 \end{pmatrix} + \begin{bmatrix} \mathbf{0} \\ \mathbf{B}_2 \end{bmatrix} \mathbf{u}_\partial, \\
\begin{bmatrix} \mathbf{M}_1 & \mathbf{0} \\ \mathbf{0} & \mathbf{M}_2 \end{bmatrix} \begin{pmatrix} \mathbf{e}_1 \\ \mathbf{e}_2 \end{pmatrix} &= \begin{pmatrix} \partial_{\boldsymbol{\alpha}_{d,1}} H_d(\boldsymbol{\alpha}_d) \\ \partial_{\boldsymbol{\alpha}_{d,2}} H_d(\boldsymbol{\alpha}_d) \end{pmatrix}, \\
\mathbf{M}_\partial \mathbf{y}_\partial &= \begin{bmatrix} \mathbf{0} & \mathbf{B}_2^\top \end{bmatrix} \begin{pmatrix} \mathbf{e}_1 \\ \mathbf{e}_2 \end{pmatrix}.
\end{aligned}
\tag{7.33}
$$

The differences with respect to formulation (7.24) reside in matrices $\mathbf{D}_{-\mathcal{L}^*}$, $\mathbf{B}_2$, whose definitions are

$$
D_{-\mathcal{L}^*}^{im} = \left\langle \boldsymbol{\phi}_1^i, \, -\mathcal{L}^* \boldsymbol{\phi}_2^m \right\rangle_{L^2(\Omega, \mathbb{A})}, \qquad B_2^{mk} = \left\langle \mathcal{N}_{\partial,2} \boldsymbol{\phi}_2^m, \, \phi_\partial^k \right\rangle_{L^2(\partial\Omega, \mathbb{R}^m)}, \tag{7.34}
$$

where $i \in \{1, n_1\}$, $m \in \{1, n_2\}$, $k \in \{1, n_\partial\}$. System (7.33) can be put in canonical form by replacing the co-energy variables by the discretized gradient.

Example: the irrotational shallow water equations Consider as an example the shallow water equations detailed in Sec. §3.3.3. The flow is assumed to be irrotational ($\nabla \times \boldsymbol{v} = 0$). As a consequence the term $\boldsymbol{\mathcal{G}}$ in Eq. (3.37) vanishes. To fulfill Assumption 3, the incoming volumetric flow is known at the boundary, so that a uniform Neumann condition is imposed. This leads to the following boundary control system, defined on an open connected set $\Omega \subset \mathbb{R}^2$

$$
\begin{aligned}
\frac{\partial}{\partial t} \begin{pmatrix} \alpha_h \\ \boldsymbol{\alpha}_v \end{pmatrix} &= - \begin{bmatrix} 0 & \operatorname{div} \\ \operatorname{grad} & \mathbf{0} \end{bmatrix} \begin{pmatrix} e_h \\ \boldsymbol{e}_v \end{pmatrix}, & \alpha_h &\in L^2(\Omega), \\
& & \boldsymbol{\alpha}_v &\in L^2(\Omega, \mathbb{R}^2), \\
\begin{pmatrix} e_h \\ \boldsymbol{e}_v \end{pmatrix} := \begin{pmatrix} \delta_{\alpha_h} H \\ \delta_{\boldsymbol{\alpha}_v} H \end{pmatrix} &= \begin{pmatrix} \frac{1}{2\rho} \left\| \boldsymbol{\alpha}_v \right\|^2 + \rho g \alpha_h, \\ \frac{1}{\rho} \alpha_h \boldsymbol{\alpha}_v. \end{pmatrix}, & e_h &\in H^1(\Omega), \\
& & \boldsymbol{e}_v &\in H^{\operatorname{div}}(\Omega, \mathbb{R}^2), \\
u_\partial &= -\boldsymbol{e}_v \cdot \boldsymbol{n}, & u_\partial &\in \mathbb{R}, \\
y_\partial &= e_h, & y_\partial &\in \mathbb{R},
\end{aligned}
\tag{7.35}
$$

where the Hamiltonian is a non linear functional in the energy variables

$$
H(\alpha_h, \boldsymbol{\alpha}_v) = \frac{1}{2} \int_\Omega \left\{ \frac{1}{\rho} \alpha_h \left\| \boldsymbol{\alpha}_v \right\|^2 + \rho g \alpha_h^2 \right\} \, \mathrm{d}\Omega.
$$

The energy and co-energy variables are related to the physical variables (fluid height and velocity) through Eqs. (3.34), (3.36). In this case $\mathbb{A} = \mathbb{R}$, $\mathbb{B} = \mathbb{R}^2$ and $\mathcal{L} = \operatorname{grad}$, $-\mathcal{L}^* = \operatorname{div}$. This implies $H^{\mathcal{L}} = H^1(\Omega)$, $H^{-\mathcal{L}^*} = H^{\operatorname{div}}(\Omega, \mathbb{R}^2)$. As shown in (3.38), the energy rate equals

$$
\dot{H} = - \left\langle \boldsymbol{e}_v, \, \operatorname{grad} e_h \right\rangle_{L^2(\Omega, \mathbb{R}^2)} - \left\langle \operatorname{div} \boldsymbol{e}_v, \, e_h \right\rangle_{L^2(\Omega)} = \left\langle -\boldsymbol{e}_v \cdot \boldsymbol{n}, \, e_h \right\rangle_{L^2(\partial\Omega)}. \tag{7.36}
$$

The boundary operators are therefore given by

$$
\begin{aligned}
u_\partial &= \mathcal{N}_{\partial,2} \boldsymbol{e}_v = -\gamma_n \boldsymbol{e}_v = -\boldsymbol{e}_v \cdot \boldsymbol{n}|_{\partial\Omega}, \\
y_\partial &= \mathcal{N}_{\partial,1} e_h = \gamma_0 e_h = e_h|_{\partial\Omega}.
\end{aligned}
\tag{7.37}
$$

This system represents a particular example of the general formulation of the general framework (7.11), together with boundary conditions (7.12). To obtain a finite dimensional system, the test variables $v_h,\ \boldsymbol{v}_v$ are introduced and the integration by parts is performed on the div operator, leading to the weak form

$$
\begin{aligned}
\langle v_h,\, \partial_t \alpha_h \rangle_{L^2(\Omega)} &= \langle \operatorname{grad} v_h,\, \boldsymbol{e}_v \rangle_{L^2(\Omega,\mathbb{R}^2)} + \langle \gamma_0 v_h,\, \boldsymbol{u}_\partial \rangle_{L^2(\partial\Omega)}\,, \\
\langle \boldsymbol{v}_v,\, \partial_t \boldsymbol{\alpha}_v \rangle_{L^2(\Omega,\mathbb{R}^2)} &= -\langle \boldsymbol{v}_v,\, \operatorname{grad} e_h \rangle_{L^2(\Omega,\mathbb{R}^2)}\,, \\
\langle v_h,\, e_h \rangle_{L^2(\Omega)} &= \left\langle v_h,\, \frac{1}{2\rho} \left\| \boldsymbol{\alpha}_v \right\|^2 + \rho g \alpha_h \right\rangle_{L^2(\Omega)}\,, \\
\langle \boldsymbol{v}_v,\, \boldsymbol{e}_v \rangle_{L^2(\Omega,\mathbb{R}^2)} &= \left\langle \boldsymbol{v}_v,\, \frac{1}{\rho} \alpha_h \boldsymbol{\alpha}_v \right\rangle_{L^2(\Omega,\mathbb{R}^2)}\,, \\
\langle v_\partial,\, y_\partial \rangle_{L^2(\partial\Omega)} &= \langle v_\partial,\, \gamma_0 e_h \rangle_{L^2(\partial\Omega)}\,.
\end{aligned}
\tag{7.38}
$$

Introducing a Galerkin approximation as in (7.23)

$$
\begin{aligned}
v_h &\approx \sum_{i=1}^{n_h} \phi_h^i(\boldsymbol{x}) v_h^i, & \alpha_h &\approx \sum_{i=1}^{n_h} \phi_h^i(\boldsymbol{x}) \alpha_h^i(t), & e_h &\approx \sum_{i=1}^{n_h} \phi_h^i(\boldsymbol{x}) e_h^i(t), & \boldsymbol{x} &\in \Omega, \\
\boldsymbol{v}_v &\approx \sum_{i=1}^{n_v} \boldsymbol{\phi}_v^i(\boldsymbol{x}) v_v^i, & \boldsymbol{\alpha}_v &\approx \sum_{i=1}^{n_2 v} \boldsymbol{\phi}_v^i(\boldsymbol{x}) \alpha_v^i(t), & \boldsymbol{e}_v &\approx \sum_{i=1}^{n_v} \boldsymbol{\phi}_v^i(\boldsymbol{x}) e_v^i(t), & \boldsymbol{x} &\in \Omega, \\
v_\partial &\approx \sum_{i=1}^{n_\partial} \phi_\partial^i(\boldsymbol{s}) v_\partial^i, & u_\partial &\approx \sum_{i=1}^{n_\partial} \phi_\partial^i(\boldsymbol{s}) u_\partial^i(t), & y_\partial &\approx \sum_{i=1}^{n_\partial} \phi_\partial^i(\boldsymbol{s}) y_\partial^i(t), & \boldsymbol{s} &\in \partial\Omega,
\end{aligned}
\tag{7.39}
$$

the finite dimensional system is obtained

$$
\begin{aligned}
\begin{bmatrix} \mathbf{M}_h & \mathbf{0} \\ \mathbf{0} & \mathbf{M}_v \end{bmatrix}
\begin{pmatrix} \dot{\boldsymbol{\alpha}}_{d,h} \\ \dot{\boldsymbol{\alpha}}_{d,v} \end{pmatrix}
&= -\begin{bmatrix} \mathbf{0} & -\mathbf{D}_{\text{grad}}^\top \\ \mathbf{D}_{\text{grad}} & \mathbf{0} \end{bmatrix}
\begin{pmatrix} \mathbf{e}_h \\ \mathbf{e}_v \end{pmatrix}
+ \begin{bmatrix} \mathbf{B}_h \\ \mathbf{0} \end{bmatrix} \mathbf{u}_\partial, \\
\begin{bmatrix} \mathbf{M}_h & \mathbf{0} \\ \mathbf{0} & \mathbf{M}_v \end{bmatrix}
\begin{pmatrix} \mathbf{e}_h \\ \mathbf{e}_v \end{pmatrix}
&= \begin{bmatrix} \partial_{\boldsymbol{\alpha}_{d,h}} H_d(\boldsymbol{\alpha}_{d,h},\, \boldsymbol{\alpha}_{d,v}) \\ \partial_{\boldsymbol{\alpha}_{d,v}} H_d(\boldsymbol{\alpha}_{d,h},\, \boldsymbol{\alpha}_{d,v}) \end{bmatrix}, \\
\mathbf{M}_\partial \mathbf{y}_\partial &= \begin{bmatrix} \mathbf{B}_h^\top & \mathbf{0} \end{bmatrix}
\begin{pmatrix} \mathbf{e}_h \\ \mathbf{e}_v \end{pmatrix}.
\end{aligned}
\tag{7.40}
$$

The matrices are defined as follows

$$
\begin{aligned}
M_h^{ij} &= \left\langle \phi_h^i,\, \phi_h^j \right\rangle_{L^2(\Omega)}\,, & D_{\text{grad}}^{mi} &= \left\langle \boldsymbol{\phi}_v^m,\, \operatorname{grad} \phi_h^i \right\rangle_{L^2(\Omega,\mathbb{R}^2)}\,, \\
M_v^{mn} &= \langle \boldsymbol{\phi}_v^m,\, \boldsymbol{\phi}_v^n \rangle_{L^2(\Omega,\mathbb{R}^2)}\,, & B_h^{ik} &= \left\langle \gamma_0 \phi_h^i,\, \phi_\partial^k \right\rangle_{L^2(\partial\Omega)}\,, \\
M_\partial^{lk} &= \left\langle \phi_\partial^l,\, \phi_\partial^k \right\rangle_{L^2(\partial\Omega)}\,,
\end{aligned}
\tag{7.41}
$$

where $i, j \in \{1, n_h\}$, $m, n \in \{1, n_v\}$, $l, k \in \{1, n_\partial\}$. The discretized gradient of the Hamiltonian reads

$$
\begin{aligned}
\partial_{\alpha_{d,h}^i} H_d(\boldsymbol{\alpha}_{d,h},\ \boldsymbol{\alpha}_{d,v}) &= \left\langle \phi_h^i,\ \frac{1}{2\rho} \left\| \sum_{r=1}^{n_v} \boldsymbol{\phi}_v^r \alpha_v^r \right\|^2 + \rho g \sum_{r=1}^{n_h} \phi_h^r \alpha_h^r \right\rangle_{L^2(\Omega)}, \qquad i \in \{1, n_h\}, \\
\partial_{\alpha_{d,v}^m} H_d(\boldsymbol{\alpha}_{d,h},\ \boldsymbol{\alpha}_{d,v}) &= \left\langle \boldsymbol{\phi}_v^m,\ \frac{1}{\rho} \left(\sum_{r=1}^{n_h} \phi_h^r \alpha_h^r \right) \left(\sum_{r=1}^{n_v} \boldsymbol{\phi}_v^r \alpha_v^r \right) \right\rangle_{L^2(\Omega, \mathbb{R}^2)}, \qquad m \in \{1, n_v\}.
\end{aligned}
\tag{7.42}
$$

One possible finite element discretization for this problem can be found in [Pir89]. The non linear nature of the problem strongly complicates the analysis. The presence of shocks has to be accounted for in the numerical discretization. The proposed methodology has to cope with finite time shocks to become a valid alternative to already well established strategies.

7.1.2 Linear case

The general framework detailed in Sec. 7.1.1 is valid for both linear and non linear systems. However, in the linear case a major simplification occurs since the constitutive law connecting energy and co-energy variables is easily invertible. This allows a description based on co-energy variables only.

To make the system linear, the additional assumption is introduced.

Assumption 4 (Quadratic separable Hamiltonian)
The Hamiltonian is assumed to be a positive quadratic functional in the energy variables $\boldsymbol{\alpha}_1$, $\boldsymbol{\alpha}_2$. *Furthermore, the Hamiltonian is considered to be separable with respect to* $\boldsymbol{\alpha}_1$, $\boldsymbol{\alpha}_2$ *(this hypothesis is always met for the systems under consideration). Therefore, it can be expressed as*

$$
H = \frac{1}{2} \langle \boldsymbol{\alpha}_1,\ \mathcal{Q}_1 \boldsymbol{\alpha}_1 \rangle_{L^2(\Omega, \mathbb{A})} + \frac{1}{2} \langle \boldsymbol{\alpha}_2,\ \mathcal{Q}_2 \boldsymbol{\alpha}_2 \rangle_{L^2(\Omega, \mathbb{B})}, \tag{7.43}
$$

where $\mathcal{Q}_1$, $\mathcal{Q}_2$ *are positive symmetric operators, bounded from below and above*

$$
m_1 \boldsymbol{I}_{\mathbb{A}} \leq \mathcal{Q}_1 \leq M_1 \boldsymbol{I}_{\mathbb{A}}, \qquad m_2 \boldsymbol{I}_{\mathbb{B}} \leq \mathcal{Q}_2 \leq M_2 \boldsymbol{I}_{\mathbb{B}}, \qquad m_1 > 0,\ m_2 > 0,\ M_1 > 0,\ M_2 > 0,
$$

where $\boldsymbol{I}_{\mathbb{A}}$, $\boldsymbol{I}_{\mathbb{B}}$ are the identity operators in $\mathbb{A}$, $\mathbb{B}$ respectively. Because of Assumption 4, the co-energy variables are given by

$$
\boldsymbol{e}_1 := \delta_{\alpha_1} H = \mathcal{Q}_1 \boldsymbol{\alpha}_1, \qquad \boldsymbol{e}_2 := \delta_{\alpha_2} H = \mathcal{Q}_2 \boldsymbol{\alpha}_2 \tag{7.44}
$$

Since $\mathcal{Q}_1$, $\mathcal{Q}_2$ are positive bounded from below and above, it is possible to invert them to obtain

$$
\boldsymbol{\alpha}_1 = \mathcal{Q}_1^{-1} \boldsymbol{e}_1 = \mathcal{M}_1 \boldsymbol{e}_1, \qquad \boldsymbol{\alpha}_2 = \mathcal{Q}_2^{-1} \boldsymbol{e}_2 = \mathcal{M}_2 \boldsymbol{e}_2, \qquad \mathcal{M}_1 := \mathcal{Q}_1^{-1},\ \mathcal{M}_2 := \mathcal{Q}_2^{-1}. \tag{7.45}
$$

The Hamiltonian is then written in terms of co-energy variables as

$$H = \frac{1}{2} \left\langle \boldsymbol{e}_1,\, \mathcal{M}_1 \boldsymbol{e}_1 \right\rangle_{L^2(\Omega,\mathbb{A})} + \frac{1}{2} \left\langle \boldsymbol{e}_2,\, \mathcal{M}_2 \boldsymbol{e}_2 \right\rangle_{L^2(\Omega,\mathbb{B})} . \tag{7.46}$$

Under assumptions 2, 3, 4, a pH linear system is expressed as

$$\begin{bmatrix} \mathcal{M}_1 & 0 \\ 0 & \mathcal{M}_2 \end{bmatrix} \partial_t \begin{pmatrix} \boldsymbol{e}_1 \\ \boldsymbol{e}_2 \end{pmatrix} = \begin{bmatrix} 0 & -\boldsymbol{L}^\top - \mathcal{L}^* \\ \boldsymbol{L} + \mathcal{L} & 0 \end{bmatrix} \begin{pmatrix} \boldsymbol{e}_1 \\ \boldsymbol{e}_2 \end{pmatrix}, \qquad \begin{aligned} \boldsymbol{e}_1 &\in H^{\mathcal{L}}, \\ \boldsymbol{e}_2 &\in H^{-\mathcal{L}^*}. \end{aligned} \tag{7.47}$$

If Eq. (7.9) holds the boundary variables equal

$$\boldsymbol{u}_\partial = \mathcal{N}_2 \boldsymbol{e}_2, \qquad \boldsymbol{y}_\partial = \mathcal{N}_1 \boldsymbol{e}_1, \qquad \boldsymbol{u}_\partial,\, \boldsymbol{y}_\partial \in \mathbb{R}^m. \tag{7.48}$$

Whereas if Eq. (7.10) holds, then

$$\boldsymbol{u}_\partial = \mathcal{N}_1 \boldsymbol{e}_1, \qquad \boldsymbol{y}_\partial = \mathcal{N}_2 \boldsymbol{e}_2, \qquad \boldsymbol{u}_\partial,\, \boldsymbol{y}_\partial \in \mathbb{R}^m. \tag{7.49}$$

From equation (7.46), the power balance reads

$$\begin{aligned} \dot{H} &= \left\langle \boldsymbol{e}_1,\, \mathcal{M}_1 \partial_t \boldsymbol{e}_1 \right\rangle_{L^2(\Omega,\mathbb{A})} + \left\langle \boldsymbol{e}_2,\, \mathcal{M}_2 \partial_t \boldsymbol{e}_2 \right\rangle_{L^2(\Omega,\mathbb{B})} , \\ &= \left\langle \boldsymbol{e}_1,\, -\mathcal{L}^* \boldsymbol{e}_2 \right\rangle_{L^2(\Omega,\mathbb{A})} + \left\langle \boldsymbol{e}_2,\, \mathcal{L} \boldsymbol{e}_1 \right\rangle_{L^2(\Omega,\mathbb{B})} , \\ &= \left\langle \mathcal{N}_{\partial,1} \boldsymbol{e}_1,\, \mathcal{N}_{\partial,2} \boldsymbol{e}_2 \right\rangle_{L^2(\partial\Omega,\mathbb{R}^m)} , \\ &= \left\langle \boldsymbol{y}_\partial,\, \boldsymbol{u}_\partial \right\rangle_{L^2(\partial\Omega,\mathbb{R}^m)} . \end{aligned} \tag{7.50}$$

To get a finite dimensional approximation the same procedure detailed in Sec. §7.1.1 is followed. The only difference is that there is no need to discretize the constitutive relations as those are already incorporated in the dynamics.

Once the system is put into weak form, if the operator $-\mathcal{L}^*$ is integrated by parts, one obtains the weak form

$$\begin{aligned} \left\langle \boldsymbol{v}_1,\, \mathcal{M}_1 \partial_t \boldsymbol{e}_1 \right\rangle_{L^2(\Omega,\mathbb{A})} &= -\left\langle \boldsymbol{v}_1,\, \boldsymbol{L}^\top \boldsymbol{e}_2 \right\rangle_{L^2(\Omega,\mathbb{A})} - \left\langle \mathcal{L} \boldsymbol{v}_1,\, \boldsymbol{e}_2 \right\rangle_{L^2(\Omega,\mathbb{B})} + \left\langle \mathcal{N}_{\partial,1} \boldsymbol{v}_1,\, \boldsymbol{u}_\partial \right\rangle_{L^2(\partial\Omega,\mathbb{R}^m)} , \\ \left\langle \boldsymbol{v}_2,\, \mathcal{M}_2 \partial_t \boldsymbol{e}_2 \right\rangle_{L^2(\Omega,\mathbb{B})} &= \left\langle \boldsymbol{v}_2,\, \boldsymbol{L} \boldsymbol{e}_1 \right\rangle_{L^2(\Omega,\mathbb{B})} + \left\langle \boldsymbol{v}_2,\, \mathcal{L} \boldsymbol{e}_1 \right\rangle_{L^2(\Omega,\mathbb{B})} , \\ \left\langle \boldsymbol{v}_\partial,\, \boldsymbol{y}_\partial \right\rangle_{L^2(\partial\Omega,\mathbb{R}^m)} &= \left\langle \boldsymbol{v}_\partial,\, \mathcal{N}_{\partial,1} \boldsymbol{e}_2 \right\rangle_{L^2(\partial\Omega,\mathbb{R}^m)} . \end{aligned} \tag{7.51}$$

Otherwise, if operator $\mathcal{L}$ is integrated by parts, it is computed

$$\begin{aligned} \left\langle \boldsymbol{v}_1,\, \mathcal{M}_1 \partial_t \boldsymbol{e}_1 \right\rangle_{L^2(\Omega,\mathbb{A})} &= -\left\langle \boldsymbol{v}_1,\, \boldsymbol{L}^\top \boldsymbol{e}_2 \right\rangle_{L^2(\Omega,\mathbb{A})} - \left\langle \boldsymbol{v}_1,\, \mathcal{L}^* \boldsymbol{e}_2 \right\rangle_{L^2(\Omega,\mathbb{A})} , \\ \left\langle \boldsymbol{v}_2,\, \mathcal{M}_2 \partial_t \boldsymbol{e}_2 \right\rangle_{L^2(\Omega,\mathbb{B})} &= \left\langle \boldsymbol{v}_2,\, \boldsymbol{L} \boldsymbol{e}_1 \right\rangle_{L^2(\Omega,\mathbb{B})} + \left\langle \mathcal{L}^* \boldsymbol{v}_2,\, \boldsymbol{e}_1 \right\rangle_{L^2(\Omega,\mathbb{A})} + \left\langle \mathcal{N}_{\partial,2} \boldsymbol{v}_2,\, \boldsymbol{u}_\partial \right\rangle_{L^2(\partial\Omega,\mathbb{R}^m)} , \\ \left\langle \boldsymbol{v}_\partial,\, \boldsymbol{y}_\partial \right\rangle_{L^2(\partial\Omega,\mathbb{R}^m)} &= \left\langle \boldsymbol{v}_\partial,\, \mathcal{N}_{\partial,2} \boldsymbol{e}_2 \right\rangle_{L^2(\partial\Omega,\mathbb{R}^m)} . \end{aligned} \tag{7.52}$$

After introducing a Galerkin approximation as in (7.23), the discretized version of the weak form (7.51) reads

$$
\begin{aligned}
\begin{bmatrix}
\mathbf{M}_{\mathcal{M}_1} & \mathbf{0} \\
\mathbf{0} & \mathbf{M}_{\mathcal{M}_2}
\end{bmatrix}
\begin{pmatrix}
\dot{\mathbf{e}}_1 \\
\dot{\mathbf{e}}_2
\end{pmatrix}
&=
\begin{bmatrix}
\mathbf{0} & -\mathbf{D}_0^\top - \mathbf{D}_{\mathcal{L}}^\top \\
\mathbf{D}_0 + \mathbf{D}_{\mathcal{L}} & \mathbf{0}
\end{bmatrix}
\begin{pmatrix}
\mathbf{e}_1 \\
\mathbf{e}_2
\end{pmatrix}
+
\begin{bmatrix}
\mathbf{B}_1 \\
\mathbf{0}
\end{bmatrix}
\mathbf{u}_\partial, \\
\mathbf{M}_\partial \mathbf{y}_\partial &= \begin{bmatrix} \mathbf{B}_1^\top & \mathbf{0} \end{bmatrix}
\begin{pmatrix}
\mathbf{e}_1 \\
\mathbf{e}_2
\end{pmatrix}.
\end{aligned}
\tag{7.53}
$$

The only difference with respect to Eq. (7.24) concerns the mass matrices

$$
M_{\mathcal{M}_1}^{ij} = \left\langle \boldsymbol{\phi}_1^i, \, \mathcal{M}_1 \boldsymbol{\phi}_1^j \right\rangle_{L^2(\Omega, \mathbb{A})}, \qquad M_{\mathcal{M}_2}^{mn} = \langle \boldsymbol{\phi}_2^m, \, \mathcal{M}_2 \boldsymbol{\phi}_2^n \rangle_{L^2(\Omega, \mathbb{B})} \qquad i, j \in \{1, n_1\}, \; m, n \in \{1, n_2\}.
\tag{7.54}
$$

If the Galerkin approximation is applied to the weak form (7.52), it is obtained

$$
\begin{aligned}
\begin{bmatrix}
\mathbf{M}_{\mathcal{M}_1} & \mathbf{0} \\
\mathbf{0} & \mathbf{M}_{\mathcal{M}_2}
\end{bmatrix}
\begin{pmatrix}
\dot{\mathbf{e}}_1 \\
\dot{\mathbf{e}}_2
\end{pmatrix}
&=
\begin{bmatrix}
\mathbf{0} & -\mathbf{D}_0^\top + \mathbf{D}_{-\mathcal{L}^*} \\
\mathbf{D}_0 - \mathbf{D}_{-\mathcal{L}^*}^\top & \mathbf{0}
\end{bmatrix}
\begin{pmatrix}
\mathbf{e}_1 \\
\mathbf{e}_2
\end{pmatrix}
+
\begin{bmatrix}
\mathbf{0} \\
\mathbf{B}_2
\end{bmatrix}
\mathbf{u}_\partial, \\
\mathbf{M}_\partial \mathbf{y}_\partial &= \begin{bmatrix} \mathbf{0} & \mathbf{B}_2^\top \end{bmatrix}
\begin{pmatrix}
\mathbf{e}_1 \\
\mathbf{e}_2
\end{pmatrix}.
\end{aligned}
\tag{7.55}
$$

In both cases, it is easy to verify that the Hamiltonian

$$
H_d = \frac{1}{2} \mathbf{e}_1^\top \mathbf{M}_{\mathcal{M}_1} \mathbf{e}_1 + \frac{1}{2} \mathbf{e}_2^\top \mathbf{M}_{\mathcal{M}_2} \mathbf{e}_2,
\tag{7.56}
$$

once differentiated in time, provides the energy rate

$$
\dot{H}_d = \mathbf{y}_\partial^\top \mathbf{M}_\partial \mathbf{u}_\partial = \widehat{\mathbf{y}}_\partial^\top \mathbf{u}_\partial, \qquad \text{where} \qquad \widehat{\mathbf{y}}_\partial := \mathbf{M}_\partial \mathbf{y}_\partial.
\tag{7.57}
$$

This result mimics its finite dimensional counterpart (7.50).

7.1.3 Linear flexible structures

In this section, some linear examples from the elasticity realms are considered. We restrict the discussion to linear problems. This case is anyway significant, as these examples are frequently encountered in engineering applications.

7.1.3.1 Euler-Bernoulli beam

We reconsider the example discussed in Sec. §3.3.2. The relation between energy and co-energy variables is given by Eqs. (3.25), (3.27)

$$
\alpha_w = \rho A \; e_w, \qquad \alpha_\kappa = \frac{1}{EI} \; e_\kappa
\tag{7.58}
$$

The coefficients ρ, A, E and I are the mass density, the cross section area, Young's modulus of elasticity and the moment of inertia of the cross section.

Control through forces and torques Given an interval $\Omega = (0,\, L)$, a thin beam under free boundary condition (forces and torques imposed at the boundary) can be modeled in terms of co-energy variables by the following system

$$
\begin{aligned}
\begin{bmatrix} \rho A & 0 \\ 0 & (EI)^{-1} \end{bmatrix} \frac{\partial}{\partial t} \begin{pmatrix} e_w \\ e_\kappa \end{pmatrix} &= \begin{bmatrix} 0 & -\partial_{xx} \\ \partial_{xx} & 0 \end{bmatrix} \begin{pmatrix} e_w \\ e_\kappa \end{pmatrix}, \qquad & \begin{matrix} e_w \in H^2(\Omega), \\ e_\kappa \in H^2(\Omega), \end{matrix} \qquad & (7.59a) \\
\boldsymbol{u}_\partial &= \begin{bmatrix} 0 & \boldsymbol{\gamma}_0 \\ 0 & -\boldsymbol{\gamma}_1 \end{bmatrix} \begin{pmatrix} e_w \\ e_\kappa \end{pmatrix}, \qquad & \boldsymbol{u}_\partial \in \mathbb{R}^4, \qquad & (7.59b) \\
\boldsymbol{y}_\partial &= \begin{bmatrix} \boldsymbol{\gamma}_1 & 0 \\ \boldsymbol{\gamma}_0 & 0 \end{bmatrix} \begin{pmatrix} e_w \\ e_\kappa \end{pmatrix}, \qquad & \boldsymbol{y}_\partial \in \mathbb{R}^4. \qquad & (7.59c)
\end{aligned}
$$

The boundary operators $\boldsymbol{\gamma}_0,\, \boldsymbol{\gamma}_1$ denote the trace and the first derivative trace along the boundary. In a one-dimensional domain the boundary degenerates to two single points

$$
\boldsymbol{\gamma}_0 a = a|_{\partial\Omega} = \begin{pmatrix} -a(0) \\ +a(L) \end{pmatrix}, \qquad \boldsymbol{\gamma}_1 a = \partial_{\boldsymbol{n}} a|_{\partial\Omega} = \begin{pmatrix} -\partial_x a(0) \\ +\partial_x a(L) \end{pmatrix}. \tag{7.60}
$$

In this case $\mathbb{A} = \mathbb{B} = \mathbb{R}$. The operators $\mathcal{M}_1,\, \mathcal{M}_2,\, \mathcal{L},\, N_{\partial,1},\, N_{\partial,2}$ read

$$
\mathcal{M}_1 = \rho A, \qquad \mathcal{M}_2 = (EI)^{-1}, \qquad \mathcal{L} = \partial_{xx}, \qquad N_{\partial,1} = \begin{bmatrix} \boldsymbol{\gamma}_1 \\ \boldsymbol{\gamma}_0 \end{bmatrix}, \qquad N_{\partial,2} = \begin{bmatrix} \boldsymbol{\gamma}_0 \\ -\boldsymbol{\gamma}_1 \end{bmatrix}. \tag{7.61}
$$

The Hamiltonian is given by

$$
H = \frac{1}{2} \int_\Omega \left\{ \rho A \ e_w^2 + (EI)^{-1} \ e_\kappa^2 \right\} \, \mathrm{d}\Omega. \tag{7.62}
$$

Applying twice the integration by parts formula, one obtains the power balance

$$
\begin{aligned}
\dot{H} &= \langle e_w,\, \rho A \ \partial_t e_w \rangle_{L^2(\Omega)} + \left\langle e_\kappa,\, (EI)^{-1} \ \partial_t e_\kappa \right\rangle_{L^2(\Omega)}, \\
&= \langle e_w,\, -\partial_{xx} e_\kappa \rangle_{L^2(\Omega)} + \langle e_\kappa,\, \partial_{xx} e_w \rangle_{L^2(\Omega)}, \\
&= \langle \boldsymbol{\gamma}_1 e_w,\, \boldsymbol{\gamma}_0 e_\kappa \rangle_{\mathbb{R}^2} + \langle \boldsymbol{\gamma}_0 e_w,\, -\boldsymbol{\gamma}_1 e_\kappa \rangle_{\mathbb{R}^2}, \\
&= \langle \boldsymbol{y}_\partial,\, \boldsymbol{u}_\partial \rangle_{\mathbb{R}^4}.
\end{aligned} \tag{7.63}
$$

Given the test functions $v_w,\, v_\kappa$, the weak form is readily obtained as

$$
\begin{aligned}
\langle v_w,\, \rho A \partial_t e_w \rangle_{L^2(\Omega)} &= \langle v_w,\, -\partial_{xx} e_\kappa \rangle_{L^2(\Omega)}, \\
\left\langle v_\kappa,\, (EI)^{-1} \partial_t e_\kappa \right\rangle_{L^2(\Omega)} &= \langle v_\kappa,\, \partial_{xx} e_w \rangle_{L^2(\Omega)}.
\end{aligned} \tag{7.64}
$$

If the integration by parts is applied twice to the first line of Eq. (7.59a), it is obtained

$$
\begin{aligned}
\langle v_w,\, \rho A \partial_t e_w \rangle_{L^2(\Omega)} &= -\langle \partial_{xx} v_w,\, e_\kappa \rangle_{L^2(\Omega)} + \langle \gamma_1 v_w,\, (u_{\partial,1}, u_{\partial,2}) \rangle_{\mathbb{R}^2} + \langle \gamma_0 v_w,\, (u_{\partial,3}, u_{\partial,4}) \rangle_{\mathbb{R}^2}, \\
\left\langle v_\kappa,\, (EI)^{-1} \partial_t e_\kappa \right\rangle_{L^2(\Omega)} &= \langle v_\kappa,\, \partial_{xx} e_w \rangle_{L^2(\Omega)}.
\end{aligned}
\tag{7.65}
$$

Introducing a Galerkin discretization for test and efforts functions

$$
v_w = \sum_{i=1}^{n_w} \phi_w^i v_w^i, \qquad e_w = \sum_{i=1}^{n_w} \phi_w^i e_w^i(t), \qquad v_\kappa = \sum_{i=1}^{n_\kappa} \phi_\kappa^i v_\kappa^i, \qquad e_\kappa = \sum_{i=1}^{n_\kappa} \phi_\kappa^i e_\kappa^i(t), \tag{7.66}
$$

and considering that $\boldsymbol{u}_\partial \in \mathbb{R}^4, \boldsymbol{y}_\partial \in \mathbb{R}^4$, the following is obtained

$$
\begin{aligned}
\begin{bmatrix} \mathbf{M}_{\rho A} & \mathbf{0} \\ \mathbf{0} & \mathbf{M}_{EI^{-1}} \end{bmatrix} \begin{pmatrix} \dot{\mathbf{e}}_w \\ \dot{\mathbf{e}}_\kappa \end{pmatrix} &= \begin{bmatrix} \mathbf{0} & -\mathbf{D}_{\partial_{xx}}^\top \\ \mathbf{D}_{\partial_{xx}} & \mathbf{0} \end{bmatrix} \begin{pmatrix} \mathbf{e}_w \\ \mathbf{e}_\kappa \end{pmatrix} + \begin{bmatrix} \mathbf{B}_w \\ \mathbf{0} \end{bmatrix} \mathbf{u}_\partial, \\
\mathbf{y}_\partial &= \begin{bmatrix} \mathbf{B}_w^\top & \mathbf{0} \end{bmatrix} \begin{pmatrix} \mathbf{e}_w \\ \mathbf{e}_\kappa \end{pmatrix}.
\end{aligned}
\tag{7.67}
$$

The matrices $\mathbf{M}_{\rho A},\ \mathbf{M}_{EI^{-1}},\ \mathbf{D}_{\partial_{xx}}$ are defined as $(i, j \in \{1, n_w\},\ m, n \in \{1, n_\kappa\})$

$$
M_{\rho A}^{ij} = \left\langle \phi_w^i,\, \rho A \phi_w^j \right\rangle_{L^2(\Omega)}, \quad M_{EI^{-1}}^{mn} = \left\langle \phi_\kappa^m,\, (EI)^{-1} \phi_\kappa^n \right\rangle_{L^2(\Omega)}, \quad D_{\partial_{xx}}^{mi} = \left\langle \phi_\kappa^m,\, \partial_{xx} \phi_w^i \right\rangle_{L^2(\Omega)}. \tag{7.68}
$$

The $\mathbf{B}_w$ is composed of four column vectors $\mathbf{B}_w = [\mathbf{b}_w^1\ \mathbf{b}_w^2\ \mathbf{b}_w^3\ \mathbf{b}_w^4]$

$$
b_w^{1,i} = -\partial_x \phi_w^i(0), \qquad b_w^{2,i} = \partial_x \phi_w^i(L), \qquad b_w^{3,i} = -\phi_w^i(0), \qquad b_w^{4,i} = \phi_w^i(L), \qquad i \in \{1, n_w\}. \tag{7.69}
$$

Control through linear and angular velocities Equivalently, the second line of Eq. (7.59a) could have been integrated by parts to control using the linear and angular velocities at the extremities. Consider the system with known forces and torques at the extremities

$$
\begin{bmatrix} \rho A & 0 \\ 0 & (EI)^{-1} \end{bmatrix} \frac{\partial}{\partial t} \begin{pmatrix} e_w \\ e_\kappa \end{pmatrix} = \begin{bmatrix} 0 & -\partial_{xx} \\ \partial_{xx} & 0 \end{bmatrix} \begin{pmatrix} e_w \\ e_\kappa \end{pmatrix}, \qquad \begin{aligned} e_w &\in H^2(\Omega), \\ e_\kappa &\in H^2(\Omega), \end{aligned} \tag{7.70a}
$$

$$
\boldsymbol{u}_\partial = \begin{bmatrix} \gamma_1 & 0 \\ \gamma_0 & 0 \end{bmatrix} \begin{pmatrix} e_w \\ e_\kappa \end{pmatrix}, \qquad \boldsymbol{u}_\partial \in \mathbb{R}^4, \tag{7.70b}
$$

$$
\boldsymbol{y}_\partial = \begin{bmatrix} 0 & \gamma_0 \\ 0 & -\gamma_1 \end{bmatrix} \begin{pmatrix} e_w \\ e_\kappa \end{pmatrix}, \qquad \boldsymbol{y}_\partial \in \mathbb{R}^4. \tag{7.70c}
$$

Once the system is put into weak form and the second line of Eq. (7.70a) is integrated twice, it is computed

$$
\begin{aligned}
\langle v_w,\, \rho A \partial_t e_w \rangle_{L^2(\Omega)} &= \langle v_w,\, -\partial_{xx} e_\kappa \rangle_{L^2(\Omega)}, \\
\left\langle v_\kappa,\, (EI)^{-1} \partial_t e_\kappa \right\rangle_{L^2(\Omega)} &= \langle \partial_{xx} v_\kappa,\, e_w \rangle_{L^2(\Omega)} + \langle \gamma_0 v_\kappa,\, (u_{\partial,1}, u_{\partial,2}) \rangle_{\mathbb{R}^2} + \langle -\gamma_1 v_\kappa,\, (u_{\partial,3}, u_{\partial,4}) \rangle_{\mathbb{R}^2}.
\end{aligned}
\tag{7.71}
$$

Replacing a Galerkin approximation, it is obtained

$$\begin{gathered}\begin{bmatrix}\mathbf{M}_{\rho A} & \mathbf{0} \\ \mathbf{0} & \mathbf{M}_{EI^{-1}}\end{bmatrix}\begin{pmatrix}\dot{\mathbf{e}}_w \\ \dot{\mathbf{e}}_\kappa\end{pmatrix} = \begin{bmatrix}\mathbf{0} & \mathbf{D}_{-\partial_{xx}} \\ -\mathbf{D}_{-\partial_{xx}}^\top & \mathbf{0}\end{bmatrix}\begin{pmatrix}\mathbf{e}_w \\ \mathbf{e}_\kappa\end{pmatrix} + \begin{bmatrix}\mathbf{0} \\ \mathbf{B}_\kappa\end{bmatrix}\mathbf{u}_\partial, \\ \mathbf{y}_\partial = \begin{bmatrix}\mathbf{0} & \mathbf{B}_\kappa^\top\end{bmatrix}\begin{pmatrix}\mathbf{e}_w \\ \mathbf{e}_\kappa\end{pmatrix}.\end{gathered} \tag{7.72}$$

The matrix $\mathbf{D}_{-\partial_{xx}}$ is defined as

$$D^{im}_{-\partial_{xx}} = \left\langle \phi_w^i, -\partial_{xx}\phi_\kappa^m \right\rangle_{L^2(\Omega)}, \qquad i, \in \{1, n_w\},\ m \in \{1, n_\kappa\}. \tag{7.73}$$

The $\mathbf{B}_\kappa$ is composed of four column vectors $\mathbf{B}_\kappa = [\mathbf{b}_\kappa^1\ \mathbf{b}_\kappa^2\ \mathbf{b}_\kappa^3\ \mathbf{b}_\kappa^4]$

$$b_\kappa^{1,m} = -\phi_\kappa^m(0), \quad b_\kappa^{2,m} = \phi_\kappa^m(L), \quad b_\kappa^{3,m} = \partial_x\phi_\kappa^m(0), \quad b_\kappa^{4,m} = -\partial_x\phi_\kappa^m(L), \quad m \in \{1, n_\kappa\}. \tag{7.74}$$

Both discretizations require the use of Hermite polynomials to meet the regularity requirement. Indeed, to lower the regularity requirement for the finite elements employed in the discretization, both lines can be integrated by parts. This will be discussed in Chap. 8.

7.1.3.2 Kirchhoff plate

The link beetween the energy and co-energy variables for the isotropic Kirchhoff model is the following (5.33)

$$\alpha_w = \rho h e_w, \qquad \boldsymbol{A}_\kappa = \boldsymbol{\mathcal{C}}_b \boldsymbol{E}_\kappa, \qquad \text{where} \qquad \boldsymbol{\mathcal{C}}_b := \boldsymbol{\mathcal{D}}_b^{-1} \tag{7.75}$$

where ρ is the mass density, h the plate thickness and $\boldsymbol{\mathcal{D}}_b$, the bending rigidity tensor, cf. Eq. (5.11). The bending compliance is given by

$$\boldsymbol{\mathcal{C}}_b = \frac{12}{Eh^3}[(1+\nu)(\cdot) - \nu\,\mathrm{Tr}(\cdot)\boldsymbol{I}_{2\times 2}]. \tag{7.76}$$

Given an open connected set $\Omega \subset \mathbb{R}^2$, the Kirchhoff plate model (5.42) in co-energy form controlled by forces and momenta is then expressed as

$$\begin{bmatrix}\rho h & 0 \\ 0 & \boldsymbol{\mathcal{C}}_b\end{bmatrix}\frac{\partial}{\partial t}\begin{pmatrix}e_w \\ \boldsymbol{E}_\kappa\end{pmatrix} = \begin{bmatrix}0 & -\operatorname{div}\operatorname{Div} \\ \operatorname{Hess} & \mathbf{0}\end{bmatrix}\begin{pmatrix}e_w \\ \boldsymbol{E}_\kappa\end{pmatrix}, \qquad \begin{aligned}&e_w \in H^2(\Omega), \\ &\boldsymbol{E}_\kappa \in H^{\operatorname{div}\operatorname{Div}}(\Omega, \mathbb{R}^{2\times 2}_{\text{sym}}),\end{aligned} \tag{7.77a}$$

$$\boldsymbol{u}_\partial = \begin{bmatrix}0 & \gamma_{nn,1} \\ 0 & \gamma_{nn}\end{bmatrix}\begin{pmatrix}e_w \\ \boldsymbol{E}_\kappa\end{pmatrix}, \qquad \boldsymbol{u}_\partial \in \mathbb{R}^2, \tag{7.77b}$$

$$\boldsymbol{y}_\partial = \begin{bmatrix}\gamma_0 & 0 \\ \gamma_1 & 0\end{bmatrix}\begin{pmatrix}e_w \\ \boldsymbol{E}_\kappa\end{pmatrix}, \qquad \boldsymbol{y}_\partial \in \mathbb{R}^2, \tag{7.77c}$$

We recall the expressions of the trace maps

$$
\begin{aligned}
\gamma_0 a &= a|_{\partial\Omega}, \qquad & \gamma_{nn,1}\boldsymbol{A} &= -\boldsymbol{n}\cdot \mathrm{Div}\,\boldsymbol{A} - \partial_{\boldsymbol{s}}(\boldsymbol{A} : (\boldsymbol{n}\otimes \boldsymbol{s}))|_{\partial\Omega}, \\
\gamma_1 a &= \partial_{\boldsymbol{n}} a|_{\partial\Omega}, \qquad & \gamma_{nn}\boldsymbol{A} &= \boldsymbol{A} : (\boldsymbol{n}\otimes\boldsymbol{n})|_{\partial\Omega}.
\end{aligned} \tag{7.78}
$$

In this case, the sets are $\mathbb{A} = \mathbb{R}$, $\mathbb{B} = \mathbb{R}^{2\times 2}_{\mathrm{sym}}$. The operators $\mathcal{M}_1$, $\mathcal{M}_2$, $\mathcal{L}$, $N_{\partial,1}$, $N_{\partial,2}$ are

$$
\mathcal{M}_1 = \rho h, \qquad \mathcal{M}_2 = \boldsymbol{\mathcal{C}}_b, \qquad \mathcal{L} = \mathrm{Hess}, \qquad N_{\partial,1} = \begin{bmatrix} \gamma_0 \\ \gamma_1 \end{bmatrix}, \qquad N_{\partial,2} = \begin{bmatrix} \gamma_{nn,1} \\ \gamma_{nn} \end{bmatrix}. \tag{7.79}
$$

The energy rate from Eq. (5.39) equals $\dot{H} = \langle \boldsymbol{y}_\partial,\, \boldsymbol{u}_\partial \rangle_{L^2(\partial\Omega,\mathbb{R}^2)}$. Introducing the test functions $(v_w,\, \boldsymbol{V}_\kappa)$ and integrating by parts twice the first line of (7.77a) one gets

$$
\begin{aligned}
&\langle v_w,\, \rho h \partial_t e_w \rangle_{L^2(\Omega)} = -\langle \mathrm{Hess}\, v_w,\, \boldsymbol{E}_\kappa \rangle_{L^2(\Omega,\mathbb{R}^{2\times 2}_{\mathrm{sym}})} + \langle \gamma_0 v_w,\, u_{\partial,1} \rangle_{L^2(\partial\Omega)} + \langle \gamma_1 v_w,\, u_{\partial,2} \rangle_{L^2(\partial\Omega)}, \\
&\langle \boldsymbol{V}_\kappa,\, \boldsymbol{\mathcal{C}}_{\boldsymbol{b}} \partial_t \boldsymbol{V}_\kappa \rangle_{L^2(\Omega,\mathbb{R}^{2\times 2}_{\mathrm{sym}})} = \langle \boldsymbol{V}_\kappa,\, \mathrm{Hess}\, e_w \rangle_{L^2(\Omega,\mathbb{R}^{2\times 2}_{\mathrm{sym}})}.
\end{aligned} \tag{7.80}
$$

Introducing a Galerkin discretization for test and efforts functions

$$
\begin{aligned}
v_w &= \sum_{i=1}^{n_w} \phi_w^i v_w^i, \qquad & \boldsymbol{V}_\kappa &= \sum_{i=1}^{n_\kappa} \boldsymbol{\Phi}_\kappa^i v_\kappa^i, \qquad & \boldsymbol{v}_\partial &= \sum_{i=1}^{n_\partial} \boldsymbol{\phi}_\partial^i v_\partial^i, \\
e_w &= \sum_{i=1}^{n_w} \phi_w^i e_w^i, \qquad & \boldsymbol{E}_\kappa &= \sum_{i=1}^{n_\kappa} \boldsymbol{\Phi}_\kappa^i e_\kappa^i \qquad & \boldsymbol{u}_\partial &= \sum_{i=1}^{n_\partial} \boldsymbol{\phi}_\partial^i u_\partial^i,
\end{aligned}
\qquad \boldsymbol{y}_\partial = \sum_{i=1}^{n_\partial} \boldsymbol{\phi}_\partial^i y_\partial^i. \tag{7.81}
$$

the following finite dimensional system is obtained

$$
\begin{aligned}
\begin{bmatrix} \mathbf{M}_{\rho h} & \mathbf{0} \\ \mathbf{0} & \mathbf{M}_{\mathcal{C}_b} \end{bmatrix}
\begin{pmatrix} \dot{\mathbf{e}}_w \\ \dot{\mathbf{e}}_\kappa \end{pmatrix}
&= \begin{bmatrix} \mathbf{0} & -\mathbf{D}_{\mathrm{Hess}}^\top \\ \mathbf{D}_{\mathrm{Hess}} & \mathbf{0} \end{bmatrix}
\begin{pmatrix} \mathbf{e}_w \\ \mathbf{e}_\kappa \end{pmatrix}
+ \begin{bmatrix} \mathbf{B}_w & \mathbf{B}_{\partial_{\boldsymbol{n}} w} \\ \mathbf{0} & \mathbf{0} \end{bmatrix} \mathbf{u}_\partial, \\
\mathbf{M}_\partial \mathbf{y}_\partial &= \begin{bmatrix} \mathbf{B}_w^\top & \mathbf{0} \\ \mathbf{B}_{\partial_{\boldsymbol{n}} w}^\top & \mathbf{0} \end{bmatrix}
\begin{pmatrix} \mathbf{e}_w \\ \mathbf{e}_\kappa \end{pmatrix}.
\end{aligned} \tag{7.82}
$$

The matrices $\mathbf{M}_{\rho h}$, $\mathbf{M}_{\mathcal{C}_b}$, $\mathbf{D}_{\mathrm{Hess}}$ are defined as $(i, j \in \{1, n_w\},\ m, n \in \{1, n_\kappa\})$

$$
M_{\rho h}^{ij} = \left\langle \phi_w^i,\, \rho h \phi_w^j \right\rangle_{L^2(\Omega)}, \qquad M_{\mathcal{C}_b}^{mn} = \langle \boldsymbol{\Phi}_\kappa^m,\, \boldsymbol{\mathcal{C}}_b \boldsymbol{\Phi}_\kappa^n \rangle_{L^2(\Omega,\mathbb{R}^{2\times 2}_{\mathrm{sym}})}, \qquad D_{\mathrm{Hess}}^{mi} = \left\langle \boldsymbol{\Phi}_\kappa^m,\, \mathrm{Hess}\, \phi_w^i \right\rangle_{L^2(\Omega)}. \tag{7.83}
$$

Matrices $\mathbf{B}_w$, $\mathbf{B}_{\partial_{\boldsymbol{n}} w}$ are given by

$$
B_w^{il} = \left\langle \gamma_0 \phi_w^i,\, \phi_{\partial,1}^l \right\rangle_{L^2(\partial\Omega)}, \qquad B_{\partial_{\boldsymbol{n}} w}^{il} = \left\langle \gamma_1 \phi_w^i,\, \phi_{\partial,2}^l \right\rangle_{L^2(\partial\Omega)}, \qquad l \in \{1, n_\partial\}. \tag{7.84}
$$

This kind of discretization requires H^2 conforming elements. The construction of those is rather involved [AFS68, Bel69] and they are computationally expensive. Nevertheless, this kind of discretization is able to handle generic boundary conditions [GSV18]. For this reason, it is the most adapted for the pH framework.

To lower the regularity requirement for the finite elements many non conforming elements have been proposed. The most employed is the Hellan-Herrmann-Johnson element [AB85, BR90]. However, this method does not handle generic non homogeneous boundary conditions. Given the unavailability of the boundary for interconnections, the modularity feature of pHs cannot be fully exploited.

Remark 10 (On the $H^{\mathrm{div}\,\mathrm{Div}}$ space)
Equivalently, the second line of Eq. (7.77a) *can be integrated by parts twice to obtain a discretized system whose inputs are the linear velocity and the angular velocity at the boundary. However, while for the* H^2 *space conforming finite elements are available, for the* $H^{\mathrm{div}\,\mathrm{Div}}$ *no conforming finite elements have been proposed. This makes the discretization unfeasible.*

7.1.3.3 Mindlin plate

Using Eqs. (5.22) and (5.24), the relation between co-energy and energy variables for the isotropic Mindlin plate is found to be

$$\begin{aligned} \alpha_w &= \rho h e_w, \qquad & \boldsymbol{\alpha}_\theta &= I_\theta \boldsymbol{e}_\theta, \qquad & I_\theta &:= \rho h^3/12, \\ \boldsymbol{A}_\kappa &= \boldsymbol{\mathcal{C}}_b \boldsymbol{E}_\kappa, \qquad & \boldsymbol{\alpha}_\gamma &= C_s \boldsymbol{e}_\gamma, \qquad & C_s &:= 1/(K_{\mathrm{sh}} G h), \end{aligned} \tag{7.85}$$

where K_{sh} is the shear correction factor, G the shear modulus. The other variables have the same meaning as in Sec. §7.1.3.2.

Control through forces and torques A pH representation in co-energy variables with known forces and momenta at the boundary is given by the system

$$
\begin{bmatrix}
\rho h & 0 & 0 & 0 \\
\mathbf{0} & I_\theta & \mathbf{0} & \mathbf{0} \\
\mathbf{0} & \mathbf{0} & \boldsymbol{\mathcal{C}}_b & \mathbf{0} \\
\mathbf{0} & \mathbf{0} & \mathbf{0} & C_s
\end{bmatrix}
\frac{\partial}{\partial t}
\begin{pmatrix} e \\ \boldsymbol{e}_\theta \\ \boldsymbol{E}_\kappa \\ \boldsymbol{e}_\gamma \end{pmatrix}
=
\begin{bmatrix}
0 & 0 & 0 & \mathrm{div} \\
\mathbf{0} & \mathbf{0} & \mathrm{Div} & \boldsymbol{I}_{2\times 2} \\
\mathbf{0} & \mathrm{Grad} & \mathbf{0} & \mathbf{0} \\
\mathrm{grad} & -\boldsymbol{I}_{2\times 2} & \mathbf{0} & \mathbf{0}
\end{bmatrix}
\begin{pmatrix} e_w \\ \boldsymbol{e}_\theta \\ \boldsymbol{E}_\kappa \\ \boldsymbol{e}_\gamma \end{pmatrix},
\qquad
\begin{aligned}
e_w &\in H^1(\Omega), \\
\boldsymbol{e}_\theta &\in H^{\mathrm{Grad}}(\Omega, \mathbb{R}^2), \\
\boldsymbol{E}_\kappa &\in H^{\mathrm{Div}}(\Omega, \mathbb{R}^{2\times 2}_{\mathrm{sym}}), \\
\boldsymbol{e}_\gamma &\in H^{\mathrm{div}}(\Omega, \mathbb{R}^2),
\end{aligned}
\tag{7.86a}
$$

$$
\boldsymbol{u}_\partial =
\begin{bmatrix}
0 & 0 & 0 & \gamma_n \\
0 & 0 & \gamma_{nn} & 0 \\
0 & 0 & \gamma_{ns} & 0
\end{bmatrix}
\begin{pmatrix} e_w \\ \boldsymbol{e}_\theta \\ \boldsymbol{E}_\kappa \\ \boldsymbol{e}_\gamma \end{pmatrix},
\qquad \boldsymbol{u}_\partial \in \mathbb{R}^3,
\tag{7.86b}
$$

$$
\boldsymbol{y}_\partial =
\begin{bmatrix}
\gamma_0 & 0 & 0 & 0 \\
0 & \gamma_n & 0 & 0 \\
0 & \gamma_s & 0 & 0
\end{bmatrix}
\begin{pmatrix} e_w \\ \boldsymbol{e}_\theta \\ \boldsymbol{E}_\kappa \\ \boldsymbol{e}_\gamma \end{pmatrix},
\qquad \boldsymbol{y}_\partial \in \mathbb{R}^3.
\tag{7.86c}
$$

The trace operators are defined as

$$
\gamma_0 a = a|_{\partial\Omega}, \qquad
\begin{aligned}
\gamma_n \boldsymbol{a} &= \boldsymbol{a} \cdot \boldsymbol{n}|_{\partial\Omega}, \qquad & \gamma_{nn} \boldsymbol{A} &= \boldsymbol{A} : (\boldsymbol{n} \otimes \boldsymbol{n})|_{\partial\Omega}, \\
\gamma_s \boldsymbol{a} &= \boldsymbol{a} \cdot \boldsymbol{s}|_{\partial\Omega}, \qquad & \gamma_{ns} \boldsymbol{A} &= \boldsymbol{A} : (\boldsymbol{n} \otimes \boldsymbol{s})|_{\partial\Omega}.
\end{aligned}
\tag{7.87}
$$

The variables assume values in the sets $\mathbb{A} = \mathbb{R} \times \mathbb{R}^2$, $\mathbb{B} = \mathbb{R}^{2\times 2}_{\mathrm{sym}} \times \mathbb{R}^2$. The mass operators are given by

$$
\mathcal{M}_1 = \begin{bmatrix} \rho h & 0 \\ \mathbf{0} & I_\theta \end{bmatrix}, \qquad
\mathcal{M}_2 = \begin{bmatrix} \boldsymbol{\mathcal{C}}_b & \mathbf{0} \\ \mathbf{0} & C_s \end{bmatrix}.
\tag{7.88}
$$

The $\boldsymbol{L}$, $\mathcal{L}$, $\mathcal{N}_{\partial,1}$, $\mathcal{N}_{\partial,1}$ operators are

$$
\boldsymbol{L} = \begin{bmatrix} \mathbf{0} & \mathbf{0} \\ \mathbf{0} & -\boldsymbol{I}_{2\times 2} \end{bmatrix}, \qquad
\mathcal{L} = \begin{bmatrix} \mathbf{0} & \mathrm{Grad} \\ \mathrm{grad} & \mathbf{0} \end{bmatrix}, \qquad
\mathcal{N}_{\partial,1} = \begin{bmatrix} \gamma_0 & 0 \\ 0 & \gamma_n \\ 0 & \gamma_s \end{bmatrix}, \qquad
\mathcal{N}_{\partial,2} = \begin{bmatrix} 0 & \gamma_n \\ \gamma_{nn} & 0 \\ \gamma_{ns} & 0 \end{bmatrix}.
\tag{7.89}
$$

The energy rate is retrieved from Eq. (5.26) $\dot{H} = \langle \boldsymbol{y}_\partial,\, \boldsymbol{u}_\partial \rangle_{L^2(\partial\Omega, \mathbb{R}^2)}$. Introducing the test functions $(v_w,\, \boldsymbol{v}_\theta,\, \boldsymbol{V}_\kappa,\, \boldsymbol{v}_\gamma)$ and integrating by parts the first two lines of (7.86a) one gets

$$
\begin{aligned}
\langle v_w,\, \rho h \partial_t e_w \rangle_{L^2(\Omega)} &= - \langle \mathrm{grad}\, v_w,\, \boldsymbol{e}_\gamma \rangle_{L^2(\Omega, \mathbb{R}^2)} + \langle \gamma_0 v_w,\, u_{\partial,1} \rangle_{L^2(\partial\Omega)}, \\
\langle \boldsymbol{v}_\theta,\, I_\theta \partial_t \boldsymbol{e}_\theta \rangle_{L^2(\Omega, \mathbb{R}^2)} &= - \langle \mathrm{Grad}\, \boldsymbol{v}_\theta,\, \boldsymbol{E}_\kappa \rangle_{L^2(\Omega, \mathbb{R}^{2\times 2}_{\mathrm{sym}})} + \langle \boldsymbol{v}_\theta,\, \boldsymbol{e}_\gamma \rangle_{L^2(\Omega)} + \langle \boldsymbol{\gamma}_0 \boldsymbol{v}_\theta,\, \boldsymbol{\gamma}_n \boldsymbol{E}_\kappa \rangle_{L^2(\partial\Omega, \mathbb{R}^2)}, \\
\langle \boldsymbol{V}_\kappa,\, \boldsymbol{\mathcal{C}_b} \partial_t \boldsymbol{E}_\kappa \rangle_{L^2(\Omega, \mathbb{R}^{2\times 2}_{\mathrm{sym}})} &= \langle \boldsymbol{V}_\kappa,\, \mathrm{Grad}\, \boldsymbol{e}_\theta \rangle_{L^2(\Omega, \mathbb{R}^{2\times 2}_{\mathrm{sym}})}, \\
\langle \boldsymbol{v}_\gamma,\, C_s \partial_t \boldsymbol{e}_\gamma \rangle_{L^2(\Omega, \mathbb{R}^2)} &= \langle \boldsymbol{v}_\gamma,\, \mathrm{grad}\, e_w \rangle_{L^2(\Omega, \mathbb{R}^2)} - \langle \boldsymbol{v}_\gamma,\, \boldsymbol{e}_\theta \rangle_{L^2(\Omega, \mathbb{R}^2)}.
\end{aligned}
\tag{7.90}
$$

The term $\langle \boldsymbol{\gamma}_0 \boldsymbol{v}_\theta,\, \boldsymbol{\gamma}_n \boldsymbol{E}_\kappa \rangle_{L^2(\partial\Omega,\mathbb{R}^2)}$ can be decomposed in its tangential and normal components

$$\langle \boldsymbol{\gamma}_0 \boldsymbol{v}_\theta,\, \boldsymbol{\gamma}_n \boldsymbol{E}_\kappa \rangle_{L^2(\partial\Omega,\mathbb{R}^2)} = \langle \gamma_n \boldsymbol{v}_\theta,\, u_{\partial,2} \rangle_{L^2(\partial\Omega)} + \langle \gamma_s \boldsymbol{v}_\theta,\, u_{\partial,3} \rangle_{L^2(\partial\Omega)} \tag{7.91}$$

Introducing a Galerkin discretization for test and efforts functions

$$\begin{aligned}
v_w &= \sum_{i=1}^{n_w} \phi_w^i v_w^i, & \boldsymbol{v}_\theta &= \sum_{i=1}^{n_\theta} \boldsymbol{\phi}_\theta^i v_\theta^i, & \boldsymbol{V}_\kappa &= \sum_{i=1}^{n_\kappa} \boldsymbol{\Phi}_\kappa^i v_\kappa^i, & \boldsymbol{v}_\gamma &= \sum_{i=1}^{n_\gamma} \boldsymbol{\phi}_\gamma^i v_\gamma^i, & \boldsymbol{v}_\partial &= \sum_{i=1}^{n_\partial} \boldsymbol{\phi}_\partial^i v_\partial^i, \\
e_w &= \sum_{i=1}^{n_w} \phi_w^i e_w^i, & \boldsymbol{e}_\theta &= \sum_{i=1}^{n_\theta} \boldsymbol{\phi}_\theta^i e_\theta^i, & \boldsymbol{E}_\kappa &= \sum_{i=1}^{n_\kappa} \boldsymbol{\Phi}_\kappa^i e_\kappa^i, & \boldsymbol{e}_\gamma &= \sum_{i=1}^{n_\gamma} \boldsymbol{\phi}_\gamma^i e_\gamma^i, & \boldsymbol{u}_\partial &= \sum_{i=1}^{n_\partial} \boldsymbol{\phi}_\partial^i u_\partial^i, \\
& & & & & & & & \boldsymbol{y}_\partial &= \sum_{i=1}^{n_\partial} \boldsymbol{\phi}_\partial^i y_\partial^i.
\end{aligned} \tag{7.92}$$

the following finite dimensional system is obtained

$$\begin{aligned}
\mathrm{Diag}\begin{bmatrix} \mathbf{M}_{\rho h} \\ \mathbf{M}_{I_\theta} \\ \mathbf{M}_{\mathcal{C}_b} \\ \mathbf{M}_{C_s} \end{bmatrix} \begin{pmatrix} \dot{\mathbf{e}}_w \\ \dot{\mathbf{e}}_\theta \\ \dot{\mathbf{e}}_\kappa \\ \dot{\mathbf{e}}_\gamma \end{pmatrix} &= \begin{bmatrix} \mathbf{0} & \mathbf{0} & \mathbf{0} & -\mathbf{D}_{\mathrm{grad}}^\top \\ \mathbf{0} & \mathbf{0} & -\mathbf{D}_{\mathrm{Grad}}^\top & -\mathbf{D}_0^\top \\ \mathbf{0} & \mathbf{D}_{\mathrm{Grad}} & \mathbf{0} & \mathbf{0} \\ \mathbf{D}_{\mathrm{grad}} & \mathbf{D}_0 & \mathbf{0} & \mathbf{0} \end{bmatrix} \begin{pmatrix} \mathbf{e}_w \\ \mathbf{e}_\theta \\ \mathbf{e}_\kappa \\ \mathbf{e}_\gamma \end{pmatrix} + \begin{bmatrix} \mathbf{B}_w & \mathbf{0} & \mathbf{0} \\ \mathbf{0} & \mathbf{B}_{\theta_n} & \mathbf{B}_{\theta_s} \\ \mathbf{0} & \mathbf{0} & \mathbf{0} \\ \mathbf{0} & \mathbf{0} & \mathbf{0} \end{bmatrix} \mathbf{u}_\partial, \\
\mathbf{M}_\partial \mathbf{y}_\partial &= \begin{bmatrix} \mathbf{B}_w^\top & \mathbf{0} & \mathbf{0} & \mathbf{0} \\ \mathbf{0} & \mathbf{B}_{\theta_n}^\top & \mathbf{0} & \mathbf{0} \\ \mathbf{0} & \mathbf{B}_{\theta_s}^\top & \mathbf{0} & \mathbf{0} \end{bmatrix} \begin{pmatrix} \mathbf{e}_w \\ \mathbf{e}_\theta \\ \mathbf{e}_\kappa \\ \mathbf{e}_\gamma \end{pmatrix}.
\end{aligned} \tag{7.93}$$

The notation Diag denotes a block diagonal matrix. The mass matrices $\mathbf{M}_{\rho h},\ \mathbf{M}_{I_\theta},\ \mathbf{M}_{\mathcal{C}_b},\ \mathbf{M}_{C_s}$ are computed as

$$\begin{aligned}
M_{\rho h}^{ij} &= \left\langle \phi_w^i,\, \rho h \phi_w^j \right\rangle_{L^2(\Omega)}, & M_{\mathcal{C}_b}^{pq} &= \langle \boldsymbol{\Phi}_\kappa^p,\, \mathcal{C}_b \boldsymbol{\Phi}_\kappa^q \rangle_{L^2(\Omega,\mathbb{R}^{2\times 2}_{\mathrm{sym}})}, \\
M_{I_\theta}^{mn} &= \langle \boldsymbol{\phi}_\kappa^m,\, I_\theta \boldsymbol{\phi}_\kappa^n \rangle_{L^2(\Omega,\mathbb{R}^2)}, & M_{C_s}^{rs} &= \left\langle \boldsymbol{\phi}_\gamma^r,\, C_s \boldsymbol{\phi}_\gamma^s \right\rangle_{L^2(\Omega,\mathbb{R}^2)},
\end{aligned} \tag{7.94}$$

where $i, j \in \{1, n_w\},\ m, n \in \{1, n_\theta\},\ p, q \in \{1, n_\kappa\},\ r, s \in \{1, n_\gamma\}$. Matrices $\mathbf{D}_{\mathrm{grad}},\ \mathbf{D}_{\mathrm{Grad}},\ \mathbf{D}_0$ assume the form

$$\begin{aligned}
D_{\mathrm{grad}}^{rj} &= \left\langle \boldsymbol{\phi}_\gamma^r,\, \mathrm{grad}\, \phi_w^j \right\rangle_{L^2(\Omega,\mathbb{R}^2)}, \\
D_{\mathrm{Grad}}^{pn} &= \langle \boldsymbol{\Phi}_\kappa^p,\, \mathrm{Grad}\, \boldsymbol{\phi}_\theta^n \rangle_{L^2(\Omega,\mathbb{R}^{2\times 2}_{\mathrm{sym}})},
\end{aligned} \qquad D_0^{rn} = -\left\langle \boldsymbol{\phi}_\gamma^r,\, \boldsymbol{\phi}_\theta^n \right\rangle_{L^2(\Omega,\mathbb{R}^2)}. \tag{7.95}$$

Matrices $\mathbf{B}_w$, $\mathbf{B}_{\theta_n}$, $\mathbf{B}_{\theta_s}$ are computed as ($l \in \{1, n_\partial\}$)

$$B_w^{il} = \left\langle \gamma_0 \phi_w^i,\, \phi_{\partial,1}^l \right\rangle_{L^2(\partial\Omega)}, \qquad B_{\theta_n}^{ml} = \left\langle \gamma_n \boldsymbol{\phi}_\theta^m,\, \phi_{\partial,2}^l \right\rangle_{L^2(\partial\Omega)}, \qquad B_{\theta_s}^{ml} = \left\langle \gamma_s \boldsymbol{\phi}_\theta^m,\, \phi_{\partial,3}^l \right\rangle_{L^2(\partial\Omega)}. \tag{7.96}$$

Control through linear and angular velocities If instead the opposite causality is considered, the continuous system reads

$$
\begin{bmatrix}
\rho h & 0 & 0 & 0 \\
\mathbf{0} & I_\theta & \mathbf{0} & \mathbf{0} \\
\mathbf{0} & \mathbf{0} & \boldsymbol{\mathcal{C}}_b & \mathbf{0} \\
\mathbf{0} & \mathbf{0} & \mathbf{0} & C_s
\end{bmatrix}
\frac{\partial}{\partial t}
\begin{pmatrix}
e \\ \boldsymbol{e}_\theta \\ \boldsymbol{E}_\kappa \\ \boldsymbol{e}_\gamma
\end{pmatrix}
=
\begin{bmatrix}
0 & 0 & 0 & \mathrm{div} \\
\mathbf{0} & \mathbf{0} & \mathrm{Div} & \boldsymbol{I}_{2\times 2} \\
\mathbf{0} & \mathrm{Grad} & \mathbf{0} & \mathbf{0} \\
\mathrm{grad} & -\boldsymbol{I}_{2\times 2} & \mathbf{0} & \mathbf{0}
\end{bmatrix}
\begin{pmatrix}
e_w \\ \boldsymbol{e}_\theta \\ \boldsymbol{E}_\kappa \\ \boldsymbol{e}_\gamma
\end{pmatrix},
\tag{7.97a}
$$

$$
\boldsymbol{u}_\partial =
\begin{bmatrix}
\gamma_0 & 0 & 0 & 0 \\
0 & \gamma_n & 0 & 0 \\
0 & \gamma_s & 0 & 0
\end{bmatrix}
\begin{pmatrix}
e_w \\ \boldsymbol{e}_\theta \\ \boldsymbol{E}_\kappa \\ \boldsymbol{e}_\gamma
\end{pmatrix},
\qquad \boldsymbol{u}_\partial \in \mathbb{R}^3,
\tag{7.97b}
$$

$$
\boldsymbol{y}_\partial =
\begin{bmatrix}
0 & 0 & 0 & \gamma_n \\
0 & 0 & \gamma_{nn} & 0 \\
0 & 0 & \gamma_{ns} & 0
\end{bmatrix}
\begin{pmatrix}
e_w \\ \boldsymbol{e}_\theta \\ \boldsymbol{E}_\kappa \\ \boldsymbol{e}_\gamma
\end{pmatrix},
\qquad \boldsymbol{y}_\partial \in \mathbb{R}^3.
\tag{7.97c}
$$

Integrating by parts the last two lines of (7.97a) one gets

$$
\begin{aligned}
\langle v_w,\, \rho h \partial_t e_w \rangle_{L^2(\Omega)} &= \langle v_w,\, \mathrm{div}\, \boldsymbol{e}_\gamma \rangle_{L^2(\Omega, \mathbb{R}^2)}\,, \\
\langle \boldsymbol{v}_\theta,\, I_\theta \partial_t \boldsymbol{e}_\theta \rangle_{L^2(\Omega, \mathbb{R}^2)} &= \langle \boldsymbol{v}_\theta,\, \mathrm{Div}\, \boldsymbol{E}_\kappa \rangle_{L^2(\Omega, \mathbb{R}^2)} + \langle \boldsymbol{v}_\theta,\, \boldsymbol{e}_\gamma \rangle_{L^2(\Omega)}\,, \\
\langle \boldsymbol{V}_\kappa,\, \boldsymbol{\mathcal{C}_b} \partial_t \boldsymbol{E}_\kappa \rangle_{L^2(\Omega, \mathbb{R}^{2\times 2}_{\mathrm{sym}})} &= - \langle \mathrm{Div}\, \boldsymbol{V}_\kappa,\, \boldsymbol{e}_\theta \rangle_{L^2(\Omega, \mathbb{R}^2)} + \langle \boldsymbol{\gamma}_n \boldsymbol{V}_\kappa,\, \boldsymbol{\gamma}_0 \boldsymbol{e}_\theta \rangle_{L^2(\partial\Omega, \mathbb{R}^2)}\,, \\
\langle \boldsymbol{v}_\gamma,\, C_s \partial_t \boldsymbol{e}_\gamma \rangle_{L^2(\Omega, \mathbb{R}^2)} &= - \langle \mathrm{div}\, \boldsymbol{v}_\gamma,\, e_w \rangle_{L^2(\Omega)} - \langle \boldsymbol{v}_\gamma,\, \boldsymbol{e}_\theta \rangle_{L^2(\Omega, \mathbb{R}^2)} + \langle \gamma_0 v_w,\, u_{\partial,1} \rangle_{L^2(\partial\Omega)}\,.
\end{aligned}
\tag{7.98}
$$

The term $\langle \boldsymbol{\gamma}_n \boldsymbol{V}_\kappa,\, \boldsymbol{\gamma}_0 \boldsymbol{e}_\theta \rangle_{L^2(\partial\Omega, \mathbb{R}^2)}$ can be decomposed in its tangential and normal components

$$
\langle \boldsymbol{\gamma}_n \boldsymbol{V}_\kappa,\, \boldsymbol{\gamma}_0 \boldsymbol{e}_\theta \rangle_{L^2(\partial\Omega, \mathbb{R}^2)} = \langle \gamma_{nn} \boldsymbol{V}_\kappa,\, u_{\partial,2} \rangle_{L^2(\partial\Omega)} + \langle \gamma_{ns} \boldsymbol{V}_\kappa,\, u_{\partial,3} \rangle_{L^2(\partial\Omega)}\,.
\tag{7.99}
$$

Plugging approximation (7.92) into this system, one computes

$$
\begin{aligned}
\mathrm{Diag}
\begin{bmatrix}
\mathbf{M}_{\rho h} \\ \mathbf{M}_{I_\theta} \\ \mathbf{M}_{\boldsymbol{\mathcal{C}}_b} \\ \mathbf{M}_{C_s}
\end{bmatrix}
\begin{pmatrix}
\dot{\mathbf{e}}_w \\ \dot{\mathbf{e}}_\theta \\ \dot{\mathbf{e}}_\kappa \\ \dot{\mathbf{e}}_\gamma
\end{pmatrix}
&=
\begin{bmatrix}
\mathbf{0} & \mathbf{0} & \mathbf{0} & \mathbf{D}_{\mathrm{div}} \\
\mathbf{0} & \mathbf{0} & \mathbf{D}_{\mathrm{Div}} & -\mathbf{D}_0^\top \\
\mathbf{0} & -\mathbf{D}_{\mathrm{Div}}^\top & \mathbf{0} & \mathbf{0} \\
-\mathbf{D}_{\mathrm{div}}^\top & \mathbf{D}_0 & \mathbf{0} & \mathbf{0}
\end{bmatrix}
\begin{pmatrix}
\mathbf{e}_w \\ \mathbf{e}_\theta \\ \mathbf{e}_\kappa \\ \mathbf{e}_\gamma
\end{pmatrix}
+
\begin{bmatrix}
\mathbf{0} & \mathbf{0} & \mathbf{0} \\
\mathbf{0} & \mathbf{0} & \mathbf{0} \\
\mathbf{0} & \mathbf{B}_{M_{nn}} & \mathbf{B}_{M_{ns}} \\
\mathbf{B}_{q_n} & \mathbf{0} & \mathbf{0}
\end{bmatrix}
\mathbf{u}_\partial, \\
\mathbf{M}_\partial \mathbf{y}_\partial &=
\begin{bmatrix}
\mathbf{0} & \mathbf{0} & \mathbf{0} & \mathbf{B}_{q_n}^\top \\
\mathbf{0} & \mathbf{0} & \mathbf{B}_{M_{nn}}^\top & \mathbf{0} \\
\mathbf{0} & \mathbf{0} & \mathbf{B}_{M_{ns}}^\top & \mathbf{0}
\end{bmatrix}
\begin{pmatrix}
\mathbf{e}_w \\ \mathbf{e}_\theta \\ \mathbf{e}_\kappa \\ \mathbf{e}_\gamma
\end{pmatrix}.
\end{aligned}
\tag{7.100}
$$

Matrices $\mathbf{D}_{\mathrm{div}}$, $\mathbf{D}_{\mathrm{Div}}$ assume the form $(i, j \in \{1, n_w\},\ m, n \in \{1, n_\theta\},\ p, q \in \{1, n_\kappa\},\ r, s \in \{1, n_\gamma\})$

$$
D_{\mathrm{div}}^{is} = \left\langle \phi_w^i,\, \mathrm{div}\, \boldsymbol{\phi}_\gamma^s \right\rangle_{L^2(\Omega)}, \qquad D_{\mathrm{Div}}^{mq} = \langle \boldsymbol{\phi}_\theta^m,\, \mathrm{Div}\, \boldsymbol{\Phi}_\kappa^q \rangle_{L^2(\Omega, \mathbb{R}^2)}\,.
\tag{7.101}
$$

Matrix $\mathbf{B}_{q_n}$, $\mathbf{B}_{M_{nn}}$, $\mathbf{B}_{M_{ns}}$ are computed as ($l \in \{1, n_\partial\}$)

$$B_{q_n}^{rl} = \left\langle \gamma_n \boldsymbol{\phi}_\gamma^r,\, \phi_{\partial,1}^l \right\rangle_{L^2(\partial\Omega)}, \quad B_{M_{nn}}^{pl} = \left\langle \gamma_{nn} \boldsymbol{\Phi}_\kappa^p,\, \phi_{\partial,2}^l \right\rangle_{L^2(\partial\Omega)}, \quad B_{M_{ns}}^{pl} = \left\langle \gamma_{ns} \boldsymbol{\Phi}_\kappa^p,\, \phi_{\partial,3}^l \right\rangle_{L^2(\partial\Omega)}. \tag{7.102}$$

This finite dimensional system represents a purely mixed discretization of the problem and is really close to the plane elasticity system. Conforming finite elements for the plane elasticity system on simplicial meshes have been constructed in [AW02]. The resulting element is rather cumbersome and computationally expensive as the stress tensor has at least 24 degrees of freedom on a triangle For this reason, many finite element discretization imposes the symmetry of the stress tensor weakly [AFW07]. To actually implement the discretization, in Chap. 8 the Mindlin plate problem is going to be reformulated so that the momenta tensor is only weakly symmetric.

7.2 Mixed boundary conditions

In this section Assumption 3 on uniform boundary condition is modified to account for general non homogeneous boundary conditions. The discretization of Stokes-Dirac structure under mixed causality has been already treated in [KML18]. However, to satisfy the power balance at a discrete level, some additional parameters are introduced. This makes the employment of this methodology not simple and dependent on the considered application. Furthermore, elasticity models do not fall within the required assumptions.

We propose here two methodologies to tackle mixed boundary conditions within the Partitioned Finite Element Method. The first introduces Lagrange multipliers, and therefore algebraic constraints, to enforce the mixed causality. Finite dimensional differential algebraic port-Hamiltonian systems (pHDAE) have been introduced in [BMXZ18] for linear systems and in [MM19] for non linear systems. This enriched description shares all the crucial features of ordinary pHs, but easily takes into account algebraic constraints, time-dependent transformations and explicit dependence on time in the Hamiltonian. The second method employs a domain decomposition technique to interconnect systems with different causalities. For sake of simplicity the illustration is restricted to the linear case.

The open connected set $\Omega \subset \mathbb{R}^d$, $d = \{1, 2, 3\}$, with Lipschitz boundary $\partial\Omega$ represents the spatial domain. The boundary is partitioned into two sets $\partial\Omega = \overline{\Gamma}_1 \cup \overline{\Gamma}_2$, $\Gamma_1 \cap \Gamma_2 = \{\emptyset\}$. The sets Γ_1, Γ_2 are considered to be connected, cf. Fig. 7.1.

Remark 11 (Connectedness of Γ_1, Γ_2)
Disconnected sets can be handled as well. This requires the introduction of an heavy notation and complicates the illustration. For sake of simplicity, the connectedness hypothesis applies.

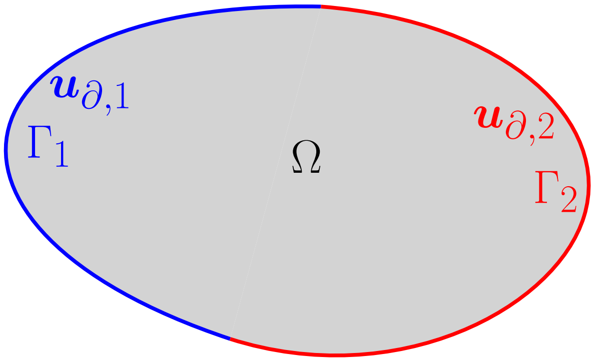

Figure 7.1: Partition of boundary into two connected sets.

For scalars $a_{\partial,*}, b_{\partial,*} \in L^2(\Gamma_*)$ and vectors $\boldsymbol{a}_{\partial,*}, \boldsymbol{b}_{\partial,*} \in L^2(\Gamma_*, \mathbb{R}^m)$ defined on the boundary partition Γ_* the inner product is defined as

$$\langle a_{\partial,*},\, b_{\partial,*}\rangle_{L^2(\Gamma_*)} = \int_{\Gamma_*} a_{\partial,*} b_{\partial,*} \, \mathrm{d}\Gamma_*, \qquad \langle \boldsymbol{a}_{\partial,*},\, \boldsymbol{b}_{\partial,*}\rangle_{L^2(\Gamma_*,\mathbb{R}^m)} = \int_{\Gamma_*} \boldsymbol{a}_{\partial,*} \cdot \boldsymbol{b}_{\partial,*} \, \mathrm{d}\Gamma_*. \tag{7.103}$$

Consider now the following boundary control linear pH system in co-energy form

$$\begin{bmatrix} \mathcal{M}_1 & 0 \\ 0 & \mathcal{M}_2 \end{bmatrix} \partial_t \begin{pmatrix} \boldsymbol{e}_1 \\ \boldsymbol{e}_2 \end{pmatrix} = \begin{bmatrix} 0 & -\boldsymbol{L}^\top - \mathcal{L}^* \\ \boldsymbol{L} + \mathcal{L} & 0 \end{bmatrix} \begin{pmatrix} \boldsymbol{e}_1 \\ \boldsymbol{e}_2 \end{pmatrix}, \qquad \begin{matrix} \boldsymbol{e}_1 \in H^{\mathcal{L}}, \\ \boldsymbol{e}_2 \in H^{-\mathcal{L}^*}, \end{matrix} \tag{7.104a}$$

$$\begin{pmatrix} \boldsymbol{u}_{\partial,1} \\ \boldsymbol{u}_{\partial,2} \end{pmatrix} = \begin{bmatrix} \mathcal{N}_{\partial,1}^{\Gamma_1} & 0 \\ 0 & \mathcal{N}_{\partial,2}^{\Gamma_2} \end{bmatrix} \begin{pmatrix} \boldsymbol{e}_1 \\ \boldsymbol{e}_2 \end{pmatrix}, \qquad \begin{matrix} \boldsymbol{u}_{\partial,1} \in \mathbb{R}^m, \\ \boldsymbol{u}_{\partial,2} \in \mathbb{R}^m, \end{matrix} \tag{7.104b}$$

$$\begin{pmatrix} \boldsymbol{y}_{\partial,1} \\ \boldsymbol{y}_{\partial,2} \end{pmatrix} = \begin{bmatrix} 0 & \mathcal{N}_{\partial,2}^{\Gamma_1} \\ \mathcal{N}_{\partial,1}^{\Gamma_2} & 0 \end{bmatrix} \begin{pmatrix} \boldsymbol{e}_1 \\ \boldsymbol{e}_2 \end{pmatrix}, \qquad \begin{matrix} \boldsymbol{y}_{\partial,1} \in \mathbb{R}^m, \\ \boldsymbol{y}_{\partial,2} \in \mathbb{R}^m. \end{matrix} \tag{7.104c}$$

The operator $\mathcal{N}_{\partial,*}^{\Gamma_\circ}$ with $*, \circ \in \{1, 2\}$ represents now the restriction of operator $\mathcal{N}_{\partial,*}$, defined in Eq. (7.8), over the subset $\Gamma_\circ$. The boundary inputs and outputs are now vectors $\mathbb{R}^{2m}$. This does not mean that the boundary conditions have been doubled, but only that the components of $\boldsymbol{u}_\partial, \boldsymbol{y}_\partial$ are only defined on the subsets Γ_1, Γ_2 of the overall boundary. This corresponds to a slight modification of Assumption 3.

Given the additive property of the integral, it is possible to write

$$\begin{aligned} \langle \mathcal{N}_{\partial,1}\boldsymbol{e}_1,\, \mathcal{N}_{\partial,2}\boldsymbol{e}_2\rangle_{L^2(\partial\Omega,\mathbb{R}^m)} &= \left\langle \mathcal{N}_{\partial,1}^{\Gamma_1}\boldsymbol{e}_1,\, \mathcal{N}_{\partial,2}^{\Gamma_1}\boldsymbol{e}_2\right\rangle_{L^2(\Gamma_1,\mathbb{R}^m)} + \left\langle \mathcal{N}_{\partial,1}^{\Gamma_2}\boldsymbol{e}_1,\, \mathcal{N}_{\partial,2}^{\Gamma_2}\boldsymbol{e}_2\right\rangle_{L^2(\Gamma_2,\mathbb{R}^m)}, \\ &= \langle \boldsymbol{u}_{\partial,1},\, \boldsymbol{y}_{\partial,1}\rangle_{L^2(\Gamma_1,\mathbb{R}^m)} + \langle \boldsymbol{y}_{\partial,2},\, \boldsymbol{u}_{\partial,2}\rangle_{L^2(\Gamma_2,\mathbb{R}^m)}. \end{aligned} \tag{7.105}$$

The continuous power balance is obtained using Eqs. (7.50) and (7.105)

$$\dot{H} = \langle \boldsymbol{u}_{\partial,1},\, \boldsymbol{y}_{\partial,1}\rangle_{L^2(\Gamma_1,\mathbb{R}^m)} + \langle \boldsymbol{y}_{\partial,2},\, \boldsymbol{u}_{\partial,2}\rangle_{L^2(\Gamma_2,\mathbb{R}^m)}. \tag{7.106}$$

7.2.1 Solution using Lagrange multipliers

This solution introduces a Lagrange multiplier for the boundary control that does not arise explicitly in the weak form. To illustrate the idea, consider again the weak form 7.51 (obtained by integration by parts of the $-\mathcal{L}^*$ partition) of Sys. 7.104

$$
\begin{aligned}
&\langle \boldsymbol{v}_1,\, \mathcal{M}_1 \partial_t \boldsymbol{e}_1 \rangle_{L^2(\Omega,\mathbb{A})} = -\langle \boldsymbol{v}_1,\, \boldsymbol{L}^\top \boldsymbol{e}_2 \rangle_{L^2(\Omega,\mathbb{A})} - \langle \mathcal{L}\boldsymbol{v}_1,\, \boldsymbol{e}_2 \rangle_{L^2(\Omega,\mathbb{B})} + \langle \mathcal{N}_{\partial,1}\boldsymbol{v}_1,\, \mathcal{N}_{\partial,2}\boldsymbol{e}_2 \rangle_{L^2(\partial\Omega,\mathbb{R}^m)}\,, \\
&\langle \boldsymbol{v}_2,\, \mathcal{M}_2 \partial_t \boldsymbol{e}_2 \rangle_{L^2(\Omega,\mathbb{B})} = \langle \boldsymbol{v}_2,\, \boldsymbol{L}\boldsymbol{e}_1 \rangle_{L^2(\Omega,\mathbb{B})} + \langle \boldsymbol{v}_2,\, \mathcal{L}\boldsymbol{e}_1 \rangle_{L^2(\Omega,\mathbb{B})}\,.
\end{aligned}
\tag{7.107}
$$

The term $\langle \mathcal{N}_{\partial,1}\boldsymbol{v}_1,\, \mathcal{N}_{\partial,2}\boldsymbol{e}_2 \rangle_{L^2(\partial\Omega,\mathbb{R}^m)}$ can be split into the two boundary contributions, as in Eq. (7.105). The variable $\boldsymbol{y}_{\partial,1}$ plays here the role of a Lagrange multiplier $\boldsymbol{y}_{\partial,1} = \boldsymbol{\lambda}_{\partial,1}$

$$
\begin{aligned}
\langle \mathcal{N}_{\partial,1}\boldsymbol{v}_1,\, \mathcal{N}_{\partial,2}\boldsymbol{e}_2 \rangle_{L^2(\partial\Omega,\mathbb{R}^m)} &= \left\langle \mathcal{N}_{\partial,1}^{\Gamma_1}\boldsymbol{v}_1,\, \mathcal{N}_{\partial,2}^{\Gamma_1}\boldsymbol{e}_2 \right\rangle_{L^2(\Gamma_1,\mathbb{R}^m)} + \left\langle \mathcal{N}_{\partial,1}^{\Gamma_2}\boldsymbol{v}_1,\, \mathcal{N}_{\partial,2}^{\Gamma_2}\boldsymbol{e}_2 \right\rangle_{L^2(\Gamma_2,\mathbb{R}^m)}\,, \\
&= \left\langle \mathcal{N}_{\partial,1}^{\Gamma_1}\boldsymbol{v}_1,\, \boldsymbol{y}_{\partial,1} \right\rangle_{L^2(\Gamma_1,\mathbb{R}^m)} + \left\langle \mathcal{N}_{\partial,1}^{\Gamma_2}\boldsymbol{v}_1,\, \boldsymbol{u}_{\partial,2} \right\rangle_{L^2(\Gamma_2,\mathbb{R}^m)}\,, \\
&= \left\langle \mathcal{N}_{\partial,1}^{\Gamma_1}\boldsymbol{v}_1,\, \boldsymbol{\lambda}_{\partial,1} \right\rangle_{L^2(\Gamma_1,\mathbb{R}^m)} + \left\langle \mathcal{N}_{\partial,1}^{\Gamma_2}\boldsymbol{v}_1,\, \boldsymbol{u}_{\partial,2} \right\rangle_{L^2(\Gamma_2,\mathbb{R}^m)}\,,
\end{aligned}
\tag{7.108}
$$

If the test functions $\boldsymbol{v}_{\partial,1},\ \boldsymbol{v}_{\partial,2} \in \mathbb{R}^m$ are introduced, the input and outputs definitions

$$
\boldsymbol{u}_{\partial,1} = \mathcal{N}_{\partial,1}^{\Gamma_1}\boldsymbol{e}_1, \qquad \boldsymbol{y}_{\partial,1} = \boldsymbol{\lambda}_{\partial,1}, \qquad \boldsymbol{y}_{\partial,2} = \mathcal{N}_{\partial,1}^{\Gamma_2}\boldsymbol{e}_1, \tag{7.109}
$$

can be put into weak form to obtain

$$
\begin{aligned}
\langle \boldsymbol{v}_{\partial,1},\, \boldsymbol{u}_{\partial,1} \rangle_{L^2(\Gamma_1,\mathbb{R}^m)} &= \left\langle \boldsymbol{v}_{\partial,1},\, \mathcal{N}_{\partial,1}^{\Gamma_1}\boldsymbol{e}_1 \right\rangle_{L^2(\Gamma_1,\mathbb{R}^m)}\,, \\
\langle \boldsymbol{v}_{\partial,1},\, \boldsymbol{y}_{\partial,1} \rangle_{L^2(\Gamma_1,\mathbb{R}^m)} &= \langle \boldsymbol{v}_{\partial,1},\, \boldsymbol{\lambda}_{\partial,1} \rangle_{L^2(\Gamma_1,\mathbb{R}^m)}\,, \\
\langle \boldsymbol{v}_{\partial,2},\, \boldsymbol{y}_{\partial,2} \rangle_{L^2(\Gamma_1,\mathbb{R}^m)} &= \left\langle \boldsymbol{v}_{\partial,2},\, \mathcal{N}_{\partial,1}^{\Gamma_2}\boldsymbol{e}_1 \right\rangle_{L^2(\Gamma_1,\mathbb{R}^m)}\,.
\end{aligned}
\tag{7.110}
$$

As usual, a Galerkin approximation is introduced

$$
\begin{aligned}
\boldsymbol{v}_1 &\approx \sum_{i=1}^{n_1} \boldsymbol{\phi}_1^i(\boldsymbol{x}) v_1^i, \qquad & \boldsymbol{e}_1 &\approx \sum_{i=1}^{n_1} \boldsymbol{\phi}_1^i(\boldsymbol{x}) e_1^i(t), \qquad & \triangle_{\partial,1} &\approx \sum_{i=1}^{n_{\partial,1}} \boldsymbol{\phi}_{\partial,1}^i(\boldsymbol{s}_1) \triangle_{\partial,1}^i, \quad \boldsymbol{s}_1 \in \Gamma_1, \\
\boldsymbol{v}_2 &\approx \sum_{i=1}^{n_2} \boldsymbol{\phi}_2^i(\boldsymbol{x}) v_2^i, \qquad & \boldsymbol{e}_2 &\approx \sum_{i=1}^{n_2} \boldsymbol{\phi}_2^i(\boldsymbol{x}) e_2^i(t), \qquad & \square_{\partial,2} &\approx \sum_{i=1}^{n_{\partial,2}} \boldsymbol{\phi}_{\partial,2}^i(\boldsymbol{s}_2) \square_{\partial,2}^i(t), \quad \boldsymbol{s}_2 \in \Gamma_2.
\end{aligned}
\tag{7.111}
$$

where $\triangle$ stays for v, u, y, λ and $\square$ for v, u, y. Replacing the approximation 7.111 into Eqs. 7.107, 7.108, 7.110, the following differential-algebraic system is constructed

$$
\begin{aligned}
&\mathrm{Diag}\begin{bmatrix}\mathbf{M}_{\mathcal{M}_1} \\ \mathbf{M}_{\mathcal{M}_2} \\ \mathbf{0}\end{bmatrix}\begin{pmatrix}\dot{\mathbf{e}}_1 \\ \dot{\mathbf{e}}_2 \\ \dot{\boldsymbol{\lambda}}_{\partial,1}\end{pmatrix} = \begin{bmatrix}\mathbf{0} & -\mathbf{D}_0^\top - \mathbf{D}_{\mathcal{L}}^\top & \mathbf{B}_{1,\Gamma_1} \\ \mathbf{D}_0 + \mathbf{D}_{\mathcal{L}} & \mathbf{0} & \mathbf{0} \\ -\mathbf{B}_{1,\Gamma_1}^\top & \mathbf{0} & \mathbf{0}\end{bmatrix}\begin{pmatrix}\mathbf{e}_1 \\ \mathbf{e}_2 \\ \boldsymbol{\lambda}_{\partial,1}\end{pmatrix} + \begin{bmatrix}\mathbf{0} & \mathbf{B}_{1,\Gamma_2} \\ \mathbf{0} & \mathbf{0} \\ \mathbf{M}_{\partial,1} & \mathbf{0}\end{bmatrix}\begin{bmatrix}\mathbf{u}_{\partial,1} \\ \mathbf{u}_{\partial,2}\end{bmatrix}, \\
&\begin{bmatrix}\mathbf{M}_{\partial,1} & \mathbf{0} \\ \mathbf{0} & \mathbf{M}_{\partial,2}\end{bmatrix}\begin{pmatrix}\mathbf{y}_{\partial,1} \\ \mathbf{y}_{\partial,2}\end{pmatrix} = \begin{bmatrix}\mathbf{0} & \mathbf{0} & \mathbf{M}_{\partial,1} \\ \mathbf{B}_{1,\Gamma_2}^\top & \mathbf{0} & \mathbf{0}\end{bmatrix}\begin{pmatrix}\mathbf{e}_1 \\ \mathbf{e}_2 \\ \boldsymbol{\lambda}_{\partial,1}\end{pmatrix}.
\end{aligned}
\tag{7.112}
$$

Apart for matrices $\mathbf{M}_{\partial,1}, \mathbf{M}_{\partial,2}, \mathbf{B}_{1,\Gamma_1}, \mathbf{B}_{1,\Gamma_2}$,

$$
\begin{aligned}
M_{\partial,1}^{lk} &= \left\langle \boldsymbol{\phi}_{\partial,1}^l, \, \boldsymbol{\phi}_{\partial,1}^k \right\rangle_{L^2(\Gamma_1,\mathbb{R}^m)}, \; (l,k) \in \{1, n_{\partial,1}\}, \quad B_{1,\Gamma_1}^{ik} = \left\langle \mathcal{N}_{\partial,1}^{\Gamma_1}\boldsymbol{\phi}_1^i, \, \boldsymbol{\phi}_{\partial,1}^k \right\rangle_{L^2(\Gamma_1,\mathbb{R}^m)}, \\
M_{\partial,2}^{fg} &= \left\langle \boldsymbol{\phi}_{\partial,2}^f, \, \boldsymbol{\phi}_{\partial,2}^g \right\rangle_{L^2(\Gamma_2,\mathbb{R}^m)}, \; (f,g) \in \{1, n_{\partial,2}\}, \quad B_{1,\Gamma_2}^{ig} = \left\langle \mathcal{N}_{\partial,1}^{\Gamma_2}\boldsymbol{\phi}_1^i, \, \boldsymbol{\phi}_{\partial,2}^g \right\rangle_{L^2(\Gamma_2,\mathbb{R}^m)},
\end{aligned}
\quad i \in \{1, n_1\},
\tag{7.113}
$$

the other matrices keep the same definition as in (7.53). The discrete Hamiltonian, whose expression is [BMXZ18]

$$
H_d = \frac{1}{2}\mathbf{e}_1^\top \mathbf{M}_{\mathcal{M}_1}\mathbf{e}_1 + \frac{1}{2}\mathbf{e}_2^\top \mathbf{M}_{\mathcal{M}_2}\mathbf{e}_2.
\tag{7.114}
$$

gives rise to the discrete power balance

$$
\begin{aligned}
\dot{H}_d &= \mathbf{e}_1^\top \mathbf{M}_{\mathcal{M}_1}\dot{\mathbf{e}}_1 + \mathbf{e}_2^\top \mathbf{M}_{\mathcal{M}_2}\dot{\mathbf{e}}_2, \\
&= -\mathbf{e}_1^\top(\mathbf{D}_0 + \mathbf{D}_{\mathcal{L}})^\top \mathbf{e}_2 + \mathbf{e}_2^\top(\mathbf{D}_0 + \mathbf{D}_{\mathcal{L}})\mathbf{e}_1 + \mathbf{e}_1^\top(\mathbf{B}_{1,\Gamma_1}\boldsymbol{\lambda}_{\partial,1} + \mathbf{B}_{1,\Gamma_2}\mathbf{u}_{\partial,2}), \\
&= \mathbf{y}_{\partial,1}^\top \mathbf{M}_{\partial,1}\mathbf{u}_{\partial,1} + \mathbf{y}_{\partial,2}^\top \mathbf{M}_{\partial,2}\mathbf{u}_{\partial,2}, \\
&= \widehat{\mathbf{y}}_{\partial,1}^\top \mathbf{u}_{\partial,1} + \widehat{\mathbf{y}}_{\partial,2}^\top \mathbf{u}_{\partial,2}, \qquad \text{where} \qquad \widehat{\mathbf{y}}_{\partial,1} := \mathbf{M}_{\partial,1}\mathbf{y}_{\partial,1}, \quad \widehat{\mathbf{y}}_{\partial,2} := \mathbf{M}_{\partial,2}\mathbf{y}_{\partial,2}.
\end{aligned}
\tag{7.115}
$$

This result is the finite dimensional equivalent of (7.106).

Equivalently, the weak form Eq.7.52 may be used as a starting point. The computation follows in a completely analogous manner. The only difference is that $\boldsymbol{y}_{\partial,2} = \boldsymbol{\lambda}_{\partial,2}$ plays the role of the Lagrange multiplier. The final finite dimensional system is then given by

$$
\begin{aligned}
&\mathrm{Diag}\begin{bmatrix}\mathbf{M}_{\mathcal{M}_1} \\ \mathbf{M}_{\mathcal{M}_2} \\ \mathbf{0}\end{bmatrix}\begin{pmatrix}\dot{\mathbf{e}}_1 \\ \dot{\mathbf{e}}_2 \\ \dot{\boldsymbol{\lambda}}_{\partial,2}\end{pmatrix} = \begin{bmatrix}\mathbf{0} & -\mathbf{D}_0^\top + \mathbf{D}_{-\mathcal{L}^*} & \mathbf{0} \\ \mathbf{D}_0 - \mathbf{D}_{-\mathcal{L}^*}^\top & \mathbf{0} & \mathbf{B}_{2,\Gamma_2} \\ \mathbf{0} & -\mathbf{B}_{2,\Gamma_2}^\top & \mathbf{0}\end{bmatrix}\begin{pmatrix}\mathbf{e}_1 \\ \mathbf{e}_2 \\ \boldsymbol{\lambda}_{\partial,2}\end{pmatrix} + \begin{bmatrix}\mathbf{0} & \mathbf{0} \\ \mathbf{B}_{2,\Gamma_1} & \mathbf{0} \\ \mathbf{0} & \mathbf{M}_{\partial,2}\end{bmatrix}\begin{bmatrix}\mathbf{u}_{\partial,1} \\ \mathbf{u}_{\partial,2}\end{bmatrix}, \\
&\begin{bmatrix}\mathbf{M}_{\partial,1} & \mathbf{0} \\ \mathbf{0} & \mathbf{M}_{\partial,2}\end{bmatrix}\begin{pmatrix}\mathbf{y}_{\partial,1} \\ \mathbf{y}_{\partial,2}\end{pmatrix} = \begin{bmatrix}\mathbf{0} & \mathbf{B}_{2,\Gamma_1}^\top & \mathbf{0} \\ \mathbf{0} & \mathbf{0} & \mathbf{M}_{\partial,2}\end{bmatrix}\begin{pmatrix}\mathbf{e}_1 \\ \mathbf{e}_2 \\ \boldsymbol{\lambda}_{\partial,2}\end{pmatrix}.
\end{aligned}
\tag{7.116}
$$

where $\mathbf{B}_{2,\Gamma_1}, \; \mathbf{B}_{2,\Gamma_2}$ are given by

$$
B_{2,\Gamma_1}^{mk} = \left\langle \mathcal{N}_{\partial,2}^{\Gamma_1}\boldsymbol{\phi}_2^m, \, \boldsymbol{\phi}_{\partial,1}^k \right\rangle_{L^2(\Gamma_1,\mathbb{R}^m)}, \quad B_{2,\Gamma_2}^{mg} = \left\langle \mathcal{N}_{\partial,2}^{\Gamma_2}\boldsymbol{\phi}_2^m, \, \boldsymbol{\phi}_{\partial,2}^g \right\rangle_{L^2(\Gamma_2,\mathbb{R}^m)},
\tag{7.117}
$$

where $m \in \{1, n_2\}, \; k \in \{1, n_{\partial,1}\}, \; g \in \{1, n_{\partial,2}\}$. This solution can be applied to incorporate

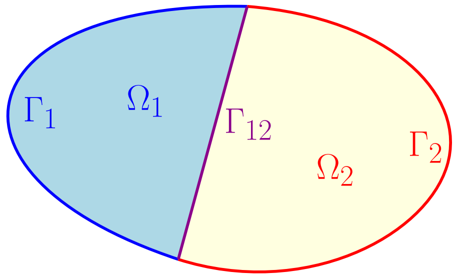

Figure 7.2: Splitting of the domain.

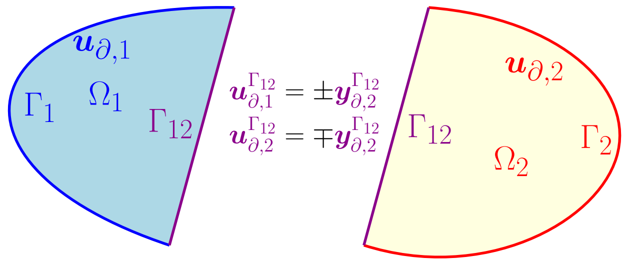

Figure 7.3: Interconnection at the interface Γ_{12}.

all possible mixed boundary conditions in a systematic manner. However the finite element discretization is required to satisfy the inf-sup condition. Simulating the resulting system is harder, since the algebraic constrains pose additional difficulties for the time integration.

7.2.2 Virtual domain decomposition

Since the boundary subsets Γ_1, Γ_2 are supposed to be connected sets, a single interface is sufficient to decompose the system appropriately. In Fig. 7.2 the splitting of the domain is accomplished by introducing the interface Γ_{12}. This separation line that separates the domain is an additional degree of freedom, as it can be freely drawn. If the finite element method is used for the basis functions, the interface should be drawn so that the meshing of the subdomains does not generate excessively skewed triangles.

The idea is based on the fact that System 7.104 can be split into two systems with uniform causality. The following set of boundary variables is used for Ω_1 subdomain

$$\begin{pmatrix} \boldsymbol{u}_{\partial,1} \\ \boldsymbol{u}_{\partial,1}^{\Gamma_{12}} \end{pmatrix} = \begin{bmatrix} \mathcal{N}_{\partial,1}^{\Gamma_1} & 0 \\ \mathcal{N}_{\partial,1}^{\Gamma_{12}} & 0 \end{bmatrix} \begin{pmatrix} \boldsymbol{e}_1 \\ \boldsymbol{e}_2 \end{pmatrix}, \qquad \begin{pmatrix} \boldsymbol{y}_{\partial,1} \\ \boldsymbol{y}_{\partial,1}^{\Gamma_{12}} \end{pmatrix} = \begin{bmatrix} 0 & \mathcal{N}_{\partial,2}^{\Gamma_1} \\ 0 & \mathcal{N}_{\partial,2}^{\Gamma_{12}} \end{bmatrix} \begin{pmatrix} \boldsymbol{e}_1 \\ \boldsymbol{e}_2 \end{pmatrix}. \tag{7.118}$$

Whereas for the Ω_2 subdomain, the boundary variables are

$$\begin{pmatrix} \boldsymbol{u}_{\partial,2} \\ \boldsymbol{u}_{\partial,2}^{\Gamma_{12}} \end{pmatrix} = \begin{bmatrix} 0 & \mathcal{N}_{\partial,2}^{\Gamma_2} \\ 0 & \mathcal{N}_{\partial,2}^{\Gamma_{12}} \end{bmatrix} \begin{pmatrix} \boldsymbol{e}_1 \\ \boldsymbol{e}_2 \end{pmatrix}, \qquad \begin{pmatrix} \boldsymbol{y}_{\partial,2} \\ \boldsymbol{y}_{\partial,2}^{\Gamma_{12}} \end{pmatrix} = \begin{bmatrix} \mathcal{N}_{\partial,1}^{\Gamma_1} & 0 \\ \mathcal{N}_{\partial,1}^{\Gamma_{12}} & 0 \end{bmatrix} \begin{pmatrix} \boldsymbol{e}_1 \\ \boldsymbol{e}_2 \end{pmatrix}. \tag{7.119}$$

The following relations then hold (cf. Fig. 7.3)

$$\boldsymbol{u}_{\partial,1}^{\Gamma_{12}} = \pm \boldsymbol{y}_{\partial,2}^{\Gamma_{12}}, \qquad \boldsymbol{u}_{\partial,2}^{\Gamma_{12}} = \mp \boldsymbol{y}_{\partial,1}^{\Gamma_{12}}. \tag{7.120}$$

The plus or minus sign is due to the fact that either $\mathcal{N}_{\partial,1}^{\Gamma_{12}}$ or $\mathcal{N}_{\partial,2}^{\Gamma_{12}}$ contains a scalar product with the outgoing normal (or the tangent unit vector) at Γ_{12} (that has opposite direction depending on which subdomain is considered). *These relations are at the core of the methodology, since they state the equivalence between a problem with mixed causalities and the interconnection of two problems with uniform causality.*

To obtain a final system with the desired causality, the weak form has to be carried out separately on each subdomain. In particular, on subdomain Ω_1 the $\mathcal{L}$ operator is integrated by parts, whereas on subdomain Ω_2 the $-\mathcal{L}^*$ operator undergoes the integration by parts. Consequently, on subdomains Ω_1 (Ω_2) the boundary input $\boldsymbol{u}_{\partial,1}$ ($\boldsymbol{u}_{\partial,2}$) explicitly appears. Let $L^2(\Omega_*, \mathbb{A})$ be the L^2 space restricted to the subdomain Ω_*, and let $L^2(\Omega_*, \mathbb{B})$ be the restriction of the L^2 space to Ω_* for $* \in \{1, 2\}$. The weak form of the dynamics (7.104a) for the Ω_1 contribution reads

$$\begin{aligned}
\langle \boldsymbol{v}_1,\, \mathcal{M}_1 \partial_t \boldsymbol{e}_1 \rangle_{L^2(\Omega_1, \mathbb{A})} &= -\langle \boldsymbol{v}_1,\, \boldsymbol{L}^\top \boldsymbol{e}_2 \rangle_{L^2(\Omega_1, \mathbb{A})} - \langle \boldsymbol{v}_1,\, \mathcal{L}^* \boldsymbol{e}_2 \rangle_{L^2(\Omega_1, \mathbb{A})} \\
\langle \boldsymbol{v}_2,\, \mathcal{M}_2 \partial_t \boldsymbol{e}_2 \rangle_{L^2(\Omega_1, \mathbb{B})} &= \langle \boldsymbol{v}_2,\, \boldsymbol{L} \boldsymbol{e}_1 \rangle_{L^2(\Omega_1, \mathbb{B})} + \langle \mathcal{L}^* \boldsymbol{v}_2,\, \boldsymbol{e}_1 \rangle_{L^2(\Omega_1, \mathbb{A})} + \langle \mathcal{N}_{\partial,2} \boldsymbol{v}_2,\, \mathcal{N}_{\partial,1} \boldsymbol{e}_1 \rangle_{L^2(\partial\Omega_1, \mathbb{R}^m)} .
\end{aligned} \tag{7.121}$$

For Ω_2, we get

$$\begin{aligned}
\langle \boldsymbol{v}_1,\, \mathcal{M}_1 \partial_t \boldsymbol{e}_1 \rangle_{L^2(\Omega_2, \mathbb{A})} &= -\langle \boldsymbol{v}_1,\, \boldsymbol{L}^\top \boldsymbol{e}_2 \rangle_{L^2(\Omega_2, \mathbb{A})} - \langle \mathcal{L} \boldsymbol{v}_1,\, \boldsymbol{e}_2 \rangle_{L^2(\Omega_2, \mathbb{B})} + \langle \mathcal{N}_{\partial,1} \boldsymbol{v}_1,\, \mathcal{N}_{\partial,2} \boldsymbol{e}_2 \rangle_{L^2(\partial\Omega_2, \mathbb{R}^m)} , \\
\langle \boldsymbol{v}_2,\, \mathcal{M}_2 \partial_t \boldsymbol{e}_2 \rangle_{L^2(\Omega_2, \mathbb{B})} &= \langle \boldsymbol{v}_2,\, \boldsymbol{L} \boldsymbol{e}_1 \rangle_{L^2(\Omega_2, \mathbb{B})} + \langle \boldsymbol{v}_2,\, \mathcal{L} \boldsymbol{e}_1 \rangle_{L^2(\Omega_2, \mathbb{B})} .
\end{aligned} \tag{7.122}$$

Since $\partial\Omega_1 = \overline{\Gamma}_1 \cup \overline{\Gamma}_{12}$ and $\partial\Omega_2 = \overline{\Gamma}_2 \cup \overline{\Gamma}_{12}$, the boundary terms can be decomposed

$$\begin{aligned}
\langle \mathcal{N}_{\partial,2} \boldsymbol{v}_2,\, \mathcal{N}_{\partial,1} \boldsymbol{e}_1 \rangle_{L^2(\partial\Omega_1, \mathbb{R}^m)} &= \langle \mathcal{N}_{\partial,2} \boldsymbol{v}_2,\, \mathcal{N}_{\partial,1} \boldsymbol{e}_1 \rangle_{L^2(\Gamma_1, \mathbb{R}^m)} + \langle \mathcal{N}_{\partial,2} \boldsymbol{v}_2,\, \mathcal{N}_{\partial,1} \boldsymbol{e}_1 \rangle_{L^2(\Gamma_{12}, \mathbb{R}^m)} , \\
&= \left\langle \mathcal{N}_{\partial,2}^{\Gamma_1} \boldsymbol{v}_2,\, \mathcal{N}_{\partial,1}^{\Gamma_1} \boldsymbol{e}_1 \right\rangle_{L^2(\Gamma_1, \mathbb{R}^m)} + \left\langle \mathcal{N}_{\partial,2}^{\Gamma_{12}} \boldsymbol{v}_2,\, \mathcal{N}_{\partial,1}^{\Gamma_{12}} \boldsymbol{e}_1 \right\rangle_{L^2(\Gamma_{12}, \mathbb{R}^m)} , \\
&= \left\langle \mathcal{N}_{\partial,2}^{\Gamma_1} \boldsymbol{v}_2,\, \boldsymbol{u}_{\partial,1} \right\rangle_{L^2(\Gamma_1, \mathbb{R}^m)} + \left\langle \mathcal{N}_{\partial,2}^{\Gamma_{12}} \boldsymbol{v}_2,\, \boldsymbol{u}_{\partial,1}^{\Gamma_{12}} \right\rangle_{L^2(\Gamma_{12}, \mathbb{R}^m)} .
\end{aligned} \tag{7.123}$$

Analogously, for the remaining boundary term we find

$$\langle \mathcal{N}_{\partial,1} \boldsymbol{v}_1,\, \mathcal{N}_{\partial,2} \boldsymbol{e}_2 \rangle_{L^2(\partial\Omega_2, \mathbb{R}^m)} = \left\langle \mathcal{N}_{\partial,1}^{\Gamma_2} \boldsymbol{v}_1,\, \boldsymbol{u}_{\partial,2} \right\rangle_{L^2(\Gamma_2, \mathbb{R}^m)} + \left\langle \mathcal{N}_{\partial,1}^{\Gamma_{12}} \boldsymbol{v}_1,\, \boldsymbol{u}_{\partial,2}^{\Gamma_{12}} \right\rangle_{L^2(\Gamma_{12}, \mathbb{R}^m)} . \tag{7.124}$$

A Galerkin approximation, analogous to (7.111), is used for each subdomain

$$\begin{aligned}
\boldsymbol{v}_{1,1} &\approx \sum_{i=1}^{n_{1,1}} \boldsymbol{\phi}_{1,1}^i(\boldsymbol{x}_1) v_{1,1}^i, \quad \boldsymbol{x}_1 \in \Omega_1, & \boldsymbol{v}_{1,2} &\approx \sum_{i=1}^{n_{1,2}} \boldsymbol{\phi}_{1,2}^i(\boldsymbol{x}_2) v_{1,2}^i, \quad \boldsymbol{x}_2 \in \Omega_2, \\
\boldsymbol{v}_{2,1} &\approx \sum_{i=1}^{n_{2,1}} \boldsymbol{\phi}_{2,1}^i(\boldsymbol{x}_1) v_{2,1}^i, & \boldsymbol{v}_{2,2} &\approx \sum_{i=1}^{n_{2,2}} \boldsymbol{\phi}_{2,2}^i(\boldsymbol{x}_2) v_{2,2}^i, \\
\boldsymbol{e}_{1,1} &\approx \sum_{i=1}^{n_{1,1}} \boldsymbol{\phi}_{1,1}^i(\boldsymbol{x}_1) e_{1,1}^i(t), & \boldsymbol{e}_{1,2} &\approx \sum_{i=1}^{n_{1,2}} \boldsymbol{\phi}_{1,2}^i(\boldsymbol{x}_2) e_{1,2}^i(t), \\
\boldsymbol{e}_{2,1} &\approx \sum_{i=1}^{n_{2,1}} \boldsymbol{\phi}_{2,1}^i(\boldsymbol{x}_1) e_{2,1}^i(t), & \boldsymbol{e}_{2,2} &\approx \sum_{i=1}^{n_{2,2}} \boldsymbol{\phi}_{2,2}^i(\boldsymbol{x}_2) e_{2,2}^i(t).
\end{aligned} \tag{7.125}$$

For the boundary variables, additional terms for the common interface are needed

$$
\begin{aligned}
\square_{\partial,1} &\approx \sum_{i=1}^{n_{\partial,1}} \boldsymbol{\phi}_{\partial,1}^{i}(\boldsymbol{s}_1)\square_{\partial,1}^{i}(t), \quad \boldsymbol{s}_1 \in \Gamma_1, \qquad & \square_{\partial,1}^{\Gamma_{12}} &\approx \sum_{i=1}^{n_{\partial,12}} \boldsymbol{\phi}_{\partial,12}^{i}(\boldsymbol{s}_{12})\square_{\partial,1}^{i,\Gamma_{12}}(t), \\
\square_{\partial,2} &\approx \sum_{i=1}^{n_{\partial,2}} \boldsymbol{\phi}_{\partial,2}^{i}(\boldsymbol{s}_2)\square_{\partial,2}^{i}(t), \quad \boldsymbol{s}_2 \in \Gamma_2. \qquad & \square_{\partial,2}^{\Gamma_{12}} &\approx \sum_{i=1}^{n_{\partial,12}} \boldsymbol{\phi}_{\partial,12}^{i}(\boldsymbol{s}_{12})\square_{\partial,2}^{i,\Gamma_{12}}(t),
\end{aligned}
\quad \boldsymbol{s}_{12} \in \Gamma_{12}.
\tag{7.126}
$$

where $\square$ stays for v, u, y.

Remark 12 (Choice of the interface basis functions)
Notice that the same basis functions $\boldsymbol{\phi}_{\partial,12}$ are used for both interface variables. This is necessary in order to dispose of the same degrees of freedom for the interconnection.

Replacing approximations 7.111, 7.126 into Eqs. 7.121, 7.123, 7.118, a finite dimensional system for the Ω_1 subdomain is obtained

$$
\begin{aligned}
&\begin{bmatrix} \mathbf{M}_{\mathcal{M}_1}^{\Omega_1} & \mathbf{0} \\ \mathbf{0} & \mathbf{M}_{\mathcal{M}_2}^{\Omega_1} \end{bmatrix}
\begin{pmatrix} \dot{\mathbf{e}}_{1,1} \\ \dot{\mathbf{e}}_{2,1} \end{pmatrix}
=
\begin{bmatrix} \mathbf{0} & -\mathbf{D}_0^{\Omega_1 \top} + \mathbf{D}_{-\mathcal{L}^*}^{\Omega_1} \\ \mathbf{D}_0^{\Omega_1} - \mathbf{D}_{-\mathcal{L}^*}^{\Omega_1 \top} & \mathbf{0} \end{bmatrix}
\begin{pmatrix} \mathbf{e}_{1,1} \\ \mathbf{e}_{2,1} \end{pmatrix}
+
\begin{bmatrix} \mathbf{0} & \mathbf{0} \\ \mathbf{B}_{2,\Gamma_1}^{\Omega_1} & \mathbf{B}_{2,\Gamma_{12}}^{\Omega_1} \end{bmatrix}
\begin{pmatrix} \mathbf{u}_{\partial,1} \\ \mathbf{u}_{\partial,1}^{\Gamma_{12}} \end{pmatrix}, \\
&\begin{bmatrix} \mathbf{M}_{\partial,1} & \mathbf{0} \\ \mathbf{0} & \mathbf{M}_{\partial,12} \end{bmatrix}
\begin{pmatrix} \mathbf{y}_{\partial,1} \\ \mathbf{y}_{\partial,1}^{\Gamma_{12}} \end{pmatrix}
=
\begin{bmatrix} \mathbf{0} & \mathbf{B}_{2,\Gamma_1}^{\Omega_1 \top} \\ \mathbf{0} & \mathbf{B}_{2,\Gamma_{12}}^{\Omega_1 \top} \end{bmatrix}
\begin{pmatrix} \mathbf{e}_{1,1} \\ \mathbf{e}_{2,1} \end{pmatrix}.
\end{aligned}
\tag{7.127}
$$

The mass and interconnection operator matrices are the restrictions to the subdomain of the matrices given in (7.116)

$$
\begin{aligned}
M_{\mathcal{M}_1}^{\Omega_1,ij} &= \left\langle \boldsymbol{\phi}_{1,1}^{i}, \, \mathcal{M}_1 \boldsymbol{\phi}_{1,1}^{j} \right\rangle_{L^2(\Omega_1,\mathbb{A})}, \quad & D_0^{\Omega_1,mj} &= \left\langle \boldsymbol{\phi}_{2,1}^{i}, \, \boldsymbol{L} \boldsymbol{\phi}_{1,1}^{j} \right\rangle_{L^2(\Omega_1,\mathbb{B})}, \qquad & i,j &\in \{1, n_{1,1}\}, \\
M_{\mathcal{M}_2}^{\Omega_1,mn} &= \left\langle \boldsymbol{\phi}_{2,1}^{m}, \, \mathcal{M}_2 \boldsymbol{\phi}_{2,1}^{n} \right\rangle_{L^2(\Omega_1,\mathbb{B})}, \quad & D_{-\mathcal{L}^*}^{\Omega_1,in} &= \left\langle \boldsymbol{\phi}_{1,1}^{m}, \, -\mathcal{L}^* \boldsymbol{\phi}_{2,1}^{n} \right\rangle_{L^2(\Omega_1,\mathbb{A})}, \qquad & m,n &\in \{1, n_{2,1}\}.
\end{aligned}
\tag{7.128}
$$

Matrix $\mathbf{M}_{\partial,1}$ is constructed as in Eq. (7.116). Matrix $\mathbf{M}_{\partial,12}$ is similarly built

$$
M_{\partial,12}^{lk} = \left\langle \boldsymbol{\phi}_{\partial,12}^{l}, \, \boldsymbol{\phi}_{\partial,12}^{k} \right\rangle_{L^2(\Gamma_{12},\mathbb{R}^m)}, \qquad l,k \in \{1, n_{\partial,12}\}.
\tag{7.129}
$$

The novel matrices $\mathbf{B}_{2,\Gamma_1}^{\Omega_1}$, $\mathbf{B}_{1,\Gamma_{12}}^{\Omega_1}$ have elements

$$
\begin{aligned}
B_{2,\Gamma_1}^{\Omega_1,mh} &= \left\langle \mathcal{N}_{\partial,2}^{\Gamma_1} \boldsymbol{\phi}_{2,1}^{m}, \, \boldsymbol{\phi}_{\partial,1}^{h} \right\rangle_{L^2(\Gamma_1,\mathbb{R}^m)}, \qquad & m \in \{1, n_{2,1}\}, \quad & h \in \{1, n_{\partial,1}\}, \\
B_{2,\Gamma_{12}}^{\Omega_1,mk} &= \left\langle \mathcal{N}_{\partial,2}^{\Gamma_{12}} \boldsymbol{\phi}_{2,1}^{m}, \, \boldsymbol{\phi}_{\partial,12}^{k} \right\rangle_{L^2(\Gamma_{12},\mathbb{R}^m)}, & & k \in \{1, n_{\partial,12}\}.
\end{aligned}
\tag{7.130}
$$

If instead the approximations are plugged into Eqs. 7.122, 7.124, 7.119, a finite dimensional system for the Ω_2 subdomain is computed

$$
\begin{bmatrix} \mathbf{M}^{\Omega_2}_{\mathcal{M}_1} & \mathbf{0} \\ \mathbf{0} & \mathbf{M}^{\Omega_2}_{\mathcal{M}_2} \end{bmatrix} \begin{pmatrix} \dot{\mathbf{e}}_{1,2} \\ \dot{\mathbf{e}}_{2,2} \end{pmatrix} = \begin{bmatrix} \mathbf{0} & -\mathbf{D}_0^{\Omega_2 \top} - \mathbf{D}_{\mathcal{L}}^{\Omega_2 \top} \\ \mathbf{D}_0^{\Omega_2} + \mathbf{D}_{\mathcal{L}}^{\Omega_2} & \mathbf{0} \end{bmatrix} \begin{pmatrix} \mathbf{e}_{1,2} \\ \mathbf{e}_{2,2} \end{pmatrix} + \begin{bmatrix} \mathbf{B}^{\Omega_2}_{1,\Gamma_2} & \mathbf{B}^{\Omega_2}_{1,\Gamma_{12}} \\ \mathbf{0} & \mathbf{0} \end{bmatrix} \begin{pmatrix} \mathbf{u}_{\partial,2} \\ \mathbf{u}^{\Gamma_{12}}_{\partial,2} \end{pmatrix},
$$
$$
\begin{bmatrix} \mathbf{M}_{\partial,2} & \mathbf{0} \\ \mathbf{0} & \mathbf{M}_{\partial,12} \end{bmatrix} \begin{pmatrix} \mathbf{y}_{\partial,2} \\ \mathbf{y}^{\Gamma_{12}}_{\partial,2} \end{pmatrix} = \begin{bmatrix} \mathbf{B}^{\Omega_2 \top}_{1,\Gamma_2} & \mathbf{0} \\ \mathbf{B}^{\Omega_2 \top}_{1,\Gamma_{12}} & \mathbf{0} \end{bmatrix} \begin{pmatrix} \mathbf{e}_{1,2} \\ \mathbf{e}_{2,2} \end{pmatrix}. \tag{7.131}
$$

The mass and interconnection operator matrices are the restrictions to the subdomain of the matrices given in (7.112)

$$
\begin{aligned}
M^{\Omega_2,ij}_{\mathcal{M}_1} &= \left\langle \phi^i_{1,2},\, \mathcal{M}_1 \phi^j_{1,2} \right\rangle_{L^2(\Omega_2,\mathbb{A})}, & D^{\Omega_2,mj}_0 &= \left\langle \phi^i_{2,2},\, \boldsymbol{L} \phi^j_{1,2} \right\rangle_{L^2(\Omega_2,\mathbb{B})}, & i,j &\in \{1, n_{1,2}\}, \\
M^{\Omega_2,mn}_{\mathcal{M}_2} &= \left\langle \phi^m_{2,2},\, \mathcal{M}_2 \phi^n_{2,2} \right\rangle_{L^2(\Omega_2,\mathbb{B})}, & D^{\Omega_2,mj}_{\mathcal{L}} &= \left\langle \phi^m_{2,2},\, \mathcal{L} \phi^n_{1,2} \right\rangle_{L^2(\Omega_2,\mathbb{B})}, & m,n &\in \{1, n_{2,2}\}.
\end{aligned} \tag{7.132}
$$

Matrix $\mathbf{M}_{\partial,2}$ is constructed as in (7.112). The elements of matrices $\mathbf{B}_{1,\Gamma_2}$, $\mathbf{B}_{1,\Gamma_{12}}$ are computed as

$$
\begin{aligned}
B^{ig}_{1,\Gamma_2} &= \left\langle \mathcal{N}^{\Gamma_2}_{\partial,1} \phi^i_{1,2},\, \phi^g_{\partial,2} \right\rangle_{L^2(\Gamma_2)}, & i &\in \{1, n_{1,2}\}, \quad g \in \{1, n_{\partial,2}\}, \\
B^{ik}_{1,\Gamma_{12}} &= \left\langle \mathcal{N}^{\Gamma_{12}}_{\partial,1} \phi^i_{1,2},\, \phi^k_{\partial,12} \right\rangle_{L^2(\Gamma_{12})}, & & k \in \{1, n_{\partial,12}\}.
\end{aligned} \tag{7.133}
$$

Systems (7.127), (7.131) are compactly rewritten as

System (7.127)

$$
\begin{aligned}
\mathbf{M}_{\Omega_1} \dot{\mathbf{e}}_{\Omega_1} &= \mathbf{J}_{\Omega_1} \mathbf{e}_{\Omega_1} + \mathbf{B}^{\Omega_1}_{\Gamma_1} \mathbf{u}_{\partial,1} + \mathbf{B}^{\Omega_1}_{\Gamma_{12}} \mathbf{u}^{\Gamma_{12}}_{\partial,1}, \\
\mathbf{M}_{\partial,1} \mathbf{y}_{\partial,1} &= \mathbf{B}^{\Omega_1 \top}_{\Gamma_1} \mathbf{e}_{\Omega_1}, \\
\mathbf{M}_{\partial,12} \mathbf{y}^{\Gamma_{12}}_{\partial,1} &= \mathbf{B}^{\Omega_1 \top}_{\Gamma_{12}} \mathbf{e}_{\Omega_1}.
\end{aligned} \tag{7.134}
$$

with Hamiltonian $H_{d,1} = \frac{1}{2} \mathbf{e}^\top_{\Omega_1} \mathbf{M}_{\Omega_1} \mathbf{e}_{\Omega_1}$

System (7.131)

$$
\begin{aligned}
\mathbf{M}_{\Omega_2} \dot{\mathbf{e}}_{\Omega_2} &= \mathbf{J}_{\Omega_2} \mathbf{e}_{\Omega_2} + \mathbf{B}^{\Omega_2}_{\Gamma_2} \mathbf{u}_{\partial,2} + \mathbf{B}^{\Omega_2}_{\Gamma_{12}} \mathbf{u}^{\Gamma_{12}}_{\partial,2}, \\
\mathbf{M}_{\partial,2} \mathbf{y}_{\partial,2} &= \mathbf{B}^{\Omega_2 \top}_{\Gamma_2} \mathbf{e}_{\Omega_2}, \\
\mathbf{M}_{\partial,12} \mathbf{y}^{\Gamma_{12}}_{\partial,2} &= \mathbf{B}^{\Omega_2 \top}_{\Gamma_{12}} \mathbf{e}_{\Omega_2}.
\end{aligned} \tag{7.135}
$$

with Hamiltonian $H_{d,2} = \frac{1}{2} \mathbf{e}^\top_{\Omega_2} \mathbf{M}_{\Omega_2} \mathbf{e}_{\Omega_2}$

To obtain a system with the desired causality, an interconnection is employed to connect the two Systems (7.134), (7.135) along the shared boundary Γ_{12}. Given (7.120), the gyrator interconnection [DMSB09] is computed as

$$
\begin{aligned}
\mathbf{u}^{\Gamma_{12}}_{\partial,1} &= \pm \mathbf{y}^{\Gamma_{12}}_{\partial,2} = \pm \mathbf{M}^{-1}_{\partial,12} \mathbf{B}^{\Omega_2 \top}_{\Gamma_{12}} \mathbf{e}_{\Omega_2}, \\
\mathbf{u}^{\Gamma_{12}}_{\partial,2} &= \mp \mathbf{y}^{\Gamma_{12}}_{\partial,1} = \mp \mathbf{M}^{-1}_{\partial,12} \mathbf{B}^{\Omega_1 \top}_{\Gamma_{12}} \mathbf{e}_{\Omega_1},
\end{aligned} \tag{7.136}
$$

The coupling matrix is then defined by

$$
\mathbf{C} := \mathbf{B}^{\Omega_1}_{\Gamma_{12}} \mathbf{M}^{-1}_{\partial,12} \mathbf{B}^{\Omega_2 \top}_{\Gamma_{12}}. \tag{7.137}
$$

Plugging Eq. (7.136) into 7.134, 7.135, the final system with mixed causality is obtained

$$
\begin{aligned}
\begin{bmatrix} \mathbf{M}_{\Omega_1} & \mathbf{0} \\ \mathbf{0} & \mathbf{M}_{\Omega_2} \end{bmatrix} \begin{pmatrix} \dot{\mathbf{e}}_{\Omega_1} \\ \dot{\mathbf{e}}_{\Omega_2} \end{pmatrix} &= \begin{bmatrix} \mathbf{J}_{\Omega_1} & \pm\mathbf{C} \\ \mp\mathbf{C}^\top & \mathbf{J}_{\Omega_2} \end{bmatrix} \begin{pmatrix} \mathbf{e}_{\Omega_1} \\ \mathbf{e}_{\Omega_2} \end{pmatrix} + \begin{bmatrix} \mathbf{B}_{\Gamma_1}^{\Omega_1} & \mathbf{0} \\ \mathbf{0} & \mathbf{B}_{\Gamma_2}^{\Omega_2} \end{bmatrix} \begin{pmatrix} \mathbf{u}_{\partial,1} \\ \mathbf{u}_{\partial,2} \end{pmatrix}, \\
\begin{bmatrix} \mathbf{M}_{\partial,1} & \mathbf{0} \\ \mathbf{0} & \mathbf{M}_{\partial,2} \end{bmatrix} \begin{pmatrix} \mathbf{y}_{\partial,1} \\ \mathbf{y}_{\partial,2} \end{pmatrix} &= \begin{bmatrix} \mathbf{B}_{\Gamma_1}^{\Omega_1\top} & \mathbf{0} \\ \mathbf{0} & \mathbf{B}_{\Gamma_2}^{\Omega_2\top} \end{bmatrix} \begin{pmatrix} \mathbf{e}_{\Omega_1} \\ \mathbf{e}_{\Omega_2} \end{pmatrix}.
\end{aligned} \tag{7.138}
$$

The total Hamiltonian is the sum

$$
H_d = H_{d,1} + H_{d,2} = \frac{1}{2}\mathbf{e}_{\Omega_1}^\top \mathbf{M}_{\Omega_1}\mathbf{e}_{\Omega_1} + \frac{1}{2}\mathbf{e}_{\Omega_2}^\top \mathbf{M}_{\Omega_2}\mathbf{e}_{\Omega_2}. \tag{7.139}
$$

So, the power rate is

$$
\begin{aligned}
\dot{H}_d &= \mathbf{e}_{\Omega_1}^\top \mathbf{M}_{\Omega_1}\dot{\mathbf{e}}_{\Omega_1} + \mathbf{e}_{\Omega_2}^\top \mathbf{M}_{\Omega_2}\dot{\mathbf{e}}_{\Omega_2}, \\
&= \mathbf{e}_{\Omega_1}^\top \mathbf{J}_{\Omega_1}\mathbf{e}_{\Omega_1} + \mathbf{e}_{\Omega_2}^\top \mathbf{J}_{\Omega_2}\mathbf{e}_{\Omega_2} \pm \mathbf{e}_{\Omega_1}^\top \mathbf{C}\,\mathbf{e}_{\Omega_2} \mp \mathbf{e}_{\Omega_2}^\top \mathbf{C}^\top \mathbf{e}_{\Omega_1} + \mathbf{e}_{\Omega_1}^\top \mathbf{B}_{\Gamma_1}^{\Omega_1}\mathbf{u}_{\partial,1} + \mathbf{e}_{\Omega_2}^\top \mathbf{B}_{\Gamma_2}^{\Omega_2}\mathbf{u}_{\partial,2}, \\
&= \mathbf{y}_{\partial,1}^\top \mathbf{M}_{\partial,1}\mathbf{u}_{\partial,1} + \mathbf{y}_{\partial,2}^\top \mathbf{M}_{\partial,2}\mathbf{u}_{\partial,2}, \\
&= \widehat{\mathbf{y}}_{\partial,1}^\top \mathbf{u}_{\partial,1} + \widehat{\mathbf{y}}_{\partial,2}^\top \mathbf{u}_{\partial,2}, \qquad \text{where} \qquad \widehat{\mathbf{y}}_{\partial,1} := \mathbf{M}_{\partial,1}\mathbf{y}_{\partial,1}, \quad \widehat{\mathbf{y}}_{\partial,2} := \mathbf{M}_{\partial,2}\mathbf{y}_{\partial,2}.
\end{aligned} \tag{7.140}
$$

Again this results mimics its corresponding infinite-dimensional (7.106).

This technique allows obtaining a system with the correct causality, but has some drawbacks. Suitable finite elements are required for both kinds of discretization detailed in §7.1.1, but the two are not always available (see Remark 10). A rigorous numerical convergence analysis of this technique appears rather involved. Some cases of mixed conditions, in particular conditions on single components of vectors, cannot be handled by this technique. For example, the simply supported condition in beams and plates imposes zero normal component of the traction at the boundary. Furthermore two different meshes are required and the interconnection has to manipulate carefully the degrees of freedom. This makes the implementation heavier than the Lagrange multiplier solution §7.2.1.

7.3 Conclusion

In this chapter a universal discretization method for multi-dimensional pHs has been detailed. The underlying Assumptions 2, 3 are indeed those that characterize the well-posedness of multi-dimensional pHs [Skr19]. For the time being, it has been shown that this technique is capable of constructing a finite-dimensional pHs from an infinite-dimensional one. For this reason, it is a structure-preserving method. The questions of numerical convergence and choice of approximation bases (in this thesis the focus is on the finite element method but spectral methods can be employed as well) are addressed in the next chapter, for the linear case only.

Chapter 8

Numerical convergence study

Aristotle maintained that women have fewer teeth than men; although he was twice married, it never occurred to him to verify this statement by examining his wives' mouths.

The Impact of Science on Society
Bertrand Russell

Contents

8.1 Discretization of the Euler-Bernoulli beam . . . 107
8.1.1 Mixed discretization for the free-free beam . . . 107
8.1.2 Mixed discretization for the clamped-clamped beam . . . 108
8.1.3 Mixed discretization with lower regularity requirement . . . 108
8.2 Plate problems using known mixed finite elements . . . 109
8.2.1 Mindlin plate mixed discretization . . . 109
8.2.2 The Hellan-Herrmann-Johnson scheme for the Kirchhoff plate . . . 112
8.3 Dual mixed discretization of plate problems . . . 113
8.3.1 Dual mixed discretization of the Mindlin plate . . . 113
8.3.2 Dual mixed discretization of the Kirchhoff plate . . . 114
8.4 Numerical experiments . . . 115
8.4.1 Numerical test for the Euler-Bernoulli beam . . . 116
8.4.2 Numerical test for the Mindlin plate . . . 118
8.4.3 Numerical test for the Kirchhoff plate . . . 120
8.5 Conclusion . . . 125

The application of the Partitioned Finite Element leads to finite-dimensional pH systems, that can be discretized using finite elements method. To quantify how well the numerical solution approximates the true one, it is important to estimate the rate of convergence of the finite elements. In this chapter convergence estimates are conjectured for beams and plates systems and numerical experiments are constructed in support to the proposed conjectures.

The first section is consecrated to the Euler-Bernoulli beam. For the discretization of this problem three methodologies are proposed. In this second section of this chapter, pH plate problems are discretized using mixed finite elements. This means that the divergence operator explicitly appears in the weak formulation. In the third part the discretization of plate problem is of dual-mixed type [A.90], meaning that the gradient operator comes out in the weak formulation. The last section gathers all the numerical results.

Remark 13

Homogeneous boundary conditions will be always considered in this chapter. This are enforced weakly or strongly depending on the specific formulation under analysis.

Notations The space of all, symmetric and skew-symmetric 2×2 matrices are denoted by $\mathbb{M}, \mathbb{S}, \mathbb{K}$ respectively. The space of $\mathbb{R}^2$ vectors is denoted by $\mathbb{V}$. The symbol $\Omega \subset \mathbb{R}^2$ denotes an open connected set. The standard notation $H^m(\Omega)$ denotes the Sobolev space of square integrable functions with m^{th} derivative in L^2 and norm

$$||u||_m^2 = \sum_{|\alpha| \leq m} \|\partial^\alpha u\|^2_{L^2(\Omega)}.$$

The space $H^{\text{Grad}}(\Omega, \mathbb{V})$ is the space of vectors with symmetric gradient in L^2

$$H^{\text{Grad}}(\Omega, \mathbb{V}) = \{\boldsymbol{u} \in L^2(\Omega, \mathbb{V}) | \ \text{Grad}(\boldsymbol{u}) \in L^2(\Omega, \mathbb{S})\},$$

and norm

$$||\boldsymbol{u}||^2_{\text{Grad}} = ||\boldsymbol{u}||^2 + ||\,\text{Grad}(\boldsymbol{u})||^2.$$

For $\mathbb{X} \subseteq \mathbb{M}$, let

$$\begin{aligned} H^{\text{div}}(\Omega, \mathbb{V}) &= \{\boldsymbol{u} \in L^2(\Omega, \mathbb{V}) | \ \text{div}(\boldsymbol{u}) \in L^2(\Omega)\}, \\ H^{\text{Div}}(\Omega, \mathbb{X}) &= \{\boldsymbol{U} \in L^2(\Omega, \mathbb{X}) | \ \text{Div}(\boldsymbol{U}) \in L^2(\Omega; \mathbb{V})\}, \end{aligned}$$

which are Hilbert spaces with the norms

$$\begin{aligned} \|\boldsymbol{u}\|^2_{\text{div}} &= \|\boldsymbol{u}\|^2_{L^2(\Omega, \mathbb{V})} + \|\text{div}(\boldsymbol{u})\|^2_{L^2(\Omega)}, \\ \|\boldsymbol{U}\|^2_{\text{Div}} &= \|\boldsymbol{U}\|^2_{L^2(\Omega, \mathbb{M})} + \|\text{Div}(\boldsymbol{U})\|^2_{L^2(\Omega, \mathbb{V})}. \end{aligned}$$

Let X be a Hilbert space, and t_f a positive real number. We denote by $L^\infty([0, t_f]; X)$ or $L^\infty(X)$ the space of functions $f : [0, t_f] \to X$ for which the time-space norm $|| \cdot ||_{L^\infty([0,t_f];X)}$ satisfies

$$||f||_{L^\infty([0,t_f];X)} = \operatorname*{ess\,sup}_{t \in [0, t_f]} ||f||_X < \infty.$$

The notation

$$||u - u_h|| \lesssim h^k$$

means $||u^{\text{ex}} - u_h|| \leq Ch^k$. The constant $C(u, t_f)$ depends only on the exact solution u and on the final time t_f.

8.1 Discretization of the Euler-Bernoulli beam

In this section the Euler-Bernoulli beam is discretized using conforming finite elements for three different formulations:

- the weak formulation (7.65) corresponding (in absence of inputs) to a free-free beam;
- the weak formulation (7.71) corresponding (for zero inputs) to a clamped-clamped beam;
- a novel weak formulation allowing to use H^1 conforming finite elements (both lines of system (7.64) are integrated by parts once).

8.1.1 Mixed discretization for the free-free beam

The weak formulation (7.65) seeks

$$\{e_w, e_\kappa\} \in H^2(\Omega) \times L^2(\Omega)$$

so that

$$\begin{aligned}
\langle v_w,\, \rho A \partial_t e_w \rangle_{L^2(\Omega)} &= - \langle \partial_{xx} v_w,\, e_\kappa \rangle_{L^2(\Omega)}\,, \qquad && \forall\, v_w \in H^2(\Omega), \\
\left\langle v_\kappa,\, (EI)^{-1} \partial_t e_\kappa \right\rangle_{L^2(\Omega)} &= \langle v_\kappa,\, \partial_{xx} e_w \rangle_{L^2(\Omega)}\,, \qquad && \forall\, v_\kappa \in L^2(\Omega).
\end{aligned} \tag{8.1}$$

Given an interval mesh $\mathcal{I}_h$ with elements E, the following conforming family of finite elements is selected for this problem

$$\begin{aligned}
H^2_{h,\mathrm{HerDG1}}(\Omega) &= \{w_h \in H^2(\Omega) |\ \forall E \in \mathcal{I}_h,\ w_h|_Q \in \mathrm{Her}\}, \\
L^2_{h,\mathrm{HerDG1}}(\Omega) &= \{M_h \in L^2(\Omega) |\ \forall E \in \mathcal{I}_h,\ M_h|_E \in \mathrm{DG}_1\},
\end{aligned} \tag{8.2}$$

where Her denotes the cubic Hermite polynomials and DG is the discontinuous Galerkin finite element [LMW+12, Chapter 3]. Since for the discretization of the static problem the use of Hermite polynomial provides optimal convergence of order 2 [Hug12], it seems logical to conjecture the following error estimates:

Conjecture 4 (Convergence of the HerDG1 elements)
Assuming a smooth solution for problem (8.1), the following error estimates hold

$$||e_w - e_w^h||_{L^\infty(H^2(\Omega))} \lesssim h^2, \qquad ||e_\kappa - e_\kappa^h||_{L^\infty(L^2(\Omega))} \lesssim h^2. \tag{8.3}$$

8.1.2 Mixed discretization for the clamped-clamped beam

The weak formulation (7.71) seeks

$$\{e_w, e_\kappa\} \in L^2(\Omega) \times H^2(\Omega)$$

so that

$$\begin{aligned}
\langle v_w,\, \rho A \partial_t e_w \rangle_{L^2(\Omega)} &= \langle v_w,\, -\partial_{xx} e_\kappa \rangle_{L^2(\Omega)}\,, \qquad && \forall\, v_w \in L^2(\Omega), \\
\left\langle v_\kappa,\, (EI)^{-1} \partial_t e_\kappa \right\rangle_{L^2(\Omega)} &= \langle \partial_{xx} v_\kappa,\, e_w \rangle_{L^2(\Omega)}\,, \qquad && \forall\, v_\kappa \in H^2(\Omega).
\end{aligned} \tag{8.4}$$

The following family of finite elements, defined on an interval mesh $\mathcal{I}_h$ with elements E, is chosen for this problem

$$\begin{aligned}
H^2_{h,\mathrm{DG1Her}}(\Omega) &= \{w_h \in L^2(\Omega) |\ \forall E \in \mathcal{I}_h,\ w_h|_Q \in \mathrm{DG}_1\}, \\
L^2_{h,\mathrm{DG1Her}}(\Omega) &= \{M_h \in H^2(\Omega) |\ \forall E \in \mathcal{I}_h,\ M_h|_E \in \mathrm{Her}\},
\end{aligned} \tag{8.5}$$

Since the formulation is symmetrical to (8.1), the following error estimates is conjectured:

Conjecture 5 (Convergence of the DG1Her elements)
Assuming a smooth solution for problem (8.4), the following error estimates hold

$$||e_w - e_w^h||_{L^\infty(L^2(\Omega))} \lesssim h^2, \qquad ||e_\kappa - e_\kappa^h||_{L^\infty(H^2(\Omega))} \lesssim h^2. \tag{8.6}$$

8.1.3 Mixed discretization with lower regularity requirement

Consider the weak formulation (7.64). If both lines are integrated by parts the following weak form is obtained: find

$$\{e_w, e_\kappa\} \in H^1(\Omega) \times H^1(\Omega)$$

so that

$$\begin{aligned}
\langle v_w,\, \rho A \partial_t e_w \rangle_{L^2(\Omega)} &= \langle \partial_x v_w,\, \partial_x e_\kappa \rangle_{L^2(\Omega)}\,, \qquad && \forall\, v_w \in H^1(\Omega), \\
\left\langle v_\kappa,\, (EI)^{-1} \partial_t e_\kappa \right\rangle_{L^2(\Omega)} &= - \langle \partial_x v_w,\, \partial_x e_\kappa \rangle_{L^2(\Omega)}\,, \qquad && \forall\, v_\kappa \in H^1(\Omega).
\end{aligned} \tag{8.7}$$

The following family of finite elements is employed for this problem

$$\begin{aligned}
H^2_{h,\mathrm{CGCG}}(\Omega) &= \{w_h \in H^1(\Omega) |\ \forall E \in \mathcal{I}_h,\ w_h|_Q \in \mathrm{CG}_k\}, \\
L^2_{h,\mathrm{CGCG}}(\Omega) &= \{M_h \in H^1(\Omega) |\ \forall E \in \mathcal{I}_h,\ M_h|_E \in \mathrm{CG}_k\},
\end{aligned} \tag{8.8}$$

where CG is the continuous Galerkin finite element [LMW+12, Chapter 3]. The following error estimates are conjectured:

Conjecture 6 (Convergence of the CGCG elements)
Assuming a smooth solution for problem (8.4), the following error estimates hold

$$||e_w - e_w^h||_{L^\infty(H^1(\Omega))} \lesssim h^k, \qquad ||e_\kappa - e_\kappa^h||_{L^\infty(H^1(\Omega))} \lesssim h^k. \tag{8.9}$$

8.2 Plate problems using known mixed finite elements

First we focused on the Mindlin plate. This problem is a combination of plane wave dynamics and plane elastodynamics. A classical mixed formulation requires H^{div} conforming elements both for the wave dynamics [BJT00] and elastodynamics [BJT01, AL14]. To obtain a suitable discretization of the Mindlin problem one has to combine the two. Additional difficulties arising from the symmetry of the stress tensor that can be imposed strongly [BJT01] or weakly [AL14].

We then discuss the mixed discretization of the Kirchhoff plate problem. For this problem the non-conforming Hellan-Herrmann-Johnson scheme [Hel67, Her67, Joh73] (HHJ) is the most successful. However, it has been analyzed under generic boundary conditions in the static case only [BR90].

8.2.1 Mindlin plate mixed discretization

We consider the weak formulation (7.98), reported in Section §7.1.2. We present first a scheme that enforces the symmetry of the momenta tensor strongly and then a scheme in which the symmetry of the momenta tensor is imposed weakly.

8.2.1.1 Mindlin plate with strongly imposed symmetry

The weak formulation with strongly imposed symmetry seeks

$$\{e_w, \boldsymbol{e_\theta}, \boldsymbol{E}_\kappa, \boldsymbol{e}_\gamma\} \in L^2(\Omega) \times L^2(\Omega, \mathbb{V}) \times H^{\mathrm{Div}}(\Omega, \mathbb{S}) \times H^{\mathrm{div}}(\Omega, \mathbb{V})$$

so that

$$\begin{aligned}
\langle v_w,\, \rho b \dot{e}_w \rangle_{L^2(\Omega)} &= \langle v_w,\, \operatorname{div} \boldsymbol{e}_\gamma \rangle_{L^2(\Omega)} + (v_w, f), && \forall\, v_w \in L^2(\Omega), \\
\langle \boldsymbol{v}_\theta,\, I_\theta \dot{\boldsymbol{e}}_\theta \rangle_{L^2(\Omega,\mathbb{V})} &= \langle \boldsymbol{v}_\theta,\, \operatorname{Div} \boldsymbol{E}_\kappa + \boldsymbol{e}_\gamma \rangle_{L^2(\Omega,\mathbb{V})} + \langle \boldsymbol{v}_\theta,\, \boldsymbol{\tau} \rangle_{L^2(\Omega,\mathbb{V})}, && \forall\, \boldsymbol{v}_\theta \in L^2(\Omega, \mathbb{V}), \\
\left\langle \boldsymbol{V}_\kappa,\, \boldsymbol{\mathcal{C}}_b \dot{\boldsymbol{E}}_\kappa \right\rangle_{L^2(\Omega,\mathbb{S})} &= - \langle \operatorname{Div} \boldsymbol{V}_\kappa,\, \boldsymbol{e}_\theta \rangle_{L^2(\Omega,\mathbb{S})}, && \forall\, \boldsymbol{V}_\kappa \in H^{\mathrm{Div}}(\Omega, \mathbb{S}), \\
\langle \boldsymbol{v}_\gamma,\, C_s \dot{\boldsymbol{e}}_\gamma \rangle_{L^2(\Omega,\mathbb{V})} &= - \langle \operatorname{div} \boldsymbol{v}_\gamma,\, e_w \rangle_{L^2(\Omega)} + \langle \boldsymbol{v}_\gamma,\, \boldsymbol{e}_\theta \rangle_{L^2(\Omega,\mathbb{V})}, && \forall\, \boldsymbol{v}_\gamma \in H^{\mathrm{div}}(\Omega, \mathbb{V}).
\end{aligned} \tag{8.10}$$

The plate thickness is indicated by the b symbol, to avoid confusion with the average mesh size indicated by h. A distributed force f and torque $\boldsymbol{\tau}$ are considered in order to find a manufactured solution for this problem.

Obtaining stable finite elements that embed the symmetry of the stress tensor for the elastodynamics problem has proven to be a difficult task [AW02]. The easiest construction is the one presented in [BJT01]. This finite element solution can be implemented in FIREDRAKE [RHM+17] thanks to the extruded mesh functionality [MBM+16]. The main disadvantage is that this scheme requires the domain to be given by a union of rectangles, as the mesh elements have to be square. However, this allows constructing a simple element for the momenta tensor. Given a regular mesh $\mathcal{R}_h$ with square elements Q the following spaces are introduced as discretization spaces

$$\begin{aligned}
L^2_{h,\mathrm{BJT}}(\Omega) &= \{w_h \in L^2(\Omega)|\ \forall Q \in \mathcal{R}_h,\ w_h|_Q \in \mathrm{DG}_{k-1}\}, \\
L^2_{h,\mathrm{BJT}}(\Omega, \mathbb{V}) &= \{\boldsymbol{\theta}_h \in L^2(\Omega, \mathbb{V})|\ \forall Q \in \mathcal{R}_h,\ \boldsymbol{\theta}_h|_Q \in (\mathrm{DG}_{k-1})^2\}, \\
H^{\mathrm{Div}}_{h,\mathrm{BJT}}(\Omega, \mathbb{S}) &= \{m_{12} \in H^1(\Omega)|\ \forall Q \in \mathcal{R}_h,\ m_{12}|_Q \in \mathrm{CG}_k\} \\
&\qquad \cup \{(m_{11}, m_{22}) \in H^{\mathrm{div}}(\Omega, \mathbb{V})|\ \forall Q \in \mathcal{R}_h,\ (m_{11}, m_{22})|_Q \in \mathrm{BDM}_k\}, \\
H^{\mathrm{div}}_{h,\mathrm{BJT}}(\Omega, \mathbb{V}) &= \{\boldsymbol{q}_h \in H^{\mathrm{div}}(\Omega, \mathbb{V})|\ \forall Q \in \mathcal{R}_h,\ \boldsymbol{q}_h|_Q \in \mathrm{BDM}_k\},
\end{aligned} \tag{8.11}$$

where BDM are the Brezzi-Douglas-Marini elements [BDM85]. BTJ stands for the initials of the authors in [BJT00, BJT01]. Combining the results of both papers, the following error estimates are conjectured.

Conjecture 7 (Convergence rate for the BJT elements)
Assuming a smooth solution to problem (8.10), the following error estimates hold

$$\begin{aligned}
||e_w - e_w^h||_{L^\infty(L^2(\Omega))} &\lesssim h^k, \qquad & ||\boldsymbol{E}_\kappa - \boldsymbol{E}_\kappa^h||_{L^\infty(L^2(\Omega,\mathbb{S}))} &\lesssim h^k, \\
||\boldsymbol{e}_\theta - \boldsymbol{e}_\theta^h||_{L^\infty(L^2(\Omega,\mathbb{V}))} &\lesssim h^k, \qquad & ||\boldsymbol{e}_\gamma - \boldsymbol{e}_\gamma^h||_{L^\infty(L^2(\Omega,\mathbb{V}))} &\lesssim h^k.
\end{aligned} \tag{8.12}$$

8.2.1.2 Mindlin plate with weakly imposed symmetry

To impose the symmetry of the momenta tensor weakly. we modify the third equation in (8.10). The symmetric gradient can be rewritten as

$$\mathrm{Grad}\ \boldsymbol{\theta} = \mathrm{grad}\,\boldsymbol{\theta} - \mathrm{skw}(\mathrm{grad}\,\boldsymbol{\theta}),$$

where $\mathrm{skw}(\boldsymbol{A}) = (\boldsymbol{A} - \boldsymbol{A}^\top)/2$ is the skew-symmetric part of matrix $\boldsymbol{A}$. Consider the weak form of the third equation in (8.10) before applying the integration by parts

$$\left\langle \boldsymbol{V}_\kappa,\, \boldsymbol{\mathcal{C}}_b \dot{\boldsymbol{E}}_\kappa \right\rangle_{L^2(\Omega,\mathbb{M})} = \left\langle \boldsymbol{V}_\kappa,\, \mathrm{Grad}\,\boldsymbol{e}_\theta \right\rangle_{L^2(\Omega,\mathbb{M})}.$$

Introducing the new variable $\boldsymbol{E}_r = \mathrm{skw}(\mathrm{grad}\,\boldsymbol{\theta})$, then $\{\boldsymbol{e}_\theta, \boldsymbol{E}_\kappa, \boldsymbol{E}_r\} \in L^2(\Omega, \mathbb{V}) \times H^{\mathrm{Div}}(\Omega, \mathbb{M}) \times L^2(\Omega, \mathbb{K})$ satisfy (remind that $\boldsymbol{e}_\theta = \partial_t \boldsymbol{\theta}$)

$$\begin{aligned}\left\langle \boldsymbol{V}_\kappa,\, \boldsymbol{\mathcal{C}}_b \dot{\boldsymbol{E}}_\kappa \right\rangle_{L^2(\Omega,\mathbb{M})} &= \langle \boldsymbol{V}_\kappa,\, \mathrm{grad}\, \boldsymbol{e}_\theta \rangle_{L^2(\Omega,\mathbb{M})} - \left\langle \boldsymbol{V}_\kappa,\, \dot{\boldsymbol{E}}_r \right\rangle_{L^2(\Omega,\mathbb{M})}, \\ &= -\langle \mathrm{Div}\, \boldsymbol{V}_\kappa,\, \boldsymbol{e}_\theta \rangle_{L^2(\Omega,\mathbb{V})} - \left\langle \boldsymbol{V}_\kappa,\, \dot{\boldsymbol{E}}_r \right\rangle_{L^2(\Omega,\mathbb{M})}.\end{aligned}$$

The momenta tensor is weakly symmetric if

$$\langle \boldsymbol{V}_r,\, \boldsymbol{E}_\kappa \rangle_{L^2(\Omega,\mathbb{M})},$$

or equivalently

$$\left\langle \boldsymbol{V}_r,\, \dot{\boldsymbol{E}}_\kappa \right\rangle_{L^2(\Omega,\mathbb{M})}.$$

The weak formulation then consists in finding

$$\{e_w, \boldsymbol{e_\theta}, \boldsymbol{E}_\kappa, \boldsymbol{e}_\gamma, \boldsymbol{E}_r\} \in L^2(\Omega) \times L^2(\Omega, \mathbb{V}) \times H^{\mathrm{Div}}(\Omega, \mathbb{M}) \times H^{\mathrm{div}}(\Omega, \mathbb{V}) \times L^2(\Omega, \mathbb{K}).$$

so that

$$\begin{aligned}\langle v_w,\, \rho b \dot{e}_w \rangle_{L^2(\Omega)} &= \langle v_w,\, \mathrm{div}\, \boldsymbol{e}_\gamma \rangle_{L^2(\Omega)} + (v_w, f), & \forall\, v_w &\in L^2(\Omega), \\ \langle \boldsymbol{v}_\theta,\, I_\theta \dot{\boldsymbol{e}}_\theta \rangle_{L^2(\Omega,\mathbb{V})} &= \langle \boldsymbol{v}_\theta,\, \mathrm{Div}\, \boldsymbol{E}_\kappa + \boldsymbol{e}_\gamma \rangle_{L^2(\Omega,\mathbb{V})} + \langle \boldsymbol{v}_\theta,\, \boldsymbol{\tau} \rangle_{L^2(\Omega,\mathbb{V})}, & \forall\, \boldsymbol{v_\theta} &\in L^2(\Omega, \mathbb{V}), \\ \left\langle \boldsymbol{V}_\kappa,\, \boldsymbol{\mathcal{C}}_b \dot{\boldsymbol{E}}_\kappa \right\rangle_{L^2(\Omega,\mathbb{M})} &= -\langle \mathrm{Div}\, \boldsymbol{V}_\kappa,\, \boldsymbol{e}_\theta \rangle_{L^2(\Omega,\mathbb{V})} - \left\langle \boldsymbol{V}_\kappa,\, \dot{\boldsymbol{E}}_r \right\rangle_{L^2(\Omega,\mathbb{M})}, & \forall\, \boldsymbol{V}_\kappa &\in H^{\mathrm{Div}}(\Omega, \mathbb{M}), \\ \langle \boldsymbol{v}_\gamma,\, C_s \dot{\boldsymbol{e}}_\gamma \rangle_{L^2(\Omega,\mathbb{V})} &= -\langle \mathrm{div} \boldsymbol{v}_\gamma,\, e_w \rangle_{L^2(\Omega)} + \langle \boldsymbol{v}_\gamma,\, \boldsymbol{e}_\theta \rangle_{L^2(\Omega,\mathbb{V})}, & \forall\, \boldsymbol{v}_\gamma &\in H^{\mathrm{div}}(\Omega, \mathbb{V}), \\ \left\langle \boldsymbol{V}_r,\, \dot{\boldsymbol{E}}_\kappa \right\rangle_{L^2(\Omega,\mathbb{M})} &= 0 & \forall\, \boldsymbol{V}_r &\in L^2(\Omega, \mathbb{K}).\end{aligned} \tag{8.13}$$

Consider a regular triangulation $\mathcal{T}_h$ with elements T. The following spaces are used as discretization spaces

$$\begin{aligned} L^2_{h,\mathrm{AFW}}(\Omega) &= \{w_h \in L^2(\Omega) |\ \forall T \in \mathcal{T}_h,\ w_h|_T \in \mathrm{DG}_{k-1}\}, \\ L^2_{h,\mathrm{AFW}}(\Omega, \mathbb{V}) &= \{\boldsymbol{\theta}_h \in L^2(\Omega, \mathbb{V}) |\ \forall T \in \mathcal{T}_h,\ \boldsymbol{\theta}_h|_T \in (\mathrm{DG}_{k-1})^2\}, \\ H^{\mathrm{Div}}_{h,\mathrm{AFW}}(\Omega, \mathbb{M}) &= \{(m_{11}, m_{12}) \in H^{\mathrm{div}}(\Omega, \mathbb{V}) |\ \forall T \in \mathcal{T}_h,\ (m_{11}, m_{12})|_T \in \mathrm{BDM}_k\} \\ &\quad \cup \{(m_{21}, m_{22}) \in H^{\mathrm{div}}(\Omega, \mathbb{V}) |\ \forall T \in \mathcal{T}_h,\ (m_{21}, m_{22})|_T \in \mathrm{BDM}_k\}, \\ H^{\mathrm{div}}_{h,\mathrm{AFW}}(\Omega, \mathbb{V}) &= \{\boldsymbol{q}_h \in H^{\mathrm{div}}(\Omega, \mathbb{V}) |\ \forall T \in \mathcal{T}_h,\ \boldsymbol{q}_h|_T \in \mathrm{RT}_{k-1}\}, \\ L^2_{h,\mathrm{AFW}}(\Omega, \mathbb{K}) &= \{\boldsymbol{R}_h \in L^2(\Omega, \mathbb{K}) |\ \forall T \in \mathcal{T}_h,\ w_h|_T \in \mathrm{DG}_{k-1}\}, \end{aligned} \tag{8.14}$$

where RT stands for the Raviart-Thomas elements [RT77]. The acronym AFW stands for Arnold-Falk-Winther, that proposed this kind on discretization for static elasticity [AFW07]. A convergence analysis for the general elastodynamics problem with weak symmetry in the $L^\infty(L^2)$ norm is detailed [AL14]. A convergence study for the wave equation with mixed finite elements in the $L^\infty(L^2)$ is presented in [Gev88]. Combining the results of the two, the following error estimates are conjectured:

Conjecture 8 (Rate of convergence for the AFW elements)
Assuming a smooth solution to problem (8.13), the following error estimates hold

$$
\begin{aligned}
&||e_w - e_w^h||_{L^\infty(L^2(\Omega))} \lesssim h^k, \qquad &&||\boldsymbol{E}_\kappa - \boldsymbol{E}_\kappa^h||_{L^\infty(L^2(\Omega,\mathbb{M}))} \lesssim h^k, \qquad && \\
&||\boldsymbol{e}_\theta - \boldsymbol{e}_\theta^h||_{L^\infty(L^2(\Omega,\mathbb{V}))} \lesssim h^k, \qquad &&||\boldsymbol{e}_\gamma - \boldsymbol{e}_\gamma^h||_{L^\infty(L^2(\Omega,\mathbb{V}))} \lesssim h^k, \qquad &&||\boldsymbol{E}_r - \boldsymbol{E}_r^h||_{L^\infty(L^2(\Omega,\mathbb{K}))} \lesssim h^k.
\end{aligned}
\tag{8.15}
$$

8.2.2 The Hellan-Herrmann-Johnson scheme for the Kirchhoff plate

For the Kirchhoff plate, the Hellan-Herrmann-Johnson scheme [Hel67, Her67, Joh73] (HHJ) can be used to obtain a structure-preserving discretization. Given the non conforming nature of this scheme, it is necessary to first introduce the discrete functional spaces and state the problem directly in discrete form. The illustration of the method follows closely [AW19]. The vertical displacement is approximated using continuous Lagrange polynomials, while the momenta tensor is discretized using the HHJ element

$$
\begin{aligned}
W_h =& \{w_h \in H_0^1(\Omega) |\ \forall T \in \mathcal{T}_h,\ w_h|_T \in P_k\}, \\
S_h =& \{\boldsymbol{M}_h \in L^2(\Omega, \mathbb{S}) |\ \forall T \in \mathcal{T}_h,\ \boldsymbol{M}_h|_T \in (P_{k-1})^{2\times 2}_{\text{sym}}, \\
& \quad \boldsymbol{M}_h \text{ is normal-normal continous across elements}\}.
\end{aligned}
\tag{8.16}
$$

The normal to normal continuity means that if two triangles T_1, T_2 share a common edge E then $\boldsymbol{n}^\top(\boldsymbol{M}_h|_{T_1})\boldsymbol{n} = \boldsymbol{n}^\top(\boldsymbol{M}_h|_{T_2})\boldsymbol{n}$ on E. Taking system (5.35) and multiplying the first equation by $v_w \in W_h$ and integrating over a triangle

$$
\begin{aligned}
-\langle v_w,\, \mathrm{div}\,\mathrm{Div}\,\boldsymbol{E}_\kappa\rangle_{L^2(T)} &= \langle \nabla v_w,\, \mathrm{Div}\,\boldsymbol{E}_\kappa\rangle_{L^2(T,\mathbb{V})} - \langle v_w,\, \mathrm{Div}\,\boldsymbol{E}_\kappa \cdot \boldsymbol{n}\rangle_{L^2(\partial T)}, \\
&= -\langle \mathrm{Hess}\, v_w,\, \boldsymbol{E}_\kappa\rangle_{L^2(T,\mathbb{S})} - \langle v_w,\, \mathrm{Div}\,\boldsymbol{E}_\kappa \cdot \boldsymbol{n}\rangle_{L^2(\partial T)}, \\
&+ \left\langle \partial_{\boldsymbol{s}} v_w,\, \boldsymbol{s}^\top \boldsymbol{E}_\kappa \boldsymbol{n}\right\rangle_{L^2(\partial T)} + \left\langle \partial_{\boldsymbol{n}} v_w,\, \boldsymbol{n}^\top \boldsymbol{E}_\kappa \boldsymbol{n}\right\rangle_{L^2(\partial T)}.
\end{aligned}
$$

A double integration by parts is applied to get the final equation. For the last term a summation over all triangles provides

$$
\sum_{T \in \mathcal{T}_h} \left\langle \partial_{\boldsymbol{n}} v_w,\, \boldsymbol{n}^\top \boldsymbol{E}_\kappa \boldsymbol{n}\right\rangle_{L^2(\partial T)} = \sum_{E \in \mathcal{E}_h} \left\langle [\![\partial_{\boldsymbol{n}} v_w]\!],\, \boldsymbol{n}^\top \boldsymbol{E}_\kappa \boldsymbol{n}\right\rangle_{L^2(E)},
$$

where $\mathcal{E}_h$ is the set of all edges belonging to the mesh and $[\![a]\!] = a|_{T_1} + a|_{T_2}$ denotes the jump of a function across shared edges. For a boundary edge it is simply the value of the function. For the other terms, it holds

$$
\langle v_w,\, \mathrm{Div}\,\boldsymbol{E}_\kappa \cdot \boldsymbol{n}\rangle_{L^2(\partial T)} = 0, \qquad \left\langle \partial_{\boldsymbol{s}} v_w,\, \boldsymbol{s}^\top \boldsymbol{E}_\kappa \boldsymbol{n}\right\rangle_{L^2(\partial T)} = 0,
$$

since v_w is continuous across the edge boundaries and the normal switches sign. We are now in a position to state the final weak form. Given the bilinear form

$$d_h(v_w,\ \boldsymbol{E}_\kappa) := -\sum_{T\in\mathcal{T}_h} \langle \mathrm{Hess}\, v_w,\ \boldsymbol{E}_\kappa\rangle_{L^2(T,\mathbb{S})} + \sum_{E\in\mathcal{E}_h} \left\langle [\![\partial_n v_w]\!],\ \boldsymbol{n}^\top \boldsymbol{E}_\kappa \boldsymbol{n}\right\rangle_{L^2(E)},$$

find $(e_w, \boldsymbol{E}_\kappa) \in W_h \times S_h$ such that

$$\begin{aligned}
\langle v_w,\ \rho b \dot{e}_w\rangle_{L^2(\Omega)} &= +d_h(v_w,\ \boldsymbol{E}_\kappa) + \langle v_w,\ f\rangle_{L^2(\Omega)}, && v_w \in W_h,\\
\left\langle \boldsymbol{V}_\kappa,\ \boldsymbol{\mathcal{C}}_b \dot{\boldsymbol{E}}_\kappa\right\rangle_{L^2(\Omega,\mathbb{S})} &= -d_h(e_w,\ \boldsymbol{V}_\kappa), && \boldsymbol{V}_\kappa \in S_h.
\end{aligned} \tag{8.17}$$

For the associated static problem, under the hypothesis of smooth solutions, optimal convergence of order $O(k)$ for $w \in H^1$ and $\boldsymbol{M} \in L^2$ has been established. So, it is natural to conjecture the following result for the dynamic problem:

Conjecture 9 (Convergence of the HHJ elements)
Assuming a smooth solution for problem (8.17), the following error estimates hold

$$||e_w - e_w^h||_{L^\infty(H^1(\Omega))} \lesssim h^k, \qquad ||\boldsymbol{E}_\kappa - \boldsymbol{E}_\kappa^h||_{L^\infty(L^2(\Omega,\mathbb{S}))} \lesssim h^k. \tag{8.18}$$

8.3 Dual mixed discretization of plate problems

In this section the discretization of the Kirchhoff and Mindlin plates is no-more a classical mixed discretization. The application of PFEM to the other partition of the system provides a discretization in which the grad and Grad operators appear.

8.3.1 Dual mixed discretization of the Mindlin plate

First of all we construct a family of finite elements capable of discretizing problem (7.90), that seeks

$$\{e_w, \boldsymbol{e}_{\boldsymbol{\theta}}, \boldsymbol{E}_\kappa, \boldsymbol{e}_\gamma\} \in H^1(\Omega) \times H^{\mathrm{Grad}}(\Omega, \mathbb{V}) \times L^2(\Omega, \mathbb{S}) \times L^2(\Omega, \mathbb{V})$$

so that

$$\begin{aligned}
\langle v_w,\ \rho h \partial_t e_w\rangle_{L^2(\Omega)} &= -\langle \mathrm{grad}\, v_w,\ \boldsymbol{e}_\gamma\rangle_{L^2(\Omega,\mathbb{R}^2)}, && \forall\ v_w \in H^1(\Omega),\\
\langle \boldsymbol{v}_\theta,\ I_\theta \partial_t \boldsymbol{e}_\theta\rangle_{L^2(\Omega,\mathbb{R}^2)} &= -\langle \mathrm{Grad}\, \boldsymbol{v}_\theta,\ \boldsymbol{E}_\kappa\rangle_{L^2(\Omega,\mathbb{R}^{2\times 2}_{\mathrm{sym}})} + \langle \boldsymbol{v}_\theta,\ \boldsymbol{e}_\gamma\rangle_{L^2(\Omega)}, && \forall\ \boldsymbol{v}_{\boldsymbol{\theta}} \in H^{\mathrm{Grad}}(\Omega, \mathbb{V}),\\
\langle \boldsymbol{V}_\kappa,\ \boldsymbol{\mathcal{C}}_{\boldsymbol{b}} \partial_t \boldsymbol{E}_\kappa\rangle_{L^2(\Omega,\mathbb{R}^{2\times 2}_{\mathrm{sym}})} &= \langle \boldsymbol{V}_\kappa,\ \mathrm{Grad}\, \boldsymbol{e}_\theta\rangle_{L^2(\Omega,\mathbb{R}^{2\times 2}_{\mathrm{sym}})}, && \forall\ \boldsymbol{V}_\kappa \in L^2(\Omega, \mathbb{S}),\\
\langle \boldsymbol{v}_\gamma,\ C_s \partial_t \boldsymbol{e}_\gamma\rangle_{L^2(\Omega,\mathbb{R}^2)} &= \langle \boldsymbol{v}_\gamma,\ \mathrm{grad}\, e_w\rangle_{L^2(\Omega,\mathbb{R}^2)} - \langle \boldsymbol{v}_\gamma,\ \boldsymbol{e}_\theta\rangle_{L^2(\Omega,\mathbb{R}^2)}, && \forall\ \boldsymbol{v}_\gamma \in L^2(\Omega, \mathbb{V}).
\end{aligned} \tag{8.19}$$

Consider a regular triangulation $\mathcal{T}_h$ with elements T. The following conforming family of finite elements is used to the weak formulation (8.19) (see also [CF05] for a similar construction for the elastodynamics problem)

$$
\begin{aligned}
H^1_{h,\mathrm{CGDG}}(\Omega) &= \{w_h \in H^1(\Omega)|\ \forall T \in \mathcal{T}_h,\ w_h|_T \in \mathrm{CG}_k\}, \\
H^{\mathrm{Grad}}_{h,\mathrm{CGDG}}(\Omega, \mathbb{R}^2) &= \{\boldsymbol{\theta}_h \in H^{\mathrm{Grad}}(\Omega, \mathbb{R}^2)|\ \forall T \in \mathcal{T}_h,\ \boldsymbol{\theta}_h|_T \in (\mathrm{CG}_k)^2\}, \\
L^2_{h,\mathrm{CGDG}}(\Omega, \mathbb{S}) &= \{\boldsymbol{M}_h \in L^2(\Omega, \mathbb{S})|\ \forall T \in \mathcal{T}_h, \boldsymbol{M}_h|_T \in (\mathrm{DG}_{k-1})^{2\times 2}_{\mathrm{sym}}\}, \\
L^2_{h,\mathrm{CGDG}}(\Omega, \mathbb{R}^2) &= \{\boldsymbol{q}_h \in L^2(\Omega, \mathbb{R}^2)|\ \forall T \in \mathcal{T}_h,\ \boldsymbol{q}_h|_T \in (\mathrm{DG}_{k-1})^2\}.
\end{aligned}
\tag{8.20}
$$

To approximate spaces $H^1_h(\Omega),\ H^{\mathrm{Grad}}_h(\Omega, \mathbb{R}^2)$ Lagrange polynomials of order k are selected. For spaces $L^2_h(\Omega, \mathbb{S}),\ L^2_h(\Omega, \mathbb{R}^2)$ Discontinous Galerkin polynomials of order $k-1$ are employed. This selection of finite elements can be seen as a standard discretization of the problem combined with a reduced integration of the stress tensor and shear vector. For this reason, the following conjecture on the error estimates is proposed.

Conjecture 10 (Convergence of the CGDG elements)
Assuming a smooth solution to problem (8.19), the following error estimates hold

$$
\begin{aligned}
||e_w - e_w^h||_{L^\infty(H^1(\Omega))} &\lesssim h^k, \qquad & ||\boldsymbol{E}_\kappa - \boldsymbol{E}_\kappa^h||_{L^\infty(L^2(\Omega))} &\lesssim h^k, \\
||\boldsymbol{e}_\theta - \boldsymbol{e}_\theta^h||_{L^\infty(H^{\mathrm{Grad}}(\Omega, \mathbb{R}^2))} &\lesssim h^k, \qquad & ||\boldsymbol{e}_\gamma - \boldsymbol{e}_\gamma^h||_{L^\infty(L^2(\Omega, \mathbb{S}))} &\lesssim h^k.
\end{aligned}
\tag{8.21}
$$

8.3.2 Dual mixed discretization of the Kirchhoff plate

The Kirchhoff plate weak formulation (7.80) seeks

$$\{e_w, \boldsymbol{E}_\kappa\} \in H^2(\Omega) \times L^2(\Omega, \mathbb{S})$$

so that

$$
\begin{aligned}
\langle v_w,\, \rho h \partial_t e_w \rangle_{L^2(\Omega)} &= - \langle \mathrm{Hess}\, v_w,\, \boldsymbol{E}_\kappa \rangle_{L^2(\Omega, \mathbb{R}^{2\times 2}_{\mathrm{sym}})}, \qquad & \forall\, v_w &\in H^2(\Omega), \\
\langle \boldsymbol{V}_\kappa,\, \boldsymbol{\mathcal{C}_b} \partial_t \boldsymbol{V}_\kappa \rangle_{L^2(\Omega, \mathbb{R}^{2\times 2}_{\mathrm{sym}})} &= \langle \boldsymbol{V}_\kappa,\, \mathrm{Hess}\, e_w \rangle_{L^2(\Omega, \mathbb{R}^{2\times 2}_{\mathrm{sym}})}. \qquad & \forall\, \boldsymbol{V}_\kappa &\in L^2(\Omega, \mathbb{S}).
\end{aligned}
\tag{8.22}
$$

Given a regular triangulation $\mathcal{T}_h$ with elements T, the following family of finite elements is conforming to the weak formulation (8.22)

$$
\begin{aligned}
H^2_{h,\mathrm{BellDG3}}(\Omega) &= \{w_h \in H^2(\Omega)|\ \forall T \in \mathcal{T}_h,\ w_h|_T \in \mathrm{Bell}\}, \\
L^2_{h,\mathrm{BellDG3}}(\Omega, \mathbb{S}) &= \{\boldsymbol{M}_h \in L^2(\Omega, \mathbb{S})|\ \forall T \in \mathcal{T}_h, \boldsymbol{M}_h|_T \in (\mathrm{DG}_3)^{2\times 2}_{\mathrm{sym}}\},
\end{aligned}
\tag{8.23}
$$

where Bell stands for the Bell element [Bel69]. No conjectured error estimates are proposed to this problem. As it will be shown in §8.4.3, the results obtained with this element are of difficult interpretation.

Remark 14
Thanks to a general approach for transforming finite elements [Kir18], H^2 conforming elements have been implemented in the Firedrake *library. Therefore, for the discretization of*

the H^2 space, the Argyris element [AFS68] is another valuable possibility. Unfortunately, the strong imposition of boundary conditions is not possible in FIREDRAKE *at the present time [KM19, Sec. 3.2]. Because of the simpler structure and ordering of its degrees of freedom, the Bell element has been privileged over the Argyris one for the convergence study. In Chap. 9 the Argyris element will be employed imposing weakly the boundary conditions.*

8.4 Numerical experiments

In this section numerical test cases are used to verify the conjectured orders of convergence for the two problems. Upon discretization, cf. Section §7.1.2, the weak formulations (8.1), (8.4), (8.7) (Euler Bernoulli beam), (8.10), (8.19) (Mindlin plate), and (8.17) (8.22) (Kirchhoff plate) assume the form

$$\underbrace{\begin{bmatrix} \mathbf{M}_1 & \mathbf{0} \\ \mathbf{0} & \mathbf{M}_2 \end{bmatrix}}_{\mathbf{M}} \begin{pmatrix} \dot{\mathbf{e}}_1 \\ \dot{\mathbf{e}}_2 \end{pmatrix} = \underbrace{\begin{bmatrix} \mathbf{0} & \mathbf{D} \\ -\mathbf{D}^\top & \mathbf{0} \end{bmatrix}}_{\mathbf{J}} \begin{pmatrix} \mathbf{e}_1 \\ \mathbf{e}_2 \end{pmatrix} + \begin{pmatrix} \mathbf{f} \\ \mathbf{0} \end{pmatrix}.$$

The mass matrix $\mathbf{M}$ is symmetric and positive definite. In case of weak enforcement of the symmetry (8.13) the final system reads

$$\underbrace{\begin{bmatrix} \mathbf{M}_1 & \mathbf{0} & \mathbf{0} \\ \mathbf{0} & \mathbf{M}_2 & \mathbf{A}_\lambda^\top \\ \mathbf{0} & \mathbf{A}_\lambda & \mathbf{0} \end{bmatrix}}_{\mathbf{M}} \begin{pmatrix} \dot{\mathbf{e}}_1 \\ \dot{\mathbf{e}}_2 \\ \dot{\boldsymbol{\lambda}} \end{pmatrix} = \underbrace{\begin{bmatrix} \mathbf{0} & \mathbf{D} & \mathbf{0} \\ -\mathbf{D}^\top & \mathbf{0} & \mathbf{0} \\ \mathbf{0} & \mathbf{0} & \mathbf{0} \end{bmatrix}}_{\mathbf{J}} \begin{pmatrix} \mathbf{e}_1 \\ \mathbf{e}_2 \\ \boldsymbol{\lambda} \end{pmatrix} + \begin{pmatrix} \mathbf{f} \\ \mathbf{0} \\ \mathbf{0} \end{pmatrix}.$$

where $\mathbf{A}_\lambda$ is the matrix obtained by discretization of $\left\langle \boldsymbol{V}_r, \, \dot{\boldsymbol{E}}_\kappa \right\rangle_{L^2(\Omega,\mathbb{M})}$.
Because of the presence of the Lagrange multiplier, the mass matrix $\mathbf{M}$ is symmetric and indefinite, giving rise to a saddle point problem. The numerical solution of this kind of problems is notoriously much harder than that of positive definite ones [BGL05]. The FIREDRAKE library [RHM+17] is used to generate the matrices. To integrate the equations in time a Crank-Nicholson scheme has been used, for all simulations. The time step is set to $\Delta t = h/10$ to have a lower impact of the time discretization error with respect to the spatial error. The final time is set to one $t_f = 1$[s] for all simulations. To compute the $L^\infty(X)$ space-time dependent norm the discrete norm $L^\infty_{\Delta t}(X)$ is used

$$|| \cdot ||_{L^\infty(X)} \approx || \cdot ||_{L^\infty_{\Delta t}(X)} = \max_{t \in t_i} || \cdot ||_X,$$

where t_i are the discrete simulation instants.

8.4.1 Numerical test for the Euler-Bernoulli beam

We consider the following exact solution for the Euler-Bernoulli beam under simply supported boundary conditions

$$w^{\text{ex}} = \sin(\pi x/L)\sin(t), \qquad \Omega = \{0, L\}. \tag{8.24}$$

The corresponding pH exact solution are then

$$\begin{aligned} e_w^{\text{ex}} &= \sin(\pi x/L)\cos(t), & e_w^{\text{ex}}|_{\partial\Omega} &= 0, \\ e_\kappa^{\text{ex}} &= -EI\,(\pi/L)^2 \sin(\pi x/L)\sin(t), & e_\kappa^{\text{ex}}|_{\partial\Omega} &= 0. \end{aligned} \tag{8.25}$$

The numerical values used for the simulations are reported in Tab. 8.1.

Beam parameters				
ρ	A	E	I	L
5600 [kg/m^3]	50 [mm^2]	[136 GPa]	4.16 [mm^4]	1 m

Table 8.1: Physical parameters for the Euler Bernoulli beam.

Results for the HerDG1 elements 8.2 The results are reported in Fig. 8.1 and Table B.2. The conjectured error estimates (8.3) are fulfilled.

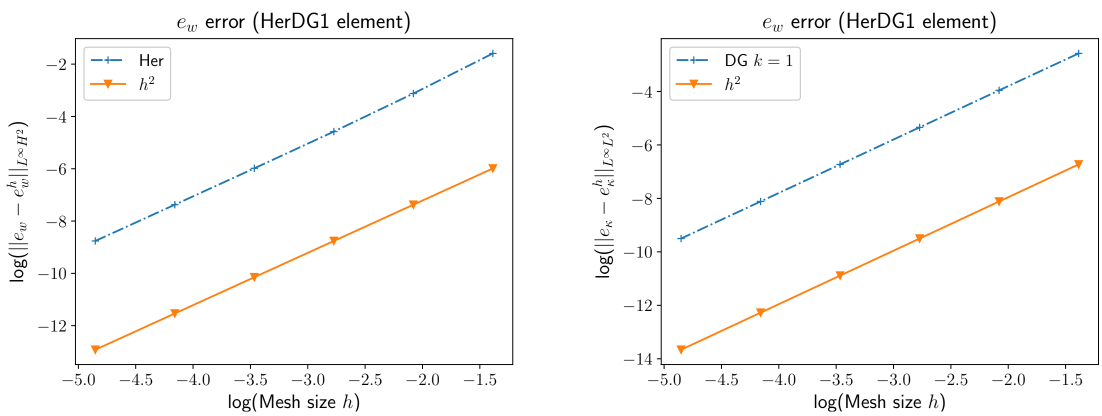

(a) $L^\infty_{\Delta t}(H^2(\Omega))$ error for e_w (b) $L^\infty_{\Delta t}(L^2(\Omega))$ error for e_κ

Figure 8.1: Error for the Euler Bernoulli beam (HerDG1 elements).

Results for the DG1Her elements 8.5 The results, reported in Fig. 8.2 and Table B.1, satisfy the predicted error (8.6).

Results for the CGCG elements 8.8 The results, reported in Fig. 8.3 and Tables B.3, B.4, B.5, verify the conjectured error (8.9).

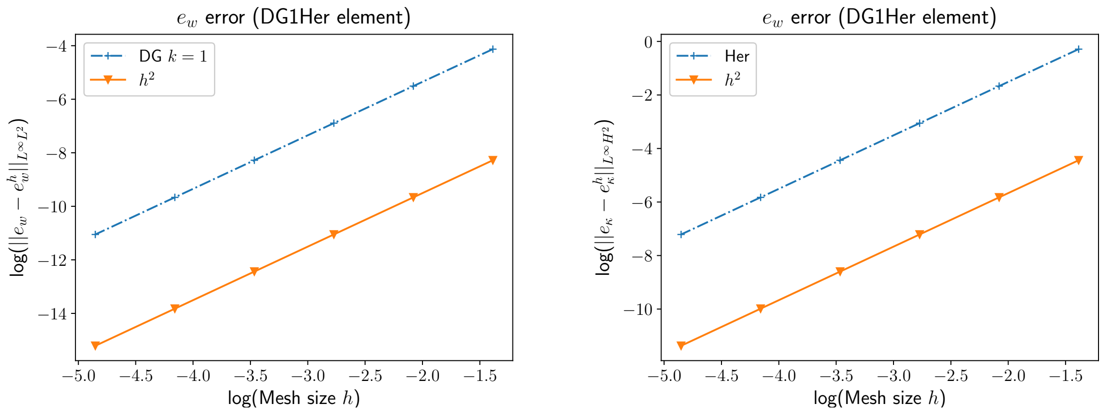

(a) $L^\infty_{\Delta t}(L^2(\Omega))$ error for e_w

(b) $L^\infty_{\Delta t}(H^2(\Omega))$ error for e_κ

Figure 8.2: Error for the Euler Bernoulli beam (DG1Her elements).

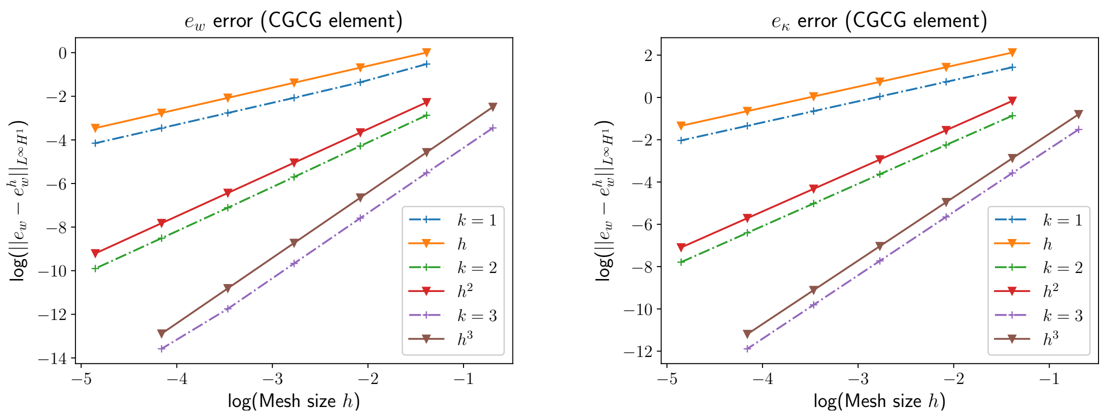

(a) $L^\infty_{\Delta t}(H^1(\Omega))$ error for e_w

(b) $L^\infty_{\Delta t}(H^1(\Omega))$ error for e_κ

Figure 8.3: Error for the Euler Bernoulli beam (CGCG elements).

8.4.2 Numerical test for the Mindlin plate

To validate the method first we test a finite element combinations on an analytic solution. Constructing an analytical solution for a vibrating Mindlin plate is far from trivial. Therefore, the solution for the static case [BadVMR13] is exploited.

Consider a distributed static force given by

$$
\begin{aligned}
f_s(x,y) = \frac{E_Y}{12(1-\nu^2)}&\{12y(y-1)(5x^2-5x+1) \\
&\times[2y^2(y-1)2+x(x-1)(5y^2-5y+1)]+12x(x-1) \\
&\times(5y^2-5y+1)[2x^2(x-1)2+y(y-1)(5x^2-5x+1)]\}.
\end{aligned}
$$

The static displacement and rotation are given by

$$
\begin{aligned}
w_s(x,y) &= \frac{1}{3}x^3(x-1)^3y^3(y-1)^3 - \frac{2b^2}{5(1-\nu)}[y^3(y-1)^3x(x-1)(5x^2-5x+1). \\
\boldsymbol{\theta}_s(x,y) &= \begin{pmatrix} y^3(y-1)^3 \ x^2(x-1)^2(2x-1) \\ x^3(x-1)^3 \ y^2(y-1)^2(2y-1) \end{pmatrix}
\end{aligned}
$$

The static solution solves the following problem defined on the square domain $\Omega = (0,1)\times(0,1)$ under clamped boundary condition:

$$
\begin{aligned}
0 &= \operatorname{div} \boldsymbol{q}_s + f_s, &\qquad \boldsymbol{\mathcal{C}}_b \boldsymbol{M}_s &= \operatorname{Grad} \boldsymbol{\theta}_s, &\qquad w_s|_{\partial\Omega} &= 0, \\
0 &= \operatorname{Div} \boldsymbol{M}_s + \boldsymbol{q}_s, & C_s \boldsymbol{q}_s &= \operatorname{grad} w_s - \boldsymbol{\theta}_s, & \boldsymbol{\theta}_s|_{\partial\Omega} &= 0.
\end{aligned} \tag{8.26}
$$

Given the linear nature of the system a solution for the dynamic problem is found by multiplying the static solution by a time dependent term. For simplicity a sinus function is chosen

$$
w_d(x,y,t) = w_s(x,y)\sin(t), \quad \boldsymbol{\theta}_d(x,y,t) = \boldsymbol{\theta}_s(x,y)\sin(t).
$$

Appropriate forcing terms have to be introduced to compensate the inertial accelerations. The force and torque in the dynamical case become

$$
f_d = f_s \sin(t) + \rho b \partial_{tt} w_d, \qquad \boldsymbol{\tau}_d = \frac{\rho b^3}{12}\partial_{tt}\boldsymbol{\theta}_d.
$$

For the port-Hamiltonian system the unknowns are the linear and angular velocities, the momenta tensor and the shear force. The exact solution and boundary conditions are thus given by

$$
\begin{aligned}
e_w^{\text{ex}} &= w_s(x,y)\cos(t), &\qquad \boldsymbol{E}_\kappa^{\text{ex}} &= \boldsymbol{\mathcal{D}}_b \operatorname{Grad} \boldsymbol{\theta}_d, &\qquad e_w^{\text{ex}}|_{\partial\Omega} &= 0, \\
\boldsymbol{e}_\theta^{\text{ex}} &= \boldsymbol{\theta}_s(x,y)\cos(t), & \boldsymbol{e}_\gamma^{\text{ex}} &= D_s(\operatorname{grad} w_d - \boldsymbol{\theta}_d), & \boldsymbol{e}_\theta^{\text{ex}}|_{\partial\Omega} &= 0.
\end{aligned} \tag{8.27}
$$

Variables $(e_w^{\text{ex}}, \boldsymbol{e}_\theta^{\text{ex}}, \boldsymbol{E}_\kappa^{\text{ex}}, \boldsymbol{e}_\gamma^{\text{ex}})$ under excitations $(f_d, \boldsymbol{\tau}_d)$ solve problem (7.86a). The solution being smooth, the conjectures 7 and 8 should hold. The numerical values of the physical parameters are reported in Table 8.2.

Plate parameters				
E	ρ	ν	K_{sh}	b
1 [Pa]	1 [kg/m^3]	0.3	5/6	0.1 [m]

Table 8.2: Physical parameters for the Mindlin plate.

Results for the mixed strong symmetry formulation (BTJ elements (8.11)**)** The weak form (8.10) and its corresponding finite elements (8.11) was implemented using Firedrake extruded mesh functionality [MBM+16]. A direct solver based on an LU preconditioner is used. In Fig. 8.4 and Tables B.6, B.7, B.8 the errors for $(e_w, \boldsymbol{e}_\theta, \boldsymbol{E}_\kappa, \boldsymbol{e}_\gamma)$ are reported. As one can notice, the conjectured error estimates (8.12) are respected for all variables.

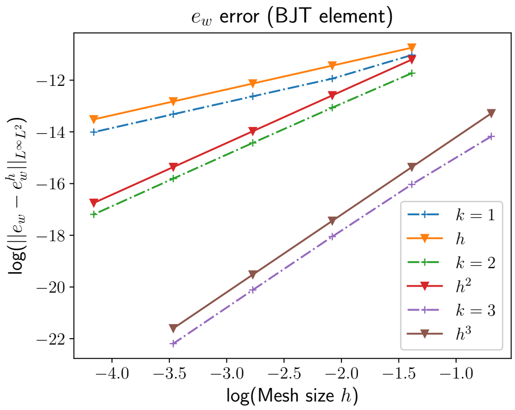

(a) $L^\infty_{\Delta t}(L^2(\Omega))$ error for e_w

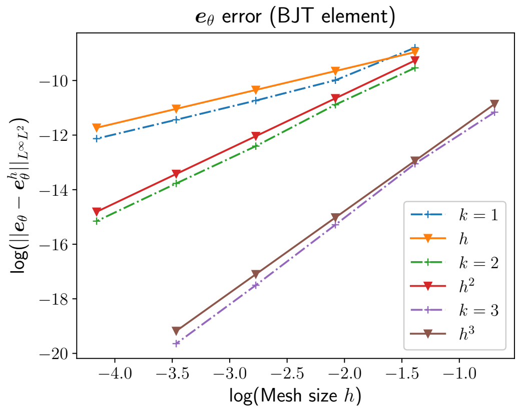

(b) $L^\infty_{\Delta t}(L^2(\Omega, \mathbb{V}))$ error for $\boldsymbol{e}_\theta$

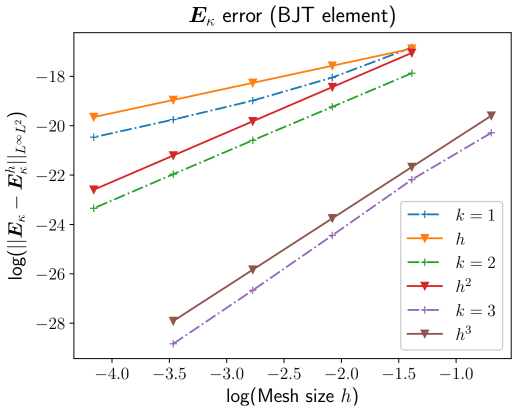

(c) $L^\infty_{\Delta t}(L^2(\Omega, \mathbb{S}))$ error for $\boldsymbol{E}_\kappa$

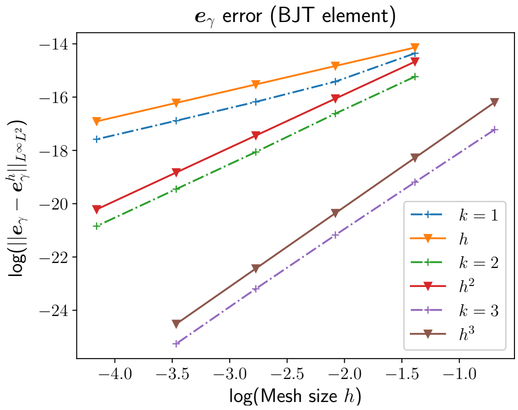

(d) $L^\infty_{\Delta t}(L^2(\Omega, \mathbb{V}))$ error for $\boldsymbol{e}_\gamma$

Figure 8.4: Error for the clamped Mindlin plate (BJT elements).

Results for the mixed weak symmetry formulation (AFW elements (8.14)**)** Formulation (8.13) and its element (8.14) are considered here. A direct solver fails for high order cases (i.e. $k = 3$). For this reason a generalized minimal residual method GMRES [SS86] is used with restart number of iterations equal to 100. In Fig. 8.5 and Tables B.9, B.10, B.11 the errors for variables $(e_w, \boldsymbol{e}_\theta, \boldsymbol{E}_\kappa, \boldsymbol{e}_\gamma)$ are reported. The errors for $(e_w, \boldsymbol{e}_\theta, \boldsymbol{e}_\gamma)$ respect the conjectured result (8.15). Variable $\boldsymbol{E}_\kappa$ exhibit a superconvergence phenomenon for the case $k = 1$. In [AL14] no numerical study was carried out for the case $k = 1$. The BDM elements might be responsible for such superconvergence. The convergence order of $(\boldsymbol{E}_\kappa, \boldsymbol{e}_\gamma)$ deteriorates for $k = 3$ for the finest mesh. This must be linked to errors due to the underlying large saddle-point problem. Indeed in [AL14] an hybridization method is used to transform the saddle-point problem into a positive definite one. The results for the Lagrange multiplier is reported in Fig. 8.5e and Table B.12. For this variable an order 2 of convergence is observed for all cases.

Results for dual mixed formulation (CGDG elements (8.20)) For this formulation have to imposed strongly on $e_w, \boldsymbol{e}_\theta$. A direct solver based on an LU preconditioner is used. In Fig. 8.6 and Tables B.13 the errors are reported. Conjecture 10 is verified for this test.

8.4.3 Numerical test for the Kirchhoff plate

The weak form (8.17) and the finite elements (8.16) are considered. The HHJ elements were included in FEniCS and Firedrake thanks to the contribution of Lizao Li [Li18]. Two numerical tests are performed to verify these elements. Both tests are solved using a direct solver with an LU preconditioner.

8.4.3.1 Simply supported test

An analytical solution for simply supported Kirchhoff plates is readily available. Consider the following solution of problem (5.20) under simply supported conditions on a square unitary domain $\Omega = (0, 1) \times (0, 1)$

$$w^{\mathrm{ex}}(x, y, t) = \sin(\pi x)\sin(\pi y)\sin(t), \quad (x, y) \in \Omega.$$

The forcing term is given by

$$f = (4D\pi^4 - \rho b)\sin(\pi x)\sin(\pi y)\sin(t), \quad D = \frac{E_Y b^3}{12(1 - \nu^2)}.$$

The corresponding variables in the port-Hamiltonian frame work are

$$e_w^{\mathrm{ex}} = \partial_t w^{\mathrm{ex}}, \quad \boldsymbol{E}_\kappa^{\mathrm{ex}} = \mathcal{D}\nabla^2 w^{\mathrm{ex}},$$

under simply supported boundary conditions

$$e_w|_{\partial\Omega} = 0, \qquad \boldsymbol{E}_\kappa : (\boldsymbol{n} \otimes \boldsymbol{n})|_{\partial\Omega} = 0.$$

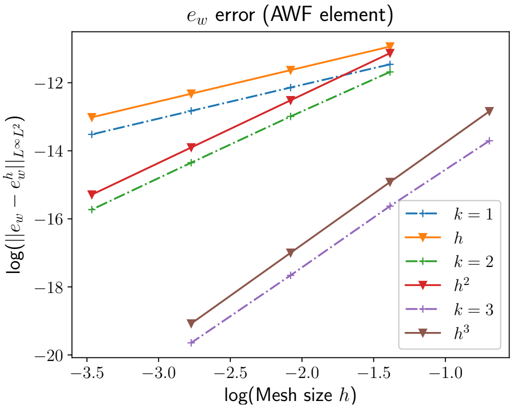

(a) $L^\infty_{\Delta t}(L^2(\Omega))$ error for e_w

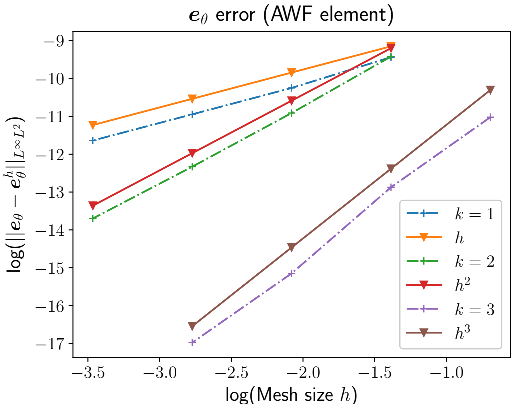

(b) $L^\infty_{\Delta t}(L^2(\Omega, \mathbb{V}))$ error for $\boldsymbol{e}_\theta$

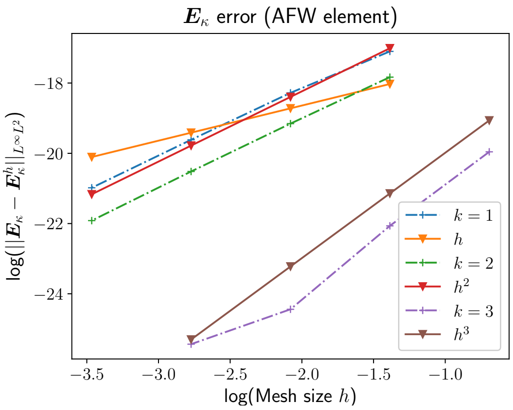

(c) $L^\infty_{\Delta t}(L^2(\Omega, \mathbb{M}))$ error for $\boldsymbol{E}_\kappa$

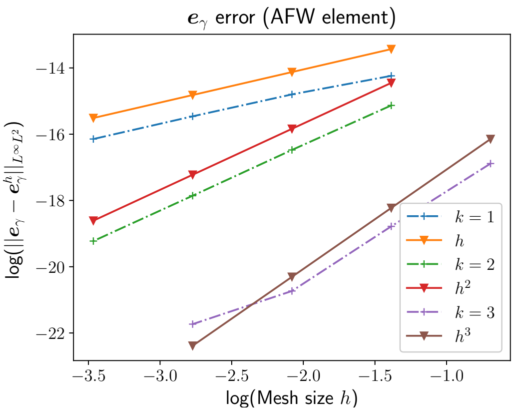

(d) $L^\infty_{\Delta t}(L^2(\Omega, \mathbb{V}))$ error for $\boldsymbol{e}_\gamma$

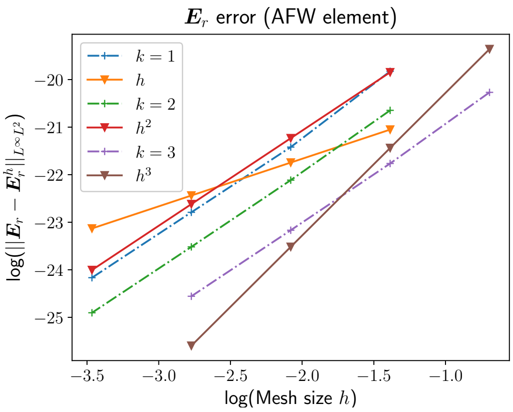

(e) $L^\infty_{\Delta t}(L^2(\Omega, \mathbb{K}))$ error for $\boldsymbol{E}_r$

Figure 8.5: Error for the clamped Mindlin plate (AFW elements).

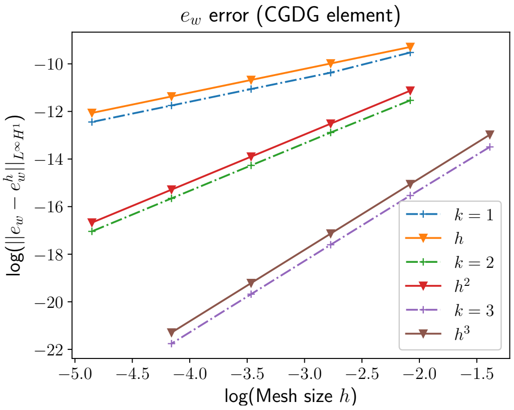

(a) $L^\infty_{\Delta t}(H^1(\Omega))$ error for e_w

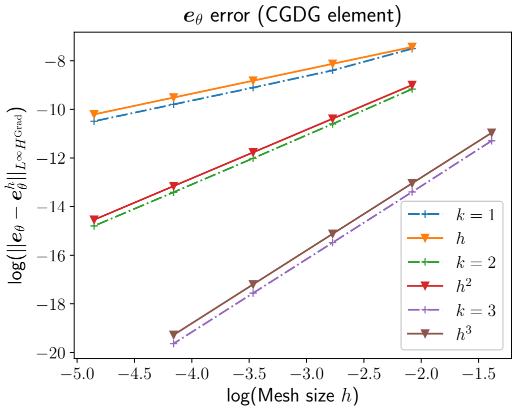

(b) $L^\infty_{\Delta t}(H^{\mathrm{Grad}}(\Omega, \mathbb{V}))$ error for $\boldsymbol{e}_\theta$

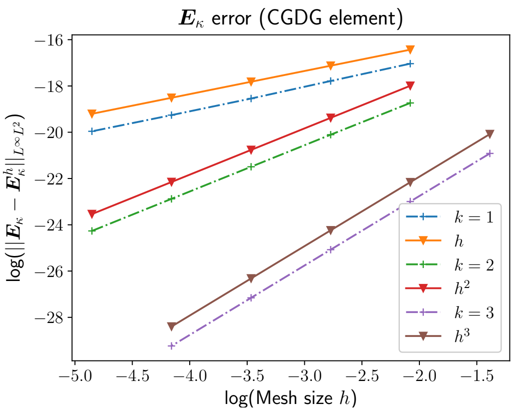

(c) $L^\infty_{\Delta t}(L^2(\Omega, \mathbb{S}))$ error for $\boldsymbol{E}_\kappa$

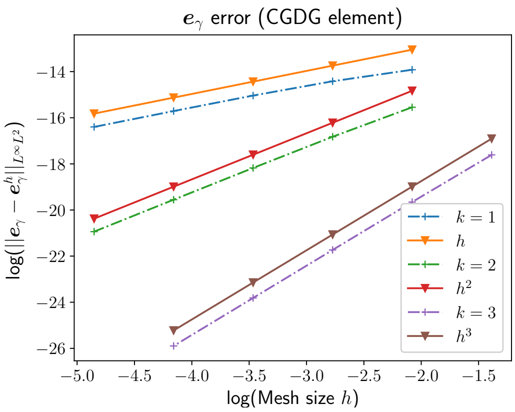

(d) $L^\infty_{\Delta t}(L^2(\Omega))$ error for $\boldsymbol{e}_\gamma$

Figure 8.6: Error for the clamped Mindlin plate (CGDG elements).

Variables $(e_w^{\mathrm{ex}}, \boldsymbol{E}_\kappa^{\mathrm{ex}})$ under excitation f solve problem (5.35). The physical parameters used in simulation are reported in Table 8.3.

Plate parameters			
E	ρ	ν	b
136 [GPa]	5600 [kg/m^3]	0.3	0.001 [m]

Table 8.3: Physical parameters for the Kirchhoff plate.

Results for the HHJ elements (8.16) Results are shown in Fig. 8.7 and Tables B.16, B.17 and B.18. The conjectured error estimates are respected.

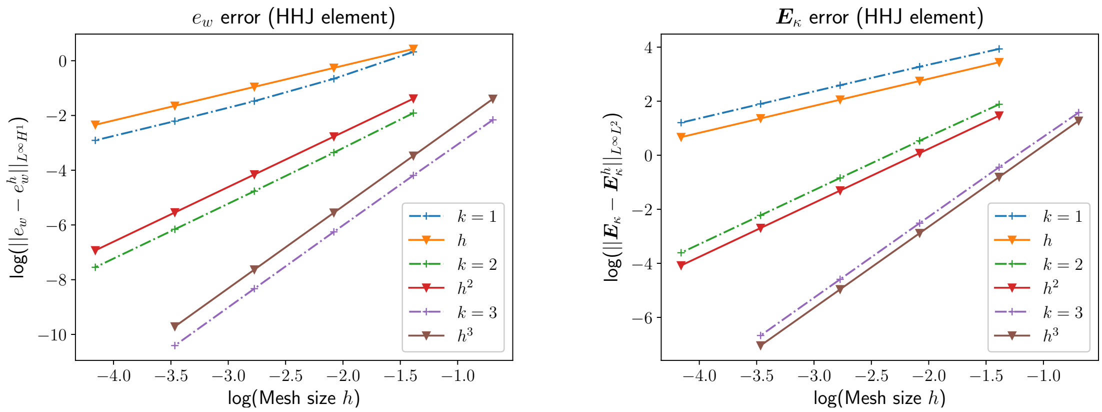

(a) $L^\infty_{\Delta t}(H^1(\Omega))$ error for e_w (b) $L^\infty_{\Delta t}(L^2(\Omega, \mathbb{S}))$ error for $\boldsymbol{E}_\kappa$

Figure 8.7: Error for the simply supported Kirchhoff plate (HHJ elements).

Results for the dual mixed formulation (BellDG3 elements) The results are reported in Fig. 8.8 and Tab. B.19. The error is computed in the $L^\infty(H^2(\Omega))$ norm for e_w and in the $L^\infty(L^2(\Omega, \mathbb{S}))$ norm for $\boldsymbol{E}_\kappa$. The convergence of the proposed elements is higher than linear, with a rate approaching 1.50 for the finest meshes. It is difficult to interpret this rate of convergence with respect to known convergence results. In particular the convergence rate for the Bell element (measured in the H^2 norm) for the classical biharmonic problem is 3 [Cia88]. The proposed method is not as performing as a standard discretization of the biharmonic problem

8.4.3.2 Mixed boundary conditions (CSFS)

We retrieve the manufactured solution for the static case from [RZ18]. Consider a square plate $\Omega = (-1, 1) \times (-1, 1)$ with simply supported top and bottom boundary, clamped left

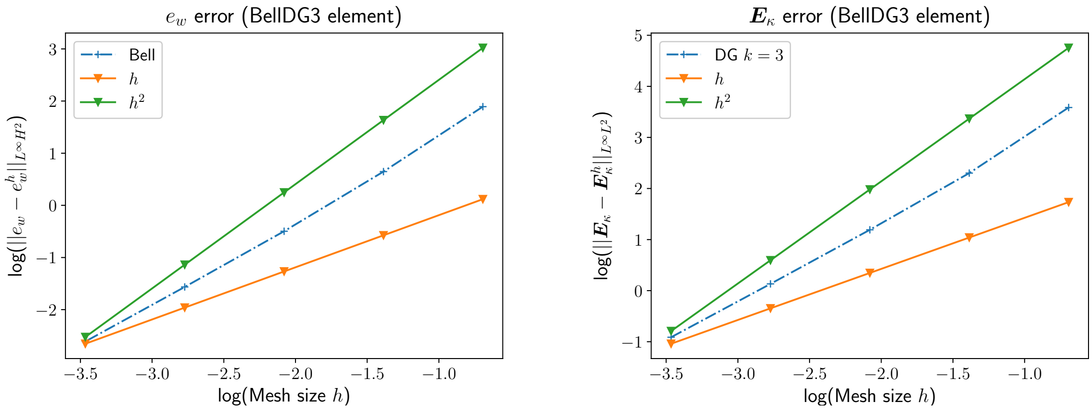

(a) $L^\infty_{\Delta t}(H^2(\Omega))$ error for e_w (b) $L^\infty_{\Delta t}(L^2(\Omega, \mathbb{S}))$ error for $\boldsymbol{E}_\kappa$

Figure 8.8: Error for the SSSS Kirchhoff plate (BellDG3 elements).

boundary and free right boundary. The stiffness tensor is the identity

$$\boldsymbol{\mathcal{D}}_b = \mathrm{Id}.$$

The density ρ and thickness b are the same as in 8.3. The static load is given by

$$f_s = 4\pi \sin(\pi x) \sin(\pi y).$$

The exact static solution is given by

$$w_s(x, y) = [(c_1 + c_2 x)\cosh(\pi x) + (c_3 + c_4 x)\sinh(\pi x) + \sin(\pi x)] \sin(\pi y).$$

The coefficient are then computed depending on the boundary conditions. For the considered case (CSFS) it is obtained

$$\begin{aligned}
c_1 &= -2\frac{\sinh(\pi) - 3\sinh(3\pi) + \pi[4\pi\sinh(\pi) + 7\cosh(\pi) - 3\cosh(3\pi)]}{5 + 8\pi^2 + 3\cosh(4\pi)}, \\
c_2 &= -\frac{8\pi[2\pi\sinh(\pi) + \cosh(\pi)]}{5 + 8\pi^2 + 3\cosh(4\pi)}, \\
c_3 &= \frac{10\cosh(\pi) + 6\cosh(\pi) + 16\pi[\sinh(\pi) + \pi\cosh(\pi)]}{5 + 8\pi^2 + 3\cosh(4\pi)}, \\
c_4 &= \frac{2\pi(5\sinh(\pi) - 3\sinh(3\pi) + 4\pi\cosh(\pi))}{5 + 8\pi^2 + 3\cosh(4\pi)}
\end{aligned}$$

The dynamical solution is constructed as in Sec. §8.4.2, meaning that a the static solution is multiplied by a sinusoidal function in time

$$w_d(x, y) = w_s(x, y)\sin(t).$$

The dynamical force is then given by

$$f_d(x,y,t) = f_s(x,y)\sin(t) + \rho b \partial_{tt} w_d$$

For the port-Hamiltonian system the exact solution are thus given by

$$e_w^{\text{ex}} = w_s(x,y)\cos(t), \qquad \boldsymbol{E}_\kappa^{\text{ex}} = \boldsymbol{\mathcal{D}}_b \,\text{Grad}\, \boldsymbol{\theta}_d. \tag{8.28}$$

The boundary conditions read

$$\begin{array}{rrrr} C & S & F & S \\ e_w^{\text{ex}}|_{x=-1} = 0, & e_w^{\text{ex}}|_{y=-1} = 0, & \partial_x E_{\kappa,xx} + \partial_y E_{\kappa,xy}|_{x=1} = 0, & e_w^{\text{ex}}|_{y=1} = 0, \\ \partial_x e_w^{\text{ex}}|_{x=-1} = 0, & E_{\kappa,yy}^{\text{ex}}|_{y=-1} = 0, & E_{\kappa,xx}^{\text{ex}}|_{x=1} = 0. & E_{\kappa,yy}^{\text{ex}}|_{y=1} = 0. \end{array} \tag{8.29}$$

Variables $(e_w^{\text{ex}}, \boldsymbol{E}_\kappa^{\text{ex}})$ under excitations f_d solve problem (7.77a).

Results for the HHJ elements (8.16) The results are reported in Fig. 8.9 and Tables B.20, B.21, B.22. Conjecture 9 is verified for all orders.

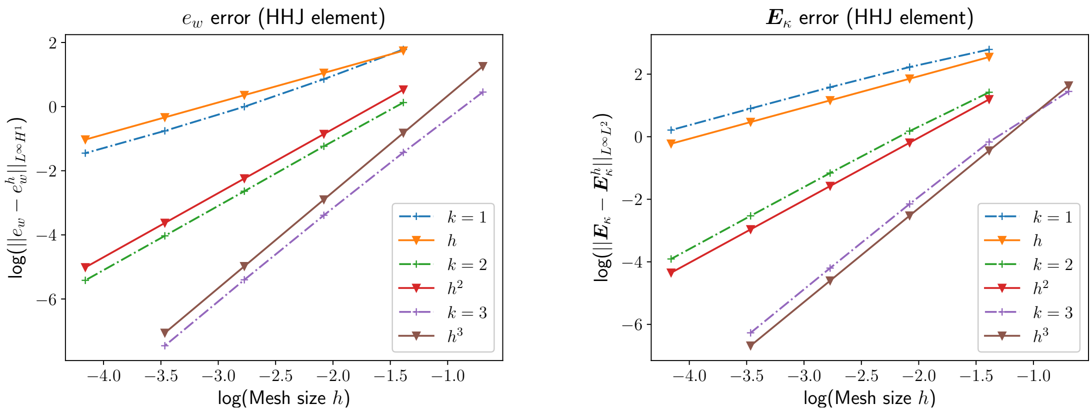

(a) $L^\infty_{\Delta t}(H^1(\Omega))$ error for e_w (b) $L^\infty_{\Delta t}(L^2(\Omega,\mathbb{S}))$ error for $\boldsymbol{E}_\kappa$

Figure 8.9: Error for the CSFS Kirchhoff plate (HHJ elements)

Results for the dual mixed formulation (BellDG3 elements) The results are reported in Fig. 8.10 and Tab. B.23. The error is computed in the $L^\infty(H^2(\Omega))$ norm for e_w and in the $L^\infty(L^2(\Omega,\mathbb{S}))$ norm for $\boldsymbol{E}_\kappa$. The convergence rate stays around 1.50 (as for the SSSS test).

8.5 Conclusion

In this chapter, the link between mixed finite element method and pH flexible structured has been studied. It was shown that existing and non-standard elements can be used to achieve

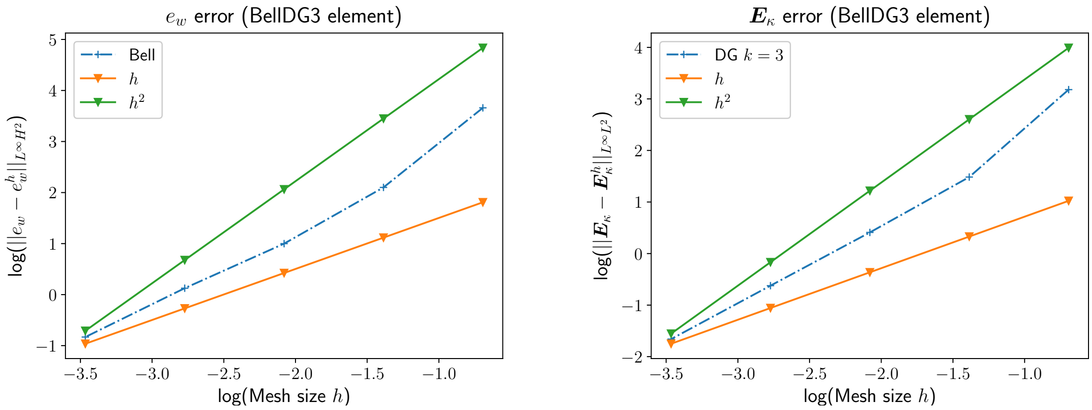

(a) $L^\infty_{\Delta t}(H^2(\Omega))$ error for e_w (b) $L^\infty_{\Delta t}(L^2(\Omega, \mathbb{S}))$ error for $\boldsymbol{E}_\kappa$

Figure 8.10: Error for the CSFS Kirchhoff plate (BellDG3 elements).

a structure-preserving discretization of the models under consideration. Apart for the dual discretization of the Kirchhoff plate, error estimates conjectures have been formulated. The numerical examples seem to confirm such conjectures. However a rigorous error analysis is still to be done.

Since the pH framework provides a powerful description of boundary control systems, it is important that numerical methods be capable of handling generic boundary conditions. Concerning this problem, the mixed discretization of Kirchhoff plate poses additional difficulties [BR90]. A promising methodology is detailed in [RZ18], but the dynamical case has not been considered yet.

Chapter 9

Numerical applications

> The most obvious characteristic of science is its application: the fact that, as a consequence of science, one has a power to do things. And the effect this power has had need hardly be mentioned. The whole industrial revolution would almost have been impossible without the development of science.
>
> *Richard Feynman*
> *The Meaning of It All: Thoughts of a Citizen-Scientist*

Contents

9.1 Boundary stabilization . . . 128
- 9.1.1 Cantilever Kirchhoff plate . . . 128
- 9.1.2 Irrotational shallow water equations . . . 130

9.2 Mixed boundary conditions enforcement . . . 135
- 9.2.1 Motion planning of a thin beam . . . 135
- 9.2.2 Vibroacoustics under mixed boundary conditions . . . 139

9.3 Thermoelastic wave propagation . . . 145

9.4 Modal analysis of plates . . . 145

The proposed finite element discretization can be employed for different numerical applications. The chapter is organized as follows:

- a boundary stabilization problem for the Kirchhoff plate and for the irrotational shallow water equations is presented in Sec. §9.1;
- Sec. §9.2 presents a comparison of the Lagrange multiplier 7.2.1 and the virtual domain decomposition method 7.2.2 for the enforcement of mixed boundary conditions;
- a thermoelastic problem for which an analytic solution is avaiable is illustrated in Sec. §9.3.

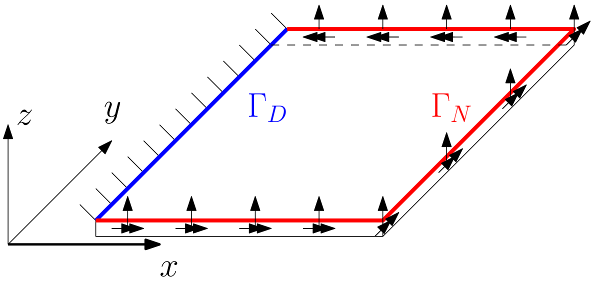

Figure 9.1: Cantilever plate subjected to a control forces on the lateral sides.

9.1 Boundary stabilization

In this section, we consider the boundary stabilization of a cantilever Kirchhoff plate of the irrotational shallow water equations. For pHs a simple proportional gain assures asymptotic system of the system thanks to the LaSalle' invariance principle [DMSB09, chapter 6, proposition 6.2]. This can be used to achieve stabilization of the undeformed configuration of the Kirchhoff plate. For the shallow water equation a reference is also added to stabilizes the system around a certain fluid height.

9.1.1 Cantilever Kirchhoff plate

Consider the problem (illustrated in Fig. 9.1)

$$\begin{bmatrix} \rho h & 0 \\ \mathbf{0} & \boldsymbol{\mathcal{C}_b} \end{bmatrix} \frac{\partial}{\partial t} \begin{pmatrix} e_w \\ \boldsymbol{E}_\kappa \end{pmatrix} = \begin{bmatrix} 0 & -\operatorname{div} \operatorname{Div} \\ \operatorname{Hess} & \mathbf{0} \end{bmatrix} \begin{pmatrix} e_w \\ \boldsymbol{E}_\kappa \end{pmatrix} \qquad (x, y) \in \Omega = [0,1] \times [0,1]$$

subjected to the following Dirichlet homogeneous conditions

$$\begin{aligned} \partial_t e_w|_{\Gamma_D} &= 0, \\ \partial_x e_w|_{\Gamma_D} &= 0, \end{aligned} \qquad \Gamma_D = \{x = 0\},$$

and Neumann boundary control

$$\begin{aligned} u_{\partial,q} = \widetilde{q}_n|_{\Gamma_N} &= -\boldsymbol{n} \cdot \operatorname{Div} \boldsymbol{E}_\kappa - \partial_{\boldsymbol{s}}(\boldsymbol{E}_\kappa : (\boldsymbol{n} \otimes \boldsymbol{s}))|_{\Gamma_N}, \\ u_{\partial,m} = m_{nn}|_{\Gamma_N} &= \boldsymbol{E}_\kappa : (\boldsymbol{n} \otimes \boldsymbol{n})|_{\Gamma_N}, \end{aligned} \qquad \Gamma_N = \{y = 0 \cup x = 1 \cup y = 1\}.$$

The corresponding boundary outputs read

$$\begin{aligned} y_{\partial,q} &= e_w|_{\Gamma_N}, \\ y_{\partial,m} &= \partial_{\boldsymbol{n}} e_w|_{\Gamma_N}. \end{aligned}$$

The initial conditions (compatible with the constraints) are given by

$$e_w(x, y, 0) = x^2, \qquad \boldsymbol{E}_\kappa(x, y, 0) = 0.$$

The following control law asymptotically stabilizes the system (cf. [Lag89])

$$\begin{aligned} u_q &= -k_q e_w|_{\Gamma_N} = -k_q y_{\partial,q}, \qquad & k_q > 0, \\ u_m &= -k_m \partial_{\boldsymbol{n}} e_w|_{\Gamma_N} = -k_m y_{\partial,m}, \qquad & k_m > 0. \end{aligned} \tag{9.1}$$

The discretization is performed as in (7.82). A structured mesh with 6 elements for side is used. Variables e_w and $\boldsymbol{E}_\kappa$ are discretized using the Argyris element and Discontinuous Galerkin elements of order 3. The Dirichlet conditions are imposed weakly using Lagrange multipliers (cf. (7.112) and Remark 14), that are discretized using Lagrange polynomials of order 2. The resulting system read

$$\begin{aligned} \begin{bmatrix} \mathbf{M}_{\rho h} & \mathbf{0} & \mathbf{0} \\ \mathbf{0} & \mathbf{M}_{\mathcal{C}_b} & \mathbf{0} \\ \mathbf{0} & \mathbf{0} & \mathbf{0} \end{bmatrix} \begin{pmatrix} \dot{\mathbf{e}}_w \\ \dot{\mathbf{e}}_\kappa \\ \dot{\boldsymbol{\lambda}}_{\Gamma_D} \end{pmatrix} &= \begin{bmatrix} \mathbf{0} & -\mathbf{D}_{\mathrm{Hess}}^\top & \mathbf{B}_{\Gamma_D} \\ \mathbf{D}_{\mathrm{Hess}} & \mathbf{0} & \mathbf{0} \\ -\mathbf{B}_{\Gamma_D}^\top & \mathbf{0} & \mathbf{0} \end{bmatrix} \begin{pmatrix} \dot{\mathbf{e}}_w \\ \dot{\mathbf{e}}_\kappa \\ \boldsymbol{\lambda}_{\Gamma_D} \end{pmatrix} + \begin{bmatrix} \mathbf{B}_{w,\Gamma_N} & \mathbf{B}_{\partial_{\boldsymbol{n}} w,\Gamma_N} \\ \mathbf{0} & \mathbf{0} \\ \mathbf{0} & \mathbf{0} \end{bmatrix} \begin{bmatrix} \mathbf{u}_{\partial,q} \\ \mathbf{u}_{\partial,m} \end{bmatrix}, \\ \begin{bmatrix} \mathbf{M}_{\Gamma_N} & \mathbf{0} \\ \mathbf{0} & \mathbf{M}_{\Gamma_N} \end{bmatrix} \begin{pmatrix} \mathbf{y}_{\partial,q} \\ \mathbf{y}_{\partial,m} \end{pmatrix} &= \begin{bmatrix} \mathbf{B}_{w,\Gamma_N}^\top & \mathbf{0} & \mathbf{0} \\ \mathbf{B}_{\partial_{\boldsymbol{n}} w,\Gamma_N}^\top & \mathbf{0} & \mathbf{0} \end{bmatrix} \begin{pmatrix} \dot{\mathbf{e}}_w \\ \dot{\mathbf{e}}_\kappa \\ \boldsymbol{\lambda}_{\Gamma_D} \end{pmatrix}, \end{aligned} \tag{9.2}$$

where $\mathbf{B}_{\Gamma_D} = [\mathbf{B}_{w,\Gamma_D} \ \mathbf{B}_{\partial_n w,\Gamma_D}]$. The discretization of the control law (9.1) provides

$$\begin{aligned} \mathbf{u}_{\partial,q} &= -k_q \mathbf{y}_{\partial,q} = -k_q \mathbf{M}_{\Gamma_N}^{-1} \mathbf{B}_{w,\Gamma_N}^\top \mathbf{e}_w, \\ \mathbf{u}_{\partial,m} &= -k_m \mathbf{y}_{\partial,m} = -k_m \mathbf{M}_{\Gamma_N}^{-1} \mathbf{B}_{\partial_{\boldsymbol{n}} w,\Gamma_N}^\top \mathbf{e}_w. \end{aligned} \tag{9.3}$$

System (9.2) now reads

$$\begin{bmatrix} \mathbf{M}_{\rho h} & \mathbf{0} & \mathbf{0} \\ \mathbf{0} & \mathbf{M}_{\mathcal{C}_b} & \mathbf{0} \\ \mathbf{0} & \mathbf{0} & \mathbf{0} \end{bmatrix} \begin{pmatrix} \dot{\mathbf{e}}_w \\ \dot{\mathbf{e}}_\kappa \\ \dot{\boldsymbol{\lambda}}_{\Gamma_D} \end{pmatrix} = \begin{bmatrix} -\mathbf{R}_w & -\mathbf{D}_{\mathrm{Hess}}^\top & \mathbf{B}_{\Gamma_D} \\ \mathbf{D}_{\mathrm{Hess}} & \mathbf{0} & \mathbf{0} \\ -\mathbf{B}_{\Gamma_D}^\top & \mathbf{0} & \mathbf{0} \end{bmatrix} \begin{pmatrix} \dot{\mathbf{e}}_w \\ \dot{\mathbf{e}}_\kappa \\ \boldsymbol{\lambda}_{\Gamma_D} \end{pmatrix}. \tag{9.4}$$

The matrix

$$\mathbf{R}_w = k_q \mathbf{B}_{w,\Gamma_N} \mathbf{M}_{\Gamma_N}^{-1} \mathbf{B}_{w,\Gamma_N}^\top + k_m \mathbf{B}_{\partial_{\boldsymbol{n}} w,\Gamma_N} \mathbf{M}_{\Gamma_N,}^{-1} \mathbf{B}_{\partial_{\boldsymbol{n}} w,\Gamma_N}^\top \succ 0$$

is positive definitive because of the collocated input-output feature of pH systems. The energy rate evaluates to ([BMXZ18] theorem 13)

$$\dot{H}_d = -\mathbf{e}_w^\top \, \mathbf{R}_w \, \mathbf{e}_w \leq 0.$$

Therefore, the Hamiltonian energy is a Lyapunov function and the asymptotic stability of configuration $\mathbf{e}_w = \mathbf{0}$, $\mathbf{e}_\kappa = \mathbf{0}$ is deduced using LaSalle' invariance principle.

The parameters for the numerical simulation are given in Table 9.1. The controller gains

Plate Parameters	
E	70 [GPa]
ρ	2700 [kg $\cdot$ m^3]
ν	0.35
h/L	0.05
$L_x = L_y$	1 [m]

Simulation Settings	
Integrator	Störmer-Verlet
Δt	1 [μs]
N° FE	6
FE spaces	Argyris $\times$ DG$_3$ $\times$ CG$_2$
t_{end}	5 [s]

Table 9.1: Settings and parameters for the boundary control of the Kirchhoff plate.

are set to

$$k_q = 10, \qquad k_m = 10. \tag{9.5}$$

The system is simulated using a Störmer-Verlet time integrator [HLW03] using a time step $\Delta t = 10^{-6}$ for a total simulation time of $t_{\mathrm{end}} = 5$ [s]. The Lagrange multiplier is eliminated using a projection method [BH15]. The control law is activated after 1 second. Snapshots of the simulation are reported in Fig. 9.3. The discrete Hamiltonian goes almost to zero in 4 seconds (Fig. 9.2).

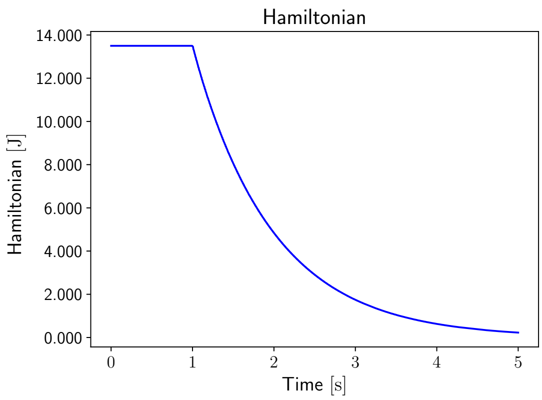

Figure 9.2: Hamiltonian trend for the cantilever Kirchhoff plate.

9.1.2 Irrotational shallow water equations

In this section we consider the boundary stabilization of a circular water tank via proportional feedback. We recall the system of equations (3.37)

$$\begin{aligned}
\frac{\partial}{\partial t}\begin{pmatrix}\alpha_h \\ \boldsymbol{\alpha}_v\end{pmatrix} &= \begin{bmatrix} 0 & -\operatorname{div} \\ -\operatorname{grad} & \mathbf{0}\end{bmatrix}\begin{pmatrix} e_h \\ \boldsymbol{e}_v\end{pmatrix}, \qquad (x,y) \in \Omega = \{x^2 + y^2 \leq R\}, \\
\begin{pmatrix} e_h \\ \boldsymbol{e}_v\end{pmatrix} &= \begin{pmatrix}\delta_{\alpha_h} H \\ \delta_{\boldsymbol{\alpha}_v} H\end{pmatrix}
\end{aligned} \tag{9.6}$$

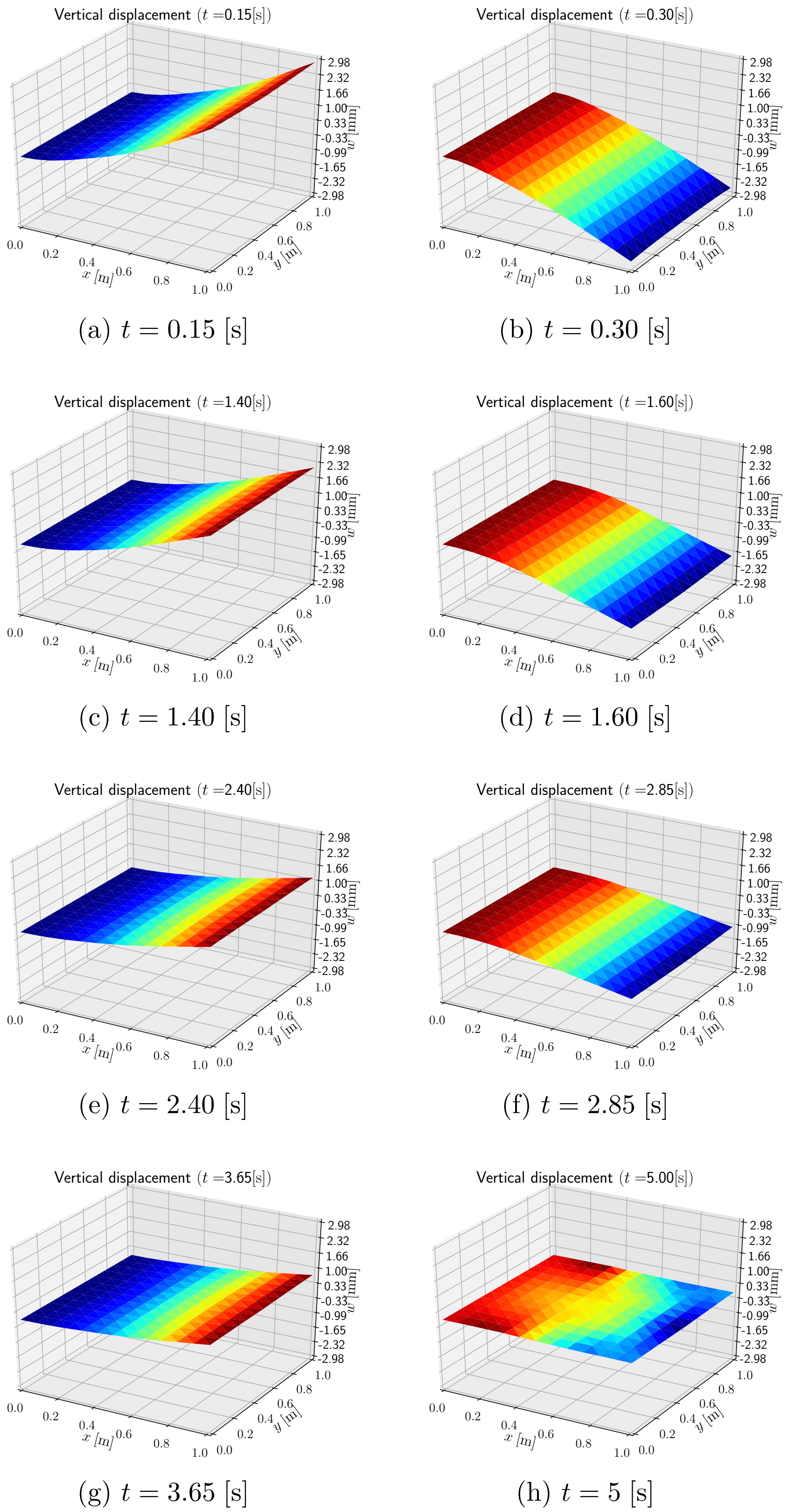

(a) $t = 0.15$ [s]
(b) $t = 0.30$ [s]
(c) $t = 1.40$ [s]
(d) $t = 1.60$ [s]
(e) $t = 2.40$ [s]
(f) $t = 2.85$ [s]
(g) $t = 3.65$ [s]
(h) $t = 5$ [s]

Figure 9.3: Snapshots at different times of the simulation of the boundary controlled cantilever Kirchhoff plate ($t_{\text{end}} = 5\,[s]$).

with

$$H(\alpha_h, \boldsymbol{\alpha}_v) = \frac{1}{2}\int_\Omega \left\{\frac{1}{\rho}\alpha_h \left\|\boldsymbol{\alpha}_v\right\|^2 + \rho g \alpha_h^2\right\} \,\mathrm{d}\Omega, \tag{9.7}$$

under Neumann boundary control

$$u_\partial = -\boldsymbol{e}_v \cdot \boldsymbol{n}|_{\partial\Omega} = -\frac{1}{\rho}\alpha_h \boldsymbol{\alpha}_v \cdot \boldsymbol{n}|_{\partial\Omega}. \tag{9.8}$$

The corresponding output reads

$$y_\partial = \boldsymbol{e}_h|_{\partial\Omega} = (\rho g \alpha_h + \frac{1}{2\rho}\left\|\boldsymbol{\alpha}_v\right\|^2)|_{\partial\Omega}. \tag{9.9}$$

The initial conditions are

$$\alpha_h = h_* + 10^{-1}\sin(\pi r/R)\cos(2\theta), \qquad r = \sqrt{x^2+y^2}, \qquad \theta = \arctan(y/r), \tag{9.10}$$

where h_* is the desired fluid height. It is known that a proportional controller exponentially stabilizes the system [DSP08]. Here, we use a simple control for stabilizing the system around the desired point h^*

$$u_\partial = -k(y_\partial - y_\partial^*), \qquad y_\partial^* = \rho g h^*, \quad k > 0. \tag{9.11}$$

This control law ensures that the Lyapunov functional

$$V = \frac{1}{2}\int_\Omega \left\{\frac{1}{2}\rho g(\alpha_h - \alpha_h^*)^2 + \frac{1}{2\rho}\alpha_h \left\|\boldsymbol{\alpha}_v\right\|^2\right\} d\Omega \geq 0, \tag{9.12}$$

where $\alpha_h^* = h^*$, has negative semi definite time derivative

$$\dot{V} = -k\int_{\partial\Omega} (y_\partial - y_\partial^*)^2 \,\mathrm{d}\Gamma \leq 0. \tag{9.13}$$

By the LaSalle' principle [Hen06] the point

$$\alpha_h = h^*, \qquad \boldsymbol{\alpha}_v = \mathbf{0}, \tag{9.14}$$

is asymptotically stable.

The discretization is performed as in (7.40). Variable α_h is discretized suing Lagrange polynomials of order 1. Discontinuous Galerkin of order 0 defined on the domain and on the boundary are used for $\boldsymbol{\alpha}_v, \boldsymbol{u}_\partial$.

$$\begin{aligned}
\begin{pmatrix} \dot{\boldsymbol{\alpha}}_{d,h} \\ \dot{\boldsymbol{\alpha}}_{d,v} \end{pmatrix} &= \begin{bmatrix} \mathbf{0} & \mathbf{M}_h^{-1}\mathbf{D}_{\mathrm{grad}}^\top \mathbf{M}_v^{-1} \\ -\mathbf{M}_v^{-1}\mathbf{D}_{\mathrm{grad}}\mathbf{M}_h^{-1} & \mathbf{0} \end{bmatrix} \begin{pmatrix} \partial_{\boldsymbol{\alpha}_{d,h}} H_d(\boldsymbol{\alpha}_{d,h},\ \boldsymbol{\alpha}_{d,v}) \\ \partial_{\boldsymbol{\alpha}_{d,v}} H_d(\boldsymbol{\alpha}_{d,h},\ \boldsymbol{\alpha}_{d,v}) \end{pmatrix} + \begin{bmatrix} \mathbf{B}_h \\ \mathbf{0} \end{bmatrix} \mathbf{u}_\partial, \\
\mathbf{M}_\partial \mathbf{y}_\partial &= \begin{bmatrix} \mathbf{B}_h^\top & \mathbf{0} \end{bmatrix} \begin{pmatrix} \partial_{\boldsymbol{\alpha}_{d,h}} H_d(\boldsymbol{\alpha}_{d,h},\ \boldsymbol{\alpha}_{d,v}) \\ \partial_{\boldsymbol{\alpha}_{d,v}} H_d(\boldsymbol{\alpha}_{d,h},\ \boldsymbol{\alpha}_{d,v}) \end{pmatrix}.
\end{aligned} \tag{9.15}$$

The control law (9.11), once discretized, is expressed as

$$\mathbf{u}_\partial = -k(\mathbf{y}_\partial - \mathbf{y}_\partial^*), \tag{9.16}$$

where $\mathbf{y}_\partial^* = \mathbf{M}_\partial^{-1} \int_{\partial\Omega} \rho g h_* \phi_\partial(s) \, \mathrm{d}\Gamma$. The closed loop system is then

$$\begin{pmatrix} \dot{\boldsymbol{\alpha}}_{d,h} \\ \dot{\boldsymbol{\alpha}}_{d,v} \end{pmatrix} = \begin{bmatrix} -\mathbf{R}_h & \mathbf{M}_h^{-1}\mathbf{D}_{\mathrm{grad}}^\top \mathbf{M}_v^{-1} \\ -\mathbf{M}_v^{-1}\mathbf{D}_{\mathrm{grad}}\mathbf{M}_h^{-1} & \mathbf{0} \end{bmatrix} \begin{bmatrix} \partial_{\boldsymbol{\alpha}_{d,h}} H_d(\boldsymbol{\alpha}_{d,h}, \ \boldsymbol{\alpha}_{d,v}) \\ \partial_{\boldsymbol{\alpha}_{d,v}} H_d(\boldsymbol{\alpha}_{d,h}, \ \boldsymbol{\alpha}_{d,v}) \end{bmatrix} + \begin{bmatrix} \mathbf{B}_h \\ \mathbf{0} \end{bmatrix} k\mathbf{y}_\partial^*, \tag{9.17}$$

Again the matrix

$$\mathbf{R}_h = k\mathbf{B}_h \mathbf{M}_\partial^{-1} \mathbf{B}_h^\top \succ 0$$

is positive definite and the discretized Lyapunov function rate reads

$$\dot{V}_d = -\partial_{\boldsymbol{\alpha}_{d,h}} H_d(\boldsymbol{\alpha}_{d,h}, \ \boldsymbol{\alpha}_{d,v})^\top \mathbf{R}_h \partial_{\boldsymbol{\alpha}_{d,h}} H_d(\boldsymbol{\alpha}_{d,h}, \ \boldsymbol{\alpha}_{d,v}) \leq 0.$$

Parameters	
ρ	1000 [kg · m^3]
g	10 [m/s^2]
R	1 [m]
h^*	1 [m]

Simulation Settings	
Integrator	Runge-Kutta 45
N° FE along R	20
FE spaces	$\mathrm{CG}_1 \times \mathrm{DG}_0 \times \mathrm{DG}_0$
t_{end}	3 [s]

Table 9.2: Settings and parameters for the irrotational shallow water equations.

The parameters for the simulation are reported in Table. (9.2). The controller gain is set to $k = 10^{-3}$. The control law is activated after 0.5 seconds. The system is simulated using a Runge-Kutta method. Snapshots are collected in Fig. 9.5. The discretized Hamiltonian and Lyapunov functional trends (Fig. 9.4) clearly show that while the Lyapunov function monotonically decrease, the Hamiltonian does not.

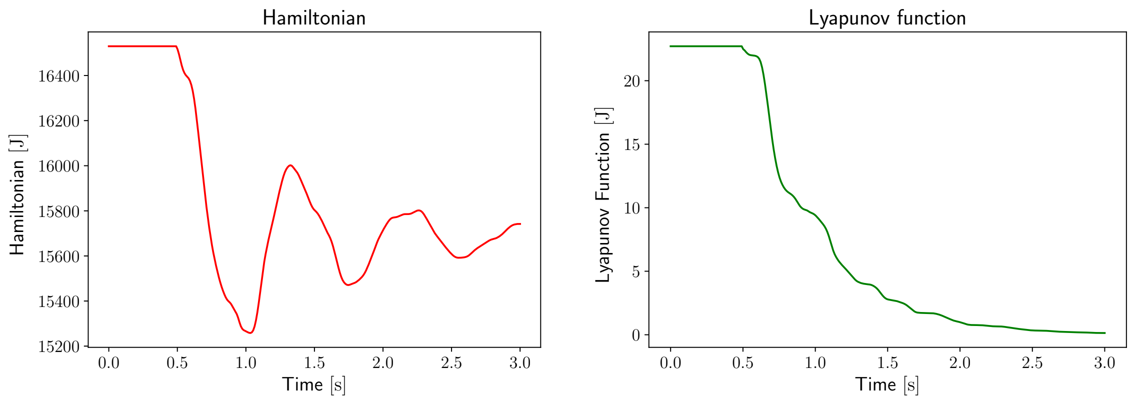

(a) Totat energy (Hamiltonian) (b) Lyapunov function

Figure 9.4: Total energy and Lyapunov function for the Shallow water equations.

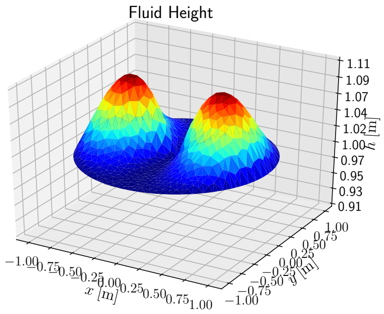

(a) $t = 0$ [s]

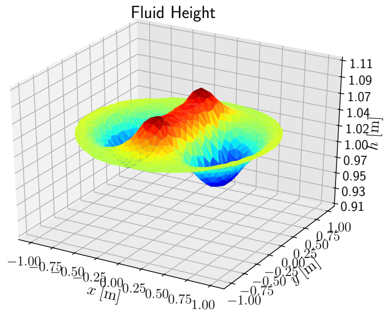

(b) $t = 0.42$ [s]

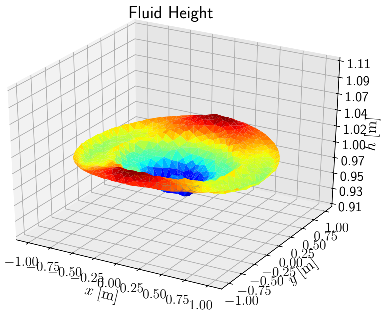

(c) $t = 0.85$ [s]

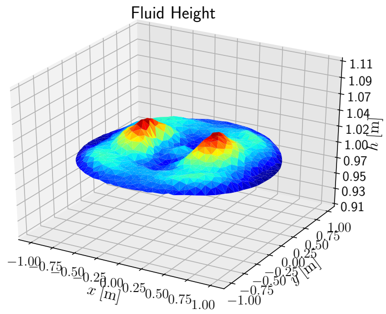

(d) $t = 1.28$ [s]

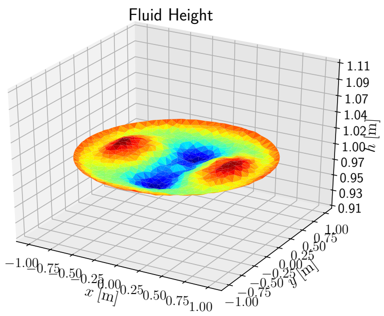

(e) $t = 1.71$ [s]

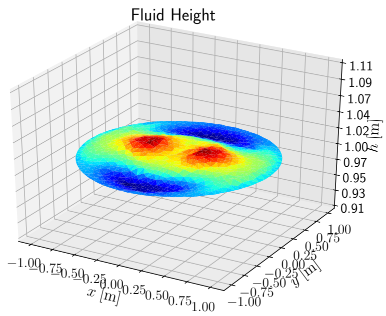

(f) $t = 2.14$ [s]

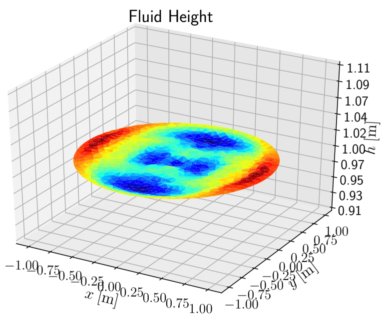

(g) $t = 2.57$ [s]

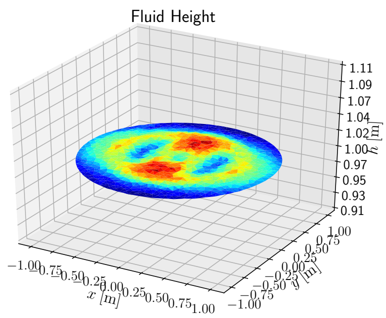

(h) $t = 3$ [s]

Figure 9.5: Snapshots at different times of the simulation for the boundary controlled irrotational shallow water equations ($t_{\mathrm{end}} = 3\,[s]$).

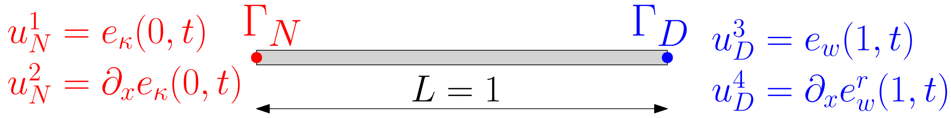

Figure 9.6: Boundary conditions for the motion planning problem.

9.2 Mixed boundary conditions enforcement

In this section the Lagrange multiplier method §7.2.1 and the virtual domain decomposition method §7.2.2 are compared for two problems:

1. a reference tracking problem for the Euler-Bernoulli beam;
2. a vibroacoustic application.

9.2.1 Motion planning of a thin beam

Consider the motion planning problem for the Euler Bernoulli beam [KS08, Chapter 12]

$$\partial_{tt}w + \partial_{xxxx}w = 0, \qquad x \in \Omega = \{0,1\} \tag{9.18}$$
$$\partial_{xx}w(0,t) = 0, \qquad \partial_{xxx}w(0,t) = 0, \tag{9.19}$$
$$w^r(0,t) = \sin(\omega t), \qquad \partial_x w^r(0,t) = 0. \tag{9.20}$$

The equation (9.18) represents the Euler-Bernoulli beam (3.24) with unitary coefficients. Conditions (9.19) represent an homogeneous free boundary conditions at the left side. To objective is to find controls $u_1 = w^r(1,t)$, $u_2 = \partial_x w^r(1,t)$ to match the reference outputs $w^r(0,t)$, $\partial_x w^r(0,t)$. The reference solution for this problem can be found by postulating the existence of a function of the form

$$w^r(x,t) = \sum_{k=0}^{\infty} a_k(t)\frac{x^k}{k!}.$$

Given the reference output $w^r(1,t) = \sin(\omega t)$, the reference solution assumes the form (cf. [KS08, Chapter 12] for details)

$$w^r(x,t) = \sum_{k=0}^{\infty} \omega^{2k}\frac{x^{4k}}{(4k)!}\sin(\omega t) = \frac{1}{2}[\cosh(\sqrt{\omega}x) + \cos(\omega x)]\sin(\omega t). \tag{9.21}$$

The inputs that assure the tracking of the outputs can be computed

$$\begin{aligned} w^r(1,t) &= \frac{1}{2}[\cosh(\sqrt{\omega}) + \cos(\omega)]\sin(\omega t), \\ \partial_x w^r(1,t) &= \frac{1}{2}[\sinh(\sqrt{\omega}) - \sin(\omega)]\sin(\omega t). \end{aligned} \tag{9.22}$$

This problem can be equivalently cast as a boundary control pH system with mixed boundary conditions (see Fig. 9.6).

$$
\frac{\partial}{\partial t}\begin{pmatrix} e_w \\ e_\kappa \end{pmatrix} = \begin{bmatrix} 0 & -\partial_{xx} \\ \partial_{xx} & 0 \end{bmatrix}\begin{pmatrix} e_w \\ e_\kappa \end{pmatrix} \tag{9.23a}
$$

$$
\begin{pmatrix} u_N^1 \\ u_N^2 \\ u_D^1 \\ u_D^2 \end{pmatrix} = \begin{pmatrix} e_\kappa(0,t) \\ -\partial_x e_\kappa(0,t) \\ e_w(1,t) \\ \partial_x e_w(1,t) \end{pmatrix} = \begin{pmatrix} 0 \\ 0 \\ \frac{1}{2}[\cosh(\sqrt{\omega}) + \cos(\omega)]\omega\cos(\omega t) \\ \frac{1}{2}[\sinh(\sqrt{\omega}) - \sin(\omega)]\omega\cos(\omega t) \end{pmatrix}, \tag{9.23b}
$$

$$
\begin{pmatrix} y_N^1 \\ y_N^2 \\ y_D^1 \\ y_D^2 \end{pmatrix} = \begin{pmatrix} -\partial_x e_w(0,t) \\ e_w(0,t) \\ \partial_x e_\kappa(1,t) \\ e_\kappa(1,t) \end{pmatrix}. \tag{9.23c}
$$

This choice of the inputs assures that the outputs $y_\partial^1 = \partial_x e_w(0,t),\ y_\partial^2 = e_w(0,t)$ verify the desired trajectories

$$
y_\partial^1 = \partial_t\partial_x w^r(0,t) = 0, \qquad y_\partial^2 = \partial_t w^r(0,t) = \omega\cos(\omega t).
$$

Next we concisely reported the discretization strategy for the imposition of mixed boundary conditions.

Lagrange multipliers If a Lagrange multipliers is used for the Neumann boundary condition

$$
\begin{aligned}
&\langle v_w,\, \partial_t e_w\rangle_\Omega = \langle v_w,\, -\partial_{xx} e_\kappa\rangle_\Omega\,, \\
&\langle v_\kappa,\, \partial_t e_\kappa\rangle_\Omega = \langle \partial_{xx} v_\kappa,\, e_w\rangle_{L^2(\Omega)} + \left\langle \begin{pmatrix} \partial_{\boldsymbol{n}} v_\kappa \\ v_\kappa \end{pmatrix},\, \begin{pmatrix} \lambda_N^1 \\ \lambda_N^2 \end{pmatrix} \right\rangle_{\Gamma_N} + \left\langle \begin{pmatrix} \partial_{\boldsymbol{n}} v_\kappa \\ v_\kappa \end{pmatrix},\, \begin{pmatrix} u_D^1 \\ u_D^2 \end{pmatrix} \right\rangle_{\Gamma_D}.
\end{aligned} \tag{9.24}
$$

Using a Galerkin method the following system is computed.

$$
\begin{aligned}
\begin{bmatrix} \mathbf{M}_w & \mathbf{0} & \mathbf{0} \\ \mathbf{0} & \mathbf{M}_\kappa & \mathbf{0} \\ \mathbf{0} & \mathbf{0} & \mathbf{0} \end{bmatrix}\begin{pmatrix} \dot{\mathbf{e}}_w \\ \dot{\mathbf{e}}_\kappa \\ \dot{\boldsymbol{\lambda}}_N \end{pmatrix} &= \begin{bmatrix} \mathbf{0} & \mathbf{D}_{-\partial_{xx}}^\top & \mathbf{0} \\ -\mathbf{D}_{-\partial_{xx}} & \mathbf{0} & \mathbf{B}_{\kappa,\Gamma_N} \\ \mathbf{0} & -\mathbf{B}_{\kappa,\Gamma_N}^\top & \mathbf{0} \end{bmatrix}\begin{pmatrix} \mathbf{e}_w \\ \mathbf{e}_\kappa \\ \boldsymbol{\lambda}_N \end{pmatrix} + \begin{bmatrix} \mathbf{0} \\ \mathbf{B}_{\kappa,\Gamma_D} \\ \mathbf{0} \end{bmatrix}\mathbf{u}_D, \\
\mathbf{y}_D &= \begin{bmatrix} \mathbf{0} & \mathbf{B}_{\kappa,\Gamma_D}^\top & \mathbf{0} \end{bmatrix}\begin{pmatrix} \mathbf{e}_p \\ \mathbf{e}_v \\ \boldsymbol{\lambda}_N \end{pmatrix}.
\end{aligned} \tag{9.25}
$$

The DG1Her element (8.5) is employed for the discretization.

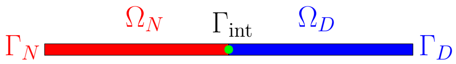

Figure 9.7: Virtual decomposition of the Euler Bernoulli beam.

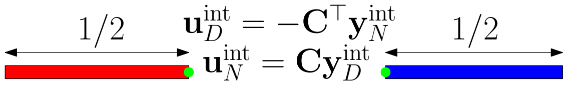

Figure 9.8: Interconnection for the Euler-Bernoulli beam.

Virtual domain decomposition For the decomposition, the beam is split into halves 9.7. Applying the PFEM methodology as in 7.2.2 two finite dimensional systems are obtained. For Ω_N the system is analogous to (7.135),

Subdomain Ω_N

$$
\begin{aligned}
\begin{bmatrix} \mathbf{M}_w & \mathbf{0} \\ \mathbf{0} & \mathbf{M}_\kappa \end{bmatrix} \begin{pmatrix} \dot{\mathbf{e}}_w \\ \dot{\mathbf{e}}_\kappa \end{pmatrix} &= \begin{bmatrix} \mathbf{0} & -\mathbf{D}_{\partial_{xx}}^\top \\ \mathbf{D}_{\partial_{xx}} & \mathbf{0} \end{bmatrix} \begin{pmatrix} \mathbf{e}_w \\ \mathbf{e}_\kappa \end{pmatrix} + \begin{bmatrix} \mathbf{B}_{w,\Gamma_{\text{int}}} \\ \mathbf{0} \end{bmatrix} \mathbf{u}_N^{\text{int}}, \\
\mathbf{y}_N^{\text{int}} &= \begin{bmatrix} \mathbf{B}_{w,\Gamma_{\text{int}}}^\top & \mathbf{0} \end{bmatrix} \begin{pmatrix} \mathbf{e}_w \\ \mathbf{e}_\kappa \end{pmatrix}.
\end{aligned} \tag{9.26}
$$

while for Ω_D to (7.134).

Subdomain Ω_D

$$
\begin{aligned}
\begin{bmatrix} \mathbf{M}_w & \mathbf{0} \\ \mathbf{0} & \mathbf{M}_\kappa \end{bmatrix} \begin{pmatrix} \dot{\mathbf{e}}_w \\ \dot{\mathbf{e}}_\kappa \end{pmatrix} &= \begin{bmatrix} \mathbf{0} & \mathbf{D}_{-\partial_{xx}} \\ -\mathbf{D}_{-\partial_{xx}}^\top & \mathbf{0} \end{bmatrix} \begin{pmatrix} \mathbf{e}_w \\ \mathbf{e}_\kappa \end{pmatrix} + \begin{bmatrix} \mathbf{0} & \mathbf{0} \\ \mathbf{B}_{\kappa,\Gamma_D} & \mathbf{B}_{\kappa,\Gamma_{\text{int}}} \end{bmatrix} \begin{pmatrix} \mathbf{u}_D \\ \mathbf{u}_D^{\text{int}} \end{pmatrix}, \\
\begin{pmatrix} \mathbf{y}_D \\ \mathbf{y}_D^{\text{int}} \end{pmatrix} &= \begin{bmatrix} \mathbf{0} & \mathbf{B}_{\kappa,\Gamma_D}^\top \\ \mathbf{0} & \mathbf{B}_{\kappa,\Gamma_{\text{int}}}^\top \end{bmatrix} \begin{pmatrix} \mathbf{e}_w \\ \mathbf{e}_\kappa \end{pmatrix}.
\end{aligned} \tag{9.27}
$$

In order to get a system with mixed causality, systems (9.27) and (9.27) have to be interconnected using a classical gyrator interconnection. The correct interconnection reads (cf. Fig. 9.8)

$$
\begin{aligned}
\mathbf{u}_N^{\text{int}} &= \begin{pmatrix} e_\kappa(1/2, t) \\ \partial_x e_\kappa(1/2, t) \end{pmatrix} = \begin{bmatrix} 1 & 0 \\ 0 & -1 \end{bmatrix} \begin{pmatrix} e_\kappa(1/2, t) \\ -\partial_x e_\kappa(1/2, t) \end{pmatrix} = \mathbf{C}\mathbf{y}_D^{\text{int}}, \\
\mathbf{u}_D^{\text{int}} &= \begin{pmatrix} -\partial_x e_w(L/2, t) \\ e_w(L/2, t) \end{pmatrix} = \begin{bmatrix} -1 & 0 \\ 0 & 1 \end{bmatrix} \begin{pmatrix} \partial_x e_w(1/2, t) \\ e_w(1/2, t) \end{pmatrix} = -\mathbf{C}^\top \mathbf{y}_N^{\text{int}} s
\end{aligned}
$$

This interconnection establishes that the power is exchanged without loss between the two systems

$$
{\mathbf{u}_D^{\text{int}}}^\top \mathbf{M}_{\Gamma_{\text{int}}} \mathbf{y}_D^{\text{int}} + {\mathbf{u}_N^{\text{int}}}^\top \mathbf{M}_{\Gamma_{\text{int}}} \mathbf{y}_N^{\text{int}} = 0. \tag{9.28}
$$

For what concerns the choice of the approximations, System (9.26) is discretized using the HerDG1 elements (8.2), while for System (9.27) the DG1Her (8.5) elements are used.

Numerical results Six elements are used for the discretization (both for the Lagrange multiplier and virtual domain decomposition method. The analytical solution for the reference dispacement and velocity together with their numerical discretization are plotted in Figs. 9.10 and 9.11. The numerical predictions perfectly match the analytical solution. In Fig. 9.9 the numerical solution for the vertical displacement obtained using the virtual domain decomposition is shown.

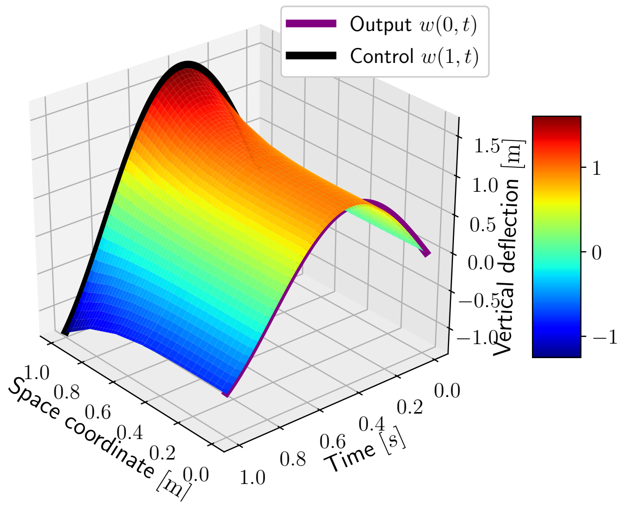

Figure 9.9: Computed vertical displacement.

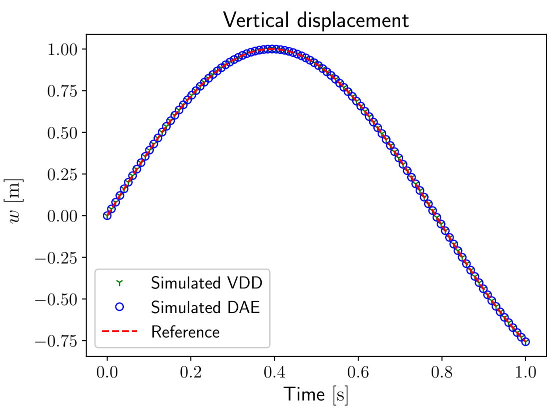

Figure 9.10: Analytical reference displacement and numerical predictions.

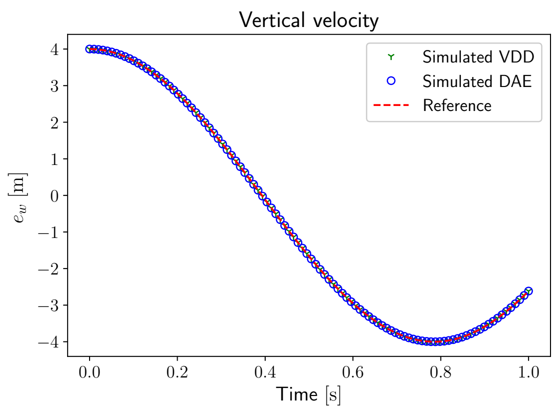

Figure 9.11: Analytical reference velocity and numerical predictions.

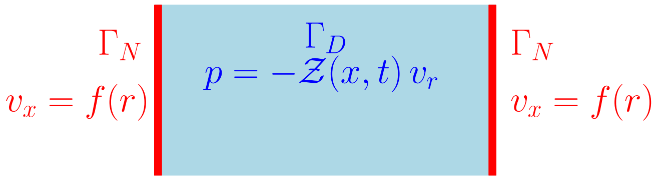

Figure 9.12: Boundary conditions for the 3D vibroacoustic problem.

9.2.2 Vibroacoustics under mixed boundary conditions

Consider the model for the propagation of sound in air 3.23

$$\begin{bmatrix} \chi_s & 0 \\ \mathbf{0} & \mu_0 \boldsymbol{I}_{3\times 3} \end{bmatrix} \frac{\partial}{\partial t} \begin{pmatrix} e_p \\ \boldsymbol{e}_v \end{pmatrix} = - \begin{bmatrix} 0 & \mathrm{div} \\ \mathrm{grad} & \mathbf{0} \end{bmatrix} \begin{pmatrix} e_p \\ \boldsymbol{e}_v \end{pmatrix}, \qquad \Omega = \{x \in [0, L], r \in [0, R], \theta = [0, 2\pi)\}, \tag{9.29}$$

where $e_p \in \mathbb{R}$ and $\boldsymbol{e}_v \in \mathbb{R}^3$ denote the variations of pressure and velocity from a steady state, μ_0 is the steady state mass density, and χ_s represents a constant adiabatic compressibility factor. With x, r, θ we denote the axial, radial and tangential cylindrical coordinates. The domain is cylindrical duct of length L and radius R. The following boundary conditions are imposed (see Fig. 9.12)

$$\begin{aligned} e_p(x, R, \theta, t) &= -\mathcal{Z}(x,t)\, e_v^r(x, R, \theta), \\ \boldsymbol{e}_v \cdot \boldsymbol{n}(0, r, \theta, t) &= -e_v^x(0, r, \theta) = -f(r), \\ \boldsymbol{e}_v \cdot \boldsymbol{n}(L, r, \theta, t) &= +e_v^x(L, r, \theta) = +f(r). \end{aligned}$$

For the initial boundary conditions, it is assumed

$$\begin{aligned} e_p^0(x, r, \theta) &= 0, & e_v^{r,0}(x, r, \theta) &= g(r), \\ e_v^{x,0}(x, r, \theta) &= f(r), & e_v^{\theta,0}(x, r, \theta) &= 0. \end{aligned} \tag{9.30}$$

The impedance and the axial and radial flows expressions are the following

$$\begin{aligned} \mathcal{Z}(x,t) &= \mathbb{1}\left\{\frac{1}{3}L \leq \; x \; \leq \frac{2}{3}L,\, t \geq 0.2\; t_{\text{fin}}\right\} \mu_0\, c_0, \\ f(r) &= \left(1 - \frac{r^2}{R^2}\right) v_0, \\ g(r) &= 16 \frac{r^2}{R^4}\, (R-r)^2\, v_0. \end{aligned}$$

The impedance operator $\mathcal{Z}$ is non invertible. If it were invertible than the impedance condition could be treated as a Robin condition. This model describes the behavior of an axis-symmetrical flow subjected to an impedance condition on the lateral surface. Because of symmetry the model can be reduced to a 2D problem in polar coordinates over the domain

$\Omega_{\mathrm{r}} = \{x \in [0, L], r \in [0, R]\}$. The reduced system reads

$$\begin{bmatrix} \chi_s & p \\ \mathbf{0} & \mu_0 \boldsymbol{I}_{2\times 2} \end{bmatrix} \frac{\partial}{\partial t} \begin{pmatrix} e_p \\ \boldsymbol{e}_v \end{pmatrix} = - \begin{bmatrix} 0 & \mathrm{div}_r \\ \mathrm{grad}_r & \mathbf{0} \end{bmatrix} \begin{pmatrix} e_p \\ \boldsymbol{e}_v \end{pmatrix}, \qquad \mathrm{div}_r = \begin{bmatrix} \partial_x & \partial_r + 1/r \end{bmatrix}, \quad \mathrm{grad}_r = \begin{bmatrix} \partial_x \\ \partial_r \end{bmatrix}. \tag{9.31}$$

The boundary conditions must now account for the symmetry condition at $r = 0$, leading to the set of boundary conditions (see Fig. 9.13)

$$u_D = e_p|_{\Gamma_D} = -\mathcal{Z}(x,t)\, e_v^r(x, R), \tag{9.32}$$

$$u_N = \boldsymbol{e}_v \cdot \boldsymbol{n}|_{\Gamma_N} = \begin{cases} -f(r), & x = 0, \\ +f(r), & x = L, \\ 0, & r = 0, \end{cases} \tag{9.33}$$

where Γ_D, Γ_D denote the boundary partitions. The Hamiltonian is then computed as

$$H = \frac{1}{2} \langle e_p, \, \chi_s e_p \rangle_{\Omega_{\mathrm{r}}} + \frac{1}{2} \langle \boldsymbol{e}_v, \, \mu_0 \boldsymbol{e}_v \rangle_{\Omega_{\mathrm{r}}}$$

where $\langle \cdot, \, \cdot \rangle_{\Omega_{\mathrm{r}}}$ is the standard L^2 inner product in polar coordinates, defined for scalar or vector fields as

$$\langle \alpha, \, \beta \rangle_{\Omega_{\mathrm{r}}} = \int_{\Omega_{\mathrm{r}}} \alpha \cdot \beta \; r \, \mathrm{d}r \, \mathrm{d}x = \int_{\Omega_{\mathrm{r}}} \alpha \cdot \beta \;\; \mathrm{d}\Omega_r.$$

The power flow is obtained by application of the Stokes theorem

$$\dot{H} = \langle e_p, \, \boldsymbol{e}_v \cdot \boldsymbol{n} \rangle_{\partial\Omega_{\mathrm{r}}} = \int_{\partial\Omega_{\mathrm{r}}} e_p \; \boldsymbol{e}_v \cdot \boldsymbol{n} \; \mathrm{d}\Gamma_r = -\int_0^L \mathcal{Z}(x,t) (e_v^r)^2 \; R \, \mathrm{d}x \leq 0$$

where $\mathrm{d}\Gamma_r = r \, \mathrm{d}s$ is the infinitesimal surface.

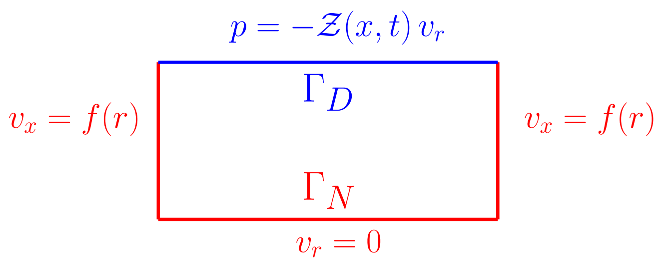

Figure 9.13: Boundary partition for the 2D vibroacoustic problem.

In the next paragraphs we provide a concise description of the discretization procedure for the two methods.

Lagrange multipliers If a Lagrange multiplier is introduced for the Dirichlet boundary condition, the following weak form is obtained

$$
\begin{aligned}
\langle v_p,\, \chi_s \partial_t e_p \rangle_{\Omega_r} &= \langle \mathrm{grad}_r v_p,\, \boldsymbol{e}_v \rangle_{\Omega_r} + \langle v_p,\, \lambda_D \rangle_{\Gamma_D} + \langle v_p,\, u_N \rangle_{\Gamma_N}\,, \\
\langle \boldsymbol{v}_v,\, \mu_0 \partial_t \boldsymbol{e}_v \rangle_{\Omega_r} &= \langle \boldsymbol{v}_v,\, \mathrm{grad}_r e_p \rangle_{\Omega_r}\,, \\
0 &= -\langle v_D,\, e_p \rangle_{\Gamma_D} + \langle v_D,\, u_D \rangle_{\Gamma_D}\,, \\
\langle v_N,\, y_N \rangle_{\Gamma_N} &= \langle v_N,\, e_p \rangle_{\Gamma_N}\,, \\
\langle v_D,\, y_D \rangle_{\Gamma_D} &= \langle v_D,\, \lambda_D \rangle_{\Gamma_D}\,,
\end{aligned}
\tag{9.34}
$$

where v_N, v_D are the test functions associated to the output discretization and $\langle \cdot,\, \cdot \rangle_{\Gamma_*}$ is the L^2 inner product on boundary Γ_*. Introducing a Galerkin approximation for the variables, one obtains the following system

$$
\begin{gathered}
\begin{bmatrix} \mathbf{M}_{\chi_s} & \mathbf{0} & \mathbf{0} \\ \mathbf{0} & \mathbf{M}_{\mu_0} & \mathbf{0} \\ \mathbf{0} & \mathbf{0} & \mathbf{0} \end{bmatrix}
\begin{pmatrix} \dot{\mathbf{e}}_p \\ \dot{\mathbf{e}}_v \\ \dot{\boldsymbol{\lambda}}_D \end{pmatrix}
=
\begin{bmatrix} \mathbf{0} & \mathbf{D}_{\mathrm{grad}}^\top & \mathbf{B}_{p,\Gamma_D} \\ -\mathbf{D}_{\mathrm{grad}} & \mathbf{0} & \mathbf{0} \\ -\mathbf{B}_{p,\Gamma_D}^\top & \mathbf{0} & \mathbf{0} \end{bmatrix}
\begin{pmatrix} \mathbf{e}_p \\ \mathbf{e}_v \\ \boldsymbol{\lambda}_D \end{pmatrix}
+
\begin{bmatrix} \mathbf{B}_{p,\Gamma_N} & \mathbf{0} \\ \mathbf{0} & \mathbf{0} \\ \mathbf{0} & \mathbf{M}_{\Gamma_D} \end{bmatrix}
\begin{pmatrix} \mathbf{u}_N \\ \mathbf{u}_D \end{pmatrix}, \\
\begin{bmatrix} \mathbf{M}_{\Gamma_N} & \mathbf{0} \\ \mathbf{0} & \mathbf{M}_{\Gamma_D} \end{bmatrix}
\begin{pmatrix} \mathbf{y}_N \\ \mathbf{y}_D \end{pmatrix}
=
\begin{bmatrix} \mathbf{B}_{p,\Gamma_D}^\top & \mathbf{0} & \mathbf{0} \\ \mathbf{0} & \mathbf{0} & \mathbf{M}_{\Gamma_D} \end{bmatrix}
\begin{pmatrix} \mathbf{e}_p \\ \mathbf{e}_v \\ \boldsymbol{\lambda}_D \end{pmatrix}.
\end{gathered}
\tag{9.35}
$$

The matrices are computed as in (7.112). To impose the actual boundary conditions consider the weak form of (9.32) $u_D = -\mathcal{Z}\lambda_D = -\mathcal{Z} y_D$:

$$
\mathbf{M}_{\Gamma_D} \mathbf{u}_D = -\mathbf{M}_{\Gamma_D, \mathcal{Z}} \mathbf{y}_D,
$$

where $\mathbf{M}_{\Gamma_D,\mathcal{Z}}$ corresponds to the mass matrix associated to the weighted inner product $\langle v_D,\, \mathcal{Z} y_D \rangle_{\Gamma_D}$. The Neumann boundary condition is imposed by projection on the u_N space. The boundary controlled system becomes

$$
\begin{bmatrix} \mathbf{M}_{\chi_s} & \mathbf{0} & \mathbf{0} \\ \mathbf{0} & \mathbf{M}_{\mu_0} & \mathbf{0} \\ \mathbf{0} & \mathbf{0} & \mathbf{0} \end{bmatrix}
\begin{pmatrix} \dot{\mathbf{e}}_p \\ \dot{\mathbf{e}}_v \\ \dot{\boldsymbol{\lambda}}_D \end{pmatrix}
=
\begin{bmatrix} \mathbf{0} & \mathbf{D}_{\mathrm{grad}}^\top & \mathbf{B}_{p,\Gamma_D} \\ -\mathbf{D}_{\mathrm{grad}} & \mathbf{0} & \mathbf{0} \\ -\mathbf{B}_{p,\Gamma_D}^\top & \mathbf{0} & -\mathbf{M}_{\Gamma_D,\mathcal{Z}} \end{bmatrix}
\begin{pmatrix} \mathbf{e}_p \\ \mathbf{e}_v \\ \boldsymbol{\lambda}_D \end{pmatrix}
+
\begin{pmatrix} \mathbf{b}_N \\ \mathbf{0} \\ \mathbf{0} \end{pmatrix}.
\tag{9.36}
$$

Virtual domain decomposition In order to apply this methodology the domain has to be split into two sub-domains. The shared boundary connecting the two sub-domains can be freely chosen. For the given geometry, the separation line that provide the most regular simplicial meshes is the trapezoidal one given in Fig. 9.14.

Applying the PFEM methodology as in 7.2.2 two finite dimensional systems are obtained. For Ω_D the system is analogous to (7.134), while for Ω_N to (7.135).

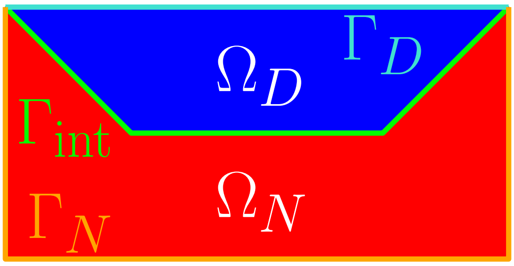

Figure 9.14: Virtual decomposition of the vibroacoustic domain.

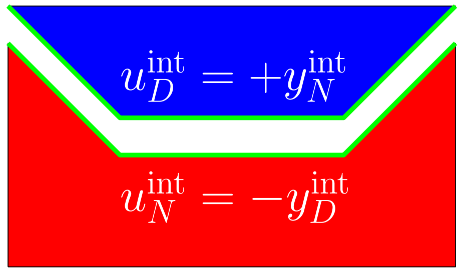

Figure 9.15: Interconnection for the vibroacoustic domain..

Subdomain Ω_D

$$\begin{aligned}
\mathbf{M}_{\Omega_D}\dot{\mathbf{e}}_{\Omega_D} &= \mathbf{J}_{\Omega_D}\mathbf{e}_{\Omega_D} + \mathbf{B}_{\Gamma_D}^{\Omega_D}\mathbf{u}_D + \mathbf{B}_{\Gamma_{\mathrm{int}}}^{\Omega_D}\mathbf{u}_D^{\mathrm{int}},\\
\mathbf{M}_{\Gamma_D}\mathbf{y}_D &= \mathbf{B}_{\Gamma_D}^{\Omega_D\top}\mathbf{e}_D,\\
\mathbf{M}_{\Gamma_{\mathrm{int}}}\mathbf{y}_D^{\mathrm{int}} &= \mathbf{B}_{\Gamma_{\mathrm{int}}}^{\Omega_D\top}\mathbf{e}_D.
\end{aligned} \tag{9.37}$$

Subdomain Ω_N

$$\begin{aligned}
\mathbf{M}_{\Omega_N}\dot{\mathbf{e}}_{\Omega_N} &= \mathbf{J}_{\Omega_N}\mathbf{e}_{\Omega_N} + \mathbf{B}_{\Gamma_N}^{\Omega_N}\mathbf{u}_N + \mathbf{B}_{\Gamma_{\mathrm{int}}}^{\Omega_N}\mathbf{u}_N^{\mathrm{int}},\\
\mathbf{M}_{\Gamma_N}\mathbf{y}_N &= \mathbf{B}_{\Gamma_N}^{\Omega_N\top}\mathbf{e}_N,\\
\mathbf{M}_{\Gamma_{\mathrm{int}}}\mathbf{y}_N^{\mathrm{int}} &= \mathbf{B}_{\Gamma_{\mathrm{int}}}^{\Omega_N\top}\mathbf{e}_N.
\end{aligned} \tag{9.38}$$

In order to get a system with mixed causality, systems (9.37) and (9.37) have to be interconnected using a classical gyrator interconnection. Considering that the pressure field is continuous at Γ_{int}, the outward normal verifies $\boldsymbol{n}_D|_{\Gamma_{\mathrm{int}}} = -\boldsymbol{n}_N|_{\Gamma_{\mathrm{int}}}$ and the corresponding degrees of freedom have to be matched, the correct interconnection reads (cf. Fig. 9.15)

$$\mathbf{u}_N^{\mathrm{int}} = -\mathbf{y}_D^{\mathrm{int}}, \qquad \mathbf{u}_D^{\mathrm{int}} = \mathbf{y}_N^{\mathrm{int}}. \tag{9.39}$$

The resulting interconnected system is written as

$$\begin{aligned}
\begin{bmatrix}\mathbf{M}_{\Omega_D} & \mathbf{0}\\ \mathbf{0} & \mathbf{M}_{\Omega_N}\end{bmatrix}\begin{pmatrix}\dot{\mathbf{e}}_{\Omega_D}\\ \dot{\mathbf{e}}_{\Omega_N}\end{pmatrix} &= \begin{bmatrix}\mathbf{J}_{\Omega_D} & \mathbf{C}\\ -\mathbf{C}^\top & \mathbf{J}_{\Omega_N}\end{bmatrix}\begin{pmatrix}\mathbf{e}_{\Omega_D}\\ \mathbf{e}_{\Omega_N}\end{pmatrix} + \begin{bmatrix}\mathbf{B}_{\Gamma_D}^{\Omega_D} & \mathbf{0}\\ \mathbf{0} & \mathbf{B}_{\Gamma_N}^{\Omega_N}\end{bmatrix}\begin{pmatrix}\mathbf{u}_D\\ \mathbf{u}_N\end{pmatrix},\\
\begin{bmatrix}\mathbf{M}_{\Gamma_D} & \mathbf{0}\\ \mathbf{0} & \mathbf{M}_{\Gamma_N}\end{bmatrix}\begin{pmatrix}\mathbf{y}_D\\ \mathbf{y}_N\end{pmatrix} &= \begin{bmatrix}\mathbf{B}_{\Gamma_D}^{\Omega_N\top} & \mathbf{0}\\ \mathbf{0} & \mathbf{B}_{\Gamma_N}^{\Omega_D\top}\end{bmatrix}\begin{pmatrix}\mathbf{e}_{\Omega_1}\\ \mathbf{e}_{\Omega_2}\end{pmatrix}.
\end{aligned} \tag{9.40}$$

where $\mathbf{C} = \mathbf{B}_{\Gamma_{\mathrm{int}}}^{\Omega_D}\mathbf{M}_{\Gamma_{\mathrm{int}}}^{-1}\mathbf{B}_{\Gamma_{\mathrm{int}}}^{\Omega_N\top}$. The actual boundary condition (9.32) can be plugged into the system leading to

$$\begin{bmatrix}\mathbf{M}_{\Omega_D} & \mathbf{0}\\ \mathbf{0} & \mathbf{M}_{\Omega_N}\end{bmatrix}\begin{pmatrix}\dot{\mathbf{e}}_{\Omega_D}\\ \dot{\mathbf{e}}_{\Omega_N}\end{pmatrix} = \begin{bmatrix}\mathbf{J}_{\Omega_D} - \mathbf{R}_{\Omega_D} & \mathbf{C}\\ -\mathbf{C}^\top & \mathbf{J}_{\Omega_N}\end{bmatrix}\begin{pmatrix}\mathbf{e}_{\Omega_D}\\ \mathbf{e}_{\Omega_N}\end{pmatrix} + \begin{pmatrix}\mathbf{0}\\ \mathbf{b}_{\Gamma_N}^{\Omega_N}\end{pmatrix}, \tag{9.41}$$

where $\mathbf{R}_{\Omega_D} = \mathbf{B}_{\Gamma_D}^{\Omega_D}\mathbf{M}_{\Gamma_D}^{-1}\mathbf{B}_{\Gamma_D}^{\Omega_D\top}$ is symmetric and positive definite.

Numerical results and discussion In this section a numerical illustration of the two methodologies is presented. The Hamiltonian and the state variables trends given by the

Physical Parameters	
L	2 [m]
R	1 [m]
μ_0	1.225 [kg/m^3]
c_0	340 [m/s]
χ_s	7.061 [μPa]$^{-1}$
v_0	1 [m/s]

Simulation Settings	
ODE Integrator	RK 45
DAE Integrator	IDA
t_{end}	0.1[s]
FE spaces	$\mathrm{CG}_1 \times \mathrm{RT}_1 \times \mathrm{CG}_1$

Table 9.3: Settings and parameters for the vibroacoustic problem.

DAE (obtained from the Lagrange's multiplier method) and the ODE (obtained from the virtual domain decomposition method) are compared with respect to a reference solution. The reference is set to the DAE solution on a very fine mesh. The physical parameters are provided in Tab. 9.3. The initial condition are selected according to (9.30):

$$e_p^0(x,r) = 0, \quad e_v^{x,0}(x,r) = f(r), \quad e_v^{r,0}(x,r) = g(r).$$

A radial component of the velocity allows highlighting the effect of the impedance. The velocity profile satisfies some regularity conditions so that the transition between Neumann and Dirichlet boundary conditions is smooth. In order to get a finite dimensional discretization the fields are approximated using the following finite element families for both approaches:

- e_p is interpolated using order 1 Lagrange polynomials;
- $\boldsymbol{e}_v$ is interpolated using order 1 Raviart-Thomas polynomials;
- Boundary variables are approximated by Lagrange polynomial of order 1 defined on the boundary Γ_D (for λ_D, u_D, y_D) or Γ_N (for u_N, y_N).

Such a choice guarantees the conformity with respect to the differential operators. The FEniCS library, that allows interpolating functions on different meshes, is used for the computations. The reference solution, obtained by using the DAE approach on a very fine mesh, is plotted in Fig. 9.16a, where the two contribution to the total energy

$$H_{p,d} \approx \frac{1}{2}\mathbf{e}_p^\top \mathbf{M}_p \mathbf{e}_p, \qquad H_{v,d} \approx \frac{1}{2}\mathbf{e}_v^\top \mathbf{M}_v \mathbf{e}_v,$$

are highlighted. The Dirichlet condition induces a continuous transfer from radial kinetic energy into pressure potential. The impedance acts by dissipating the radial component of the velocity so that only the axial flow contribution is left. The total energy at the initial time of the simulation is given only by the kinetic energy

$$H_v^0 = H_{vx}^0 + H_{vr}^0 = \frac{1}{2}\int_0^L \int_0^R \mu_0 \left\|\boldsymbol{e}_v\right\|^2 \; r \,\mathrm{d}r\,\mathrm{d}x.$$

Given the physical parameters in Tab. 9.3, the numerical values of the energy contribution are readily found

$$H_v^0 = 0.453[J], \quad H_{vx}^0 = 0.204[J], \quad H_{vr}^0 = 0.249[J].$$

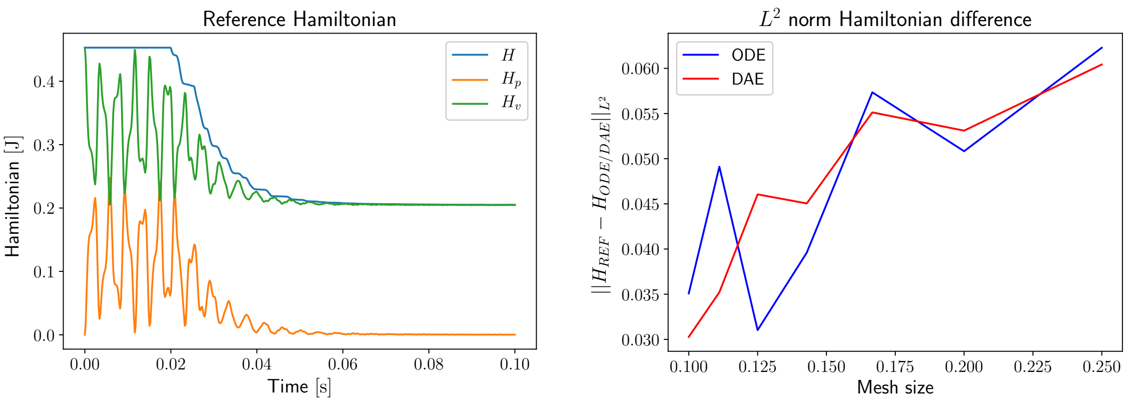

(a) Reference Hamiltonian. (b) L^2 Hamiltonian error.

Figure 9.16: Reference Hamiltonian and L^2 error.

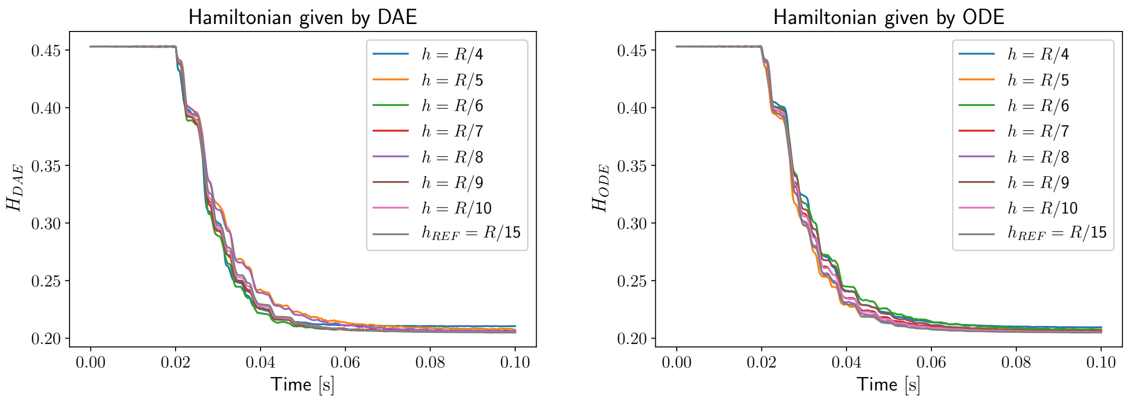

(a) DAE system (9.36). (b) ODE system (9.41).

Figure 9.17: Hamiltonian trend for different mesh size.

In order to demonstrate the consistency of the two proposed approaches the following measures are adopted

$$\varepsilon^H_{\text{ODE/DAE}} = \frac{||H_{\text{REF}} - H_{\text{ODE/DAE}}||_{L^2}}{||H_{\text{REF}}||_{L^2}},$$
$$\varepsilon^p_{\text{ODE/DAE}} = \frac{||p_{\text{REF}} - p_{\text{ODE/DAE}}||_{L^2}}{||p_{\text{REF}}||_{L^2}},$$
$$\varepsilon^v_{\text{ODE/DAE}} = \frac{||\boldsymbol{v}_{\text{REF}} - \boldsymbol{v}_{\text{ODE/DAE}}||_{L^2}}{||\boldsymbol{v}_{\text{REF}}||_{L^2}}.$$

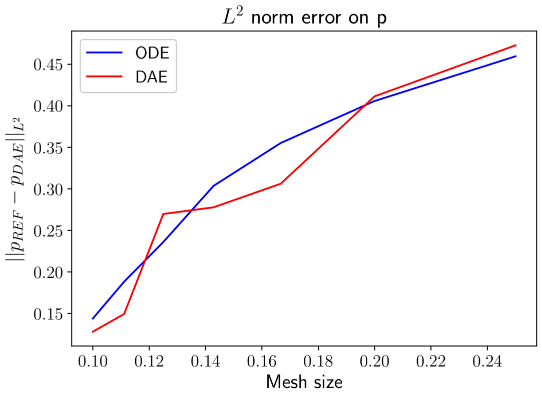

(a) L^2 pressure error.

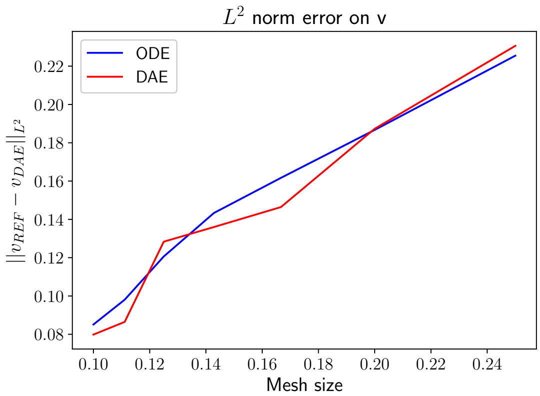

(b) L^2 velocity error.

Figure 9.18: Error on the state variables for different mesh size.

h mesh	$\Delta t_{\mathrm{DAE}}[s]$	$\Delta t_{\mathrm{ODE}}[s]$
$R_{\mathrm{ext}}/4$	98.95	124.43
$R_{\mathrm{ext}}/5$	415.99	255.54
$R_{\mathrm{ext}}/6$	798.24	893.63
$R_{\mathrm{ext}}/7$	1408.76	1120.69
$R_{\mathrm{ext}}/8$	3054.78	2271.28
$R_{\mathrm{ext}}/9$	6929.24	5792.89
$R_{\mathrm{ext}}/10$	12648.15	8835.09

Table 9.4: Elapsed simulation time for the vibroacoustic experiment.

The total energy obtained with several meshes is shown in Figs. 9.17a, 9.17b for the DAE and ODE approach respectively. It can be noticed that the Hamiltonian tends to the value H_{vx}^0 as expected. The overall Hamiltonian trend is well captured and even for coarse meshes the relative error does not exceed 6% (see Fig. 9.16b). Both methods converge monotonically to the reference solution, as illustrated in Figs. 9.18a, 9.18b. The faster convergence of one method on the other cannot be established. For what concerns the computational cost, in Tab. 9.4 the simulation time required by each solver is shown. The ODE approach is less time consuming for mesh size sufficiently small.

9.3 Thermoelastic wave propagation

9.4 Modal analysis of plates

Part IV

Port-Hamiltonian flexible multibody dynamics

Chapter 10

Modular multibody systems in port-Hamiltonian form

10.1 Reminder of the rigid case

10.2 Flexible floating body

10.3 Modular construction of multibody systems

Chapter 11

Validation

11.1 Beam systems

11.1.1 Modal analysis of a flexible mechanism

11.1.2 Non-linear crank slider

11.1.3 Hinged beam

11.2 Plate systems

11.2.1 Boundary interconnection with a rigid element

11.2.2 Actuated plate

Conclusion

Conclusions and future directions

Je n'ai cherché de rien prouver, mais de bien peindre et d'éclairer bien ma peinture.

André Gide
Préface de L'Immoraliste

Appendix A

Mathematical tools

A.1 Differential operators

The space of all, symmetric and skew-symmetric $d \times d$ matrices are denoted by $\mathbb{M}$, $\mathbb{S}$, $\mathbb{K}$ respectively. The space of $\mathbb{R}^d$ vectors is denoted by $\mathbb{V}$. $\Omega \subset \mathbb{R}^d$ is an open connected set. For a scalar field $u : \Omega \to \mathbb{R}$ the gradient is defined as

$$\mathrm{grad}(u) = \nabla u := \left(\partial_{x_1} u \dots \partial_{x_d} u\right)^\top .$$

For a vector field $\boldsymbol{u} : \Omega \to \mathbb{V}$, with components u_i, the gradient (Jacobian) is defined as

$$\mathrm{grad}(\boldsymbol{u})_{ij} := (\nabla \boldsymbol{u})_{ij} = \partial_{x_i} u_j .$$

The symmetric part of the gradient operator Grad (i. e. the deformation gradient in continuum mechanics) is thus given by

$$\mathrm{Grad}(\boldsymbol{u}) := \frac{1}{2}\left(\nabla \boldsymbol{u} + (\nabla \boldsymbol{u})^\top\right) \in \mathbb{S}.$$

The Hessian operator of u is then computed as follows

$$\mathrm{Hess}(u) = \nabla^2 u = \mathrm{Grad}(\mathrm{grad}(u)).$$

For a tensor field $\boldsymbol{U} : \Omega \to \mathbb{M}$, with components u_{ij}, the divergence is a vector, defined column-wise as

$$\mathrm{Div}(\boldsymbol{U}) = \nabla \cdot \boldsymbol{U} := \left(\sum_{i=1}^{d} \partial_{x_i} u_{ij}\right)_{j=1,\dots,d} .$$

The double divergence of a tensor field $\boldsymbol{U}$ is then a scalar field defined as

$$\mathrm{div}(\mathrm{Div}(\boldsymbol{U})) := \sum_{i=1}^{d} \sum_{j=1}^{d} \partial_{x_i} \partial_{x_j} u_{ij} .$$

Definition 7 (Formal adjoint, Def. 5.80 [RR04])
Consider the differential operator defined on Ω

$$\mathcal{L}(\boldsymbol{x}, \partial) = \sum_{|\alpha| \leq k} a_\alpha(\boldsymbol{x}) \partial^\alpha, \tag{A.1}$$

where $\alpha := (\alpha_1, \dots, \alpha_d)$ *is a multi-index of order* $|\alpha| := \sum_{i=1}^{d} \alpha_i$*,* a_α *are a set of real scalars and* $\partial^\alpha := \partial_{x_1}^{\alpha_1} \dots \partial_{x_d}^{\alpha_d}$ *is a differential operator of order* $|\alpha|$ *resulting from a combination of spatial derivatives. The formal adjoint of* $\mathcal{L}$ *is the operator defined by*

$$\mathcal{L}^*(\boldsymbol{x}, \partial)u = \sum_{|\alpha| \le k} (-1)^\alpha \partial^\alpha (a_\alpha(\boldsymbol{x}) u(\boldsymbol{x})). \tag{A.2}$$

The importance of this definition lies in the fact that

$$\langle \phi,\, \mathcal{L}(\boldsymbol{x}, \partial)\psi \rangle_\Omega = \langle \mathcal{L}^*(\boldsymbol{x}, \partial)\phi,\, \psi \rangle_\Omega \tag{A.3}$$

for every $\phi, \psi \in C_0^\infty(\Omega)$. If the assumption of compact support is removed, then (A.3) no longer holds; instead the integration by parts yields additional terms involving integrals over the boundary $\partial\Omega$. However, these boundary terms vanish if ϕ and ψ satisfy certain restrictions on the boundary.

A.2 Integration by parts

Theorem 4 (Integration by parts for tensors)
Consider a smooth tensor-valued function $\boldsymbol{A} \in \mathbb{R}^{d\times d}$ *and vector-valued function* $\boldsymbol{b} \in \mathbb{V} = \mathbb{R}^d$*. The following integration by parts formula holds*

$$\int_\Omega \{\mathrm{Div}(\boldsymbol{A}) \cdot \boldsymbol{b} + \boldsymbol{A} : \mathrm{grad}(\boldsymbol{b})\}\ \mathrm{d}\Omega = \int_\Omega \mathrm{div}(\boldsymbol{A}\boldsymbol{b})\ \mathrm{d}\Omega = \int_{\partial\Omega} (\boldsymbol{A}^\top \boldsymbol{n}) \cdot \boldsymbol{b}\ \mathrm{d}S, \tag{A.4}$$

where $\boldsymbol{n}$ *is the outward normal at the boundary and* $\mathrm{d}S$ *the infinitesimal surface.*

Proof. Consider the components expression of Eq. (A.4)

$$\begin{aligned}
\int_\Omega \{\mathrm{Div}(\boldsymbol{A}) \cdot \boldsymbol{b} + \boldsymbol{A} : \mathrm{grad}(\boldsymbol{b})\}\ \mathrm{d}\Omega &= \int_\Omega \sum_{i=1}^{d}\sum_{j=1}^{d} \{(\partial_{x_i} A_{ij}) b_j + A_{ij}(\partial_{x_i} b_j)\}\ \mathrm{d}\Omega, \\
&= \int_\Omega \sum_{i=1}^{d}\sum_{j=1}^{d} \partial_{x_i}(A_{ij} b_j)\ \mathrm{d}\Omega = \int_\Omega \mathrm{div}(\boldsymbol{A}\boldsymbol{b})\ \mathrm{d}\Omega, \\
&= \int_{\partial\Omega} \sum_{i=1}^{d}\sum_{j=1}^{d} (n_i A_{ij}) b_j\ \mathrm{d}S = \int_{\partial\Omega} (\boldsymbol{A}^\top \boldsymbol{n}) \cdot \boldsymbol{b}\ \mathrm{d}S.
\end{aligned} \tag{A.5}$$

□

The previous result can be specialized for symmetric tensor field [BBF+13, Chapter 1].

Theorem 5 (Integration by parts for symmetric tensors)
Consider a smooth tensor-valued function $\boldsymbol{M} \in \mathbb{S} = \mathbb{R}^{d\times d}_{sym}$ *and vector-valued function* $\boldsymbol{b} \in \mathbb{V} =$

$\mathbb{R}^d$. *Then, it holds*

$$\int_\Omega \{\mathrm{Div}(\boldsymbol{M}) \cdot \boldsymbol{b} + \boldsymbol{M} : \mathrm{Grad}(\boldsymbol{b})\} \, \mathrm{d}\Omega = \int_\Omega \mathrm{div}(\boldsymbol{M}\boldsymbol{b}) \, \mathrm{d}\Omega = \int_{\partial\Omega} (\boldsymbol{M}\,\boldsymbol{n}) \cdot \boldsymbol{b} \, \mathrm{d}S. \tag{A.6}$$

Proof. Consider the components expression of Eq. (A.6)

$$\int_\Omega \{\mathrm{Div}(\boldsymbol{M}) \cdot \boldsymbol{b} + \boldsymbol{M} : \mathrm{Grad}(\boldsymbol{b})\} \, \mathrm{d}\Omega = \int_\Omega \sum_{i=1}^d \sum_{j=1}^d \left\{ (\partial_{x_i} M_{ij}) b_j + M_{ij} \frac{1}{2} (\partial_{x_i} b_j + \partial_{x_j} b_i) \right\} \, \mathrm{d}\Omega, \tag{A.7}$$

The term $M_{ij}\frac{1}{2}(\partial_{x_i} b_j + \partial_{x_j} b_i)$ can be manipulated exploiting the symmetry of the tensor $\boldsymbol{M}$

$$\begin{aligned} \sum_{i=1}^d \sum_{j=1}^d \frac{1}{2}(M_{ij}\partial_{x_i} b_j + M_{ij}\partial_{x_j} b_i) &= \sum_{i=1}^d \sum_{j=1}^d \frac{1}{2}(M_{ij}\partial_{x_i} b_j + M_{ji}\partial_{x_i} b_j), \\ &= \sum_{i=1}^d \sum_{j=1}^d \frac{1}{2}(M_{ij} + M_{ji})\partial_{x_i} b_j \qquad \text{Since } \boldsymbol{M} \text{ is symmetric,} \\ &= \sum_{i=1}^d \sum_{j=1}^d M_{ij}\partial_{x_i} b_j = \boldsymbol{M} : \mathrm{grad}(\boldsymbol{b}) \end{aligned} \tag{A.8}$$

Then it holds

$$\int_\Omega \{\mathrm{Div}(\boldsymbol{M}) \cdot \boldsymbol{b} + \boldsymbol{M} : \mathrm{Grad}(\boldsymbol{b})\} \, \mathrm{d}\Omega = \int_\Omega \{\mathrm{Div}(\boldsymbol{M}) \cdot \boldsymbol{b} + \boldsymbol{M} : \mathrm{grad}(\boldsymbol{b})\} \, \mathrm{d}\Omega \tag{A.9}$$

Using Eq (A.4) then

$$\begin{aligned} \int_\Omega \{\mathrm{Div}(\boldsymbol{M}) \cdot \boldsymbol{b} + \boldsymbol{M} : \mathrm{Grad}(\boldsymbol{b})\} \, \mathrm{d}\Omega &= \int_\Omega \{\mathrm{Div}(\boldsymbol{M}) \cdot \boldsymbol{b} + \boldsymbol{M} : \mathrm{grad}(\boldsymbol{b})\} \, \mathrm{d}\Omega, \\ &= \int_{\partial\Omega} (\boldsymbol{M}^\top \boldsymbol{n}) \cdot \boldsymbol{b} \, \mathrm{d}S, \qquad \text{Since } \boldsymbol{M} \text{ is symmetric,} \\ &= \int_{\partial\Omega} (\boldsymbol{M}\,\boldsymbol{n}) \cdot \boldsymbol{b} \, \mathrm{d}S. \end{aligned} \tag{A.10}$$

This concludes the proof. □

A.3 Bilinear forms

Definition 8 (Skew-symmetric bilinear form)
A bilinear form on the Hilbert space H

$$\begin{aligned} b : H \times H &\longrightarrow \mathbb{R}, \\ (\boldsymbol{v}, \boldsymbol{u}) &\longrightarrow b(\boldsymbol{v}, \boldsymbol{u}), \end{aligned}$$

is skew-symmetric iff

$$b(\boldsymbol{v}, \boldsymbol{u}) = -b(\boldsymbol{u}, \boldsymbol{v}).$$

Appendix B

Supplementary material: tabulated results of Chapter 8

$\frac{1}{h}$	$\|\|e_w - e_w^h\|\|_{L^\infty(L^2)}$ Error	Order	$\|\|\boldsymbol{E}_\kappa - \boldsymbol{E}_\kappa^h\|\|_{L^\infty(L^2)}$ Error	Order
4	2.03e-01	—	7.58e-02	—
8	4.39e-02	2.21	1.90e-02	1.99
16	1.02e-02	2.09	4.77e-03	1.99
32	2.52e-03	2.02	1.19e-03	1.99
64	6.27e-04	2.00	2.98e-04	1.99
128	1.56e-04	2.00	7.47e-05	1.99

Table B.1: Euler Bernoulli convergence result for the HerDG1 scheme.

$\frac{1}{h}$	$\|\|e_w - e_w^h\|\|_{L^\infty(L^2)}$ Error	Order	$\|\|\boldsymbol{E}_\kappa - \boldsymbol{E}_\kappa^h\|\|_{L^\infty(L^2)}$ Error	Order
4	1.61e-02	—	7.48e-01	—
8	4.05e-03	1.99	1.88e-01	1.99
16	1.01e-03	1.99	4.71e-02	1.99
32	2.53e-04	1.99	1.17e-02	1.99
64	6.34e-05	1.99	2.94e-03	1.99
128	1.58e-05	1.99	7.37e-04	1.99

Table B.2: Euler Bernoulli convergence result for the DG1Her scheme.

$\frac{1}{h}$	$\|\|e_w - e_w^h\|\|_{L^\infty(L^2)}$ Error	Order	$\|\|\boldsymbol{E}_\kappa - \boldsymbol{E}_\kappa^h\|\|_{L^\infty(L^2)}$ Error	Order
4	5.93e-01	—	4.16e-00	—
8	2.57e-01	1.20	2.08e-00	0.99
16	1.26e-01	1.02	1.04e-00	0.99
32	6.29e-02	1.00	5.22e-01	0.99
64	3.14e-02	1.00	2.61e-01	0.99
128	1.57e-02	1.00	1.30e-01	0.99

Table B.3: Euler Bernoulli convergence result for the CGCG scheme $k = 1$.

$\frac{1}{h}$	$\lvert\lvert e_w - e_w^h \rvert\rvert_{L^\infty(L^2)}$		$\lvert\lvert \boldsymbol{E}_\kappa - \boldsymbol{E}_\kappa^h \rvert\rvert_{L^\infty(L^2)}$	
	Error	Order	Error	Order
4	5.66e-02	—	4.20e-01	—
8	1.38e-02	2.03	1.05e-01	1.99
16	3.34e-03	2.05	2.65e-02	1.99
32	8.16e-04	2.03	6.62e-03	1.99
64	2.01e-04	2.01	1.65e-03	1.99
128	5.01e-05	2.00	4.14e-04	2.00

Table B.4: Euler Bernoulli convergence result for the CGCG scheme $k = 2$.

$\frac{1}{h}$	$\lvert\lvert e_w - e_w^h \rvert\rvert_{L^\infty(L^2)}$		$\lvert\lvert \boldsymbol{E}_\kappa - \boldsymbol{E}_\kappa^h \rvert\rvert_{L^\infty(L^2)}$	
	Error	Order	Error	Order
2	3.16e-02	—	2.19e-01	—
4	4.04e-03	2.97	2.80e-02	2.96
8	5.06e-04	2.99	3.51e-03	2.99
16	6.33e-05	3.00	4.39e-04	2.99
32	7.91e-06	3.00	5.50e-05	2.99
64	1.26e-06	2.64	6.88e-06	2.99

Table B.5: Euler Bernoulli convergence result for the CGCG scheme $k = 3$.

$\frac{1}{h}$	$\lvert\lvert e_w - e_w^h \rvert\rvert_{L^\infty(L^2)}$		$\lvert\lvert \boldsymbol{e}_\theta - \boldsymbol{e}_\theta^h \rvert\rvert_{L^\infty(L^2)}$		$\lvert\lvert \boldsymbol{E}_\kappa - \boldsymbol{E}_\kappa^h \rvert\rvert_{L^\infty(L^2)}$		$\lvert\lvert \boldsymbol{e}_\gamma - \boldsymbol{e}_\gamma^h \rvert\rvert_{L^\infty(L^2)}$	
	Error	Order	Error	Order	Error	Order	Error	Order
4	1.62e-05	—	1.51e-04	—	4.89e-08	—	5.83e-07	—
8	6.52e-06	1.31	4.59e-05	1.71	1.45e-08	1.75	2.01e-07	1.53
16	3.28e-06	0.98	2.17e-05	1.07	5.69e-09	1.34	9.41e-08	1.09
32	1.64e-06	0.99	1.07e-05	1.01	2.63e-09	1.10	4.64e-08	1.02
64	8.24e-07	0.99	5.39e-06	1.00	1.29e-09	1.02	2.31e-08	1.00

Table B.6: Mindlin plate convergence result for the BJT scheme $k = 1$.

$\frac{1}{h}$	$\lvert\lvert e_w - e_w^h \rvert\rvert_{L^\infty(L^2)}$		$\lvert\lvert \boldsymbol{e}_\theta - \boldsymbol{e}_\theta^h \rvert\rvert_{L^\infty(L^2)}$		$\lvert\lvert \boldsymbol{E}_\kappa - \boldsymbol{E}_\kappa^h \rvert\rvert_{L^\infty(L^2)}$		$\lvert\lvert \boldsymbol{e}_\gamma - \boldsymbol{e}_\gamma^h \rvert\rvert_{L^\infty(L^2)}$	
	Error	Order	Error	Order	Error	Order	Error	Order
4	8.05e-06	—	7.22e-05	—	1.72e-08	—	2.42e-07	—
8	2.12e-06	1.92	1.87e-05	1.94	4.42e-09	1.96	6.06e-08	2.00
16	5.42e-07	1.96	4.09e-06	2.19	1.14e-09	1.95	1.43e-08	2.07
32	1.36e-07	1.99	1.04e-06	1.97	2.89e-10	1.97	3.56e-09	2.00
64	3.41e-08	1.99	2.62e-07	1.99	7.26e-11	1.99	8.88e-10	2.00

Table B.7: Mindlin plate convergence result for the BJT scheme $k = 2$.

$\frac{1}{h}$	$\|\|e_w - e_w^h\|\|_{L^\infty(L^2)}$ Error	Order	$\|\|\boldsymbol{e}_\theta - \boldsymbol{e}_\theta^h\|\|_{L^\infty(L^2)}$ Error	Order	$\|\|\boldsymbol{E}_\kappa - \boldsymbol{E}_\kappa^h\|\|_{L^\infty(L^2)}$ Error	Order	$\|\|\boldsymbol{e}_\gamma - \boldsymbol{e}_\gamma^h\|\|_{L^\infty(L^2)}$ Error	Order
2	6.98e-07	—	1.42e-05	—	1.54e-09	—	3.31e-08	—
4	1.09e-07	2.67	2.14e-06	2.72	2.31e-10	2.73	4.61e-09	2.84
8	1.44e-08	2.91	2.29e-07	3.22	2.42e-11	3.25	6.36e-10	2.85
16	1.83e-09	2.97	2.05e-08	3.19	2.62e-12	3.20	8.44e-11	2.91
32	2.30e-10	2.99	2.94e-09	3.08	3.00e-13	3.12	1.07e-11	2.97

Table B.8: Mindlin plate convergence result for the BJT scheme $k = 3$.

$\frac{1}{h}$	$\|\|e_w - e_w^h\|\|_{L^\infty(L^2)}$ Error	Order	$\|\|\boldsymbol{e}_\theta - \boldsymbol{e}_\theta^h\|\|_{L^\infty(L^2)}$ Error	Order	$\|\|\boldsymbol{E}_\kappa - \boldsymbol{E}_\kappa^h\|\|_{L^\infty(L^2)}$ Error	Order	$\|\|\boldsymbol{e}_\gamma - \boldsymbol{e}_\gamma^h\|\|_{L^\infty(L^2)}$ Error	Order
4	1.05e-05	—	7.96e-05	—	3.75e-08	—	6.54e-07	—
8	5.33e-06	0.98	3.53e-05	1.17	1.15e-08	1.70	3.73e-07	0.80
16	2.68e-06	0.99	1.75e-05	1.00	3.02e-09	1.92	1.92e-07	0.95
32	1.34e-06	0.99	8.80e-06	0.99	7.71e-10	1.97	9.72e-08	0.98

Table B.9: Mindlin plate convergence result for the AFW scheme $k = 1$.

$\frac{1}{h}$	$\|\|e_w - e_w^h\|\|_{L^\infty(L^2)}$ Error	Order	$\|\|\boldsymbol{e}_\theta - \boldsymbol{e}_\theta^h\|\|_{L^\infty(L^2)}$ Error	Order	$\|\|\boldsymbol{E}_\kappa - \boldsymbol{E}_\kappa^h\|\|_{L^\infty(L^2)}$ Error	Order	$\|\|\boldsymbol{e}_\gamma - \boldsymbol{e}_\gamma^h\|\|_{L^\infty(L^2)}$ Error	Order
4	8.43e-06	—	8.10e-05	—	1.80e-08	—	2.68e-07	—
8	2.28e-06	1.88	1.82e-05	2.15	4.79e-09	1.90	6.99e-08	1.93
16	5.85e-07	1.96	4.41e-06	2.04	1.22e-09	1.96	1.75e-08	1.99
32	1.47e-07	1.98	1.12e-06	1.97	3.03e-10	2.01	4.47e-09	1.97

Table B.10: Mindlin plate convergence result for the AFW scheme $k = 2$.

$\frac{1}{h}$	$\|\|e_w - e_w^h\|\|_{L^\infty(L^2)}$ Error	Order	$\|\|\boldsymbol{e}_\theta - \boldsymbol{e}_\theta^h\|\|_{L^\infty(L^2)}$ Error	Order	$\|\|\boldsymbol{E}_\kappa - \boldsymbol{E}_\kappa^h\|\|_{L^\infty(L^2)}$ Error	Order	$\|\|\boldsymbol{e}_\gamma - \boldsymbol{e}_\gamma^h\|\|_{L^\infty(L^2)}$ Error	Order
2	1.11e-06	—	1.63e-05	—	2.14e-09	—	4.63e-08	—
4	1.63e-07	2.77	2.56e-06	2.67	2.61e-10	3.04	6.96e-09	2.73
8	2.13e-08	2.93	2.63e-07	3.28	2.42e-11	3.42	9.90e-10	2.81
16	2.93e-09	2.86	4.24e-08	2.63	8.99e-12	1.43	3.64e-10	1.44

Table B.11: Mindlin plate convergence result for the AFW scheme $k = 3$.

$\frac{1}{h}$	$\|\|\boldsymbol{E}_r - \boldsymbol{E}_r^h\|\|_{L^\infty(L^2)}$					
	$k = 1$		$k = 2$		$k = 3$	
	Error	Order	Error	Order	Error	Order
4	2.45e-09	—	1.07e-09	—	1.57e-09	—
8	4.98e-10	2.29	2.48e-10	2.11	3.52e-10	2.15
16	1.26e-10	1.97	6.11e-11	2.02	8.67e-11	2.02
32	3.19e-11	1.98	1.52e-11	1.99	2.16e-11	2.00

Table B.12: Mindlin plate convergence result for the Lagrange multiplier $\boldsymbol{E}_r$.

$\frac{1}{h}$	$\|\|e_w - e_w^h\|\|_{L^\infty(H^1)}$		$\|\|\boldsymbol{e}_\theta - \boldsymbol{e}_\theta^h\|\|_{L^\infty(H^{\text{Grad}})}$		$\|\|\boldsymbol{E}_\kappa - \boldsymbol{E}_\kappa^h\|\|_{L^\infty(L^2)}$		$\|\|\boldsymbol{e}_\gamma - \boldsymbol{e}_\gamma^h\|\|_{L^\infty(L^2)}$	
	Error	Order	Error	Order	Error	Order	Error	Order
8	7.30e-05	—	5.52e-04	—	3.99e-08	—	9.02e-07	—
16	3.13e-05	1.22	2.26e-04	1.28	1.88e-08	1.08	5.47e-07	0.72
32	1.57e-05	0.99	1.11e-04	1.02	8.84e-09	1.09	2.94e-07	0.89
64	7.87e-06	0.99	5.57e-05	0.99	4.31e-09	1.03	1.50e-07	0.97
128	3.94e-06	0.99	2.78e-05	0.99	2.14e-09	1.01	7.55e-08	0.99

Table B.13: Mindlin plate convergence result for the CGDG scheme $k = 1$.

$\frac{1}{h}$	$\|\|e_w - e_w^h\|\|_{L^\infty(H^1)}$		$\|\|\boldsymbol{e}_\theta - \boldsymbol{e}_\theta^h\|\|_{L^\infty(H^{\text{Grad}})}$		$\|\|\boldsymbol{E}_\kappa - \boldsymbol{E}_\kappa^h\|\|_{L^\infty(L^2)}$		$\|\|\boldsymbol{e}_\gamma - \boldsymbol{e}_\gamma^h\|\|_{L^\infty(L^2)}$	
	Error	Order	Error	Order	Error	Order	Error	Order
8	9.78e-06	—	1.04e-04	—	7.30e-09	—	1.77e-07	—
16	2.53e-06	1.95	2.49e-05	2.07	1.85e-09	1.97	4.93e-08	1.84
32	6.35e-07	1.99	6.06e-06	2.04	4.63e-10	1.99	1.27e-08	1.95
64	1.58e-07	1.99	1.50e-06	2.01	1.15e-10	2.00	3.21e-09	1.98
128	3.97e-08	2.00	3.74e-07	2.00	2.89e-11	2.00	8.06e-10	1.99

Table B.14: Mindlin plate convergence result for the CGDG scheme $k = 2$.

$\frac{1}{h}$	$\|\|e_w - e_w^h\|\|_{L^\infty(H^1)}$		$\|\|\boldsymbol{e}_\theta - \boldsymbol{e}_\theta^h\|\|_{L^\infty(H^{\text{Grad}})}$		$\|\|\boldsymbol{E}_\kappa - \boldsymbol{E}_\kappa^h\|\|_{L^\infty(L^2)}$		$\|\|\boldsymbol{e}_\gamma - \boldsymbol{e}_\gamma^h\|\|_{L^\infty(L^2)}$	
	Error	Order	Error	Order	Error	Order	Error	Order
4	1.38e-06	—	1.24e-05	—	8.24e-10	—	2.24e-08	—
8	1.79e-07	2.94	1.51e-06	3.03	1.03e-10	2.99	2.90e-09	2.94
16	2.26e-08	2.98	1.88e-07	3.00	1.28e-11	3.00	3.64e-10	2.99
32	2.83e-09	2.99	2.36e-08	2.99	1.60e-12	3.00	4.54e-11	3.00
64	3.54e-10	2.99	2.95e-09	2.99	2.00e-13	3.00	5.67e-12	3.00

Table B.15: Mindlin plate convergence result for the CGDG scheme $k = 3$.

$\frac{1}{h}$	$\|\|e_w - e_w^h\|\|_{L^\infty(L^2)}$		$\|\|\boldsymbol{E}_\kappa - \boldsymbol{E}_\kappa^h\|\|_{L^\infty(L^2)}$	
	Error	Order	Error	Order
4	1.38e-00	—	5.11e+01	—
8	5.17e-01	1.41	2.64e+01	0.95
16	2.28e-01	1.18	1.33e+01	0.98
32	1.09e-01	1.05	6.68e-00	0.99
64	5.45e-02	1.01	3.34e-00	0.99

Table B.16: Kirchoff plate convergence result for the HHJ scheme $k = 1$ (SSSS test).

$\frac{1}{h}$	$\|\|e_w - e_w^h\|\|_{L^\infty(L^2)}$		$\|\|\boldsymbol{E}_\kappa - \boldsymbol{E}_\kappa^h\|\|_{L^\infty(L^2)}$	
	Error	Order	Error	Order
4	1.47e-01	—	6.58e-00	—
8	3.48e-02	2.08	1.70e-00	1.94
16	8.51e-03	2.03	4.31e-01	1.98
32	2.11e-03	2.00	1.08e-01	1.99
64	5.28e-04	2.00	2.70e-02	1.99

Table B.17: Kirchoff plate convergence result for the HHJ scheme $k = 2$ (SSSS test).

$\frac{1}{h}$	$\|\|e_w - e_w^h\|\|_{L^\infty(L^2)}$		$\|\|\boldsymbol{E}_\kappa - \boldsymbol{E}_\kappa^h\|\|_{L^\infty(L^2)}$	
	Error	Order	Error	Order
2	1.15e-01	—	4.85e-00	—
4	1.51e-02	2.92	6.42e-01	2.91
8	1.92e-03	2.97	8.10e-02	2.98
16	2.41e-04	2.99	1.01e-02	2.99
32	3.02e-05	2.99	1.26e-03	3.00

Table B.18: Kirchoff plate convergence result for the HHJ scheme $k = 3$ (SSSS test).

$\frac{1}{h}$	$\|\|e_w - e_w^h\|\|_{L^\infty(L^2)}$		$\|\|\boldsymbol{E}_\kappa - \boldsymbol{E}_\kappa^h\|\|_{L^\infty(L^2)}$	
	Error	Order	Error	Order
2	6.63e-00	—	3.60e+01	—
4	1.91e-00	1.79	9.99e-00	1.85
8	6.08e-01	1.64	3.29e-00	1.60
16	2.09e-01	1.54	1.14e-00	1.52
32	7.34e-02	1.50	4.01e-01	1.50

Table B.19: Kirchoff plate convergence result for the BellDG3 scheme (SSSS test).

$\frac{1}{h}$	$\|\|e_w - e_w^h\|\|_{L^\infty(L^2)}$		$\|\|\boldsymbol{E}_\kappa - \boldsymbol{E}_\kappa^h\|\|_{L^\infty(L^2)}$	
	Error	Order	Error	Order
4	5.94e-00	—	1.62e+01	—
8	2.35e-00	1.33	9.27e-00	0.81
16	9.98e-01	1.23	4.86e-00	0.93
32	4.69e-01	1.08	2.46e-00	0.98
64	2.34e-01	1.00	1.23e-00	0.99

Table B.20: Kirchoff plate convergence result for the HHJ scheme $k = 1$ (CSFS test).

$\frac{1}{h}$	$\|\|e_w - e_w^h\|\|_{L^\infty(L^2)}$ Error	Order	$\|\|\boldsymbol{E}_\kappa - \boldsymbol{E}_\kappa^h\|\|_{L^\infty(L^2)}$ Error	Order
4	1.13e-00	—	4.14e-00	—
8	2.90e-01	1.96	1.19e-00	1.79
16	7.14e-02	2.02	3.13e-01	1.93
32	1.77e-02	2.00	7.96e-02	1.97
64	4.43e-03	2.00	2.00e-02	1.98

Table B.21: Kirchoff plate convergence result for the HHJ scheme $k = 2$ (CSFS test).

$\frac{1}{h}$	$\|\|e_w - e_w^h\|\|_{L^\infty(L^2)}$ Error	Order	$\|\|\boldsymbol{E}_\kappa - \boldsymbol{E}_\kappa^h\|\|_{L^\infty(L^2)}$ Error	Order
2	1.57e-00	—	4.25e-00	—
4	2.39e-01	2.71	8.44e-01	2.33
8	3.37e-02	2.82	1.16e-01	2.85
16	4.50e-03	2.90	1.49e-02	2.95
32	5.76e-04	2.96	1.89e-03	2.98

Table B.22: Kirchoff plate convergence result for the HHJ scheme $k = 3$ (CSFS test).

$\frac{1}{h}$	$\|\|e_w - e_w^h\|\|_{L^\infty(L^2)}$ Error	Order	$\|\|\boldsymbol{E}_\kappa - \boldsymbol{E}_\kappa^h\|\|_{L^\infty(L^2)}$ Error	Order
2	3.88e+01	—	2.40e+01	—
4	8.17e-00	2.24	4.41e-00	2.44
8	2.71e-00	1.58	1.50e-00	1.54
16	1.13e-00	1.25	5.36e-01	1.49
32	4.35e-01	1.38	1.90e-01	1.49

Table B.23: Kirchoff plate convergence result for the BellDG3 scheme (CSFS test).

Appendix C

Implementation using FEniCS and Firedrake

Bibliography

[A.90] Douglas N. A. Mixed finite element methods for elliptic problems. *Computer Methods in Applied Mechanics and Engineering*, 82(1):281 – 300, 1990. Proceedings of the Workshop on Reliability in Computational Mechanics.

[AB85] D. Arnold and F. Brezzi. Mixed and nonconforming finite element methods: implementation, postprocessing and error estimates. *ESAIM: Mathematical Modelling and Numerical Analysis-Modélisation Mathématique et Analyse Numérique*, 19(1):7–32, 1985.

[Abe12] R. Abeyaratne. *Lecture Notes on the Mechanics of Elastic Solids. Volume II: Continuum Mechanics*. Cambridge, MA and Singapore, 1st edition, 2012.

[AFS68] J.H. Argyris, I. Fried, and D. W. Scharpf. The tuba family of plate elements for the matrix displacement method. *The Aeronautical Journal (1968)*, 72(692):701–709, 1968.

[AFW07] D. Arnold, R. Falk, and R. Winther. Mixed finite element methods for linear elasticity with weakly imposed symmetry. *Mathematics of Computation*, 76(260):1699–1723, 2007.

[AL00] G. Avalos and I. Lasiecka. Boundary controllability of thermoelastic plates via the free boundary conditions. *SIAM Journal on Control and Optimization*, 38(2):337–383, 2000.

[AL14] D. Arnold and J. Lee. Mixed methods for elastodynamics with weak symmetry. *SIAM Journal on Numerical Analysis*, 52(6):2743–2769, 2014.

[AW02] D. Arnold and R. Winther. Mixed finite elements for elasticity. *Numerische Mathematik*, 92(3):401–419, 2002.

[AW19] D. Arnold and S. W. Walker. The Hellan-Herrmann-Johnson method with curved elements, 2019. arXiv preprint arXiv:1909.09687.

[BadVMR13] L. Beirão da Veiga, D. Mora, and R. Rodríguez. Numerical analysis of a locking-free mixed finite element method for a bending moment formulation of Reissner-Mindlin plate model. *Numerical Methods for Partial Differential Equations*, 29(1):40–63, 2013.

[BBF$^+$13] D. Boffi, F. Brezzi, M. Fortin, et al. *Mixed finite element methods and applications*, volume 44. Springer, 2013.

[BDM85] F. Brezzi, J. Jr. Douglas, and L.D. Marini. Two families of mixed finite elements for second order elliptic problems. *Numerische Mathematik*, 47:217–236, 1985.

[Bel69] K. Bell. A refined triangular plate bending finite element. *International Journal for Numerical Methods in Engineering*, 1(1):101–122, 1969.

[BGL05] M. Benzi, G. H. Golub, and J. Liesen. Numerical solution of saddle point problems. *Acta Numerica*, 14:1–137, 2005.

[BH15] P. Benner and J. Heiland. Time-dependent Dirichlet conditions in finite element discretizations. *ScienceOpen Research*, 2015.

[Bio56] M.A. Biot. Thermoelasticity and irreversible thermodynamics. *Journal of Applied Physics*, 27(3):240–253, 1956.

[BJT00] E. Bécache, P. Joly, and C. Tsogka. An analysis of new mixed finite elements for the approximation of wave propagation problems. *SIAM Journal on Numerical Analysis*, 37(4):1053–1084, 2000.

[BJT01] E. Bécache, P. Joly, and C. Tsogka. A new family of mixed finite elements for the linear elastodynamic problem. *SIAM Journal on Numerical Analysis*, 39:2109–2132, 06 2001.

[BMXZ18] C. Beattie, V. Mehrmann, H. Xu, and H. Zwart. Linear port-Hamiltonian descriptor systems. *Mathematics of Control, Signals, and Systems*, 30(4):17, 2018.

[BR90] H. Blum and R. Rannacher. On mixed finite element methods in plate bending analysis. *Computational Mechanics*, 6(3):221–236, May 1990.

[Bre08] F. Brezzi. *Mixed finite elements, compatibility conditions, and applications*. Springer, 2008.

[Car73] D. E. Carlson. Linear thermoelasticity. In C. Truesdell, editor, *Linear Theories of Elasticity and Thermoelasticity: Linear and Nonlinear Theories of Rods, Plates, and Shells*, pages 297–345. Springer, Berlin, Heidelberg, 1973.

[CF05] G. Cohen and S. Fauqueux. Mixed spectral finite elements for the linear elasticity system in unbounded domains. *SIAM Journal on Scientific Computing*, 26(3):864–884, 2005.

[Cha62] P. Chadwick. On the propagation of thermoelastic disturbances in thin plates and rods. *Journal of the Mechanics and Physics of Solids*, 10(2):99–109, 1962.

[Cia88] P. G. Ciarlet. *Mathematical Elasticity: Three-Dimensional Elasticity*. Studies in mathematics and its applications. North-Holland, 1988.

[CMKO11] S.H. Christiansen, H.Z. Munthe-Kaas, and B. Owren. Topics in structure-preserving discretization. *Acta Numerica*, 20:1–119, 2011.

[Cou90] T.J. Courant. Dirac manifolds. *Transactions of the American Mathematical Society*, 319(2):631–661, 1990.

[CR16] F.L. Cardoso Ribeiro. *Port-Hamiltonian modeling and control of fluid-structure system.* PhD thesis, Université de Toulouse, Dec. 2016.

[CRML18] F.L. Cardoso-Ribeiro, D. Matignon, and L. Lefèvre. A structure-preserving partitioned finite element method for the 2d wave equation. *IFAC-PapersOnLine*, 51(3):119 – 124, 2018. 6th IFAC Workshop on Lagrangian and Hamiltonian Methods for Nonlinear Control LHMNC 2018.

[CRML19] F.L. Cardoso-Ribeiro, D. Matignon, and L. Lefèvre. A partitioned finite element method for power-preserving discretization of open systems of conservation laws, 2019. arXiv preprint arXiv:1906.05965.

[CRMPB17] F.L. Cardoso-Ribeiro, D. Matignon, and V. Pommier-Budinger. A port-Hamiltonian model of liquid sloshing in moving containers and application to a fluid-structure system. *Journal of Fluids and Structures*, 69:402–427, February 2017.

[DHNLS99] R. Durán, L. Hervella-Nieto, E. Liberman, and J. Solomin. Approximation of the vibration modes of a plate by Reissner-Mindlin equations. *Mathematics of Computation of the American Mathematical Society*, 68(228):1447–1463, 1999.

[DMSB09] V. Duindam, A. Macchelli, S. Stramigioli, and H. Bruyninckx. *Modeling and Control of Complex Physical Systems.* Springer Verlag, 2009.

[DSP08] V. Dos Santos and C. Prieur. Boundary control of open channels with numerical and experimental validations. *IEEE transactions on Control systems technology*, 16(6):1252–1264, 2008.

[Gev88] T. Geveci. On the application of mixed finite element methods to the wave equations. *ESAIM: M2AN*, 22(2):243–250, 1988.

[Gri15] M. Grinfeld. *Mathematical Tools for Physicists.* John Wiley & Sons Inc, 2nd edition, jan 2015.

[GSV18] T. Gustafsson, R. Stenberg, and J. Videman. A posteriori estimates for conforming kirchhoff plate elements. *SIAM Journal on Scientific Computing*, 40(3):A1386–A1407, 2018.

[GV64] I.M. Gel'fand and N.Ya. Vilenkin. *Generalized functions: Applications of harmonic analysis*, volume 4. Academic press, 1964.

[HE09] R.B. Hetnarski and M.R. Eslami. *Thermal stresses: advanced theory and applications*, volume 158. Springer, 2009.

[Hel67] K. Hellan. Analysis of elastic plates in flexure by a simplified finite element method. *Acta Polytechnica Scandinavica*, 1967.

[Hen06] D. Henry. *Geometric theory of semilinear parabolic equations*, volume 840. Springer, 2006.

[Her67] L.R. Herrmann. Finite-element bending analysis for plates. *Journal of the Engineering Mechanics Division*, 93(5):13–26, 1967.

[HLW03] E. Hairer, C. Lubich, and G. Wanner. Geometric numerical integration illustrated by the Störmer–Verlet method. *Acta numerica*, 12:399–450, 2003.

[HM78] T. J.R. Hughes and J.E. Marsden. Classical elastodynamics as a linear symmetric hyperbolic system. *Journal of Elasticity*, 8(1):97–110, 1978.

[Hug12] T. J.R. Hughes. *The finite element method: linear static and dynamic finite element analysis*. Courier Corporation, 2012.

[HZ97] S.W. Hansen and B.Y. Zhang. Boundary control of a linear thermoelastic beam. *Journal of Mathematical Analysis and Applications*, 210(1):182–205, 1997.

[Joh73] C. Johnson. On the convergence of a mixed finite-element method for plate bending problems. *Numerische Mathematik*, 21(1):43–62, 1973.

[JZ12] B. Jacob and H. Zwart. *Linear Port-Hamiltonian Systems on Infinite-dimensional Spaces*. Number 223 in Operator Theory: Advances and Applications. Springer Verlag, Germany, 2012. https://doi.org/10.1007/978-3-0348-0399-1.

[Kir18] R.C. Kirby. A general approach to transforming finite elements. *The SMAI journal of computational mathematics*, 4:197–224, 2018.

[KK15] R.C. Kirby and T. T. Kieu. Symplectic-mixed finite element approximation of linear acoustic wave equations. *Numerische Mathematik*, 130(2):257–291, Jun 2015.

[KM19] R.C. Kirby and L. Mitchell. Code generation for generally mapped finite elements. *ACM Trans. Math. Softw.*, 45(4), December 2019.

[KML18] P. Kotyczka, B. Maschke, and L. Lefèvre. Weak form of Stokes-Dirac structures and geometric discretization of port-Hamiltonian systems. *Journal of Computational Physics*, 361:442 – 476, 2018.

[Kot19] P. Kotyczka. *Numerical Methods for Distributed Parameter Port-Hamiltonian Systems*. TUM University Press, 2019.

[KS08] M. Krstic and A. Smyshlyaev. *Boundary control of PDEs: A course on backstepping designs*, volume 16. Society for Industrial and Applied Mathematics, 2008.

[KZ15] M. Kurula and H. Zwart. Linear wave systems on n-d spatial domains. *International Journal of Control*, 88(5):1063–1077, 2015. https://www.tandfonline.com/doi/abs/10.1080/00207179.2014.993337.

[KZvdSB10] M. Kurula, H. Zwart, A. J. van der Schaft, and J. Behrndt. Dirac structures and their composition on Hilbert spaces. *Journal of mathematical analysis and applications*, 372(2):402–422, 2010. https://doi.org/10.1016/j.jmaa.2010.07.004.

[Lag89] J.E. Lagnese. *Boundary Stabilization of Thin Plates*. Society for Industrial and Applied Mathematics, 1989.

[Lee12] J. Lee. *Mixed methods with weak symmetry for time dependent problems of elasticity and viscoelasticity*. PhD thesis, University of Minnesota, 2012.

[LGZM05] Y. Le Gorrec, H. Zwart, and B. Maschke. Dirac structures and Boundary Control Systems associated with Skew-Symmetric Differential Operators. *SIAM Journal on Control and Optimization*, 44(5):1864–1892, 2005. https://doi.org/10.1137/040611677.

[Li18] L. Li. *Regge finite elements with applications in solid mechanics and relativity*. PhD thesis, University of Minnesota, 2018.

[LMW+12] A. Logg, K.A. Mardal, G.N. Wells, et al. *Automated Solution of Differential Equations by the Finite Element Method*. Springer, 2012.

[LPKL12] L.D. Landau, L.P. Pitaevskii, A.M. Kosevich, and E.M. Lifshitz. *Theory of Elasticity*. Butterworth Heinemann, third edition, Dec 2012.

[LR00] R. Lifshitz and M. L. Roukes. Thermoelastic damping in micro-and nanomechanical systems. *Physical review B*, 61(8):5600, 2000.

[MBM+16] A. T. T. McRae, G.-T. Bercea, L. Mitchell, D. A. Ham, and C. J. Cotter. Automated generation and symbolic manipulation of tensor product finite elements. *SIAM Journal on Scientific Computing*, 38(5):S25–S47, 2016.

[Min51] R.D. Mindlin. Influence of rotatory inertia and shear on flexural motions of isotropic elastic Plates. *Journal of Applied Mechanics*, 18:31–38, March 1951.

[MM19] V. Mehrmann and R. Morandin. Structure-preserving discretization for port-hamiltonian descriptor systems. In *2019 IEEE 58th Conference on Decision and Control (CDC)*, pages 6863–6868, 2019.

[MMB05] A. Macchelli, C. Melchiorri, and L. Bassi. Port-based modelling and control of the Mindlin plate. In *Proceedings of the 44th IEEE Conference on Decision and Control*, pages 5989–5994, Dec. 2005. https://doi.org/10.1109/CDC.2005.1583120.

[Nor06] A.N. Norris. Dynamics of thermoelastic thin plates: A comparison of four theories. *Journal of Thermal Stresses*, 29(2):169–195, 2006.

[NY04] G. Nishida and M. Yamakita. A higher order Stokes-Dirac structure for distributed-parameter port-Hamiltonian systems. In *Proceedings of the 2004 American Control Conference*, volume 6, pages 5004–5009 vol.6, 2004.

[Olv93] P. J. Olver. *Applications of Lie groups to differential equations*, volume 107 of *Graduate texts in mathematics*. Springer-Verlag New York, 2nd edition, 1993.

[Pir89] O.A. Pironneau. *Finite element methods for fluids*. John Wiley and Sons, 1989.

[PZ18] D. Pauly and W. Zulehner. The divdiv-complex and applications to biharmonic equations. *Applicable Analysis*, pages 1–52, 2018.

[PZ20] D. Pauly and W. Zulehner. The elasticity complex, 2020. arXiv preprint arXiv:2001.11007.

[Red03] J.N. Reddy. *Mechanics of laminated composite plates and shells: theory and analysis*. CRC press, 2003.

[Red06] J.N. Reddy. *Theory and analysis of elastic plates and shells*. CRC press, 2006.

[Rei47] E. Reissner. On bending of elastic plates. *Quarterly of Applied Mathematics*, 5(1):55–68, 1947.

[RHM+17] F. Rathgeber, D.A. Ham, L. Mitchell, M. Lange, F. Luporini, A.T.T. McRae, G.T. Bercea, G.R. Markall, and P.H.J. Kelly. Firedrake: automating the finite element method by composing abstractions. *ACM Transactions on Mathematical Software (TOMS)*, 43(3):24, 2017.

[RR04] M. Renardy and R.C. Rogers. *An Introduction to Partial Differential Equations*. Number 13 in Texts in Applied Mathematics. Springer-Verlag New York, 2nd edition, 2004.

[RT77] P.A. Raviart and J.M. Thomas. A mixed finite element method for 2-nd order elliptic problems. In Ilio Galligani and Enrico Magenes, editors, *Mathematical Aspects of Finite Element Methods*, pages 292–315, Berlin, Heidelberg, 1977. Springer Berlin Heidelberg.

[RZ18] K. Rafetseder and W. Zulehner. A decomposition result for Kirchhoff plate bending problems and a new discretization approach. *SIAM Journal on Numerical Analysis*, 56(3):1961–1986, 2018.

[SHM19a] A. Serhani, G. Haine, and D. Matignon. Anisotropic heterogeneous n-D heat equation with boundary control and observation: I. Modeling as port-Hamiltonian system. *IFAC-PapersOnLine*, 52(7):51 – 56, 2019. 3rd IFAC Workshop on Thermodynamic Foundations for a Mathematical Systems Theory TFMST 2019.

[SHM19b] A. Serhani, G. Haine, and D. Matignon. Anisotropic heterogeneous n-D heat equation with boundary control and observation: II. Structure-preserving discretization. *IFAC-PapersOnLine*, 52(7):57 – 62, 2019. 3rd IFAC Workshop on Thermodynamic Foundations for a Mathematical Systems Theory TFMST 2019.

[Sim99] J.G. Simmonds. Major simplifications in a current linear model for the motion of a thermoelastic plate. *Quarterly of Applied Mathematics*, 57(4):673–679, 1999.

[Skr19] N. Skrepek. Well-posedness of linear first order port-Hamiltonian systems on multidimensional spatial domains, 2019. arXiv preprint arXiv:1910.09847.

[SS86] Y. Saad and M.H. Schultz. Gmres: A generalized minimal residual algorithm for solving nonsymmetric linear systems. *SIAM Journal on Scientific and Statistical Computing*, 7(3):856–869, 1986.

[SS17] M. Schöberl and K. Schlacher. Variational Principles for Different Representations of Lagrangian and Hamiltonian Systems. In Hans Irschik, Alexander Belyaev, and Michael Krommer, editors, *Dynamics and Control of Advanced Structures and Machines*, pages 65–73. Springer International Publishing, 2017.

[TRLGK18] V. Trenchant, H. Ramírez, Y. Le Gorrec, and P. Kotyczka. Finite differences on staggered grids preserving the port-Hamiltonian structure with application to an acoustic duct. *Journal of Computational Physics*, 373, 06 2018.

[TW09] M. Tucsnak and G. Weiss. *Observation and control for operator semigroups*. Springer Science & Business Media, 2009.

[TWK59] S. Timoshenko and S. Woinowsky-Krieger. *Theory of plates and shells*. Engineering societies monographs. McGraw-Hill, 1959.

[vdSM02] A.J. van der Schaft and B. Maschke. Hamiltonian formulation of distributed-parameter systems with boundary energy flow. *Journal of Geometry and Physics*, 42(1):166 – 194, 2002.

[Vil07] J.A. Villegas. *A Port-Hamiltonian Approach to Distributed Parameter Systems*. PhD thesis, University of Twente, May 2007.

[Yao11] P.F. Yao. *Modeling and Control in Vibrational and Structural Dynamics: A Differential Geometric Approach*. Chapman & Hall/CRC Applied Mathematics & Nonlinear Science. Taylor & Francis, 2011.

Résumé — Malgré l'abondante littérature sur le formalisme pH, les problèmes d'élasticité en deux ou trois dimensions géométriques n'ont presque jamais été considérés. Cette thèse vise à étendre l'approche port-Hamiltonienne (pH) à la mécanique des milieux continus. L'originalité apportée réside dans trois contributions majeures. Tout d'abord, la nouvelle formulation pH des modèles de plaques et des phénomènes thermoélastiques couplés est présentée. L'utilisation du calcul tensoriel est obligatoire pour modéliser les milieux continus et l'introduction de variables tensorielles est nécessaire pour obtenir une description pH équivalente qui soit intrinsèque, c'est-à-dire indépendante des coordonnées choisies. Deuxièmement, une technique de discrétisation basée sur les éléments finis et capable de préserver la structure du problème de la dimension infinie au niveau discret est développée et validée. La discrétisation des problèmes d'élasticité nécessite l'utilisation d'éléments finis non standard. Néanmoins, l'implémentation numérique est réalisée grâce à des bibliothèques open source bien établies, fournissant aux utilisateurs externes un outil facile à utiliser pour simuler des systèmes flexibles sous forme pH. Troisièmement, une nouvelle formulation pH de la dynamique multicorps flexible est dérivée. Cette reformulation, valable sous de petites hypothèses de déformations, inclut toutes sortes de modèles élastiques linéaires et exploite la modularité intrinsèque des systèmes pH.

Mots clés : Systèmes port-Hamiltonien, méchanique des solides, discretisation symplectique, méthode des éléments finis, dynamique multicorps

---

Abstract — Despite the large literature on pH formalism, elasticity problems in higher geometrical dimensions have almost never been considered. This work establishes the connection between port-Hamiltonian distributed systems and elasticity problems. The originality resides in three major contributions. First, the novel pH formulation of plate models and coupled thermoelastic phenomena is presented. The use of tensor calculus is mandatory for continuum mechanical models and the inclusion of tensor variables is necessary to obtain an equivalent and intrinsic, i.e. coordinate free, pH description. Second, a finite element based discretization technique, capable of preserving the structure of the infinite-dimensional problem at a discrete level, is developed and validated. The discretization of elasticity problems requires the use of non-standard finite elements. Nevertheless, the numerical implementation is performed thanks to well-established open-source libraries, providing external users with an easy to use tool for simulating flexible systems in pH form. Third, flexible multibody systems are recast in pH form by making use of a floating frame description valid under small deformations assumptions. This reformulation include all kinds of linear elastic models and exploits the intrinsic modularity of pH systems.

Keywords: Port-Hamiltonian systems, continuum mechanics, structure preserving discretization, finite element method, multibody dynamics.
